U.PORTO

DOUTORAMENTO

BIOLOGIA BÁSICA e APLICADA

Graphene-based materials for blood-contacting devices

Andreia Trindade Pereira

D

2020

U.PORTO

Andreia Trindade Pereira
Graphene-based materials for blood-contacting devices

Graphene-based materials for blood-contacting devices

Andreia Trindade Pereira

D.ICBAS 2020

SEDE ADMINISTRATIVA

INSTITUTO DE CIÊNCIAS BIOMÉDICAS ABEL SALAZAR
FACULDADE DE CIÊNCIAS
FACULDADE DE MEDICINA

ANDREIA SOFIA TRINDADE PEREIRA

GRAPHENE-BASED MATERIALS FOR BLOOD-CONTACTING DEVICES

Tese de Candidatura ao grau de Doutor em Biologia Básica e Aplicada submetida ao Instituto de Ciências Biomédicas Abel Salazar da Universidade do Porto.

Orientadora – Doutora Inês de Castro Gonçalves Almada Lobo

Categoria – Investigadora Principal

Afiliação – i3S – Instituto de Investigação e Inovação em Saúde, INEB – Instituto de Engenharia Biomédica; ICBAS – Instituto de Ciências Biomédicas Abel Salazar da Universidade do Porto; FEUP – Faculdade de Engenharia da Universidade do Porto.

Coorientadora – Professora Helga Bergmeister

Categoria – Professora Assistente

Afiliação – Center for Biomedical Research Medical University of Vienna, Vienna, Austria and Ludwig Boltzmann Cluster of Cardiovascular Research, Vienna, Austria.

Coorientador – Doutora M. Cristina L. Martins

Categoria – Investigadora Principal

Afiliação – i3S – Instituto de Investigação e Inovação em Saúde, INEB – Instituto de Engenharia Biomédica, ICBAS – Instituto de Ciências Biomédicas Abel Salazar da Universidade do Porto.

PhD program and institutions involved in this thesis:

Funding:

This work was financially supported by PhD grant of Andreia Sofia Trindade Pereira PD/BD/114156/2016 and projects PTDC/CTM-COM/32431/2017 and PTDC/CTM-BIO/4033/2014 funded by national funds through FCT/MCTES (PIDDAC).

To my father, my mother,
my brother, Íris, Pedro
all of my friends

Acknowledgments

I want to show my tremendous gratitude to my supervisor, Inês Gonçalves, for believing in my potential and ability as a researcher along this work. Since the first day, you got my attention due to your peculiar way of talking about the research that you do. This contagious “motto” was crucial to show me the way and to achieve the goals of this project. As supervisor, you were tireless and dedicated, promoting several scientific discussions that always culminated with several points of view that I did not think before and teaching me a lot of things. Besides the good researcher, you are a great friend, always showing your maternal character and care about all the students and me - you make the “Graphene team” a top place to work. I would like also to thank you for all the opportunities that you gave to me, namely, the possibility to visit different labs, to participate in several national/international congress (where we shared funny stories) and to promote my interdisciplinarity. Inês, you made me grow as a researcher and most important as a person. Thank you for making everything easier, possible and encouraging me.

I would like to thank my co-supervisor, Prof. Helga Bergmeister, for receiving me in your lab, all the scientific support always giving me your clinical point of view in this work. Your skills as one of the best vascular surgeons were crucial to achieve the main goals of this work. I also want to point out that you enlarge my abilities as a researcher, teaching me a lot about vascular grafts and allow me to participate in different courses and seminars. Your support during my stay in Vienna was incredible. You helped me with the most variety of issues. I still remember those afternoons in your office, all the evenings that we shared, and the way that you showed me how to have the full “Viennese” experience.

Special thanks to my co-supervisor, Cristina Martins, for accepting me in your group, for your sympathy and kind words that guided and encouraged me during this journey, not only during experimental part of Ph.D., but also during my decision process of thesis topic. Your scientific input was crucial for the development of this work always showing me how to be clear in all the ideas that I want to spread. As the leader of our group, you promote the good and relaxing environment emblematic of our group and gives the example of how hard work results in fantastic outcomes.

To Professor Fernão Magalhães, that despite not being an "official supervisor" followed this work closely, always giving a crucial scientific input. Your help was essential for me to understand several issues related to chemistry and mechanical properties of polymers. Thank you for all your dedication to this work.

To scientific committee of GABBA program for betting on me as a researcher, allowing me to embrace this challenge. Without doubt, this is best PhD program, since it gave me the freedom to explore the research topic that I most appreciate in the places that I felt to be the best to do it.

To all institutions engaged in this work, their Scientific Platforms and technicians that always helped to make this work easier, namely to Maria Lázaro from bioimaging, Rui Fernandes from HEMS, André Maia from BioSciences Screening members of the PPBI (PPBI-POCI-01-0145-FEDER-022122), to Ricardo from BN all from INEB/i3s. To Daniela Silva, Rui Rocha and Engenheiro Carlos Sá from CEMUP. To center from biomedical research from Medical University of Vienna (CBR), ICBAS, FCUP, FMUP, Laboratório de Engenharia de Processos, Ambiente, Biotecnologia e Energia (Lepabe – FEUP).

To my “gabbinhas collegues”, Diogo, Miguel, Joana and João for sharing with me all the rotational theoretical classes during the first year of Ph.D. Special to my friends, Rita, for being always there, Vânia, for all the “TUSH", Telmo, for all the cocktails that we enjoied, Francisca for being my flatmate during one of the best seasons in Porto. Thank you, Francisca, for listening and supporting me and helping me in to think rationally about all the issues.

To Bioengineered Surfaces group for being the best group of INEB/i3S and surroundings, for supporting this work scientifically during the lab meetings, for your daily encouragement, and for all our group activities. Thank you all! Special to Fabiola, for being the entrepreneur even in lab activities, Cláudia, which shares with me the love for biochemistry, Parreira, which use to call me “Andreia Mariana” in really friendly way, Catarina Seabra, for hosting me in my first times in the lab, Helena, for reading carefully my thesis, Guilherme, "the sushi guy", Duarte, which will continue the "pHEMA saga", Sofia Melo, for being always available for a 2 minutes of talk, Rita Gomes, for all the moments that you helped me, Inês Borges, for the hilarious moments together, namely during "chill outs", you always embraced my craziest ideas, Maura, Pedro, Diana, Renato, and Sofia.

I also would like to express my deep gratitude to my lab and outreach activities partner, Patrícia Henriques. Without you, I won’t say that would be impossible, because “impossible is nothing”, but it would be much more painful. You catalyzed all this process, with your everyday inexhaustible motivational words, therapeutical coffees, hugs, and “pizzas of sweet potato”, all our “dates”, sunsets, trips, etc and your unconditional help and support. Not only of fun, this catalyzation was supported, since, within all our scientific discussions, several questions were also raised, which contribute to this work maturation and to my growth as a scientist. I can’t also forget that you were my support in the lab teaching me a lot. You were always there, even when more than 2000 km split us. I am sure that I won’t find another “bartnina”.

To all people from INEB/i3S, especially to my dear friends Claudia Martins, for all ours “provinciana/auditorio” nights, conversations about random issues, for your knowhow about nanoparticles and cells, I know you will be there in all “my falls”, Ana Gerós, for being always helpful trying to show me the simplest solution for my problems and Francisca Araújo, for yours golden advice which were important during this journey. I would like to thank all the people that shared the lunchtime with me, Luis Leitão, special thank for the last month support, Tiago, Zé, Rita and Francisco. People that shared with me moments of fun, Elsa, I have a lot of “estima” for you, Angela, for your perpetual smile, Flávia Castro, Tatiana, Catarina, ... Tália and Silvia Bidarra for the help with HUVECs culturing, Dra Cristina Barrias and Sara for the support in this project.

To people from LEPABE, namely Diana Paiva and Diana Bogas, for helping me in the lab, and Artur Pinto, for sharing with me the knowledge and protocols about graphene materials.

To all of the people that I met in Vienna with who I had the pleasure to share seven months. To Karl, for all yours scientific inputs and discussions (I have a “to do list” with all our pendant ideas), to teach me everything about how to work with decellularized matrices, for all the unexpected “SEM” expeditions, for being a great friend that I count on. To Prof. Bruno Podesser for hosting me in his renowned institute, CBR, making me always feel like part. To Sabrina for being always with a great smile, even in the early morning. To Maria and Barbara for their indispensable role in keeping the lab "in shape", to Karin Huber for taking care of all the bureaucratic things associated with my visits, to Vesna for all the cakes and good conversation, to Atilla Kiss for his kindness, to Luiza and to Ouafa. To Professor Edward Leonard for sharing with me him know how about blood contacting devices. I want to thank people from OR, for their incredible work preparing everything in advance and all support during surgical proceeds, especially to Patrizia, for set up of GO-pro step up, Olga and Antonia. To guys from “students room” to Pia and Gabi, to make me feel at home during my first stay, to Patrick for keeping the good mood in the room, to Aldina and Ibo. To group “Party tomorrow”, Viki, Diego, Emil, and Bende that besides the support in the lab also shared with me several funny moments that helped me to relax during moments of pressure, I won’t forget about our parties at FIZZ, really great times. I would also like to thank Dr. Nagy Bendeguz, “the fake doctor”, for being a really great friend, for all scientific discussions, historical inputs, gastronomic experiences, and your availability to help me, even to carry my stuffs in the last day.

I wish to acknowledge all the support and great love of my childhood friends, Mariana Santos and Sofia Brito. Mariana Santos, best, for being always available to give me unconditional support, even when you did not understand the issues that I was worry about. To Sofia, for motivating me through her dedication to her own work and her words, which pushed me up during the hard moments. Thank you for all the pleasing moments that we shared together and for being my BFF’s.

To my family, specially to my sweet cousins, Cristina & Carolina, for being always available to give me a friendly word, supporting me in all moments and for sharing with me the trends of social networks, to Tono, to my Grandmother that always has a funny thing to tell me helping me just with her smile.

I would like to offer my special thanks to the wonderful people that were always one my side since my first day, my brother, my father, and my mother. “Manito” you are, without a doubt, my “guru”. Your wise advices during all my journey always added me as a person and professional. Special during Ph.D., you were crucial to teach me how to deal with stress and to define my priorities. I also appreciate all our scientific discussions, which were of great importance for this work. I could not forget to thank you, my sweet little niece, Iris Martina, for your “Titis”, smiles and first supporting words (at least in my interpretation). To Clara for her friendship and motivational words always encouraging me to start a Ph.D. Thank you for your scientific inputs and knowhow about “carbon materials” and how to deal with stress. To my parents, I owe my deepest gratitude for all that they taught me, namely the great values of the human life. You helped me a lot during all my journeys. I know all the things that I achieved until now were only possible because of yours’ unconditional friendship, love, dedication…, any word will define… Thank you for always believing in me, “Obrigada Papis”.

I owe a very important debt to Pedro for sharing with me the last years. You are my endless source of friendship, serenity, love, and happiness that support me as a person and as a researcher. Thank you for being always available to discuss with me about all the topics that I already worked on, poor you, and to think loud with me about these issues. Thank you for all the patience in all the “my stressing” moments, and for all the good times that we spent together, that were my refuge.

Resumo

Uma das principais restrições no setor de saúde, está relacionada com desempenho dos dispositivos para contato com sangue (BCDs), sendo responsável pela redução da qualidade de vida e sobrevivência dos pacientes. O papel universal dos BCDs no diagnóstico e tratamento de várias doenças levou a um crescimento do seu mercado global em cerca de ~ 22,2 bilhões de dólares (americanos) em 2018. Apesar de vários esforços, poucos biomateriais foram encontrados com potencial para serem usados como BCDs. Atualmente, os biomateriais comercialmente disponíveis, estão associados a várias complicações, como ocorrência de trombose, infeção e fibrose.

Esta tese tem como objetivo desenvolver biomateriais inovadores para serem utilizados como BCDs. Para isso, materiais à base de grafeno (GBMs), foram utilizados para suprimir as limitadas propriedades mecânicas, que restringem a aplicação de materiais hemo e/ou biocompatíveis no desenvolvimento de BCDs, uma vez que o grafeno, é o material mais forte do mundo. Dois biomateriais com características distintas foram selecionados, nomeadamente, o poli(2-hidroxietil metacrilato) (pHEMA), um polímero antiadesivo com baixa interação com o sangue e o tecidos adjacente (estratégia passiva), e artérias descelularizadas da placenta e do cordão umbilical, que promovem a reconstrução dos vasos nativos após a sua implantação (estratégia bioativa).

Na estratégia passiva, as propriedades mecânicas do pHEMA foram moduladas pela incorporação de: i) diferentes concentrações de óxido de grafeno (GO), variando de 0,1 até 5% (m/v), e ii) diferentes GBMs que variam em espessura, tamanho lateral e grau de oxidação, nomeadamente GO, Nanoplaquetas de Grafeno (GNP com 5 ou 15 μm) e asrespetivas formas oxidadas. Foi observado um efeito da concentração tendo-se obtido hidrogéis com uma excelente rigidez (módulo de Young até 6,5 MPa, 730% maior que o pHEMA) e resistência à tração (resistência à tração máxima até 1,1 MPa, 640% maior que o pHEMA) após incorporação de 5% de GO (m/v), sem afetar a capacidade de absorção de água, a hidrofilicidade e a citocompatibilidade do pHEMA. Estes valores de rigidez e resistência à tração são maiores que os da maioria dos hidrogéis (~ 0,300 MPa), atingindo-se uma rigidez comparável ao polidimetilsiloxano (PDMS), cartilagem ou paredes das artérias e uma resistência à tração semelhante a espumas rígidas, PDMS e cortiça. Particularmente, para a aplicação no desenvolvimento de BCDs, a concentração de 1% GO (m/v) mostrou ser a que permite obter propriedades mecânicas apropriadas. Nesta concentração, o grau de oxidação revelou ser o fator crucial para melhorar as propriedades de tração do pHEMA, uma vez que incorporação de GBMs não oxidados não influencia as suas propriedades mecânicas. A espessura dos GBMs oxidados também exerce um papel activo, sendo os maiores melhoramentos obtidos com a incorporação dos GBMs oxidados mais finos,

nomeadamento o GO, gerando hidrogéis com um módulo de Young de 1,8 MPa e uma resistência à tração de 0,70 MPa. Além disso, é observado um aumento na rugosidade da superfície dos hidrogéis após a incorporação de formas oxidadas de GBMs, embora o inchamento e a molhabilidade não sejam afetados na maioria das formulações testadas. As características biológicas do pHEMA não são comprometidas, uma vez que os GBMs oxidados não afetam a hemo/citocompatibilidade, mantendo-se assim as suas propriedades antiadesivas para células endoteliais, plaquetas sanguíneas e bactérias. Um estudo *in vivo* de hemocompatibilidade aguda num modelo de fístula arteriovenosa (AV) em porcos não heparinizados comprovou a baixa adesão dos componentes sanguíneos ao excerto pHEMA/GO 1% (m/v), revelando que este suporta o fluxo sanguíneo sem rutura e sem formação de coágulos.

Na abordagem bioativa, o revestimento interno de artérias decelularizadas do cordão umbilical com GO aumenta 29% a sua pressão de rutura, atingindo valores de 1960 mmHg, que são semelhantes aos da veia safena humana (~ 2100 mmHg), usualmente utilizada para excertos vasculares. Notavelmente, os revestimentos com GO também reduziram a adesão das plaquetas humanas às artérias decelularizadas do cordão umbilical e do córion da placenta, sendo também observada uma diminuição na adesão bacteriana das últimas, sem comprometer a adesão das células endoteliais. O modelo *in vivo* de fístula AV em porcos não heparinizados revelou que, à semelhança do que é realizado quando são implantadas artérias descelularizadas não revestidas, a compatibilidade sanguínea dos vasos descelularizados revestidos com GO pode ser alcançada após heparinização destes biomateriais.

O uso de GBMs revela-se assim uma excelente estratégia para reforçar as propriedades mecânicas de dois biomateriais com carateristicas distintas sem comprometer sua hemo / biocompatibilidade. Esta tese dá um passo em frente na área dos BCDs, abrindo caminho para uma futura aplicação de compósitos de pHEMA reforçado com GO e de artérias do cordão umbilical decelularizadas revestidas com GO.

Abstract

One of the main constraints on the health care sector is related to blood-contacting devices (BCDs) performance, being responsible for reduced quality of life and survival of patients. BCDs universal role in the diagnosis and treatment of several diseases, led to a rising global market of around ~ 22.2 billion USD in 2018. Despite several efforts, few biomaterials were found with high potential for use as BCDs. The commercial biomaterials used nowadays are associated with undesirable effects such as high thrombogenicity, infection, and fibrosis occurrence.

This thesis aims to develop innovative biomaterials to be used as BCDs. For this, graphene-based materials (GBMs) were used to suppress the limited mechanical features that restrain the application of hemo and/or biocompatible materials in the design of BCDs, since graphene is the strongest material in the world. Two biomaterials with distinct features were select, namely Poly(2-hydroxyethyl methacrylate) (pHEMA), a non-fouling polymer that has minimal interaction with blood and surrounding tissue (passive strategy), and decellularized placenta chorion and umbilical cord arteries, which may promote the reconstruction of native vessels upon implantation (bioactive strategy).

In the passive strategy, the mechanical properties of pHEMA were modulated through the incorporation of: i) different concentrations of graphene oxide (GO), ranging from 0.1 up to 5 % (w/v) and ii) different GBMs varying in thickness, lateral size and oxidation degree, namely GO, Graphene Nanoplatelets (GNP with 5 or 15 μm) and respective oxidized forms. A concentration effect was observed having obtained hydrogels with outstanding stiffness (Young's modulus of up to 6.5 MPa, 730% higher than neat pHEMA) and tensile resistance (ultimate tensile strength of up to 1.1 MPa, 640% higher than neat pHEMA) upon incorporation of 5% of GO, without affecting the water absorption capacity, surface wettability and cytocompatibility of pHEMA. These stiffness and tensile resistance values are higher than the ones of most hydrogels (~ 0.300 MPa), achieving a stiffness comparable to polydimethylsiloxane (PDMS), cartilage or artery walls and a tensile resistance similar to rigid foams, PDMS and cork. Particularly for application as BCDs, 1% GO (w/v) allows the achievement of appropriate mechanical features. Within this concentration, GBMs oxidation reveals to be a crucial factor to improve the tensile properties of pHEMA, since incorporation of non-oxidized GBMs does not influence the mechanical features. GBMs thickness also plays a role, with best improvements obtained upon incorporation of the thinnest oxidized GBM, GO, which generates hydrogels with 1.8 MPa of Young's Modulus and 0.70 MPa of tensile strength. Moreover, an increase in surface roughness of the hydrogels is observed upon the incorporation of oxidized forms of GBMs while swelling and surface wettability are not affected for most tested formulations. Biological features are not compromised, as oxidized GBMs did

not affect the hemo/cytocompatibility of pHEMA, maintaining the anti-adhesive properties towards endothelial cells, blood platelets, and bacteria. An acute hemocompatibility *in vivo* study using a non-heparinized porcine arteriovenous (AV)-shunt model proved the low adhesion of blood components to pHEMA/GO 1% (w/v) conduit, revealing that they can withstand blood flow without rupture and clot formation.

In the bioactive approach, GO coating of umbilical cord decellularized arteries lumen increase 29% of their burst pressure, reaching values of 1960 mmHg, which are similar to the human saphenous vein (~2100 mmHg), the gold standard for any prosthetic vascular conduit. Remarkably, GO coatings also reduced human platelets adhesion to umbilical cord and placenta chorion decellularized arteries, without compromising endothelial cells adhesion. The *in vivo* non-heparinized pig AV-shunt model revealed that similarly to what is performed when uncoated decellularized arteries are used, blood compatibility of GO coated decellularized vessels can be achieved after a heparinization step.

In summary, the use of GBMs unveil to be an excellent strategy to reinforce the mechanical properties of two biomaterials with distinct properties without compromising their hemo/biocompatibility. This thesis is a steppingstone in the field of BCDs, paving the way for a future application of biocompatible GO-reinforced pHEMA composites and GO-coated decellularized umbilical cord arteries.

Table of Contents

List of Abbreviations

AAm – Acrylamide

ADP – Adenosine diphosphate

adsHep – Adsorbed heparina

APS – Ammonium persulfate

ATR – Attenuated Total Reflection

AV-shunt – Arteriovenous-shunt

BCDs – Blood-contacting devices

BSA – Bovine serum albumin

covHep –Covalently heparinized

dArtery – Decellularized artery

DLS – Dynamic light scattering

DMEM – Dulbecco's modified Eagle's medium

ECGS – Endothelial cell growth supplement

ECM – Extracellular matrix

ECs – Endothelial cells

ePTFE – expanded-Polytetrafluoroethylene,

F – Activation of factor

FBS – Fetal bovine serum

FDA – Food & Drug Administration

FLG – Dew-layer Graphene

FLGox – Oxidized few-layer Graphene

Fmax – Maximal loaded radial force

FTIR – Fourier-transform infrared spectroscopy

FWHM – Full width at half-maximum

GACs – Glycosaminoglycans

GBMs – Graphene-based materials

GNP – Graphene nanoplatelets

GO – Graphene oxide

Gt – Graphite

GtO – Graphite oxide

H&E – Hematoxylin/Eosin

HEMA – 2-hydroxyethyl methacrylate

HUVECs – Human Umbilical Vein Endothelial Cells

iPSCs – Induced Pluripotent Stem Cells

ITA – Internal thoracic artery

I.D. – inner diameter

l – Length

MHM – Modified Hummers' method

MLG – Multi-layer Graphene

MLGox – Oxidized Multi-layer Graphene

MSCs – Mesenchymal Stem Cells

N.A. – Not Available

nGO – Commercially available GO (795534, Aldrich)

NSCs – Neural stem cells

PAA – poly(acrylic acid)

PAF – Platelet activating factor

PAM – poly(acrylamide)

PBS – Phosphate buffered saline

PC – Platelets concentrate

PCL – poly(caprolactone)

PDMA-stat-PAPBA – poly(N,N-dimethylacrylmide-stat-3-acrylamidophenylboronic acid)

PDMS – Polydimethylsiloxane

PEG – polyethylene glycol

PGA – poly(glycolic acid)

PGMA – poly(glycerol monomethacrylate)

pHEMA – poly(2-hydroxyethyl methacrylate)

PI – Propidium iodide

PLA – poly(lactic acid)

PLGA – poly(lactic acid-co-glycolic acid)

poly(AA-AANa) – poly(acrylic acid–sodium acrylate)

poly(AMPS) – poly(2-acrylamido-2-methylpropane sulfonic acid)

poly(CBAA) – poly(carboxybetaine acrylamide)

poly(HPMA) – poly[N-(2-hydroxypropyl) methacrylamide]

poly(MeOEGMA)) – poly[oligo(ethylene glycol) methylether methacrylate]

PU – Polyurethane

PVA – poly(vinyl alcohol)

PVC – poly(vinyl chloride)

r – Luminal radius

RBCs – Red Blood Cells

RT – Room temperature

SEM – Scanning Electron Microscopy

SMB – Sodium metabisulfite

SMCs – Smooth muscle cells

SV – Saphenous vein

TCPET – Tissue culture polyethylene terephthalate

T.E. – Tissue engineering

TEGDMA – Tetraethylene glycol dimethacrylate

TEM – Transmission Electron Microscopy

TF – Tissue factor

TSA – Tryptic Soy Agar

TSB – Trypticase Soy Broth

UTS – Ultimate tensile strength

Wd – Weight of the dry polymer

Ws – Weight of the swollen

XPS – X-ray Photoelectron Spectroscopy

XRD – X-Ray Diffraction (XRD)

YM – Young's Modulus

Chapter 1

Motivation, objectives, thesis outline and list of contributions

1.1 Motivation

Blood contacting devices (BCDs), such as catheters, vascular grafts, cannula and heart valves have a universal role in the diagnosis and treatment of several diseases. Nowadays, the available materials for the design of BCDs, such as silicone, polypropylene, polyethylene terephthalate, polyvinylchloride are associated with poor outcomes when applied for long periods of times due to the occurrence of thrombosis, infection, hemolysis, and fibrous tissue. This, in combination with the increase of several diseases prevalence (due to constantly rising in aging population, sedentary lifestyle and obesity) explains the global market of BCDs, moving ~ 22 billion USD in 2017-2018, with an expected average annual growth rate of 7.6% within the next three years. Thus, the search for new biomaterials, which could improve the general performance of BCDs, has been one of the main focus and challenges in the bioengineering research field [1-8].

To overcome these limitations, some strategies have been proposed, such as the development of passive (non-fouling) or bioactive surfaces [3, 8]. A non-fouling surface prevents the adhesion of blood components, cells and bacteria, being an attractive approach to prevent thrombosis and biomaterials related infections. Hydrophilic non-charged polymers, such as poly(2-hydroxyethyl methacrylate) (pHEMA), are described with non-fouling properties [9] and good hemocompatibility [10] but lack the mechanical properties to be applied as BCDs. Another strategy that has been suggested is the development of bioactive surfaces [1-3, 11] that keep the hemostasis upon blood and biomaterials interaction through the promotion of an anticoagulant and fibrinolytic environment locally. This could be achieved through the incorporation of anticoagulant molecules, seeding of endothelial cells before implantation, or promoting a rapid endothelialization upon implantation of the material. Regarding the last approach, the use of decellularized matrices of vascular tissue as an acellular scaffold has been proposed [12-22], namely due to preservation of tissue architecture and some cues crucial for cell adhesion [23, 24]. However, the lack of required mechanical properties and the high thrombogenic potential and susceptibility to infection, due to collagen fibers exposure [25], disable their usage as BCDs without further modification. Although these

approaches exhibit promising features to fill the gap of suitable materials for BCDs, their optimization is a demand to allow their future application.

1.2 Objectives

The main objective of this work is to develop novel biomaterials with suitable features to apply in the design of blood contacting devices (BCDs).

More specifically, this work aims to explore materials that are described in the literature as having a good hemo and/or biocompatibility, but that are not applied yet as BCDs due to weak mechanical properties. Since graphene is the strongest material in the world, the use of graphene-based materials (GBMs) is proposed to tune the mechanical properties of these biomaterials aspiring to reach the desired features for BCDs.

To achieve this main aim, two different approaches are followed: one that focuses on the development of an inert material that has minimal interaction with blood and surrounding tissues (**passive approach**) and another that aims to promote the reconstruction of native tissue upon implantation (**bioactive approach**).

In the **passive approach** two specific goals were stablished, namely the assessment of:

i. the required amount of GBMs to reach suitable mechanical properties for pHEMA application as BCDs without compromising its hydrogel-like non-fouling features.

ii. which GBMs are more suitable for the design of pHEMA based BCDs regarding mechanical properties, antimicrobial potential and hemo/biocompatibility.

In the **bioactive approach** a specific goal was stablished, namely the assessment of:

iii. the effect of graphene oxide coatings in the mechanical and antimicrobial properties and hemo/biocompatibility of decellularized arteries.

1.3 Thesis outline

This thesis is divided into six chapters, comprising a literature overview, three chapters with the manuscripts containing the main experimental work and the concluding remarks.

Chapter 1 comprises the motivation, main objectives for this study, as well as a thesis outline and list of contribution.

Chapter 2 introduces the main problems associated with blood-biomaterials interactions and recent developments in the design of blood-contacting devices (BCDs), along with the general properties and application of graphene-based materials (GBMs), specifically their interaction with biological systems and their use in the mechanical reinforcement of polymers.

Chapter 3 investigates the incorporation of different amounts of graphene oxide (GO) on the pHEMA and its impact on the physical/chemical and cytocompatibility of pHEMA/GO composites. Hydrogels are characterized regarding their surface wettability, swelling capacity and mechanical properties – Young's modulus (stiffness) and ultimate tensile strength (tensile resistance) – while investigating their cytocompatibility. From this exploratory study, which proposed pHEMA/GO application in different fields, it was possible to reach a filler concentration where these hydrogels exhibit the required mechanical properties to be apply in the design of BCDs.

Chapter 4 is dedicated to understand the effect of oxidation degree, thickness and lateral size of GBMs on the mechanical and biological properties of the composites, using the filler concentration disclaimed in **chapter 3**. The material with highest potential to be applied in the design of BCDs was investigated regarding its acute *in vivo* hemocompatibility.

Chapter 5 addresses the bioactive approach and explores the influence of GO coatings on the mechanical properties – tensile tests and suture retention – and biological features – biocompatibility, thrombogenicity and infectious potential – of decellularized matrices of umbilical cord and placenta chorion arteries. These *in vitro* experiments are complemented with assessment of acute *in vivo* hemocompatibility.

In **Chapter 6,** a general discussion, concisely correlating results from **Chapters 3-5,** is presented as well as the main conclusions, finishing with suggested directions to guide future research.

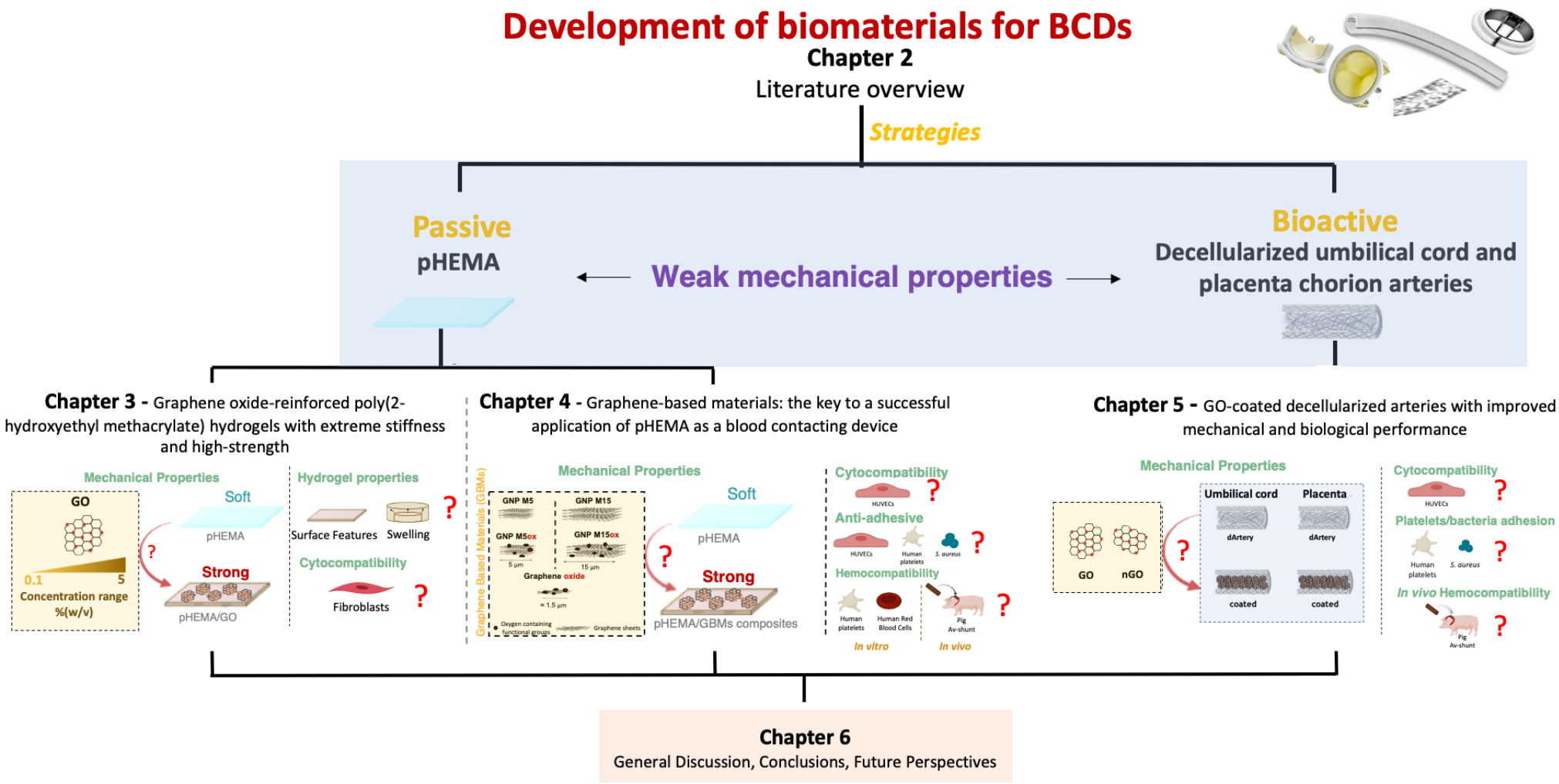

Figure. 1.1 – Schematic diagram illustrating the different topics covered in this thesis and their articulation.

1.4 List of Contributions

Under the scope of this thesis, 1 research article was published in an international peer reviewed journal, being 2 more in preparation, 1 book chapter is under proof revision, 8 oral and 6 poster presentations were performed in international/national conferences. The work was distinguished through attribution of a travel award to attend the conference “Graphene week 2019”, in Helsinki, Finland. A workshop on pHEMA/GBMs work was performed in the VIII AEICBAS Biomedical Congress. Due to the novelty of this research work a patent was submitted, which highlights the potential of commercialization. Other publications and presentations in collaboration on related topics were also achieved as described in the *curriculum vitae*.

Publications in the framework of this thesis

Papers in international refereed journals

1. **A. T. Pereira**, P. C Henriques, P. Costa, M. C. L. Martins, F. D. Magalhães, I. C. Gonçalves, Graphene oxide-reinforced poly(2-hydroxyethyl methacrylate) hydrogels with extreme stiffness and high-strength, Composites Science and Technology 184, **2019**.
2. **A. T. Pereira**, P. C. Henriques, K. H. Schneider, A. L. Pires, A. M. Pereira, M. C. L. Martins, F.D. Magalhães, H. Bergmeister, I.C. Gonçalves, Graphene-based materials: the key to a successful application of pHEMA as a blood contacting device, **in preparation.**
3. **A. T. Pereira**, K. H. Schneider, P. C. Henriques, S. Melo, C. Grasl, A. L. Pires, A. M. Pereira, M. C. L. Martins, H. Bergmeister*, I. C. Gonçalves*, GO-coated decellularized arteries with improved mechanical and biological performance, **in preparation.**

Patents

1. WO2019197504-A1 (PCT 2019.04); (P610.7 PP. 2018.04.11). STIFF AND STRONG HYDROGELS, PRODUCTION METHOD AND USES THEREOF. **A. T. Pereira**, F. D. Magalhães, I C Gonçalves.

Book chapter

1. A. M. Pinto, **A. T. Pereira**, I. C. Gonçalves, *Carbon Biomaterials*, Biomaterials Science Biomaterials Science, 4th Edition, Elsevier, **under proof revisions.**

Oral communications

1. **A. T. Pereira**, H. Bergmeister, I. C. Gonçalves, Multitasking role of graphene-based materials in the development of blood contacting devices, 22nd Gabba Meeting, Porto, **2019.**
2. **A. T. Pereira**, P. C. Henriques, K. Schneider, C. Grasl, P. Costa, M. C. L. Martins, F. D. Magalhães, H. Bergmeister, I. C. Gonçalves, Graphene oxide: the key for a successful application of pHEMA as a blood contacting device, Chirurigsche Forschung, Schlaming, Austria, **2019.**
3. **A. T. Pereira**, P. C. Henriques, K. Schneider, C. Grasl, P. Costa, M. C. L. Martinns, F. D. Magalhães, H. Bergmeister, I. C. Gonçalves, Graphene oxide: the key for a successful application of pHEMA as a blood contacting device, 30th European Conference on Biomaterials (ESB), Dresden, Germany, **2019.**
4. **A. T. Pereira**, P. C. Henriques, K. Schneider, C. Grasl, P. Costa, M. C. L. Martins, F. D. Magalhães, H. Bergmeister, I. C. Gonçalves, Biomaterials containing graphene-based materials (GBMs) for the development of small diameter vascular grafts, 21st GABBA Meeting, Porto, **2018.**
5. **A. T. Pereira**, P. C. Henriques, M. C. L. Martins, F. D. Magalhães, I. C. Gonçalves. New biocompatible graphene oxide-containing hydrogel with extreme mechanical properties. i3S Annual Meeting 2018, Póvoa do Varzim, **2018.**
6. **A. T. Pereira**, P. C. Henriques, M. C. L. Martins, F. D. Magalhães, I. C. Gonçalves. New biocompatible hydrogels with extreme mechanical properties. 29th European Conference on Biomaterials (ESB), Maastricht, **2018.**
7. **A. T. Pereira**, P. C. Henriques, A. M. Pinto, M. C. L. Martins, F. D. Magalhães, I. C. Gonçalves. Designing new hydrogels for blood contacting applications. i3S Annual Meeting 2017, Póvoa do Varzim, **2017.**
8. **A. T. Pereira**, P. C. Henriques, A. M. Pinto, M. C. L. Martins, F. D. Magalhães, I. C. Gonçalves. New era of strong materials for blood contacting devices, 20th GABBA Meeting, Porto, **2017.**

Poster communications

1. **A. T. Pereira**, K. Schneider, C. Grasl, M. C. L. Martins, H. Bergmeister, I. C. Gonçalves, Graphene-coated decellularized vessels as cell-free scaffolds for vascular applications, i3S Annual Meeting 2019, Póvoa do Varzim, **2019.**
2. **A. T. Pereira**, P. C. Henriques, K. Schneider, P. Costa, M. C. L. Martins, F. D. Magalhães, H. Bergmeister, I. C. Gonçalves, Biocompatible graphene oxide-containing hydrogels with extreme stiffness and high-strength, Graphene week, Helsinki, Finland, **2019.**

3. **A. T. Pereira**, P. C. Henriques, A. M. Pinto, M. C. L. Martins, F. D. Magalhães, I. C. Gonçalves. Tailoring the mechanical properties of hydrogels for blood contacting applications. International Symposium on Bioinspired Macromolecular Systems, Aveiro, Portugal, **2017**.
4. **A. T. Pereira**, H. Bergmeister, C. Grasl, M. C. L. Martins, F. D. Magalhães, I. C. Gonçalves "Composites of Polymers/carbon nano-fillers for blood contact aplications", 6th China-Europe of Biomaterials in Regenerative Medicine (CESB 2017), Porto, Portugal, **2017**.
5. **A. T. Pereira**, P. C Henriques, A. M Pinto, M. C. L. Martins, F. D. Magalhães, I. C. Gonçalves, "Polymers loaded with carbon nano-fillers for blood contact applicaRons" Graphene 2017, Barcelona, Spain, **2017**.
6. **A. T. Pereira**, H. Bergmeister, C. Grasl, M. C. L. Martins, F. D. Magalhães, I. C. Gonçalves, "Carbon nano-fillers loaded polymers for blood contact applications", Jornadas Nacionais de Caracterização de Materiais, Aveiro, Portugal, **2017**.

Award

1. Graphene Week 2019 Student Grant, Helsinky, Finland, **2019.**

Workshop organization

1. Super strong graphene containing hydrogels, Workshop at VII AEICBAS Biomedical congress, Porto, Portugal, **2019.**

1.5 References

[1] I. Sotiri, M. Robichaud, D. Lee, S. Braune, M. Gorbet, B.D. Ratner, J.L. Brash, R.A. Latour, I. Reviakine, BloodSurf 2017: News from the blood-biomaterial frontier, Acta Biomater 87 (2019) 55-60.

[2] B.D. Ratner, Biomaterials: Been There, Done That, and Evolving into the Future, Annu Rev Biomed Eng 21 (2019) 171-191.

[3] M.F. Maitz, M.C.L. Martins, N. Grabow, C. Matschegewski, N. Huang, E.L. Chaikof, M.A. Barbosa, C. Werner, C. Sperling, The blood compatibility challenge. Part 4: Surface modification for hemocompatible materials: Passive and active approaches to guide blood-material interactions, Acta Biomater 94 (2019) 33-43.

[4] I.H. Jaffer, J.I. Weitz, The blood compatibility challenge. Part 1: Blood-contacting medical devices: The scope of the problem, Acta Biomater 94 (2019) 2-10.

[5] M. Gorbet, C. Sperling, M.F. Maitz, C.A. Siedlecki, C. Werner, M.V. Sefton, The blood compatibility challenge. Part 3: Material associated activation of blood cascades and cells, Acta Biomater 94 (2019) 25-32.

[6] J.L. Brash, T.A. Horbett, R.A. Latour, P. Tengvall, The blood compatibility challenge. Part 2: Protein adsorption phenomena governing blood reactivity, Acta Biomater 94 (2019) 11-24.

[7] R. Gbyli, A. Mercaldi, H. Sundaram, K.A. Amoako, Achieving Totally Local Anticoagulation on Blood Contacting Devices, Adv Mater Interfaces 5(4) (2018).

[8] K.S. Lavery, C. Rhodes, A. McGraw, M.J. Eppihimer, Anti-thrombotic technologies for medical devices, Advanced drug delivery reviews 112 (2017) 2-11.

[9] F. Surman, T. Riedel, M. Bruns, N.Y. Kostina, Z. Sedlakova, C. Rodriguez-Emmenegger, Polymer brushes interfacing blood as a route toward high performance blood contacting devices, Macromol Biosci 15(5) (2015) 636-46.

[10] A.S. Hoffman, Hydrogels for biomedical applications, Advanced Drug Delivery Reviews 54(1) (2002) 3-12.

[11] C.H. Lin, K. Hsia, C.H. Tsai, H. Ma, J.H. Lu, R.Y. Tsay, Decellularized porcine coronary artery with adipose stem cells for vascular tissue engineering, Biomed Mater 14(4) (2019) 045014.

[12] J. Cheng, C. Wang, Y. Gu, Combination of freeze-thaw with detergents: A promising approach to the decellularization of porcine carotid arteries, Biomed Mater Eng 30(2) (2019) 191-205.

[13] H. Bai, A. Dardik, Y. Xing, Decellularized Carotid Artery Functions as an Arteriovenous Graft, J Surg Res 234 (2019) 33-39.

[14] M. van Steenberghe, T. Schubert, C. Bouzin, C. Caravaggio, Y. Guiot, D. Xhema, P. Gianello, Enhanced Vascular Biocompatibility and Remodeling of Decellularized and Secured Xenogeneic/Allogeneic Matrices in a Porcine Model, Eur Surg Res 59(1-2) (2018) 58-71.
[15] M. van Steenberghe, T. Schubert, C. Bouzin, C. Caravaggio, Y. Guiot, D. Xhema, P. Gianello, Decellularized and Secured Porcine Arteries with NaOH-based Process: Proof of Concept, Ann Vasc Surg 49 (2018) 179-190.
[16] H. Qi, C. Cheng, X. Wang, X. Yu, Preparation and investigation of novel SrCl2/DCMC-modified (via DOPA) decellularized arteries with excellent physicochemical properties and cytocompatibility for vascular scaffolds, RSC Advances 8(53) (2018) 30098-30105.
[17] L. Pu, J. Wu, X. Pan, Z. Hou, J. Zhang, W. Chen, Z. Na, M. Meng, H. Ni, L. Wang, Y. Li, L. Jiang, Determining the optimal protocol for preparing an acellular scaffold of tissue engineered small-diameter blood vessels, J Biomed Mater Res B Appl Biomater 106(2) (2018) 619-631.
[18] A. Porzionato, E. Stocco, S. Barbon, F. Grandi, V. Macchi, R. De Caro, Tissue-Engineered Grafts from Human Decellularized Extracellular Matrices: A Systematic Review and Future Perspectives, International journal of molecular sciences 19(12) (2018).
[19] N. Jeinsen, L. Magel, D. Jonigk, M. Klingenberg, A. Haverich, M. Wilhelmi, U. Boer, Biocompatibility of Intensified Decellularized Equine Carotid Arteries in a Rat Subcutaneous Implantation Model and in a Human In Vitro Model, Tissue Eng Part A 24(3-4) (2018) 310-321.
[20] N.J. Kristofik, L. Qin, N.E. Calabro, S. Dimitrievska, G. Li, G. Tellides, L.E. Niklason, T.R. Kyriakides, Improving in vivo outcomes of decellularized vascular grafts via incorporation of a novel extracellular matrix, Biomaterials 141 (2017) 63-73.
[21] Z. Syedain, J. Reimer, M. Lahti, J. Berry, S. Johnson, R.T. Tranquillo, Tissue engineering of acellular vascular grafts capable of somatic growth in young lambs, Nat Commun 7 (2016) 12951.
[22] S. Pashneh-Tala, S. MacNeil, F. Claeyssens, The Tissue-Engineered Vascular Graft-Past, Present, and Future, Tissue Eng Part B Rev 22(1) (2016) 68-100.
[23] C.H. Lin, K. Hsia, H. Ma, H. Lee, J.H. Lu, In Vivo Performance of Decellularized Vascular Grafts: A Review Article, International journal of molecular sciences 19(7) (2018).
[24] H. Bergmeister, R. Plasenzotti, I. Walter, C. Plass, F. Bastian, E. Rieder, W. Sipos, A. Kaider, U. Losert, G. Weigel, Decellularized, xenogeneic small-diameter arteries: transition from a muscular to an elastic phenotype in vivo, J Biomed Mater Res B Appl Biomater 87(1) (2008) 95-104.

Chapter 2

Introduction

2.1 Blood-Biomaterials interaction

2.1.1 Hemostasis mechanisms

Blood is constituted by water, proteins, platelets, red blood cells (RBCs) and white blood cells. To keep hemostasis, blood has several mechanisms, such as the coagulation cascade, platelets adhesion/activation, complement system and inflammatory response.

The coagulation cascade (Fig. 2.1.) is an important pathway for blood to keep hemostasis, since it limits blood loss upon a vascular injury. However, it can also be triggered in reaction to a tissue damage or an implanted biomaterial, leading to thrombus formation which can block blood flow and generate a pathogenic situation. Regulation of this mechanism involves the activation of zymogens (inert precursor enzymes) which circulate in blood as inactivated molecules, being activated by a sequence of proteolytic reactions. The coagulation cascade is divided into extrinsic (tissue factor) and intrinsic (contact) pathway, which merges upon activation of facto (F) X.

Extrinsic pathway can be activated by tissue factor (TF), which is expressed in the surface of endothelial cells (ECs), monocytes, monocyte-derived microparticles, neutrophils, eosinophils, and platelets. TF, a glycosylated integral-membrane protein, and FVIIa in presence of calcium, converts FX into FXa.

Intrinsic pathway seems to play only an active role in the pathogenic thrombus formation without a strong contribution for hemostasis. It can be activated upon blood contact with artificial surface (especially if negatively charged), platelet-derived polyphosphate, mast cell, extracellular RNA/DNA, collagen, misfolded proteins, kaolin, dextran sulfate, oversulfate chondroitin sulfate, glass and plastic. This contact leads to a conformational change and subsequent activation of FXVII to FXIIa. FXIIa converts FXI into FXIa. FXIa in the presence of calcium ions and phospholipids which activates FIX into FIXa. A serine protease “tenase” constituted by FIXa and FVIIIa, calcium and phospholipids activate FX into FXa.

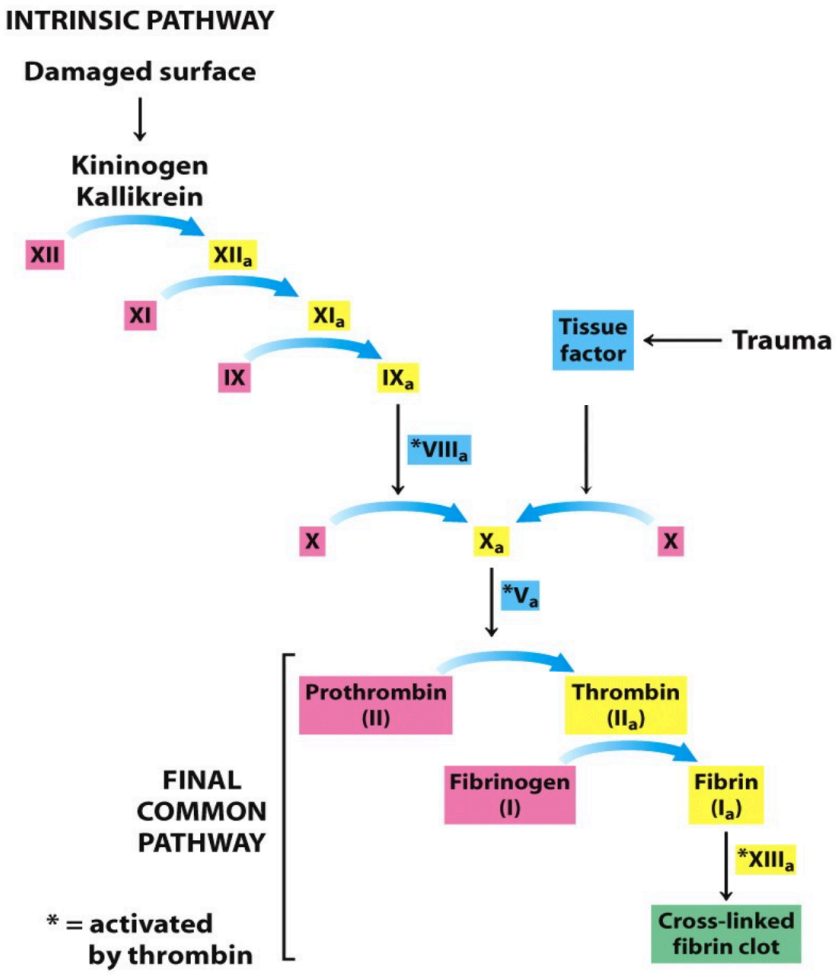

Figure 2.1 - Blood coagulation cascade. Reprinted with permission from ref. [1], copyright 2012, W.H. Freeman & Company.

In common branch of these two pathways, FXa interacts with FVa a serine protease called "prothrombinase" that converts prothrombin (FII) into thrombin. Thrombin acts on fibrinogen, releasing fibrin monomer that is cross-linked by FXIIIa forming a fibrin polymer clot.

Another hemostasis mechanism consists on platelets adhesion/activation. Platelets are disc shaped, anucleate cellular fragments derived from megakaryocytes with 2–3 μm of diameter. They circulate in inactivated form (round shape) with an average concentration of 200 x 10^6 plaquetas/mL, that can range between 150-400 x 10^6 plaquetas/mL and can be activated through several factors such as thrombin, fibrinogen, cytokines, vascular wall constituents (i.g. collagen), platelet activating factor (PAF), cathepsin G or artificial materials. Upon activation, platelets release the stored compounds, such as factor 4, thrombospondin, b-thromboglobulin, adenosine diphosphate (ADP), serotonin and P-selectin which play a role in platelets adhesion to neutrophils, monocytes and lymphocytes. After that, platelets change their structure to promote adhesion to the surface (Fig. 2.2) and their interaction between them. The rearrangement in platelets plasma membrane and the release of arachidonic acid, a precursor

of prostaglandins and thromboxane B_2 synthesis, promote “tenase” formation from coagulation cascade.

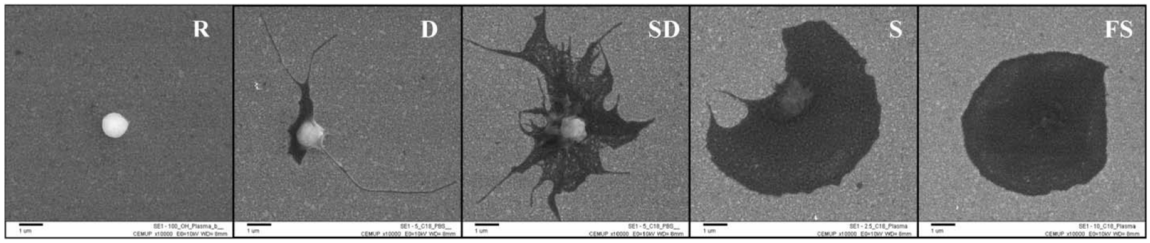

Figure 2.2 – SEM images of adherent platelets in different activation states. R – round or discoid; D – dendritic or early pseudopodial; SD – spread-dendritic, S – spreading or late pseudopodial and FS – fully spread. Reprinted with permission from ref. [2], copyright 2006, Elsevier.

Besides coagulation cascade and platelets, the complement system, which consists in more than 20 plasma proteins, also shows an essential role in the body’s defense mechanisms against infection and ‘‘non-self’’ elements. The complement system can be activated by three different pathways, classic, lectin and alternative, generating different complement products such as C3b, C4b and iC3b which bind to surfaces, particles, bacteria or immune complexes allowing their uptake by inflammatory cells. Moreover, release of anaphylotoxins C3a, C4a and C5a induces different cellular responses such as chemotaxis, cell adhesion and activation and vasodilation.

Leukocytes, which comprise monocytes, lymphocytes, eosinophils, basophils and neutrophils, are the major players in the inflammatory response. Upon an inflammatory stimulus, neutrophils increase their half-life time while monocytes can migrate to the damaged tissue or blood vessel, where they differentiate into macrophages. Bacteria, cell adhesion, platelet activating factor, cytokines, β-thromboglobulin and platelet-derived growth factor (PDGF) can activate this pathway.

2.2 Interplay between blood contacting devices and hemostasis mechanisms

Blood contacting devices (BCDs) comprise all the materials that are used in contact with blood, being widely BCDs that require some mechanical resistance, such as stent, guidewires and cannulas are mostly produced by steel while heart valves, vascular grafts and catheters are produced with polymers (Table 2).

Table 2.1 – Global Market of BCDs.

BCDs	Global market (USD) 2018 - Millions	%Compound annual growth rate	Materials	Companies	Ref
Stent	8000	6.6	Nitinol Stainless steels Other metallic alloys Nylon PU Styrene-isobutylene	Biotronik SE & Co. KG Cardinal Health Cook C. R. Bard, Inc. MicroPort Scientific Corporation Terumo Corporation B. Braun Melsungen AG Abbott Boston Scientific Corporation Medtronic	[3]
Heart Valves	6200	11.5	Dacron Fixed natural tissue Pyrolytic carbon	Medtronic Edwards Lifesciences Corporation Boston Scientific Corporation St. Jude Medical, Inc. LivaNova PLC, Symetis SA Jenavalve Technology, Inc. CryoLife, Inc. TTK HealthCare Colibri Heart Valve, LLC Lepu Medical Technology Co., Ltd. Braile Biomédica	[4]
Catheters	3500	5.1	PU PVC Silicone Teflon	Becton Dickinson and Company Boston Scientific Corporation Medtronic	[5]
Vascular grafts	2010	6.4	Dacron ePTFE	Gore Medical Cardinal Health R. Bard Terumo LeMaitre Vascular Medtronic Endologix Braun Melsugen AG Cook Medical Maquet	[6]
Ventricular assist device	1150	11.4	PU	Medtronic Abbott Berlin Heart Abiomed Cardiac Assist, Inc. ReliantHeart.	[7]
Guidewires	883	5.4	Steel coated with hydrophilic or a hydrophobic polymer	Abbott Laboratories B. Braun Melsungen AG Becton Dickinson and Company Biotronik SE & Co. KG Boston Scientific Corporation Cardinal Health, Inc. Cook Medical Inc. Olympus Corporation Terumo Corporation	[8]
Extracorporeal Membrane Oxygenation	268	6.5	Silicone rubber	CAPIOX FX Oxygenator Medtronic Plc	[9]
Cannulas	112	7.5	Stainless steel PU	Medtronic Becton Dickinson (BD) Edward Lifesciences LivaNova Smiths Medical Boston Scientific Corporation	[9]

ePTFE – expanded-Polytetrafluoroethylene, PU – Polyurethane, PVC - Polyvinyl chloride

By definition, a “blood compatible” device fully exerts its function in contact with blood without inducing adverse responses. Mechanisms involved in the hemostasis modulate in an interconnected way the response towards biomaterial (Fig. 2.3).

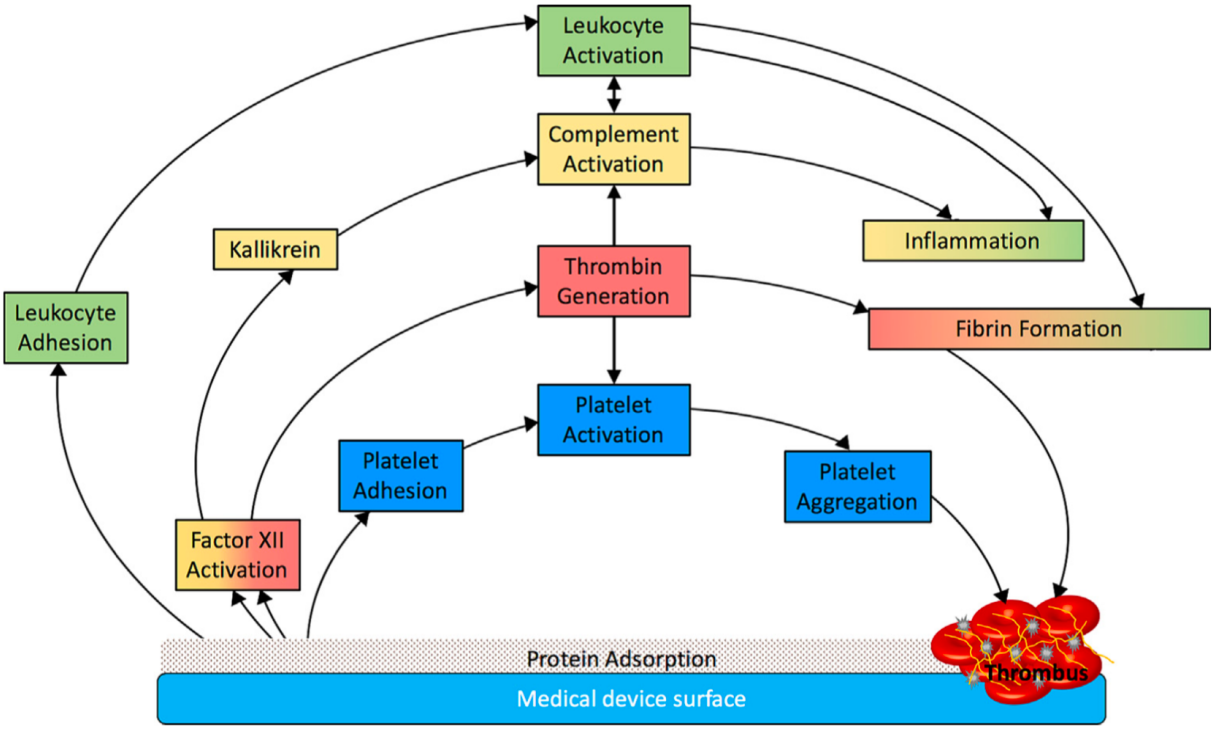

Figure 2.3 – Blood-contacting medical device associated thrombosis. Reprinted with permission from ref. [10] copyright 2019, Elsevier.

Plasma protein adsorption onto material surfaces is a trigger event in thrombus formation because it mediates the subsequent reactions. This phenomenon depends on surface chemistry and it is reversible, changing its composition over time. Platelets have capacity to recognize specific amino acid sequences that mediate their activation, namely RGD present in adsorbed proteins, namely fibrinogen (first plasma proteins to deposit), fibronectin and von Willebrand factor. Adsorbed fibrinogen can be replaced by factor XII which induces the intrinsic pathway of coagulation cascade as well as complement system activation, amplifying the pathways of thrombus formation. Leukocytes can adhere to the biomaterial surface and, due to size constrains, they are incapable to engulf the material, which leads to the release of reactive oxygen species, proteolytic enzymes and mediators of complement system and coagulation cascade. All these events culminate in thrombus formation, which is by definition a coagulated mixture of fibrin, platelets, RBCs and other cellular elements [11]. Even in conjugation with anticoagulant therapy, occurrence of thrombosis is the major cause of BCDs failure. This can cause local problems by occluding the vessel in which the device is present, requiring the replacement of BCDs. Furthermore, it can origin systemic complications if clot dislocates from original place and travels to the lungs, brain, or other organs.

2.2.1 Design of biomaterials for blood-contacting devices

BCDs performance varies with the used material, body response and exposure time, being their outcomes more limited for long-term application. Moreover, the good blood compatibility of materials in specific applications cannot be extrapolated for others. For example, extended-polytetrafluoroethylene (ePTFE) [12] and Dacron polyester [12, 13], which are synthetic and biostable materials, exhibit good performance in the replacement of large diameter arteries. However, when employed for the replacement of small diameter grafts (<4 mm), their outcomes are poor, exhibiting 54% failure rate upon 3 months of implantation [14], due to compliance mismatch and high thrombogenicity. In general, these materials do not support endothelial cell (EC) adhesion (without a coating), are thrombogenic and mismatch the mechanical properties of native vessels, exhibiting a compliance of around 1.5-1.9% which is not comparable to the 25.6% of saphenous veins [15, 16].

Despite thrombosis being the primary cause of BCDs failure, with high prevalence in heart valves, vascular grafts, and catheters, the occurrence of hemolysis, infection, and fibrosis also compromises the BCDs performance. Aiming the improvement of BCDs performance, two general strategies have been used; using passive and bioactive surfaces (Fig. 2.4), to prevent thrombus formation.

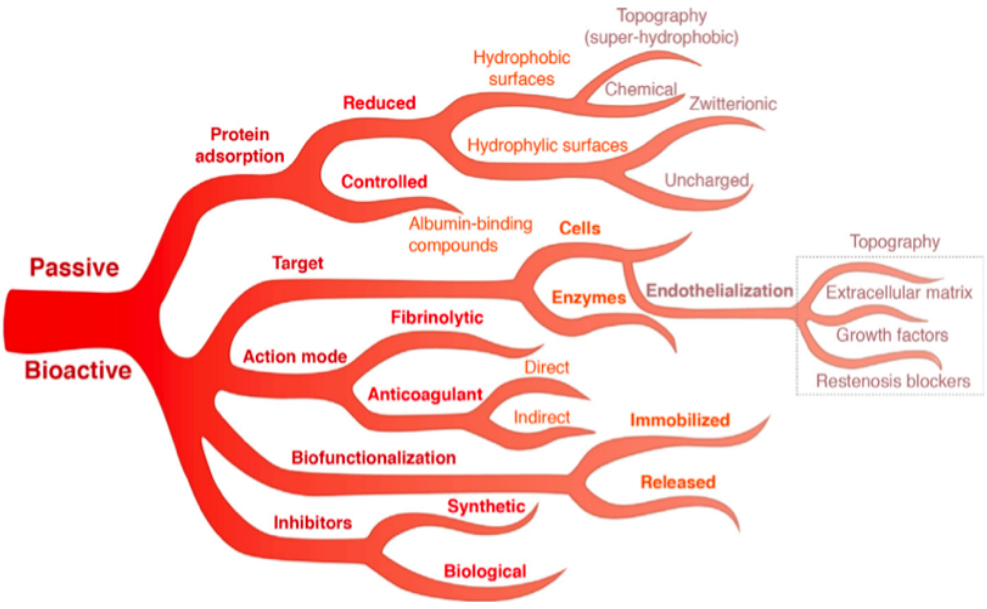

Figure 2.4 – Surfaces integrating passive vs active strategies for the design of BCDs. Reprinted with permission from ref. [17] copyright 2019, Elsevier.

2.2.1.1 Passivation strategy

Surface passivation strategy aims to prevent or to control protein adsorption to biomaterial. This strategy involves the use of uncharged or zwitterionic hydrophilic brushes or super-hydrophobic surfaces, allowing a high hydration degree or preventing the wetting by water or blood, respectively, and aims to impair proteins adsorption [10]. The passive strategy also includes approaches that promote the adsorption of thrombus protective proteins such as albumin.

Surfaces containing hydrophilic non charged polymers such as polyethylene glycol (PEG), polyethylene oxide, poly(2-hydroxyethyl methacrylate) (pHEMA), polyvinylpyrrolidone and poly(vinyl alcohol) (PVA) show low potential to adhere proteins and platelets on their surface. However, it is difficult to rank these polymers based on their performance. Surman *et al.* compared the non-fouling properties of poly[oligo(ethylene glycol) methylether methacrylate] (poly(MeOEGMA)), poly(hydroxyethyl methacrylate) (p(HEMA)), poly[N-(2-hydroxypropyl) methacrylamide] (poly(HPMA)), and poly(carboxybetaine acrylamide) (poly(CBAA)) coatings in gold glass slides [18]. Lower protein adsorption to pHEMA surface was observed despite the higher platelets adhesion comparing with the others. However, platelets adhere to less than 1% of pHEMA surface area [18], which comparing with other polymers is really low. Since its development in 1945, pHEMA has been used in several biological applications, such as design of drug delivery systems, blood compatible surfaces [19, 20] and as a scaffold when modified with molecules that promote cell adhesion [21], due to its biocompatibility and/or non-fouling properties. The high amount of hydroxyl groups and ester bonds in pHEMA structure, allows the binding of water molecules through hydrogen bonds forming a layer of structured water molecules on top of its surfaces that prevents protein adsorption (Fig. 2.5). In agreement with this, polyurethane grafted with the monomer 2-hydroxyethyl methacrylate (HEMA) presented good blood compatibility featured by the low platelet adhesion [22]. This effect is common to all hydrophilic non charged polymers, however, some of them exhibit a low stability, such as PEG, which is sensitive to oxidative and enzymatic degradation comprising its long-term usage [23].

A zwitterionic molecule is dipolar having at least one positively and another negatively charged functional group, being its total charge zero. Besides their high hydration capacity, due to their hydrophilic character, some zwitterionic molecules mimic the cellular membrane, which has a synergic effect for the prevention of thrombus occurrence. Coatings with poly(2-methacryloyloxyethyl phosphorylcholine), poly(sulfobetaine methacrylate) and N-(3-sulfopropyl)-N-methacryloxyethyl-N,N-dimethyl-ammoniumbetaine)) offer an improved hemocompatibility comparing with neat polymer [18].

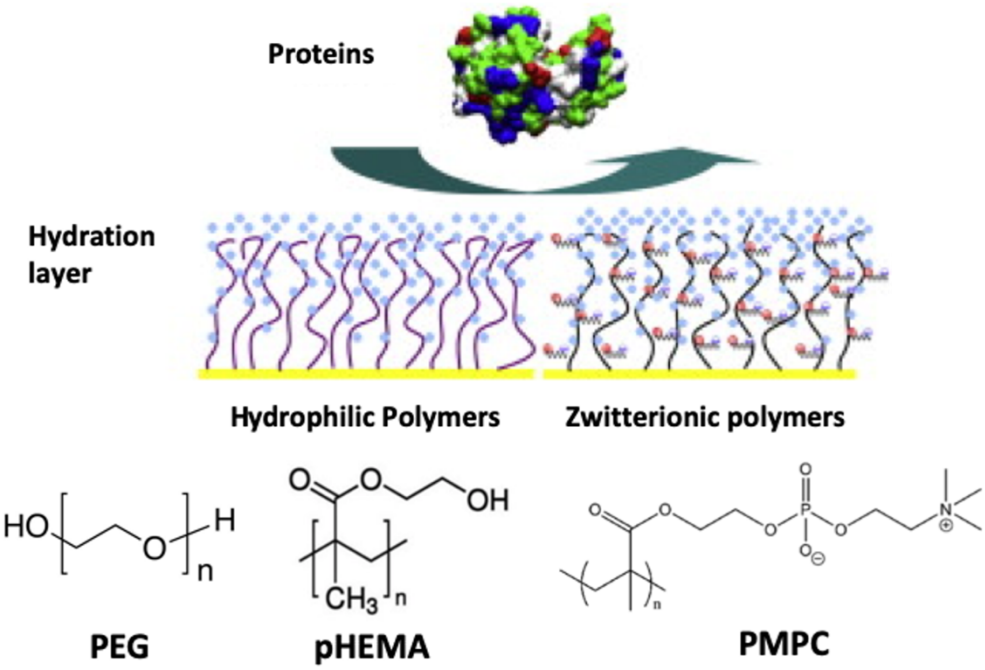

Figure 2.5 – Hydrophilic and zwitterionic polymers. Adapted from [23, 24] copyright 2010, Elsevier.

Non-fouling properties of hydrophilic non charged and zwitterionic polymers also prevent cellular and microbe attachment. Due to their week mechanical properties, as a consequence of high-water content, hydrophilic non charged and zwitterionic polymers have been only used as a coating or in conjugation with a copolymer. Thus, their performance depends always on the chemistry used for immobilization, the binding place, coating stability, their amount at the surface, the used copolymer and the proportion.

Superhydrophobic surfaces prevent liquid from entering and spreading in polymer surface, due to high energy barrier, promoted by nanostructured geometry, leading to the formation of water/blood droplet [25, 26]. Regarding platelet adhesion to super hydrophobic surfaces, it has been shown to be reduced, namely for nanotextured titania surfaces [27] and laser-ablated steel and titanium structures coated with hydrophobic material [28].

2.2.1.2 Bioactive strategy

Inspired by normal endothelial function, a bioactive strategy comprises the development of materials that keep the hemostasis upon their contact with blood providing an anticoagulant and fibrinolytic environment locally. This can be achieved through the inclusion of anticoagulant molecules, promoting endothelialization upon implantation and/or endothelialization before implantation. Heparin, a natural glycosaminoglycan, is the mostly used anticoagulant to coat surfaces in contact with blood. It promotes the interaction between thrombin–antithrombin and factor Xa–antithrombin inhibiting the coagulation cascade [29, 30].

This molecule has been conjugated with polyurethane [31], poly(ethersulfone) [32, 33], poly-(DL-lactic acid) [34] and 316L stainless steel [35]. Due to the promising features of heparin modified surfaces, it is already used in clinics for the design of vascular grafts, CarmedaBioActive Surface (CBAS®) technology [36]. A combination of two bioactive molecules has also been explored, namely using heparin and fibronectin. Yang *et al.* showed that heparin and fibronectin coatings have a synergic effect in the improvement of anticoagulation properties of titanium surfaces [37, 38]. These coatings sometimes involve complex chemical process for molecules immobilization being time consuming, expensive and can also compromise the activity of the molecule. Moreover, their efficacy depends on saturation, consumption and also the possible degradation during storage or when implanted.

Anti-CD34, anti-CD133, anti-cadherin, DNA or peptide aptamers are some of the molecules that have been immobilized at biomaterials surface to promote a fast endothelialization upon *in vivo* implantation [17, 23]. However, this approach shows to promote an unspecific cell adhesion.

Natural and synthetic polymers with capacity to sustain cell growth have also been explored, especially for the development of vascular grafts with inner diameter < 4 mm, cardiac valves and patches (promotion of cardiac cell growth) [39]. Natural polymers, mainly the ones derived from extracellular matrix (ECM), such as elastin, collagen and fibrin, exhibit a chemical structure and biological cues similar to the host vessel and are biodegraded upon implantation. Thus, grafts produced with these polymers integrate easily the host vessel being remodeled. However, problems associated to their weaker mechanical properties and high heterogeneity have been pointed as the main disadvantages. Synthetic polymers have as main advantages their controllable fabrication process, reproducibility and relative low production costs. Moreover, the mechanical properties of these polymers can be modulated allowing the production of grafts with capacity to sustain high blood pressure. Their highest disadvantage is the lack of cell binding sites, which compromise cell attachment and infiltration [40].

Both natural and synthetic polymers can be implanted after their *in vitro* cellularization or as an acellular graft. *In vitro* cellularization of grafts reveals to improve their mechanical resistance, blood compatibility and remodelling capacity. However, it is limited to long production time, the associated costs and to a selection of cell type appropriated to this approach, since they should be easy to harvest, able to proliferate and to perform their function upon implantation [41].

Biodegradable and FDA approved synthetic polymers such as poly(lactic acid) (PLA), poly(glycolic acid) (PGA), and their copolymers poly(lactic acid-co-glycolic acid) (PLGA), and poly(caprolactone) (PCL) have been explored specially for the design of small diameter vascular grafts. High degradation rates of PGA and PLA have been pointed as the central problem for their application in development of tissue engineered vascular tissue [12, 16] since

they can not support arterial pressure during tissue regeneration leading to the occurrence of aneurysm and consequent graft failure. PCL exhibits slower degradation kinetics (longer than 24 months), which allow cellular ingrowth and tissue regeneration [42]. Electrospun PCL grafts with 2 mm exhibited complete endothelization by 12 weeks when implanted in the abdominal aorta of rats. A regression in tissue regeneration is observed after 12 months of implantation as well as a decrease in angiogenic factors, cell infiltration and macrophages in remodelling area, leading to the starving of myoblast and a consequent graft calcification [42].

Most of the natural materials explored in the design of vascular grafts are a constituent of the extracellular matrix (ECM), such as collagen and elastin. The first tissue-engineered blood vessel was developed by Weinberg and Bell in mid 1980s using the principal constituent of ECM, collagen, as a scaffold. Bovine endothelial cells (ECs), fibroblasts, and smooth muscle cells (SMCs) were co-cultured in a 2D sheet of a collagen matrix, which was shaped posteriorly into 3D mold to form a tube. Despite exhibiting a similar structure to the native vessel, its mechanical properties were reduced. Besides the high potential to support ECs and SMCs growth [43], collagen is also easily recognized by platelets, activating them. Thus, it cannot be used as acellular scaffold without further modification, such as heparinization [44]. Oppositely to collagen, tropoelastin, a small soluble precursor of elastin, does not allow the attachment of platelets at its surface, being an attractive material for the design of tissue engineered vascular grafts [45]. However, tropoelastin scaffolds lack the tensile resistance, being used in combination with PCL or PLGA and collagen [46]. Despite not belonging to ECM, silk supports the migration and proliferation of endothelial and smooth muscle cells [47]. This material is biocompatible and non-thrombogenic exhibiting an excellent performance upon 1 year of implantation in the abdominal aorta with 85% of patency [48]. Decellularized grafts have been proposed for the vascular replacement/access, being some of them already available in the market such as Artegraft® (Bovine carotid artery), Solcograft (Bovine carotid artery), ProCol® (Bovine mesenteric vein), and SynerGraft® (Bovine ureter). After implantation, the natural matrix induces tissue remodeling and regeneration. However, their outcomes are similar to synthetic materials, failing due to thrombosis, infection, or aneurysm occurrence, and the higher associated costs explain their reduced usage in clinics [49, 50]. Even when allografts are used, such as SynerGraft® processed human cadaver vein allograft, their performance is similar to decellularized xenografts [49, 50].

2.3 Graphene-based materials (GBMs)[1]

Graphene is a 2D material with a crystalline form of carbon containing sp^2 hybridized atoms. It is the basic building block of hexagonally bonded carbon materials and consists of a 6-ring honeycomb lattice structure where each carbon atom is bonded to three neighboring atoms. Graphene was firstly isolated in 2004, and since then, along with its derived graphene-based materials (GBMs), has been remarkably studied. Graphene can be produced by top-down approaches, using graphite as raw material, and/or bottom-up approaches, using alternative carbon sources as raw material (Fig. 2.6) [51]. GBMs are a broad class of materials which involve single layer graphene, few-layer graphene (2-5 layers graphene layers packed together, FLG) and multi-layer Graphene (MLG), also called Graphene nanoplatelets (GNP) (2-10 layers), while materials with more than 10 layers are considered graphite (Gt). Each of this class of materials can be oxidized (usually by Modified Hummers Method), being referred as Graphene oxide (GO), oxidized FLG (FLGox), oxidized MLG (MLGox) and Gt oxide (GtO).

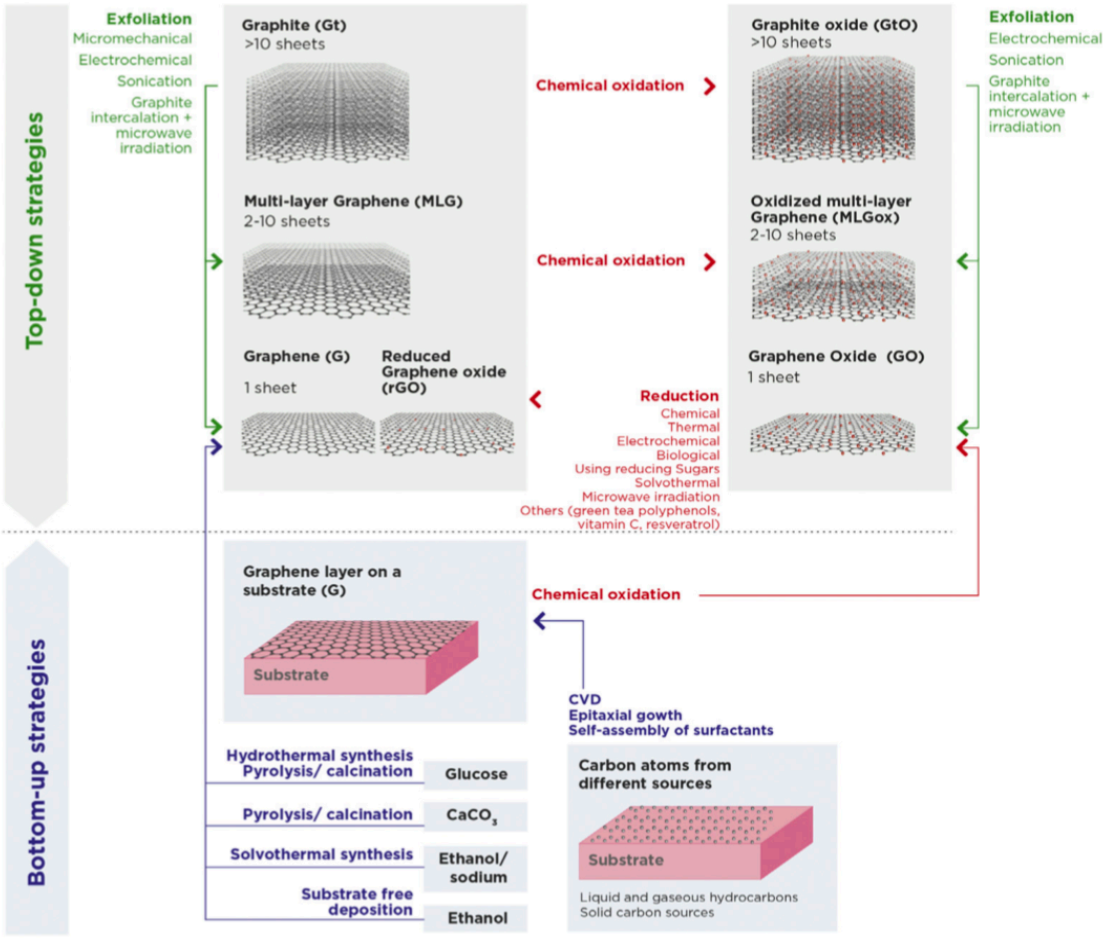

Figure 2.6 – Graphene-based materials family and their production methods. Reprinted with permission from ref. [51] copyright 2018, Elsevier.

[1]This section was partially based on the book chapter: A. M. Pinto, A. T. Pereira, I. C. Gonçalves, Carbon Biomaterials, Biomaterials Science Biomaterials Science, 4th Edition, Elsevier, under proof revisions

In addition to its unique thermal (~5000 W/mK) and electrical (6000 s/cm) conductivity, G is the strongest (ultimate tensile strength 130 GPa and Young's modulus of 1 TPa) [52], thinnest and lightest material in the world. However, with the increase of graphene layers a decrease in electric conductivity is observed. GBMs oxidation disrupts the aromatic system, introducing oxygen in the form of hydroxyl (–OH) and epoxide (–O–) groups at the bulk surface and carbonyl (C=O) and carboxyl groups (O-C=O) at the edges of the sheets (Fig. 2.7).

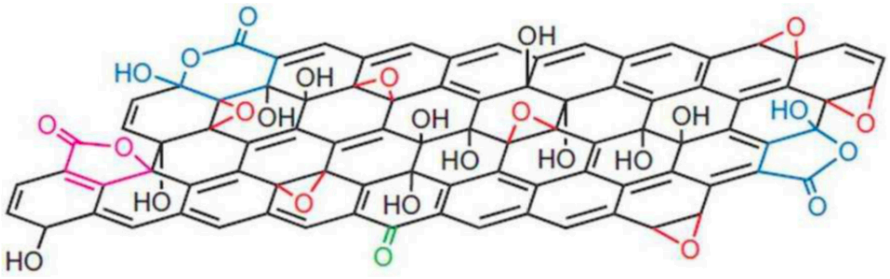

Figure 2.7 – Graphene oxide structure. Reprinted with permission from ref. [53] copyright 2009, Springer Nature.

This also leads to a decrease of conductivity, which can be partially reestablished by reduction, resulting in rGO (when GO is used). Due to their unique properties, research in graphene and GBMs has been increasing since 2007, reaching the 33750/year publications in 2019 (Fig 2.8). From these studies, only around 17% focus on GBMs interaction with biological systems, being energy, synthesis, electronics and sensors the main topics of graphene related research.

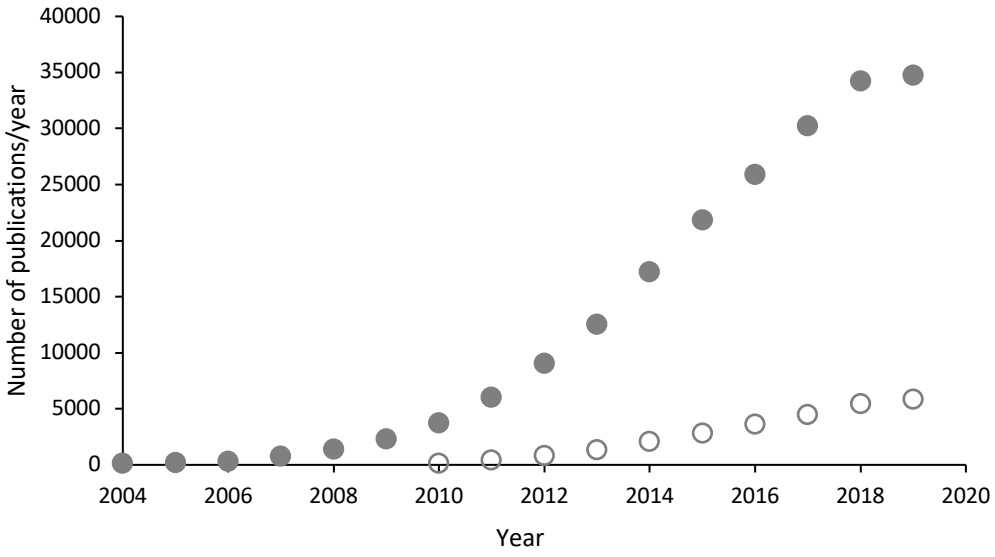

Figure 2.8 – Number of publications using "graphene" (●) and "graphene+bio*" (○) as keywords. Source: isi web of knowledge.

2.3.1 Biomedical applications of GBMs

Despite many of us not always being aware of it, carbon materials are part of our daily routines, being present in things like coal, jewelry, pencils, biomaterials, graphite lubricants, etc. Their recognition as biocompatible dates back to ancient times, where man made permanent tattoos using pulverized charcoal, as they knew it could be placed under the skin without apparent adverse effects. However, it was only in late 1960s that a pyrolytic form of carbon was found to have remarkable blood compatibility and the structural properties needed for application in long-term artificial heart valves [54].

Depending on the biological application, GBMs can be used as colloids, free-standing materials, coatings or composites (Table 2.2). GBMs in the colloidal form have been mainly explored for drug delivery, specially the oxidized forms, due to high loading capacity and high dispersibility in aqueous solvents, for phototherapy, due to the need of lower radiation energy, [59] and as antimicrobial agents.

Free-standing materials comprise free-standing films, that can be quickly and cheaply produced through vacuum filtration or direct evaporation methods [55], and carbon aerogels, generally produced by critical point drying, 3D printing or freeze-drying methods [56]. GBMs free-standing materials have been mainly explored for the development of biosensors due to their electrical conductivity, large surface area, and high electron transfer potential, as antibacterial surfaces, in cardiac, orthopedic and neurological tissue engineering applications and in skin wound healing [57-59].

GBMs coatings can be obtained by chemical vapor deposition, Langmuir-Blodgett, dip coating, drop casting, spin coating, spray coating or electrophoretic deposition [51], resulting in GBMs deposition in a flat or random orientation. GBMs coatings are being investigated for biosensors, antimicrobial applications, orthopedic and oral implants, catheters, contact lenses and tissue engineering of cardiac and bone tissues [58, 60]

As graphene composites, GBMs are combined with polymers, ceramic or metals. GBMs composites can be produced using different techniques, as *in-situ* polymerization, melt blending and solvent-mixing (followed by casting, doctor blading, electrospinning, 3D printing,…) [61, 62]. The final features of the produced materials are highly dependent on the used GBM, production technique and also on base polymer. Thus, playing with all these features allows the production of a wide range of materials. Applications in drug delivery, antimicrobial materials, design of mechanical heart valves, tissue engineering of cardiac, bone, cartilage, neuronal and muscle and skin wound healing have been envisaged .

Table 2.2 - Examples of the main potential applications under investigation of the different GBMs colloids, free-standing materials, coatings and composites.

Potential application of GBMs	Colloids	Free-standing	Coatings	Composites
	- Drug delivery - Phototherapy - Antimicrobial	- Biosensors - Antimicrobial - T.E. (Cardiac; Bone; Neuronal; Muscle) - Skin wound healing	- Biosensors - Antimicrobial - Orthopedic Implants - Catheter - Contact Lenses - Oral Implants - T.E. (Cardiac; Bone)	- Drug delivery - Antimicrobial - Mechanical Heart Valves - T.E. (Cardiac; Bone; Cartilage; Neuronal; Muscle) - Skin wound healing

T.E. – Tissue engineering

2.3.1.1 Biocompatibility

GBMs interaction with biological systems is an issue of high importance for its application, not only as a biomaterial but in all other materials fields since their contact with biological systems (e.g. environment) will be inherent (Fig. 2.9). Despite several studies and reviews focusing on this issue, the biological response mechanisms to GBMs are not fully understood, probably due to their recent appearance [63-67].

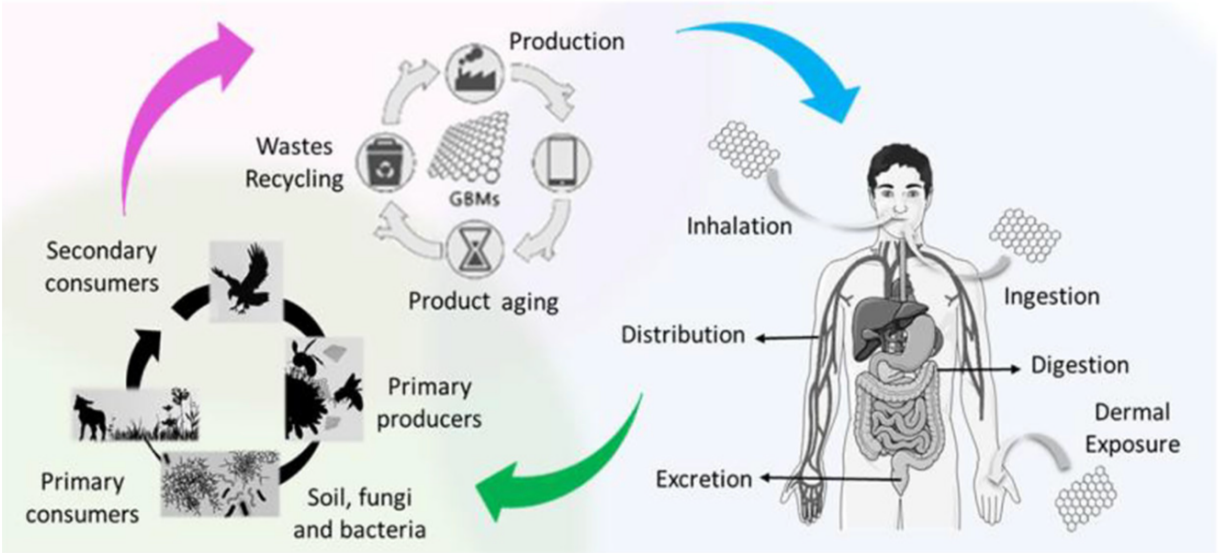

Figure 2.9 – Graphene-Based Materials interaction with biological systems. Reprinted with permission from ref. [63] copyright 2019, American Chemical Society.

GBMs interaction with biological systems depends on their oxidation degree, number of graphene layers and lateral dimension. Regarding biodegradation of GBMs, Kotchey *et al.* [68] showed that GO is susceptible to degradation in the presence of low amounts of horseradish peroxidase, while reduced GO is not affected. Moreover, thinner oxidized (single layer) GBMs are completely degraded by myeloperoxidase upon 24 h, while thicker GBMs remain almost intact [68] (Fig. 2.10). GO with different lateral sizes also exhibit a high degradation potential by neutrophils, being shown that degradation products are non-genotoxic to human lung cells [69]. Recently, D. Li *et al.* [70] showed that GBMs can be degraded in blood after 14 days, being the degradation process highly dependent on their oxidization degree. Active substances in blood plasma (e.g., •OH and •O2) attack carbon atoms connected with oxygen-containing groups in their basal planes, leading to break of C-C and C=C bonds, forming holey sheets and aromatic hydrocarbons, which exhibit higher biocompatibility than pristine material (Fig. 2.10) [70]. Thus, for GBMs containing low oxygen amounts, this biotransformation is slower due to the lower number of active sites. Degradation of oxidized nano-FLG was also reported *in vivo*. These materials, which tend to agglomerate in lungs, liver, kidneys and spleen, exhibit some signals of degradation in the edges of its structure upon 90 days [71].

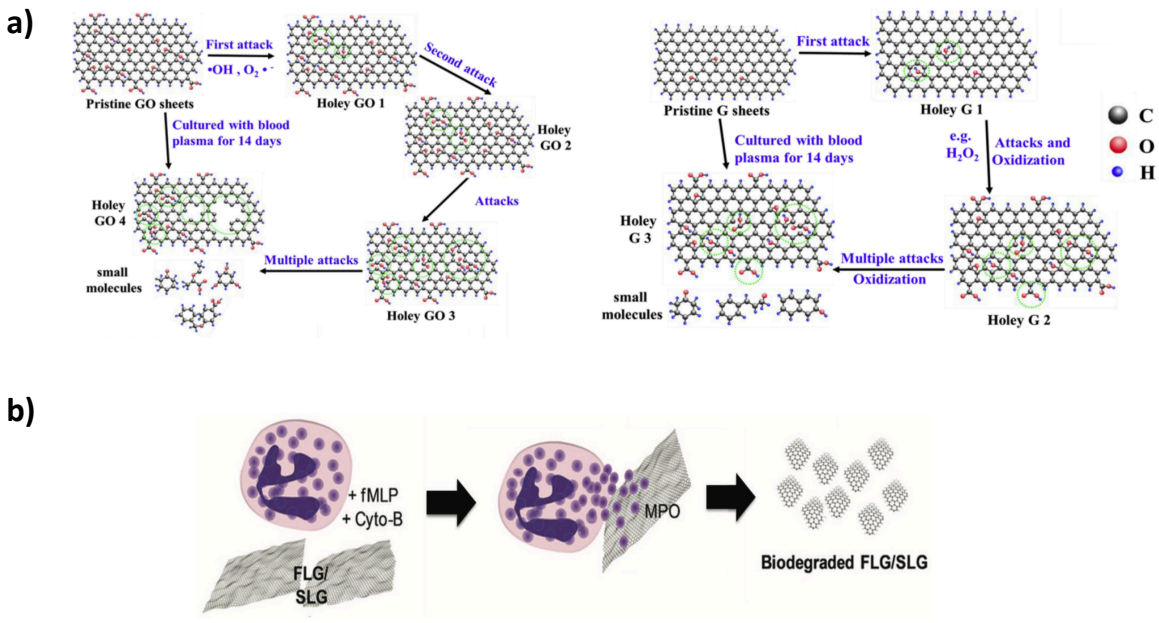

Figure 2.10 – Biodegradation mechanism of Graphene-Based Materials. Proposed mechanism of GBMs biodegradation by blood plasma (a) and (b) myeloperoxidase. Adapted with permission from ref. [70] (a), copyright 2019, Elsevier and ref [68] (b), copyright 2011, American Chemical Society

Regarding biodistribution of GBMs *in vivo*, Liu *et al.* showed that for a concentration of 1.0 mg/kg, small GO (148-160 nm) particles tend to remain longer in circulation than large ones (556-780 nm) [72]. They also observed that the small GO tends to accumulate mainly in the liver (slightly decreasing at 180 min) with a lower amount in spleen and lungs, while the larger GO was mostly present in lungs. When the amount of injected GO, is increased 10 times, small GO tends to accumulate in lungs instead of liver [72]. Radiolabelled GO, ^{188}Re–GO, with lateral size ranging 10–800 nm, exhibits long blood circulation time (half-time 5.3 ± 1.2 h) after intravenous administrated in mice (1 mg/kg) and low uptake by the reticuloendothelial system [73]. No pathological changes were observed in examined organs when mice were exposed to 1 mg/kg body weight of GO for 14 days [73].

Strategies to promote GBMs degradation and to tune the biodistribution and accumulation have been explored namely by their functionalization with native subtracts of HRP, cathecol or cumarin, which promote their degradation [63].

Besides the study of GBMs biodegradation, their cytotoxicity towards different cell lines, has been addressed. Although, the inconsistency between some studies, it is established that cytotoxicity of GBMs depends on doses, exposure time, oxidation degree, lateral size, and also of the used cell type [64, 74-76]. Smaller and more oxidized GBMs particles exhibit a better biocompatibility *in vitro* towards HFF-1 cells [64, 77]. Cheng *et al.* showed that HUVECs viability in the presence of 20 μg/mL of GO and rGO is around 95%, decreasing to 60% for a concentration of 100 μg/mL [78]. Due to GBMs capacity to interact with cell membranes as well as their capacity to be internalized, they can induce different mechanisms within cells. Regarding internalization capacity, oxidized particles are more internalized in the cell than non-oxidized GBMs, which tend to accumulate in cellular plasma membrane. The accumulation of graphene nanosheets on cellular plasma membrane may result in the blocking of ion channels and nutrient uptakes, leading to the disturbance of the balance of various intracellular events, including the intracellular redox equilibrium [79-81]. Eventually, this may elicit considerable intracellular oxidative stress, resulting in programmed cell death. Thus, smaller and more oxidized GBMs seem to be more cytocompatible than non-oxidized and larger particles [77].

Interaction of GBMs with blood has also been addressed [75, 82-85], namely, with proteins and blood cells. Regarding protein adsorption, it has been shown that hydrophobic GBMs have a higher capacity to adsorb albumin at their surfaces than hydrophilic ones. This could be related to hydrophobic interactions via π – π stacking of albumin aromatic aminoamides and graphene sheets [39]. However, the direct comparison of the protein binding capacity of G/rGO and GO is challenging, since rGO exhibits poor stability in aqueous solutions, and its surface composition highly depends on the reduction method [83]. However, GO adsorbs better fibrinogen than albumin, while non-oxidized GBMs adsorbs albumin in higher amounts [83]. For the same GO concentration, larger particles (1 μm) exhibit a higher capacity to adsorb

albumin, a small protein, in their surface than smaller particles (100 nm). An opposite effect is observed for fibrinogen, a large protein [86].

For GBMs interaction with red blood cells (RBCs), contradictory results have been described in the literature. Pinto *et al.* reported a low hemolytic effect (<3%) of MLG and MLGox with a lateral size of <2 μm or 5 μm for a concentration of up to 500 μg/mL [77]. In contrast, an hemolytic percentage of 96% was shown by Feng *et al.* [87], for GO with an average lateral size of 0.5 μm, in the same concentration. A higher hemolytic potential is associated to smaller particles, with lateral size lower than a few nm [88-90]. Hydrophobic interaction between GO and RBCs membrane as well as glycocalyx and hydroxyl/carboxyl groups of GO [87] have been pointed as one of the reasons for the hemolytic potential of GO Functionalization of GO with NH2 groups (GO-NH2) reduces the hemolytic potential of GO through the decrease of its interaction with phosphatidylcholine [85, 88]. Moreover, interaction of GO with phosphatidylcholine of cell membrane could also explain the high hemolysis. Proteins adsorbed on GBMs surface, such as bovine serum albumin (BSA), seem to have a protective effect regarding their hemolytic potential [91-94].

Regarding platelets and coagulation, *in vitro* results show a thrombogenic effect for concentration of GO higher than 500 μg/mL [87, 90]. GO also shows a thrombogenic effect in *in vivo* studies for concentrations around 250 mg/kg body weight [95].

Some studies report that GO activates as well the complement system, although the reduction of oxygen content and the pre-coating with blood corona proteins might prevent this effect [96]. This activation leads to expression of pro inflammatory cytokines, in a size dependent way, being more activated for smaller GO (< 1 μm) particles than for larger ones (> 10 μm) [97]. Macrophages, one of the major players in inflammatory response, show high potential to phagocyte GO, depending on its lateral size. Larger GO sheets can align with the cellular membrane inducing the M1 macrophage polarization [98, 99], and its apoptosis is promoted in the presence of GO concentrations of 50 μg/mL [90, 100-102].

In summary, biocompatibility of GBMs colloids depends on their concentration, oxidation degree, lateral size and dispersibility. For lower amounts of GBMs, the effects in inflammation, cells and blood components is diminished. Oxidized and smaller GBMs are biodegraded in the body, which contributes for their higher biocompatibility.

As described above, depending on GBMs application they could be in colloid dispersion, free-standing, surface coating or composite. In particular, GBMs-integrated surfaces exhibit different features of GBMs colloids, since they seem to promote cell attachment and proliferation as shown for GO coatings on titanium [103] or nitinol [104], as well as PCL/GO [105], collagen/GO [106], PU/GO [107] and tropoelastin/GO [108] composites. In these last three studies, the presence of GO promoted cell proliferation. GBMs can influence cell

attachment, growth, proliferation and phenotypes due to their high capacity to recruit and adsorb medium components such as nutrients and cell growth and differentiation factors on their surface [109]. Moreover, GBMs showed potential to support growth, proliferation and differentiation of mesenchymal, neural or induced pluripotent stem cells into different tissue lineages, through tuning of different surface properties of graphene nanomaterials, as review by Huang *et al.* [109]. These features potentiate their use in design of scaffolds for tissue engineering approaches.

2.3.1.2 Antimicrobial properties

Antimicrobial properties of GBMs have been described several times in literature [51, 105, 110-113]. There are two main events caused by GBMs which lead to antibacterial effect: oxidative stress induction and membrane damaging. However, their efficiency depends on the used GBMs and also if they are in colloidal, exposed to surface or incorporated in a composite form. Regarding colloids, the antibacterial activity of GBM has been described to be higher for GO than for rGO [114, 115]. Differences are explained by different state of dispersion and amount of oxygen-containing functional groups, which impact on both membrane and oxidative stress. Large GO nanosheets, which can cover bacteria preventing proliferation, have been pointed out as having stronger antibacterial effect. By contrast, some results indicate that small GO sheets have higher oxidative and antibacterial capacity [116, 117]. There are three different molecular initiating events caused by GBMs which lead to antibacterial effects: redox reaction with biomolecules, mechanical destruction of membranes and catalysis of extracellular metabolites (Fig. 2.11).

In 2D films particles lateral size and oxidation degree seem to have a crucial impact on the antimicrobial activity (Fig. 2.11). Films containing smaller GO particles have a stronger antimicrobial effect than films containing large particles and/or rGO [51, 118], and these smaller GO particles seem to induce higher oxidative stress in bacteria. Besides surface chemistry, the roughness of GBM free-standing 2D films also influences their antimicrobial properties. Rough surfaces that expose the sharp edges were showed to promote bacteria killing while smooth surface promoted bacterial adhesion [51, 119]. Possible piercing of the bacterial cell wall and membrane by exposure of sharp edges has been pointed as the main mechanism for this phenomena, although some authors defend a low probability of it occurring [119, 120] (Fig. 2.11). The covalent link of GO to a collagen scaffold, followed by its reduction, showed to decrease *Escherichia coli*, *Staphylococcus aureus* and *Streptococcus pyogenes* adhesion to surface [121].

The antimicrobial performance of GBM containing composites depends not only on the incorporated GBMs and their amount but also of the adopted composite production technique. Production techniques which promote GBM exposure at composites surface generate

composites with higher antimicrobial properties [51]. Due to the poor characterization of incorporated GBMs and resulting composites, comparisons between different studies are difficult. However, incorporation of GO to create polymeric composites such as CS/GO [122], CS/polyvinylpyrrolidone/GO [123], PLA/PU/GO [124] and Agar/GO [125] hydrogel showed to promote an antimicrobial effect between 50-100%, in different bacteria species.

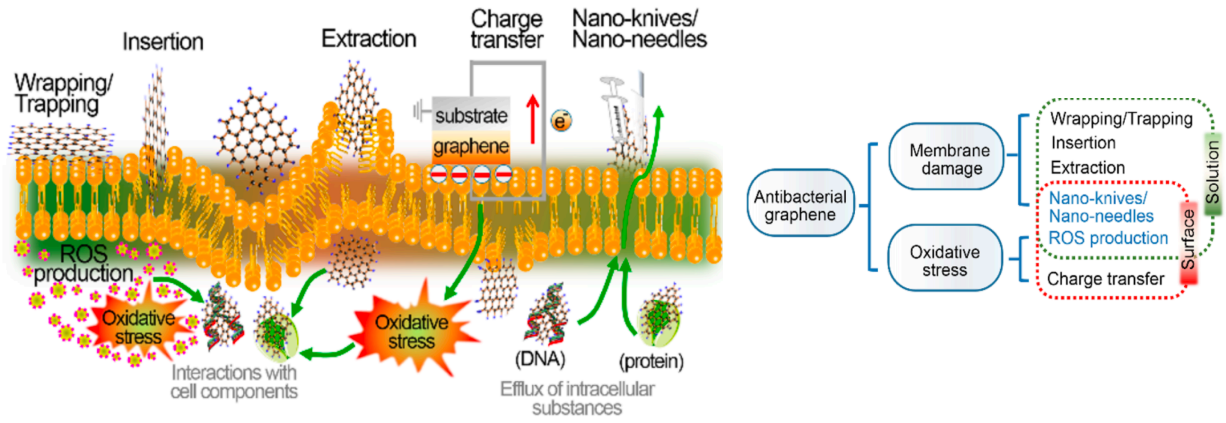

Figure 2.11 – Antimicrobial mechanisms of GBMs colloids and surfaces. Adapted with permission from ref. [126] copyright 2016, American Chemical Society.

2.3.2 Graphene Based Materials in Mechanical Reinforcement

As the strongest material in the world, graphene and GBMs have been recurrently used in the mechanical reinforcement of polymers. In most of the studies, GBMs are incorporated in polymeric matrices, as composites, being GBMs coatings much less explored. This fact could be explained by an expected more effective mechanical action of GBMs when included within the polymer matrices than as a coating. GBMs were proposed as a filler of several polymers such as epoxy, polyurethanes, polypropylene, PTFE, among others, showing a consistent improvement for most of the polymers in 15-250% in ultimate tensile strength (tensile resistance) and Young's Modulus (stiffness), under tensile stress as reviewed by *Papageorgiou et al.* [61]. The performance of GBMs in the mechanical reinforcement of polymers depends on its intrinsic features, such as lateral size, thickness and oxidation degree, interaction with base polymer and production technique. Regarding production techniques, solution mixing or *in situ* polymerization techniques allow a more homogenous dispersion of GBMs in polymer matrix then melt-blending. Besides the production technique, GBMs can be modified to covalently link to polymer chains to promote a stronger interaction.

a) Hydrogels reinforced with GBMs

Due to the high-water content in their composition, hydrogels are fragile materials with a limited application in several load-bearing fields. Incorporation of GBMs in hydrogels network plays an important role in decreasing crack propagation and delaying the hydrogels' failure, which consequently improves their mechanical properties. This effect seems to be promoted by a strong interaction between GBMs and the polymeric network, which can be covalent or non-covalent. Regarding the covalent interaction, it requires the chemical modification of GBMs in order to stablish a covalent bond with the polymeric network. In non-covalent interactions, GBMs can stablish hydrophilic interactions, such as hydrogen bonds, or hydrophobic such as π-π interactions. Moreover, hydration state of hydrogels during the mechanical measurements also plays an important role in the achieved improvements, since GO incorporation in the hydrogel network seems to lead higher improvements in dry state than in swollen state [127, 128]. In general, non-covalent incorporation of GBMs in polymeric networks leads to average increase in neat properties of hydrogel around 3 x for Young's Modulus (YM) and ultimate tensile strength (UTS) (Table 2.3). This has been reported for several hydrogels such as cellulose [129, 130], chitosan [131], polyacrylamide (PAM) [132-136], poly(acrylic acid) (PAA) [137-139], poly(vinyl-alcohol) (PVA) [127, 140-148], tannins [149], silk [150] and starch/polyacrylamide [151] (Table 2.3). The highest increase was recently reported by Wang, Y. T. *et al.* achieved for GO 8% (w/w) incorporation in PAA [138], increasing 10x the UTS and 8.5x the YM of neat hydrogel. When GO is covalently associated to the polymer network, it is possible to obtain even more remarkable improvements, such as in the case of PAM/GOP hydrogels, where the UTS is 24x higher than neat hydrogel. Besides this, GBMs incorporation also increase the elasticity capacity of some hydrogels. This could be explained by the interaction between the filler and polymeric network (Table 2.3).

Increases in compressive strength are also reported, namely upon incorporation of GO in chitosan (163%) [152], poly(sulfobetaine methacrylate) (400%) [153], double networking hydrogels based on κ-carrageenan, PAM [154] and poly(N-isopropylacrylamide) (400%) [155].

Table 2.3 – Tensile properties and swelling capacity of hydrogels containing GBMs

	Hydrogel	GBMs concentration	↑ UTS	UTS (MPa)	↑ YM	YM (MPa)	↑ Elongation at break	Elongation at Break	↑ Swelling capacity	Swelling capacity	Ref.
Physically incorporated	cellulose/G	0.5% (w/w)	1.5	0.60	2.2	4500	0	27%	-	-	[129]
	cellulose/G	0.3% (w/w)	1.9	1.75	4.0	38	-2	10%	-	-	[130]
	chitosan/rGO	3% (w/w)	1.3	0.4	N.A.	N.A.	0	52%	-4.7	75%	[131]
	Gelatin/PAM/GO	0.5 (mg/mL)	1.3	0.32	2.7	175	-1.7	45000%	-2.7	15000	[156]
	GO-g-PAA/PAM rGO-g-PAA/PAM	1.2% (w/w)	4.0	0.40	2.0	1	1.1	950%	-1.3	1500%	[157]
	PAA/gelatin/GO	0.3% (w/w)	1.7	0.25	N.A.	N.A.	1.3	55%	N.A.	N.A.	[137]
	PAA/gelatin/GO	0.5% (w/w)	3.3	0.25	N.A.	N.A.	2	60%	N.A.	N.A.	[139]
	PAA/GO	8 % (w/w)	10.0	0.75	8.5	1	2.9	2500%	-1.8	60%	[158]
	PAM/GO	0.3% (w/w)	4.0	0.10	2.0	0.02	1.2	1200%	N.A.	N.A.	[154]
	PAM/G	0.1% (w/w)	2.5	0.10	0.0	0	1.2	1050%	N.A.	N.A.	[136]
	PAM/GO	3 (mg/mL)	2.0	0.10	N.A.	N.A.	2.2	130000%	N.A.	N.A.	[159]
	p(2-hydroxyethyl acrylate)/GO	1% (w/w)	5.8	0.08	3.1	2	2.1	40%	N.A.	N.A.	[128]
	p(AMPS-co-Aam/GO	1% (w/w)	4.5	0.90	N.A.	N.A.	2.5	300%	N.A.	N.A.	[160]
	p(AMPS-coAAm)/GO	1 (mg/mL)	5.0	0.10	N.A.	N.A.	2.4	300%	N.A..	N.A.	[138]
	p(AMPS)/poly(AA-AANa)/GO	0.5 % (w/w)	1.4	0.86	3.8	1	2.1	334%	-2.0	90%	[161]
	p(N-isopropylacrylamide)/GO	0.1% (w/w)	2.5	0.10	4.0	0	0	800%	N.A.	N.A.	[161]
	polyacrylamide/aG	0.1% (w/w)	2.0	0.10	0.0	0	0.1	1100%	N.A.	N.A.	[136]
	PU/GO	8 (w/w)	2.2	7.35	3.4	3.5	1.2	936%	0	57%	[162]
	PVA/G	10% (w/w)	4.7	20.90	10.5	115	1.6	115%	N.A.	N.A.	[141]
	PVA/GO	0.1% (w/w)	2.4	0.60	N.A.	N.A.	1.6	547%	0	94%	[140]
	PVA/GO	0.8% (w/w)	2.5	N.A.	N.A.	N.A.	1.6	160%	0	80%	[142]
	PVA/GO	8 (mg/mL)	3.0	1.85	N.A.	N.A.	N.A.	425%	N.A.	97%	[143]
	PVA/GO	3 (mg/mL)	1.5	1.50	N.A.	N.A.	2.5	750%	0	80%	[144]
	PVA/GO	0.2 % (w/w)	2.3	1.40	N.A.	N.A.	1.5	380%	1.1	80%	[145]
	PVA/GO	0.5% (w/w)	N.A.	N.A.	0.2	1	N.A.	N.A.	N.A..	75%	[127]
	PVA/GO ɣ-ray	1% (w/w)	1.8	60.00	1.6	1200	-2.5	6%	0	8%	[146]
	PVA/GO-PEG	1.5% (w/w)	2.7	4.20	N.A.	N.A.	1.4	250%		N.A.	[147]
	PVA/GO/cellulose	1% (w/w)	1.4	N.A.	N.A.	N.A.	2.3	238%	1.4	250%	[148]
	Silk/GO	0.5% (w/w)	1.3	4.50	N.A.	N.A.	-3.7	1100%	N.A.	N.A.	[150]
	Sodium Acrylate/PAM/GO	5% (w/w)	1.6	0.20	1.5	0	-1.3	600%	-1.9	800	[163]
	Tannin/GO	0.5 (mg/mL)	2.0	0.20	N.A.	N.A.	1.5	3100%	N.A.	N.A.	[149]
Covalently linked	PAMPS/GO	0.2% (w/w)	1.6	40.00	1.6	202	1.5	43%	1.4	107	[164]
	PAM/GOP	3 (mg/mL)	24.0	1.20	N.A.	N.A.	8.9	5300%	N.A.	N.A.	[159]
	PDMA-stat-PAPBA/PGMA coated rGO-dopamine	0.5 % (w/w)	5.5	0.00	N.A.	N.A.	1.6	825%	N.A.	N.A.	[165]
	PVA/GO Modified with shift base	3 (mg/mL)	2.0	2.00	N.A.	N.A.	2.7	80000%	0	80	[144]

AAm – Acrylamide, N.A. – not available, PAA – Polyacrylic acid, poly(AMPS) – poly(2-acrylamido-2-methylpropane sulfonic acid), PAM – polyacrylamide, PDMA-stat-PAPBA - poly(N,N-dimethylacrylmide-stat-3-acrylamidophenylboronic acid), poly(AA-AANa) – poly(acrylic acid–sodium acrylate), PGMA - poly(glycerol monomethacrylate), PVA – Polyvynil alcohol

Besides the increase in mechanical properties, GO incorporation in hydrogels seems to interfere with their swelling capacity. In some cases, it increases the swelling capacity, such as for boron crosslinked GO/PVA [140], while a decrease was reported for hydroxyethyl cellulose/GO [166] and GO/PVA hydrogels [167]. This effect seems to be dependent on the amount of GO incorporated in the hydrogel. In lower amounts, GO promotes a faster diffusion of water molecules due to the presence of hydrophilic groups on its surface. However, for high amounts, hydrogen bonds possible form between the polymer, and therefore physical concerns due to GO presence decrease the swelling capacity.

b) Extracellular matrices-based materials

Development of GBMs composites comprising extracellular matrix (ECM) polymers, namely collagen, elastin and ECM-derived materials, to improve their mechanical properties has received increasing attention in the biomaterials field, especially in the last two years[168-183]. Covalent crosslinking of GO (800 μg/mL) to collagen scaffolds followed by GO reduction show to highly increase their stiffness under tensile stress in around 800%. rGO or GO adsorption to acellular dermal matrix show an increase of 35% or 10% in tensile resistance and 44% and 111% in stiffness [172], respectively. Incorporation of GO in collagen aerogels or scaffolds show an increase in compressive resistance of around 150 % [171] and increase in compressive stiffness 100%, respectively [176].

2.4 References

[1] Biochemistry, 7th Edition edition ed., W.H. Freeman & Company.

[2] S.N. Rodrigues, I.C. Goncalves, M.C. Martins, M.A. Barbosa, B.D. Ratner, Fibrinogen adsorption, platelet adhesion and activation on mixed hydroxyl-/methyl-terminated self-assembled monolayers, Biomaterials 27(31) (2006) 5357-67.

[3] F.B. Insights, Healthcare | Cardiovascular Stents Market, 2019. https://www.fortunebusinessinsights.com/industry-reports/cardiovascular-stents-market-100061.

[4] M.S. Future, Cardiac Valve Market Research Report - Global Forecast till 2025, 2019. https://www.marketresearchfuture.com/reports/cardiac-valve-market-560.

[5] P.T. Community, Global Cardiovascular Catheters Industry, 2019. https://www.ptcommunity.com/wire/global-cardiovascular-catheters-industry.

[6] G.V. Research, Vascular Graft Market Size, Share, Global Industry Report, 2019-2026, 2019. https://www.grandviewresearch.com/industry-analysis/vascular-graft-market.

[7] G.V. Research, Ventricular Assist Device Market Size, Industry Report, 2019-2025, 2019. https://www.grandviewresearch.com/industry-analysis/ventricular-assist-devices-market.

[8] A.M. Research, Global Vascular Guidewires Market Expected to Reach $1,336 Million by 2025, 2017. https://www.alliedmarketresearch.com/press-release/vascular-guidewires-market.html.

[9] G.V. Research, Extracorporeal Membrane Oxygenation (ECMO) Machine Market Report, 2026, 2019. https://www.grandviewresearch.com/industry-analysis/extracorporeal-membrane-oxygenation-ecmo-market.

[10] I.H. Jaffer, J.I. Weitz, The blood compatibility challenge. Part 1: Blood-contacting medical devices: The scope of the problem, Acta Biomater 94 (2019) 2-10.

[11] M. Gorbet, C. Sperling, M.F. Maitz, C.A. Siedlecki, C. Werner, M.V. Sefton, The blood compatibility challenge. Part 3: Material associated activation of blood cascades and cells, Acta Biomater 94 (2019) 25-32.

[12] D.G. Seifu, A. Purnama, K. Mequanint, D. Mantovani, Small-diameter vascular tissue engineering, Nat Rev Cardiol 10(7) (2013) 410-21.

[13] J.B. Pietzsch, B.P. Geisler, M.R. Jaff, T. Zeller, M. Brodmann, Economic Analysis of Endovascular Interventions for The Treatment of Femoropopliteal Peripheral Artery Disease in Austria, Value Health 19(7) (2016) A690-A690.

[14] W.C. Johnson, Preliminary experience with expanded polytetrafluoroethylene grafts, Surgery 85(2) (1979) 123-8.

[15] A. Edwards, R.J. Carson, S. Bowald, W.C. Quist, Development of a microporous compliant small bore vascular graft, J Biomater Appl 10(2) (1995) 171-87.

[16] B. Nottelet, E. Pektok, D. Mandracchia, J.C. Tille, B. Walpoth, R. Gurny, M. Moller, Factorial design optimization and in vivo feasibility of poly(epsilon-caprolactone)-micro- and nanofiber-based small diameter vascular grafts, J Biomed Mater Res A 89(4) (2009) 865-75.
[17] M.F. Maitz, M.C.L. Martins, N. Grabow, C. Matschegewski, N. Huang, E.L. Chaikof, M.A. Barbosa, C. Werner, C. Sperling, The blood compatibility challenge. Part 4: Surface modification for hemocompatible materials: Passive and active approaches to guide blood-material interactions, Acta Biomater 94 (2019) 33-43.
[18] F. Surman, T. Riedel, M. Bruns, N.Y. Kostina, Z. Sedlakova, C. Rodriguez-Emmenegger, Polymer brushes interfacing blood as a route toward high performance blood contacting devices, Macromol Biosci 15(5) (2015) 636-46.
[19] L. Indolfi, F. Causa, P.A. Netti, Coating process and early stage adhesion evaluation of poly(2-hydroxy-ethyl-methacrylate) hydrogel coating of 316L steel surface for stent applications, Journal of materials science. Materials in medicine 20(7) (2009) 1541-51.
[20] B. Chen, J. Chen, L. Yang, G. Zhao, G. Ding, Electrodepositing salicylate modified PHEMA on stainless steel surface for hemocompatibility, Surf Eng 30(10) (2014) 768-775.
[21] A. Badea, J.M. McCracken, E.G. Tillmaand, M.E. Kandel, A.W. Oraham, M.B. Mevis, S.S. Rubakhin, G. Popescu, J.V. Sweedler, R.G. Nuzzo, 3D-Printed pHEMA Materials for Topographical and Biochemical Modulation of Dorsal Root Ganglion Cell Response, Acs Appl Mater Inter 9(36) (2017) 30318-30328.
[22] C. He, M. Wang, X. Cai, X. Huang, L. Li, H. Zhu, J. Shen, J. Yuan, Chemically induced graft copolymerization of 2-hydroxyethyl methacrylate onto polyurethane surface for improving blood compatibility, Appl Surf Sci 258(2) (2011) 755-760.
[23] X. Liu, L. Yuan, D. Li, Z. Tang, Y. Wang, G. Chen, H. Chen, J.L. Brash, Blood compatible materials: state of the art, J Mater Chem B 2(35) (2014) 5718-5738.
[24] S. Chen, L. Li, C. Zhao, J. Zheng, Surface hydration: Principles and applications toward low-fouling/nonfouling biomaterials, Polymer 51(23) (2010) 5283-5293.
[25] V. Jokinen, E. Kankuri, S. Hoshian, S. Franssila, R.H.A. Ras, Superhydrophobic Blood-Repellent Surfaces, Adv Mater 30(24) (2018) e1705104.
[26] M. Paven, P. Papadopoulos, S. Schottler, X. Deng, V. Mailander, D. Vollmer, H.J. Butt, Super liquid-repellent gas membranes for carbon dioxide capture and heart-lung machines, Nat Commun 4 (2013) 2512.
[27] S. Movafaghi, V. Leszczak, W. Wang, J.A. Sorkin, L.P. Dasi, K.C. Popat, A.K. Kota, Response to "Correspondence Concerning Hemocompatibility of Superhemophobic Titania Surfaces", Adv Healthc Mater 6(17) (2017).
[28] S. Moradi, N. Hadjesfandiari, S.F. Toosi, J.N. Kizhakkedathu, S.G. Hatzikiriakos, Effect of Extreme Wettability on Platelet Adhesion on Metallic Implants: From Superhydrophilicity to Superhydrophobicity, Acs Appl Mater Inter 8(27) (2016) 17631-41.

[29] E. Gray, J. Hogwood, B. Mulloy, The anticoagulant and antithrombotic mechanisms of heparin, Handb Exp Pharmacol (207) (2012) 43-61.
[30] K.S. Lavery, C. Rhodes, A. McGraw, M.J. Eppihimer, Anti-thrombotic technologies for medical devices, Advanced drug delivery reviews 112 (2017) 2-11.
[31] K. Ishihara, Y. Liu, Y. Inoue, Enhancing polyurethane blood compatibility, in: S.L. Cooper, J. Guan (Eds.), Advances in Polyurethane Biomaterials, Woodhead Publishing2016, pp. 319-348.
[32] C. Hou, Q. Yuan, D. Huo, S. Zheng, D. Zhan, Investigation on clotting and hemolysis characteristics of heparin-immobilized polyether sulfones biomembrane, J Biomed Mater Res A 85(3) (2008) 847-52.
[33] L. Wang, Y. Cai, Y. Jing, B. Zhu, L. Zhu, Y. Xu, Route to hemocompatible polyethersulfone membranes via surface aminolysis and heparinization, J Colloid Interface Sci 422 (2014) 38-44.
[34] T. Sharkawi, V. Darcos, M. Vert, Poly(DL-lactic acid) film surface modification with heparin for improving hemocompatibility of blood-contacting bioresorbable devices, J Biomed Mater Res A 98(1) (2011) 80-7.
[35] Z. Yang, J. Wang, R. Luo, M.F. Maitz, F. Jing, H. Sun, N. Huang, The covalent immobilization of heparin to pulsed-plasma polymeric allylamine films on 316L stainless steel and the resulting effects on hemocompatibility, Biomaterials 31(8) (2010) 2072-83.
[36] R. Larm O Fau - Larsson, P. Larsson R Fau - Olsson, P. Olsson, A new non-thrombogenic surface prepared by selective covalent binding of heparin via a modified reducing terminal residue, (0090-5488 (Print)).
[37] G. Li, Y. Zhang F Fau - Liao, P. Liao Y Fau - Yang, N. Yang P Fau - Huang, N. Huang, Coimmobilization of heparin/fibronectin mixture on titanium surfaces and their blood compatibility, (1873-4367 (Electronic)).
[38] G. Li, P. Yang, Y. Liao, N. Huang, Tailoring of the titanium surface by immobilization of heparin/fibronectin complexes for improving blood compatibility and endothelialization: an in vitro study, Biomacromolecules 12(4) (2011) 1155-68.
[39] D.F. Williams, Challenges With the Development of Biomaterials for Sustainable Tissue Engineering, Front Bioeng Biotechnol 7 (2019) 127.
[40] D. Radke, W. Jia, D. Sharma, K. Fena, G. Wang, J. Goldman, F. Zhao, Tissue Engineering at the Blood-Contacting Surface: A Review of Challenges and Strategies in Vascular Graft Development, Adv Healthc Mater 7(15) (2018) e1701461.
[41] M.A. Hiob, S. She, L.D. Muiznieks, A.S. Weiss, Biomaterials and Modifications in the Development of Small-Diameter Vascular Grafts, Acs Biomater Sci Eng 3(5) (2016) 712-723.

[42] S. de Valence, J.C. Tille, D. Mugnai, W. Mrowczynski, R. Gurny, M. Moller, B.H. Walpoth, Long term performance of polycaprolactone vascular grafts in a rat abdominal aorta replacement model, Biomaterials 33(1) (2012) 38-47.
[43] F. Boccafoschi, J. Habermehl, S. Vesentini, D. Mantovani, Biological performances of collagen-based scaffolds for vascular tissue engineering, Biomaterials 26(35) (2005) 7410-7.
[44] H. Bergmeister, F. Bastian, C. Plass, E. Rieder, U. Losert, G. Weigel, 563: In vivo remodeling of decellularized xenogeneic arteries: Impact of heparin-crosslinking on graft stability, J Heart Lung Transp 26(2) (2007) S262-S262.
[45] S.G. Wise, M.J. Byrom, A. Waterhouse, P.G. Bannon, A.S. Weiss, M.K.C. Ng, Corrigendum to “A multilayered synthetic human elastin/polycaprolactone hybrid vascular graft with tailored mechanical properties” [Acta Biomater. 7 (2011) 295–303], Acta Biomater 7(3) (2011) 1429-1429.
[46] M.J. McClure, S.A. Sell, D.G. Simpson, B.H. Walpoth, G.L. Bowlin, A Three Layered Electrospun Matrix to Mimic Native Arterial Architecture Using Polycaprolactone, Elastin, and Collagen: A Preliminary Study, Proceedings of the Asme Summer Bioengineering Conference, 2010 (2010) 513-514.
[47] M. Lovett, G. Eng, J.A. Kluge, C. Cannizzaro, G. Vunjak-Novakovic, D.L. Kaplan, Tubular silk scaffolds for small diameter vascular grafts, Organogenesis 6(4) (2010) 217-24.
[48] S. Enomoto, M. Sumi, K. Kajimoto, Y. Nakazawa, R. Takahashi, C. Takabayashi, T. Asakura, M. Sata, Long-term patency of small-diameter vascular graft made from fibroin, a silk-based biodegradable material, J Vasc Surg 51(1) (2010) 155-64.
[49] S. Pashneh-Tala, S. MacNeil, F. Claeyssens, The Tissue-Engineered Vascular Graft-Past, Present, and Future, Tissue engineering. Part B, Reviews 22(1) (2016) 68-100.
[50] C.H. Lin, K. Hsia, H. Ma, H. Lee, J.H. Lu, In Vivo Performance of Decellularized Vascular Grafts: A Review Article, International journal of molecular sciences 19(7) (2018).
[51] P.C. Henriques, I. Borges, A.M. Pinto, F.D. Magalhães, I.C. Gonçalves, Fabrication and antimicrobial performance of surfaces integrating graphene-based materials, Carbon 132 (2018) 709-732.
[52] C. Lee, X. Wei, J.W. Kysar, J. Hone, Measurement of the elastic properties and intrinsic strength of monolayer graphene, Science 321(5887) (2008) 385-8.
[53] W. Gao, L.B. Alemany, L.J. Ci, P.M. Ajayan, New insights into the structure and reduction of graphite oxide, Nat Chem 1(5) (2009) 403-408.
[54] A.D. Haubold, R.B. More, J.C. Bokros, Carbons, in: W. Murphy, J. Black, G. Hastings (Eds.), Handbook of biomaterial properties2016.
[55] F. Gong, H. Li, W. Wang, D. Xia, Q. Liu, D. Papavassiliou, Z. Xu, Recent Advances in Graphene-Based Free-Standing Films for Thermal Management: Synthesis, Properties, and Applications, Coatings 8(2) (2018).

[56] H.M. Duong, Z. Fan, S.T. Nguyen, Graphene/Carbon Nanotube Aerogels, in: K.D. Sattler (Ed.), Carbon Nanomaterials Source Book2016, pp. 563-579.
[57] S. Priyadarsini, S. Mohanty, S. Mukherjee, S. Basu, M. Mishra, Graphene and graphene oxide as nanomaterials for medicine and biology application, J Nanostructure Chem 8(2) (2018) 123-137.
[58] K. Tadyszak, J.K. Wychowaniec, J. Litowczenko, Biomedical Applications of Graphene-Based Structures, Nanomaterials-Basel 8(11) (2018).
[59] K. Ghosal, K. Sarkar, Biomedical Applications of Graphene Nanomaterials and Beyond, Acs Biomater Sci Eng 4(8) (2018) 2653-2703.
[60] Y.C. Shin, S.J. Song, S.W. Hong, S.J. Jeong, W. Chrzanowski, J.C. Lee, D.W. Han, Multifaceted Biomedical Applications of Functional Graphene Nanomaterials to Coated Substrates, Patterned Arrays and Hybrid Scaffolds, Nanomaterials (Basel) 7(11) (2017).
[61] D.G. Papageorgiou, I.A. Kinloch, R.J. Young, Mechanical properties of graphene and graphene-based nanocomposites, Prog Mater Sci 90 (2017) 75-127.
[62] V.B. Mohan, K.-t. Lau, D. Hui, D. Bhattacharyya, Graphene-based materials and their composites: A review on production, applications and product limitations, Compos Part B: Eng 142 (2018) 200-220.
[63] B. Fadeel, C. Bussy, S. Merino, E. Vazquez, E. Flahaut, F. Mouchet, L. Evariste, L. Gauthier, A.J. Koivisto, U. Vogel, C. Martin, L.G. Delogu, T. Buerki-Thurnherr, P. Wick, D. Beloin-Saint-Pierre, R. Hischier, M. Pelin, F. Candotto Carniel, M. Tretiach, F. Cesca, F. Benfenati, D. Scaini, L. Ballerini, K. Kostarelos, M. Prato, A. Bianco, Safety Assessment of Graphene-Based Materials: Focus on Human Health and the Environment, ACS Nano 12(11) (2018) 10582-10620.
[64] A.M. Pinto, I.C. Goncalves, F.D. Magalhaes, Graphene-based materials biocompatibility: a review, Colloids and surfaces. B, Biointerfaces 111 (2013) 188-202.
[65] A. Bianco, Graphene: safe or toxic? The two faces of the medal, Angew Chem Int Ed Engl 52(19) (2013) 4986-97.
[66] G. Lalwani, M. D'Agati, A.M. Khan, B. Sitharaman, Toxicology of graphene-based nanomaterials, Advanced drug delivery reviews 105(Pt B) (2016) 109-144.
[67] C.J. Bullock, C. Bussy, Biocompatibility Considerations in the Design of Graphene Biomedical Materials, Adv Mat Interfaces (2019).
[68] G.P. Kotchey, B.L. Allen, H. Vedala, N. Yanamala, A.A. Kapralov, Y.Y. Tyurina, J. Klein-Seetharaman, V.E. Kagan, A. Star, The enzymatic oxidation of graphene oxide, ACS Nano 5(3) (2011) 2098-108.
[69] S.P. Mukherjee, A.R. Gliga, B. Lazzaretto, B. Brandner, M. Fielden, C. Vogt, L. Newman, A.F. Rodrigues, W. Shao, P.M. Fournier, M.S. Toprak, A. Star, K. Kostarelos, K. Bhattacharya,

B. Fadeel, Graphene oxide is degraded by neutrophils and the degradation products are non-genotoxic, Nanoscale 10(3) (2018) 1180-1188.
[70] D. Li, X. Hu, S. Zhang, Biodegradation of graphene-based nanomaterials in blood plasma affects their biocompatibility, drug delivery, targeted organs and antitumor ability, Biomaterials 202 (2019) 12-25.
[71] C.M. Girish, A. Sasidharan, G.S. Gowd, S. Nair, M. Koyakutty, Confocal Raman imaging study showing macrophage mediated biodegradation of graphene in vivo, Adv Healthc Mater 2(11) (2013) 1489-500.
[72] J.H. Liu, S.T. Yang, H. Wang, Y. Chang, A. Cao, Y. Liu, Effect of size and dose on the biodistribution of graphene oxide in mice, Nanomedicine (Lond) 7(12) (2012) 1801-12.
[73] X. Zhang, J. Yin, C. Peng, W. Hu, Z. Zhu, W. Li, C. Fan, Q. Huang, Distribution and biocompatibility studies of graphene oxide in mice after intravenous administration, Carbon 49(3) (2011) 986-995.
[74] A. Piperno, A. Scala, A. Mazzaglia, G. Neri, R. Pennisi, M.T. Sciortino, G. Grassi, Cellular Signaling Pathways Activated by Functional Graphene Nanomaterials, International journal of molecular sciences 19(11) (2018).
[75] X. Zhang, Q. Zhou, W. Zou, X. Hu, Molecular Mechanisms of Developmental Toxicity Induced by Graphene Oxide at Predicted Environmental Concentrations, Environ Sci Technol 51(14) (2017) 7861-7871.
[76] I.M. Martinez Paino, F. Santos, V. Zucolotto, Biocompatibility and toxicology effects of graphene oxide in cancer, normal, and primary immune cells, J Biomed Mater Res A 105(3) (2017) 728-736.
[77] A.M. Pinto, C. Gonçalves, D.M. Sousa, A.R. Ferreira, J.A. Moreira, I.C. Gonçalves, F.D. Magalhães, Smaller particle size and higher oxidation improves biocompatibility of graphene-based materials, Carbon 99 (2016) 318-329.
[78] C. Cheng, S. Nie, S. Li, H. Peng, H. Yang, L. Ma, S. Sun, C. Zhao, Biopolymer functionalized reduced graphene oxide with enhanced biocompatibility via mussel inspired coatings/anchors, J Mater Chem B 1(3) (2013) 265-275.
[79] R. Kurapati, F. Bonachera, J. Russier, A.R. Sureshbabu, C. Ménard-Moyon, K. Kostarelos, A. Bianco, Covalent chemical functionalization enhances the biodegradation of graphene oxide, 2d Mater 5(1) (2017).
[80] S. Jaworski, E. Sawosz, M. Grodzik, A. Winnicka, M. Prasek, M. Wierzbicki, A. Chwalibog, In vitro evaluation of the effects of graphene platelets on glioblastoma multiforme cells, Int J Nanomed 8 (2013) 413-20.
[81] L. Ou, B. Song, H. Liang, J. Liu, X. Feng, B. Deng, T. Sun, L. Shao, Toxicity of graphene-family nanoparticles: a general review of the origins and mechanisms, Part Fibre Toxicol 13(1) (2016) 57.

[82] P.T. Yin, S. Shah, M. Chhowalla, K.B. Lee, Design, synthesis, and characterization of graphene-nanoparticle hybrid materials for bioapplications, Chem Rev 115(7) (2015) 2483-531.
[83] V. Palmieri, G. Perini, M. De Spirito, M. Papi, Graphene oxide touches blood: in vivo interactions of bio-coronated 2D materials, Nanoscale Horizons 4(2) (2019) 273-290.
[84] Kenry, K.P. Loh, C.T. Lim, Molecular Hemocompatibility of Graphene Oxide and Its Implication for Antithrombotic Applications, Small 11(38) (2015) 5105-17.
[85] S.K. Singh, M.K. Singh, P.P. Kulkarni, V.K. Sonkar, J.J. Gracio, D. Dash, Amine-modified graphene: thrombo-protective safer alternative to graphene oxide for biomedical applications, ACS Nano 6(3) (2012) 2731-40.
[86] Kenry, K.P. Loh, C.T. Lim, Molecular interactions of graphene oxide with human blood plasma proteins, Nanoscale 8(17) (2016) 9425-41.
[87] R. Feng, Y. Yu, C. Shen, Y. Jiao, C. Zhou, Impact of graphene oxide on the structure and function of important multiple blood components by a dose-dependent pattern, J Biomed Mater Res A 103(6) (2015) 2006-14.
[88] K.H. Liao, Y.S. Lin, C.W. Macosko, C.L. Haynes, Cytotoxicity of graphene oxide and graphene in human erythrocytes and skin fibroblasts, Acs Appl Mater Inter 3(7) (2011) 2607-15.
[89] M. De Spirito, M. Papi, G. Maolucci, G. Ciasca, V. Palmieri, M.C.C. Lauriola, Plasma Protein Corona Reduces the Haemolytic Activity of the Graphene Oxide Nano and Micro Flakes, Biophys J 110(3) (2016) 167a-167a.
[90] A. Sasidharan, L.S. Panchakarla, A.R. Sadanandan, A. Ashokan, P. Chandran, C.M. Girish, D. Menon, S.V. Nair, C.N. Rao, M. Koyakutty, Hemocompatibility and macrophage response of pristine and functionalized graphene, Small 8(8) (2012) 1251-63.
[91] W. Hu, C. Peng, M. Lv, X. Li, Y. Zhang, N. Chen, C. Fan, Q. Huang, Protein corona-mediated mitigation of cytotoxicity of graphene oxide, ACS Nano 5(5) (2011) 3693-700.
[92] Y. Chong, C. Ge, Z. Yang, J.A. Garate, Z. Gu, J.K. Weber, J. Liu, R. Zhou, Reduced Cytotoxicity of Graphene Nanosheets Mediated by Blood-Protein Coating, ACS Nano 9(6) (2015) 5713-24.
[93] G. Duan, S.G. Kang, X. Tian, J.A. Garate, L. Zhao, C. Ge, R. Zhou, Protein corona mitigates the cytotoxicity of graphene oxide by reducing its physical interaction with cell membrane, Nanoscale 7(37) (2015) 15214-24.
[94] Y. Li, L. Feng, X. Shi, X. Wang, Y. Yang, K. Yang, T. Liu, G. Yang, Z. Liu, Surface coating-dependent cytotoxicity and degradation of graphene derivatives: towards the design of non-toxic, degradable nano-graphene, Small 10(8) (2014) 1544-54.

[95] S.K. Singh, M.K. Singh, M.K. Nayak, S. Kumari, S. Shrivastava, J.J. Gracio, D. Dash, Thrombus inducing property of atomically thin graphene oxide sheets, ACS Nano 5(6) (2011) 4987-96.
[96] P.P. Wibroe, S.V. Petersen, N. Bovet, B.W. Laursen, S.M. Moghimi, Soluble and immobilized graphene oxide activates complement system differently dependent on surface oxidation state, Biomaterials 78 (2016) 20-6.
[97] M. Orecchioni, C. Menard-Moyon, L.G. Delogu, A. Bianco, Graphene and the immune system: Challenges and potentiality, Advanced drug delivery reviews 105(Pt B) (2016) 163-175.
[98] J. Ma, R. Liu, X. Wang, Q. Liu, Y. Chen, R.P. Valle, Y.Y. Zuo, T. Xia, S. Liu, Crucial Role of Lateral Size for Graphene Oxide in Activating Macrophages and Stimulating Pro-inflammatory Responses in Cells and Animals, ACS Nano 9(10) (2015) 10498-515.
[99] J. Russier, E. Treossi, A. Scarsi, F. Perrozzi, H. Dumortier, L. Ottaviano, M. Meneghetti, V. Palermo, A. Bianco, Evidencing the mask effect of graphene oxide: a comparative study on primary human and murine phagocytic cells, Nanoscale 5(22) (2013) 11234-47.
[100] Y. Li, Y. Liu, Y. Fu, T. Wei, L. Le Guyader, G. Gao, R.S. Liu, Y.Z. Chang, C. Chen, The triggering of apoptosis in macrophages by pristine graphene through the MAPK and TGF-beta signaling pathways, Biomaterials 33(2) (2012) 402-11.
[101] H. Zhou, K. Zhao, W. Li, N. Yang, Y. Liu, C. Chen, T. Wei, The interactions between pristine graphene and macrophages and the production of cytokines/chemokines via TLR- and NF-kappaB-related signaling pathways, Biomaterials 33(29) (2012) 6933-42.
[102] S.P. Mukherjee, M. Bottini, B. Fadeel, Graphene and the Immune System: A Romance of Many Dimensions, Front Immunol 8 (2017) 673.
[103] C.J. Pan, L.Q. Pang, F. Gao, Y.N. Wang, T. Liu, W. Ye, Y.H. Hou, Anticoagulation and endothelial cell behaviors of heparin-loaded graphene oxide coating on titanium surface, Mat Sci Eng C-Mater 63 (2016) 333-40.
[104] R. Podila, T. Moore, F. Alexis, A.M. Rao, Graphene coatings for enhanced hemo-compatibility of nitinol stents, Rsc Adv 3(6) (2013) 1660-1665.
[105] S.N. Sofia Melo, Andreia T Pereira, Inês Borges, Pedro Granja, Fernão Magalhães, Inês Gonçalves, Incorporation of graphene oxide into poly(ε-caprolactone) 3D printed fibrous scaffolds improves their antimicrobial properties, Materials Science & Engineering C (2020).
[106] M.H. Norahan, M. Amroon, R. Ghahremanzadeh, M. Mahmoodi, N. Baheiraei, Electroactive graphene oxide-incorporated collagen assisting vascularization for cardiac tissue engineering, J Biomed Mater Res A 107(1) (2019) 204-219.
[107] X. Jing, H.Y. Mi, M.R. Salick, T.M. Cordie, X.F. Peng, L.S. Turng, Electrospinning thermoplastic polyurethane/graphene oxide scaffolds for small diameter vascular graft applications, Mat Sci Eng C-Mater 49 (2015) 40-50.

[108] N. Annabi, S.R. Shin, A. Tamayol, M. Miscuglio, M.A. Bakooshli, A. Assmann, P. Mostafalu, J.Y. Sun, S. Mithieux, L. Cheung, X.S. Tang, A.S. Weiss, A. Khademhosseini, Highly Elastic and Conductive Human-Based Protein Hybrid Hydrogels, Adv Mater 28(1) (2016) 40-9.
[109] Kenry, W.C. Lee, K.P. Loh, C.T. Lim, When stem cells meet graphene: Opportunities and challenges in regenerative medicine, Biomaterials 155 (2018) 236-250.
[110] R.N. Gomes, I. Borges, A.T. Pereira, A.F. Maia, M. Pestana, F.D. Magalhães, A.M. Pinto, I.C. Gonçalves, Antimicrobial graphene nanoplatelets coatings for silicone catheters, Carbon 139 (2018) 635-647.
[111] E. Shams, H. Yeganeh, H. Naderi-Manesh, R. Gharibi, Z. Mohammad Hassan, Polyurethane/siloxane membranes containing graphene oxide nanoplatelets as antimicrobial wound dressings: in vitro and in vivo evaluations, Journal of materials science. Materials in medicine 28(5) (2017) 75.
[112] F. Perreault, A.F. de Faria, S. Nejati, M. Elimelech, Antimicrobial Properties of Graphene Oxide Nanosheets: Why Size Matters, ACS Nano 9(7) (2015) 7226-36.
[113] X. Wu, S. Tan, Y. Xing, Q. Pu, M. Wu, J.X. Zhao, Graphene oxide as an efficient antimicrobial nanomaterial for eradicating multi-drug resistant bacteria in vitro and in vivo, Colloids Surf B Biointerfaces 157 (2017) 1-9.
[114] S. Liu, T.H. Zeng, M. Hofmann, E. Burcombe, J. Wei, R. Jiang, J. Kong, Y. Chen, Antibacterial activity of graphite, graphite oxide, graphene oxide, and reduced graphene oxide: membrane and oxidative stress, ACS Nano 5(9) (2011) 6971-80.
[115] S. Gurunathan, J.W. Han, A.A. Dayem, V. Eppakayala, J.H. Kim, Oxidative stress-mediated antibacterial activity of graphene oxide and reduced graphene oxide in Pseudomonas aeruginosa, Int J Nanomed 7 (2012) 5901-14.
[116] L. Shi, J. Chen, L. Teng, L. Wang, G. Zhu, S. Liu, Z. Luo, X. Shi, Y. Wang, L. Ren, The Antibacterial Applications of Graphene and Its Derivatives, Small 12(31) (2016) 4165-84.
[117] H. Zheng, R. Ma, M. Gao, X. Tian, Y.-Q. Li, L. Zeng, R. Li, Antibacterial applications of graphene oxides: structure-activity relationships, molecular initiating events and biosafety, Sci Bull 63(2) (2018) 133-142.
[118] S.P. Singh, Y. Li, A. Be'er, Y. Oren, J.M. Tour, C.J. Arnusch, Laser-Induced Graphene Layers and Electrodes Prevents Microbial Fouling and Exerts Antimicrobial Action, Acs Appl Mater Inter 9(21) (2017) 18238-18247.
[119] V.T. Pham, V.K. Truong, M.D. Quinn, S.M. Notley, Y. Guo, V.A. Baulin, M. Al Kobaisi, R.J. Crawford, E.P. Ivanova, Graphene Induces Formation of Pores That Kill Spherical and Rod-Shaped Bacteria, ACS Nano 9(8) (2015) 8458-67.

[120] S. Romero-Vargas Castrillón, F. Perreault, A.F. de Faria, M. Elimelech, Interaction of Graphene Oxide with Bacterial Cell Membranes: Insights from Force Spectroscopy, Environ Sci Tech Let 2(4) (2015) 112-117.
[121] M.H. Norahan, M. Pourmokhtari, M.R. Saeb, B. Bakhshi, M. Soufi Zomorrod, N. Baheiraei, Electroactive cardiac patch containing reduced graphene oxide with potential antibacterial properties, Mat Sci Eng C-Mater 104 (2019) 109921.
[122] M. Mazaheri, O. Akhavan, A. Simchi, Flexible bactericidal graphene oxide–chitosan layers for stem cell proliferation, Appl Surf Sci 301 (2014) 456-462.
[123] N. Mahmoudi, F. Ostadhossein, A. Simchi, Physicochemical and antibacterial properties of chitosan-polyvinylpyrrolidone films containing self-organized graphene oxide nanolayers, J Appl Polym Sci 133(11) (2016) n/a-n/a.
[124] X. An, H. Ma, B. Liu, J. Wang, Graphene Oxide Reinforced Polylactic Acid/Polyurethane Antibacterial Composites, J Nanomater 2013 (2013) 1-7.
[125] M. Papi, V. Palmieri, F. Bugli, M. De Spirito, M. Sanguinetti, C. Ciancico, M.C. Braidotti, S. Gentilini, L. Angelani, C. Conti, Biomimetic antimicrobial cloak by graphene-oxide agar hydrogel, Sci Rep 6(1) (2016) 12.
[126] Z. Jia, Y. Shi, P. Xiong, W. Zhou, Y. Cheng, Y. Zheng, T. Xi, S. Wei, From Solution to Biointerface: Graphene Self-Assemblies of Varying Lateral Sizes and Surface Properties for Biofilm Control and Osteodifferentiation, Acs Appl Mater Inter 8(27) (2016) 17151-65.
[127] Y. Zhao, W. Terai, Y. Hoshijima, K. Gotoh, K. Matsuura, K. Matsumura, Development and Characterization of a Poly (Vinyl Alcohol)/Graphene Oxide Composite Hydrogel as An Artificial Cartilage Material, Appl Sci 8(11) (2018).
[128] F. Sánchez-Correa, C. Vidaurre-Agut, Á. Serrano-Aroca, A.J. Campillo-Fernández, Poly(2-hydroxyethyl acrylate) hydrogels reinforced with graphene oxide: Remarkable improvement of water diffusion and mechanical properties, J Appl Polym Sci 135(15) (2018).
[129] H. Si, H. Luo, G. Xiong, Z. Yang, S.R. Raman, R. Guo, Y. Wan, One-step in situ biosynthesis of graphene oxide-bacterial cellulose nanocomposite hydrogels, Macromol Rapid Comm 35(19) (2014) 1706-11.
[130] H. Luo, J. Dong, X. Xu, J. Wang, Z. Yang, Y. Wan, Exploring excellent dispersion of graphene nanosheets in three-dimensional bacterial cellulose for ultra-strong nanocomposite hydrogels, Compos Part A Appl Sci Manuf 109 (2018) 290-297.
[131] S. Sayyar, E. Murray, B.C. Thompson, J. Chung, D.L. Officer, S. Gambhir, G.M. Spinks, G.G. Wallace, Processable conducting graphene/chitosan hydrogels for tissue engineering, J Mater Chem B 3(3) (2015) 481-490.
[132] P. Zhu, Y. Deng, C. Wang, Graphene/cyclodextrin-based nanocomposite hydrogel with enhanced strength and thermo-responsive ability, Carbohyd Polym 174 (2017) 804-811.

[133] R. Liu, S. Liang, X.-Z. Tang, D. Yan, X. Li, Z.-Z. Yu, Tough and highly stretchable graphene oxide/polyacrylamide nanocomposite hydrogels, J Mater Chem 22(28) (2012) 14160-14167.
[134] C. Pan, L. Liu, Q. Chen, Q. Zhang, G. Guo, Tough, Stretchable, Compressive Novel Polymer/Graphene Oxide Nanocomposite Hydrogels with Excellent Self-Healing Performance, Acs Appl Mater Inter 9(43) (2017) 38052-38061.
[135] J. Liu, G. Song, C. He, H. Wang, Self-healing in tough graphene oxide composite hydrogels, Macromol Rapid Comm 34(12) (2013) 1002-7.
[136] J.M. Gonzalez-Dominguez, C. Martin, O.J. Dura, S. Merino, E. Vazquez, Smart Hybrid Graphene Hydrogels: A Study of the Different Responses to Mechanical Stretching Stimulus, Acs Appl Mater Inter 10(2) (2018) 1987-1995.
[137] M. Zhong, Y.-T. Liu, X.-M. Xie, Self-healable, super tough graphene oxide–poly(acrylic acid) nanocomposite hydrogels facilitated by dual cross-linking effects through dynamic ionic interactions, J Mater Chem B 3(19) (2015) 4001-4008.
[138] Y. Wang, Q. Chang, R. Zhan, K. Xu, Y. Wang, X. Zhang, B. Li, G. Luo, M. Xing, W. Zhong, Tough but self-healing and 3D printable hydrogels for E-skin, E-noses and laser controlled actuators, J Mater Chem A 7(43) (2019) 24814-24829.
[139] S. Faghihi, A. Karimi, M. Jamadi, R. Imani, R. Salarian, Graphene oxide/poly(acrylic acid)/gelatin nanocomposite hydrogel: experimental and numerical validation of hyperelastic model, Materials science & engineering. C, Materials for biological applications 38 (2014) 299-305.
[140] Y. Huang, M. Zhang, W. Ruan, High-water-content graphene oxide/polyvinyl alcohol hydrogel with excellent mechanical properties, J Mater Chem A 2(27) (2014) 10508-10515.
[141] A. Alam, M. Moussa, Preparation of graphene/poly(vinyl alcohol) composite hydrogel films with enhanced electrical and mechanical properties, Polym Compos (2019).
[142] L. Zhang, Z. Wang, C. Xu, Y. Li, J. Gao, W. Wang, Y. Liu, High strength graphene oxide/polyvinyl alcohol composite hydrogels, J Mater Chem 21(28) (2011) 10399-10406.
[143] Q. Luo, Y. Shan, X. Zuo, J. Liu, Anisotropic tough poly(vinyl alcohol)/graphene oxide nanocomposite hydrogels for potential biomedical applications, Rsc Adv 8(24) (2018) 13284-13291.
[144] J. Chen, X. Shi, L. Ren, Y. Wang, Graphene oxide/PVA inorganic/organic interpenetrating hydrogels with excellent mechanical properties and biocompatibility, Carbon 111 (2017) 18-27.
[145] Y. Shi, D. Xiong, J. Li, N. Wang, The water-locking and cross-linking effects of graphene oxide on the load-bearing capacity of poly(vinyl alcohol) hydrogel, Rsc Adv 6(86) (2016) 82467-82477.

[146] M. Frounchi, S. Dadbin, M. Tabatabaei, Poly (vinyl alcohol)/graphene oxide nanocomposite films and hydrogels prepared by gamma ray, Plast Rubber and Compos 48(2) (2018) 42-47.
[147] Y. Meng, L. Ye, P. Coates, P. Twigg, In Situ Cross-Linking of Poly(vinyl alcohol)/Graphene Oxide–Polyethylene Glycol Nanocomposite Hydrogels as Artificial Cartilage Replacement: Intercalation Structure, Unconfined Compressive Behavior, and Biotribological Behaviors, J Phys Chem C 122(5) (2018) 3157-3167.
[148] X. Rui-Hong, R. Peng-Gang, H. Jian, R. Fang, R. Lian-Zhen, S. Zhen-Feng, Preparation and properties of graphene oxide-regenerated cellulose/polyvinyl alcohol hydrogel with pH-sensitive behavior, Carbohydrate polymers 138 (2016) 222-8.
[149] Q. Guo, Z. Shi, H. Xu, X. Ma, J. Yin, M. Tian, Fabrication of Super Extensible and Highly Tough Graphene Composite Hydrogels by Thermal Treatment Strategy for the Mixture of Tannin and Graphene Oxide, Macromol Chem Phys 218(6) (2017).
[150] R. Balu, S. Reeder, R. Knott, J. Mata, L. de Campo, N.K. Dutta, N.R. Choudhury, Tough Photocrosslinked Silk Fibroin/Graphene Oxide Nanocomposite Hydrogels, Langmuir 34(31) (2018) 9238-9251.
[151] A.M. Nzenguet, M. Aqlil, Y. Essamlali, O. Amadine, A. Snik, M. Larzek, M. Zahouily, Novel bionanocomposite films based on graphene oxide filled starch/polyacrylamide polymer blend: structural, mechanical and water barrier properties, J Polym Res 25(4) (2018) 86.
[152] Y. Huang, M. Zeng, J. Chen, Y. Wang, Q. Xu, Multi-structural network design and mechanical properties of graphene oxide filled chitosan-based hydrogel nanocomposites, Materials & Design 148 (2018) 104-114.
[153] Z. Wang, J. Li, L. Jiang, S. Xiao, Y. Liu, J. Luo, Zwitterionic Hydrogel Incorporated Graphene Oxide Nanosheets with Improved Strength and Lubricity, Langmuir 35(35) (2019) 11452-11462.
[154] S. Tarashi, H. Nazockdast, G. Sodeifian, Reinforcing effect of graphene oxide on mechanical properties, self-healing performance and recoverability of double network hydrogel based on κ-carrageenan and polyacrylamide, Polymer 183 (2019).
[155] X. Ma, Y. Li, W. Wang, Q. Ji, Y. Xia, Temperature-sensitive poly(N-isopropylacrylamide)/graphene oxide nanocomposite hydrogels by in situ polymerization with improved swelling capability and mechanical behavior, Eur Polym J 49(2) (2013) 389-396.
[156] X. Yan, J. Yang, F. Chen, L. Zhu, Z. Tang, G. Qin, Q. Chen, G. Chen, Mechanical properties of gelatin/polyacrylamide/graphene oxide nanocomposite double-network hydrogels, Comp Sci Tec 163 (2018) 81-88.
[157] B. Li, C. Wu, C. Wang, Z. Luo, J. Cao, Fabrication of tough, self-recoverable, and electrically conductive hydrogels by
in situ

reduction of poly(acrylic acid) grafted graphene oxide in polyacrylamide hydrogel matrix, J Appl Polym Sci (2019).
[158] Y. Wang, Q. Chang, R. Zhan, K. Xu, Y. Wang, X. Zhang, B. Li, G. Luo, M. Xing, W. Zhong, Tough but self-healing and 3D printable hydrogels for E-skin, E-noses and laser controlled actuators, Journal of Materials Chemistry A 7(43) (2019) 24814-24829.
[159] J. Liu, C. Chen, C. He, J. Zhao, X. Yang, H. Wang, Synthesis of graphene peroxide and its application in fabricating super extensible and highly resilient nanocomposite hydrogels, ACS Nano 6(9) (2012) 8194-202.
[160] C. Yang, Z. Liu, C. Chen, K. Shi, L. Zhang, X.J. Ju, W. Wang, R. Xie, L.Y. Chu, Reduced Graphene Oxide-Containing Smart Hydrogels with Excellent Electro-Response and Mechanical Properties for Soft Actuators, Acs Appl Mater Inter 9(18) (2017) 15758-15767.
[161] M. Kheirabadi, R. Bagheri, K. Kabiri, D.A. Ossipov, E. Jokar, E. Asadian, Improvement in Mechanical Performance of Anionic Hydrogels Using Full-Interpenetrating Polymer Network Reinforced with Graphene Oxide Nanosheets, Adv Pol Tec 35(4) (2016) 386-395.
[162] M. Javadi, Q. Gu, S. Naficy, S. Farajikhah, J.M. Crook, G.G. Wallace, S. Beirne, S.E. Moulton, Conductive Tough Hydrogel for Bioapplications, Macromol Biosci 18(2) (2018).
[163] J. Fan, Z. Shi, M. Lian, H. Li, J. Yin, Mechanically strong graphene oxide/sodium alginate/polyacrylamide nanocomposite hydrogel with improved dye adsorption capacity, J Mater Chem A 1(25) (2013) 7433-7443.
[164] M. Gorji, M. Karimi, G. Mashaiekhi, S. Ramazani, Superabsorbent, Breathable Graphene Oxide-Based Nanocomposite Hydrogel as a Dense Membrane for Use in Protective Clothing, Polym-Plast Tech Mat 58(2) (2018) 182-192.
[165] W. Huang, C. Qi, Y. Gao, Injectable Self-Healable Nanocomposite Hydrogels with Mussel-Inspired Adhesive Properties for 3D Printing Ink, Acs Appl Nano Mater 2(8) (2019) 5000-5008.
[166] Y. Bai, X. Chen, A fast water-induced shape memory polymer based on hydroxyethyl cellulose/graphene oxide composites, Compos Part A Appl Sci Manuf 103 (2017) 9-16.
[167] X. Fu, Y. Zhan, Y. Meng, Y. Li, C. Liao, Z. Lu, Graphene oxide/poly(vinyl alcohol) hydrogels with good tensile properties and reusable adsorption properties, Plast Rubber and Compos 46(2) (2017) 53-59.
[168] B.L. Zimba, M. Wang, J. Hao, X. Yu, Y. Li, C. Chen, G. Xiong, Q. Wu, Preparation of collagen/carboxylated graphene oxide nanofibrous membranes by electrospinning and their hemocompatibilities, Mater Res Express 6(10) (2019).
[169] C. Tang, B.D. Holt, Z.M. Wright, A.M. Arnold, A.C. Moy, S.A. Sydlik, Injectable amine functionalized graphene and chondroitin sulfate hydrogel with potential for cartilage regeneration, J Mater Chem B 7(15) (2019) 2442-2453.

[170] M.H. Norahan, M. Amroon, R. Ghahremanzadeh, N. Rabiee, N. Baheiraei, Reduced graphene oxide: osteogenic potential for bone tissue engineering, Iet Nanobiotechnol 13(7) (2019) 720-725.
[171] S. Liu, C. Zhou, S. Mou, J. Li, M. Zhou, Y. Zeng, C. Luo, J. Sun, Z. Wang, W. Xu, Biocompatible graphene oxide-collagen composite aerogel for enhanced stiffness and in situ bone regeneration, Mat Sci Eng C-Mater 105 (2019) 110137.
[172] J. Fu, Y. Zhang, J. Chu, X. Wang, W. Yan, Q. Zhang, H. Liu, Reduced Graphene Oxide Incorporated Acellular Dermal Composite Scaffold Enables Efficient Local Delivery of Mesenchymal Stem Cells for Accelerating Diabetic Wound Healing, Acs Biomater Sci Eng 5(8) (2019) 4054-4066.
[173] Y. Chen, Z. Zheng, R. Zhou, H. Zhang, C. Chen, Z. Xiong, K. Liu, X. Wang, Developing a Strontium-Releasing Graphene Oxide-/Collagen-Based Organic-Inorganic Nanobiocomposite for Large Bone Defect Regeneration via MAPK Signaling Pathway, Acs Appl Mater Inter 11(17) (2019) 15986-15997.
[174] D. Zhang, X. Wu, J. Chen, K. Lin, The development of collagen based composite scaffolds for bone regeneration, Bioact Mater 3(1) (2018) 129-138.
[175] J. Wang, Y. Wang, D. Liu, Q. Yang, C. Huang, C. Yang, Q. Zhang, Preparation and cytological study of collagen/nano-hydroxyapatite/graphene oxide composites, Acta Bioeng Biomech 20(4) (2018) 65-74.
[176] S. Liu, S. Mou, C. Zhou, L. Guo, A. Zhong, J. Yang, Q. Yuan, J. Wang, J. Sun, Z. Wang, Off-the-Shelf Biomimetic Graphene Oxide-Collagen Hybrid Scaffolds Wrapped with Osteoinductive Extracellular Matrix for the Repair of Cranial Defects in Rats, ACS Appl Mater Interfaces 10(49) (2018) 42948-42958.
[177] E. Kolanthai, P.A. Sindu, D.K. Khajuria, S.C. Veerla, D. Kuppuswamy, L.H. Catalani, D.R. Mahapatra, Graphene Oxide-A Tool for the Preparation of Chemically Crosslinking Free Alginate-Chitosan-Collagen Scaffolds for Bone Tissue Engineering, Acs Appl Mater Inter 10(15) (2018) 12441-12452.
[178] Z. Bazrafshan, G.K. Stylios, High Performance of Covalently Grafting onto Collagen in The Presence of Graphene Oxide, Nanomaterials (Basel) 8(9) (2018).
[179] J. Wang, Z. Zhang, G. Su, X. Sun, Y. Wang, Z. Fang, M. Chen, Q. Zhang, Graphene Oxide Incorporated Collagen/Nano-Hydroxyapatite Composites with Improved Mechanical Properties for Bone Repair Materials, J Biomater Tiss Eng 7(10) (2017) 1000-1007.
[180] M.K. Jaiswal, J.R. Xavier, J.K. Carrow, P. Desai, D. Alge, A.K. Gaharwar, Mechanically Stiff Nanocomposite Hydrogels at Ultralow Nanoparticle Content, ACS Nano 10(1) (2016) 246-56.
[181] A.F. Girão, G. Gonçalves, K.S. Bhangra, J.B. Phillips, J. Knowles, G. Irurueta, M.K. Singh, I. Bdkin, A. Completo, P.A.A.P. Marques, Electrostatic self-assembled graphene oxide-

collagen scaffolds towards a three-dimensional microenvironment for biomimetic applications, Rsc Adv 6(54) (2016) 49039-49051.
[182] S. Kang, J.B. Park, T.-J. Lee, S. Ryu, S.H. Bhang, W.-G. La, M.-K. Noh, B.H. Hong, B.-S. Kim, Covalent conjugation of mechanically stiff graphene oxide flakes to three-dimensional collagen scaffolds for osteogenic differentiation of human mesenchymal stem cells, Carbon 83 (2015) 162-172.
[183] S. Ebrahimi, A. Montazeri, H. Rafii-Tabar, Molecular dynamics study of the interfacial mechanical properties of the graphene–collagen biological nanocomposite, Comput Mater Sci 69 (2013) 29-39.

Chapter 3

Graphene oxide-reinforced poly(2-hydroxyethyl methacrylate) hydrogels with extreme stiffness and high-strength

Designing hydrogels with high-strength and stiffness remains a challenge, limiting their usage in several applications that involve load-bearing. In this work, in situ incorporation of different amounts of graphene oxide (GO) into poly(2-hydroxyethyl methacrylate) (pHEMA) was used to create hydrogels with outstanding stiffness (Young's modulus of up to 6.5 MPa, 8.3x higher than neat pHEMA) and tensile resistance (ultimate tensile strength of up to 1.14 MPa, 7.4x higher than neat pHEMA) without affecting the water absorption capacity, surface wettability and cytocompatibility of pHEMA. Such magnitude of improvement in Young's modulus and ultimate tensile strength was never before described for GO incorporation in hydrogels. Moreover, these stiffness and tensile resistance values are higher than the ones of most hydrogels (few hundred kPa), achieving a stiffness comparable to polydimethylsiloxane (PDMS), cartilage and artery walls and a tensile resistance similar to rigid foams, PDMS and cork. These new materials open a wide range of application for pHEMA in different fields.

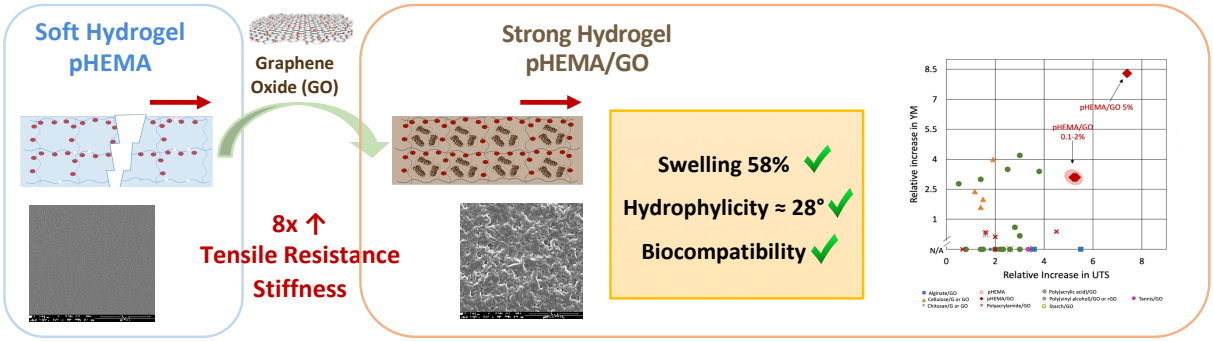

Keywords: *Biomaterials, Compressive strength, Graphene Oxide, Mechanical Properties, poly(2-hydroxyethyl methacrylate), Strong Hydrogels, Tensile Strength1*

This chapter is based on the following published paper:

A.T. Pereira, P.C. Henriques, P.C. Costa, M.C.L. Martins, F.D. Magalhães, I.C. Gonçalves, Graphene oxide-reinforced poly(2-hydroxyethyl methacrylate) hydrogels with extreme stiffness and high-strength, Composites Science Technology 184 (2019) 107819.

3.1 Introduction

Hydrogels are hydrophilic polymer networks capable of absorbing large amounts of water [1]. By taking advantage of this swelling capacity, several uses have been devised, like contact lenses [2] or systems for removal of dye and heavy metal from water. Potential applications in tissue engineering, biosensors and drug delivery systems have also been explored [3, 4]. However, poor mechanical properties have hampered their widespread use in load-bearing applications [5, 6]. To surpass this limitation, several approaches have been proposed: use of a combination and/or higher amounts of crosslinking agents [7-9], brittle/ductile inter-penetrating networks (double-network hydrogels), [6, 10-14] nanofillers [6, 15-24] and micro/nanostructured hydrogels [25-27]. However, these often lead to the loss of key features, like swelling capacity, hemo/biocompatibility and non-fouling characteristics, and/or to difficulties in preparation [28, 29]. As such, the design and production of strong hydrogels remains a central issue in the materials science field.

Poly(2-hydroxyethyl methacrylate) (pHEMA) is a synthetic hydrogel produced through *in situ* polymerization of 2-hydroxyethyl methacrylate (HEMA) monomers [1]. Described as a non-fouling material, pHEMA limits the adsorption of proteins, platelets and cells on its surface [30]. Due to its biocompatibility, pHEMA is a Food & Drug Administration (FDA) approved hydrogel being currently used in clinics for the production of contact lenses and keratoprosthetics [31, 32]. pHEMA applications could be far more widened by developing new composites with improved mechanical properties while preserving its biocompatibility.

Graphene is a single-layer sheet of sp^2-bonded carbon atoms in a two-dimensional (2D) honeycomb lattice. This material was firstly isolated in 2004 and has been described as the strongest material in the world. Due to this unique property, Graphene and Graphene-Based Materials (GBMs) have been proposed as appealing nano-fillers for mechanical reinforcement of polymers, including hydrogels such as polyacrylamide, cellulose, alginate and polyvinyl alcohol [6, 33-39]. For most of the hydrogels, incorporation of GBMs induces an increase in the polymer's intrinsic tensile resistance of up to 2 times [6, 33]. GBMs can also be used as building blocks to make 3D materials such as aerogels and graphene-based hydrogel [40-42], which exhibit promising features regarding electrical conductivity, thermal resistance and adsorption capacity and also a high elasticity and compressive resistance but a weak tensile resistance, in the order of few kPa [43-45].

Beyond the filler efficiency, GBMs biocompatibility is a crucial factor to allow a future biological application. Among available GBMs, G oxide (GO), which contains different oxygen groups (hydroxyl, epoxide, carbonyl and carboxylic groups) at its surface, has been described as having lower cytotoxicity than G [46-48]. *In vivo* studies reveal that when intravenously administrated, GO accumulation in lungs, liver, kidneys and/or spleen depends on its lateral

size [48-50]. Moreover, a recent study showed that GO can be degraded *in vitro* by neutrophils generating non-genotoxic by-products [51].

The present study proposes for the first time the use of GO to improve pHEMA mechanical properties, aiming to obtain a new hydrogel with outstanding performance under tensile and compressive stress. Additionally, this work aims to meet the requirements of several load-bearing applications (stiffness and tensile resistance in the order of MPa) and to preserve the biocompatibility of the neat polymer. To achieve this goal, an accessible and industrially applicable approach was established, which consists on the *in situ* free-radical polymerization of the monomer (2-hydroxyethyl methacrylate; HEMA) and crosslinking agent (tetraethylene glycol dimethacrylate; TEGDMA) in the presence of different contents of GO (0%, 0.1%, 0.25%, 1%, 2% and 5%). An in-depth characterization of the new pHEMA/GO composites was conducted regarding their mechanical behavior under tensile and compressive stress, in order to evaluate their potential in future usage in load-bearing applications. Physical-chemical characteristics as well as cytocompatibility of pHEMA/GO composites were evaluated to reveal whether the main features of pHEMA are maintained upon GO incorporation, thus enabling application in biomedical field.

3.2 Methods

3.2.1 Synthesis of Graphene Oxide (GO)

Carbon graphite micropowder (purity: ≥99% and lateral size: 7-11 μm, American Elements) was oxidized by modified Hummers' method, as described before [47, 52, 53]. Briefly, 3 g of carbon graphite were added to 150 mL of H_2SO_4/H_3PO_4 (4:1) mixture followed by cooling and addition of $KMnO_4$ (18 g). The reaction was kept at 35 ˚C and stirred for 2 h. Afterwards, the mixture was cooled to 0 ˚C and 450 mL of distilled water added slowly. Excess of $KMnO_4$ was eliminated by adding H_2O_2 until oxygen release stopped. After overnight resting, the material was consecutively centrifuged at 4000 rpm during 20 min, until pH of supernatant reached the pH of distilled water. The suspension was sonicated during 6 h in ultrasonic water bath to obtain GO. GO powder was obtained by freeze-drying the suspension at -80 °C and 0.008 mBar for 3 days.

3.2.2 pHEMA/GO composites production

Poly(2-hydroxyethyl methacrylate) (pHEMA)/GO composites were produced by *in situ* polymerization of 2-hydroxyethyl methacrylate (HEMA) monomers as previously described for pHEMA [54]. 7.5 ml of 2-hydroxyethyl methacrylate monomer (HEMA; >99.5%, Polysciences) were added to a water/ethylene glycol (Sigma Aldrich) mixed solvent (1.5 mL/2.25 mL) with 0%, 0.1%, 0.25%, 1%, 2%, 5% (w/v) of GO. The mixture was vortexed for 30 sec and sonicated

in an ultrasonic water bath during 15 min. After that, 0.345 mL of the crosslinking agent, tetraethylene glycol dimethacrylate (TEGDMA; Polysciences) and 1.5 mL of redox initiators solution, 40% ammonium persulfate (APS; 98%, Aldrich) and 15% sodium metabisulfite (SMB; 97%), were added to the mixture. The mixture was poured between two clean glass plates with a 0.54 mm thick Teflon gasket and allowed to polymerize overnight (although the gel sets within 1 h for pHEMA and 5 min for pHEMA/GO composites). Neat pHEMA and pHEMA/GO composites with cylindrical shape were also produced using 24-well plate as mould (Ø = 15.6 mm and height = 17.0 mm) to evaluate their compressive properties. All the hydrogels were released from the glass plates or from 24-well plate and soaked in distilled water for 4 h (water renewed every hour) to leach out unreacted monomers, initiators and oligomer residues. 5% (w/v) of GO was the maximum amount of GO that could be incorporated in pHEMA due to the high increase in the pHEMA/GO mixture viscosity before polymerization, which prevented its moulding between the glass plates.

3.2.3 GO and pHEMA/GO composites characterization

3.2.3.1 Physical-chemical characterization

X-ray photoelectron spectroscopy (XPS) was used to evaluate the oxidation degree of GO. Briefly, GO pellet (prepared in a manual hydraulic press) was analyzed using a Kratos Axis Ultra HAS (Kratos Analytical, UK) equipment. An Al monochromator with 15 kW was used as X-ray source. The survey spectrum of GO was obtained at 80 eV and the C1s high resolution spectra at 40 eV. C1s spectral component was set at a binding energy of 284.6 eV to correct the contribution of charge effect.

Fourier-transform infrared spectroscopy (FTIR) was performed to evaluate the presence of oxygen-containing functional groups in GO and also to assess pHEMA polymerization. The analysis was performed with dehydrated samples on a Perkin Elmer Frontier spectrophotometer coupled to universal Attenuated Total Reflection (ATR) sampling accessory. All spectra were obtained in duplicate using 100 scans and 2 cm^{-1} of resolution being baseline corrected and smoothed.

Raman spectroscopy was performed to characterize vibrational modes of GO and to evaluate its presence in pHEMA/GO composites. The spectra were acquired using a confocal Raman microscope, LabRAM HR800 UV, Horiba Jobin-Yvon. The excitation was provided by a 515.2 nm laser with an acquisition time of 30 sec. A 50x objective (Olympus) lens with a numerical aperture of 0.55 was used. Measurements were performed using dehydrated samples and at least 5 spectra were acquired for each condition. Spectra were baseline corrected and smoothed.

Transmission electron microscopy (TEM) of GO powders was performed to evaluate lateral size, exfoliation and morphology of GO sheets. The images were acquired using a JEOL JEM

1400 TEM (Tokyo, Japan) coupled to a digital camera CCD Orious 1100 W (Tokyo, Japan). Visualization of GO was performed after ultrasonic dispersion of the GO dried powder in water and dropping the suspension on 200 mesh copper TEM grids.

Scanning electron microscopy (SEM) was performed to visualize GO morphology as well as surface and cross-section topographies of pHEMA and pHEMA/GO composites. To improve samples conductivity, the materials were dried in vacuum oven at 60 ºC and coated with a thin layer of gold/palladium by sputtering. A FEI Quanta 400FEG ESEM / EDAX Genesis X4M SEM with accelerating voltage of 15 kV (GO) and 10 kV (pHEMA/GO composites) was used to visualize the samples.

Optical microscopy images of hydrated composites were acquired to visualize GO dispersion on composites using an Inverted Fluorescence Microscope (Axiovert 200, Zeiss) in brightfield mode.

Contact angles of hydrated pHEMA and pHEMA/GO composites were measured to evaluate surface wettability alterations upon GO incorporation on pHEMA. For this, captive air-bubble contact angles were measured by the inverted drop method using a goniometer, Data Physics, model OCA 15, equipped with a video CCD-camera. Each sample was attached to a steel slide and placed into an ultrapure water-filled glass chamber. After that, a 10 µL air bubble was released from a J-shaped needle underneath the sample's surface and the contact angle was measured using the software SCA. At least 6 drops of each conditions were considered.

The swelling profile of neat pHEMA and pHEMA/GO composites was determined by gravimetric analysis. A pre-weighed dehydrated disc of each composite was immersed in water during 4 h, being removed at different time points, blotted with filter paper and weighed. The swelling degree was calculated using the following equation:

$$Swelling\ degree\ (\%) = \frac{Ws - Wd}{Wd} \times 100 \quad \text{Equation 2}$$

where W_d is the weight of the dry polymer and W_s the weight of the swollen polymer. The swelling profile of each material was evaluated at least 3 times.

3.2.3.2 Mechanical characterization

Tensile properties of hydrated hydrogels were evaluated with a Mecmesin Multitest-1d motorized test frame machine, at room temperature, using a loading cell of 10 N or 200 N and displacement rate of 10 mm/min. The test parameters were in agreement with Standard Test Method for Tensile Properties, ASTM D 882-02 [55]. Measurements were performed using samples with 60.0 mm of length, 15.0 mm of width and 0.54 mm of thickness. For each condition at least 15 samples of 3 different batches of materials were tested.

Compression properties of hydrated hydrogels were evaluated with a texture analyzer (TA-XT2i, Stable Micro Systems), at room temperature, using a loading cell of 5 kG, a cylindrical Delrin probe with a 12.7 mm diameter with 126.7 mm^2 of area and a displacement rate of 60 mm/min. Measurements were performed using samples with 15.6 mm of diameter and 17.0 mm of height. For each condition at least 2 samples of different batches were tested in triplicate.

3.2.4 Cytocompatibility of pHEMA/GO composites

The *in vitro* biocompatibility of pHEMA and pHEMA/GO composites was evaluated by the incubation of mouse fibroblasts NIH 3T3 cells with extracts of materials. The extracts were prepared as described in ISO 10993-12:2012 [56]. Briefly, neat pHEMA and pHEMA/GO composites were cut with Ø = 13 mm and sterilized with ethanol 70% (v/v). After the sterilization step, materials were rinsed with PBS and extracted with DMEM+ culture medium (Dulbecco's modified Eagle's medium (DMEM, Gibco) supplemented with 10% (v/v) Fetal bovine serum (FBS, Gibco) and 1% (v/v) penicillin/streptomycin (biowest)) during 24 h at 37 ºC in an orbital shaker at 100 rpm. Cells were seeded in 96-well plates at density of 1×10^5 cells/mL and maintained in culture for 24 h in DMEM+. After that, the culture medium was replaced by material extracts, according to ISO 10993-5:2009(E) [57]. After 24 h of incubation at 37 ºC, mitochondrial metabolic activity of cells was quantified by resazurin assay. Extracts of TCPET discs were used as positive control of cells growth while a solution of DMEM with 1 mM H_2O_2 was used as negative control. Assays were performed with n=5 and repeated twice.

3.3 Results and Discussion

3.3.1 Graphene Oxide (GO)

Graphene oxide was prepared through graphite oxidation by modified Hummers' method followed by exfoliation using an ultrasonic water bath. XPS analysis was performed to characterize the chemical composition of GO, namely its oxidation degree and the functional groups present at GO surface. Fig. 1a shows that GO is constituted by 66.8% of carbon atoms and 33.2% of oxygen atoms, confirming the successful oxidation of graphite which has a low amount of oxygen atoms (around 8%), as previously characterized [58]. C1s high resolution spectrum of GO exhibits two peaks that could be deconvoluted in five bands attributed to sp^2 C=C (284.3 eV), sp^3 C-C (284.7 eV), C-O-C and C-OH (286.6 eV), C=O (287.8 eV) and O-C=O (288.7 eV) bonds (Fig. 1a). The 21.1% of sp^2 C=C bonds present in GO are associated to the 2D honeycomb crystal lattice structure characteristic of GBMs, whereas the 20.6% of sp^3 C-C bonds are formed during the oxidation process upon breakage of same of the sp^2 C=C bonds originally present in graphite. Regarding the oxygen containing functional groups on GO

structure, the epoxy and alcohol groups (C-O-C and C-OH), which emerge on the basal planes of GO sheets, represent 50.2% of carbon bonds being most prevalent than carbonyl (C=O) and carboxylic groups ($^{-}$O-C=O), which appear on GO edges and represent only 4.7% and 3.3%, respectively.

FTIR spectrum of GO exhibits a broad absorption band in the 3750-2300 cm^{-1} characteristic of OH stretching which is associated to hydroxyl and carboxyl groups into GO structure and also to water molecules [59]. The bands around 1047 cm^{-1} and 1225 cm^{-1} are associated to C-O-C (epoxide) and C-O bonds (epoxide, hydroxyl and carboxylic acids) respectively [60]. At a wavelength of 1715 cm^{-1}, a well-recognized band is assigned by C=O bonds which could be associated with carboxylic acids or carbonyl moieties mostly present along GO edges [61, 62]. The band at 1611 cm^{-1} is associated with C=C bonds present in the hexagonal lattice of graphene oxide [63]. These results show successful oxidation of graphite being the epoxide groups the most prevalent oxygen containing groups in GO structure, which corroborate XPS spectrum.

Fig. 1c shows the Raman spectrum of GO where it is possible to identify the presence of the G-band at 1580 cm^{-1} and the D-band at 1350 cm^{-1} [64, 65]. The G peak corresponds to the bond stretching of sp^2 atoms in six-atom carbon rings while D peak is associated to the structural defects in these rings mostly introduced during oxidation process due to the presence of epoxy, alcohol, carbonyl and carboxylic groups. Raman spectrum does not exhibit the peak signed by non-regular rings (1700-1780 cm^{-1}) [66], confirming the preservation of the ring-structure characteristic of GO.

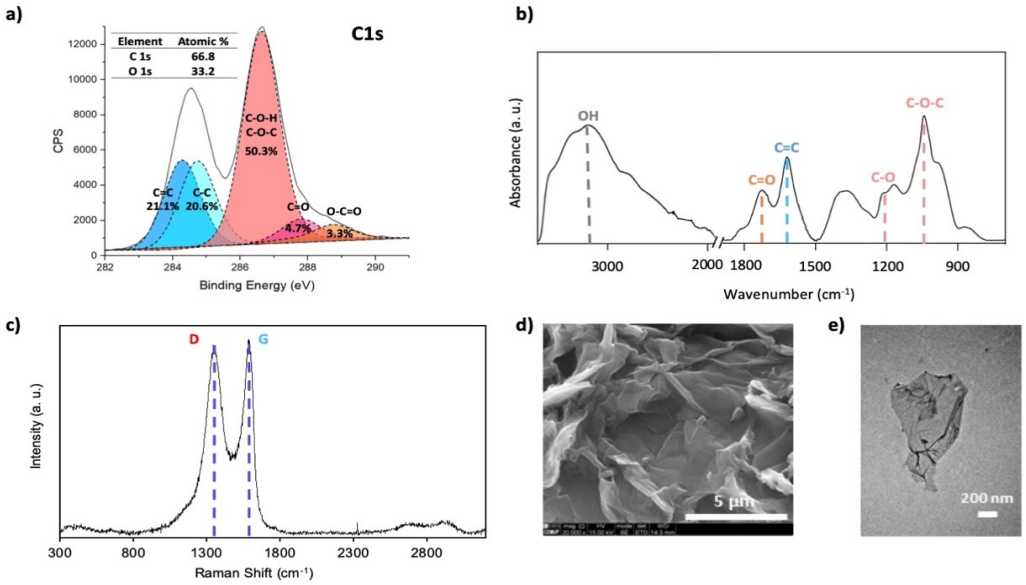

Figure 1 – Characterization of GO: a) elemental composition (Atomic %) and C1s high resolution spectrum obtained by XPS, b) FTIR and c) RAMAN spectra, and d) SEM and e) TEM images of GO powders.

Morphology of GO sheets was evaluated by SEM and TEM. Fig. 1d and 1e show that GO sheets exhibit a wrinkled structure with folded edges. This is due to the presence of oxygen-containing functional groups on GO structure, which leads to hydrogen bonding within each sheet's surface [67, 68]. TEM images also allow inferring on exfoliation and lateral size of GO. GO sheets exhibit good dispersion in water (Fig. 1e), which could be explained by the hydrophilic nature of GO. The evaluation of several TEM images indicates that the lateral size of GO is around 1.5 (± 0.5) μm (Fig. 1e). Altogether, the techniques confirm the successful oxidation and exfoliation of graphite, obtaining GO.

3.3.2 Physical-chemical characterization of pHEMA/GO composites

pHEMA/GO composites were produced by *in situ* polymerization of HEMA in the presence of different amounts of GO (0%, 0.1%, 0.25%, 1%, 2% and 5% (w/v)). Chemical composition of GO, neat pHEMA and pHEMA/GO composites was evaluated by FTIR analysis and is present in Fig. 2a. FTIR spectra of neat pHEMA and pHEMA/GO composites are similar and exhibit pHEMA characteristic bands C=O (1727 cm^{-1}), CH_2 (1277 cm^{-1}), C-O-C (1158 cm^{-1}) and C-O or CH_2 (1079 cm^{-1}) [69, 70]. The characteristic band of HEMA monomers, C=C (1635 cm^{-1}) [71], is not present in any of the spectra, demonstrating that pHEMA polymerization occurs even in the presence of GO. Since GO characteristic bands were not detected in pHEMA/GO composites by FTIR (probably due to the low amounts present), RAMAN analysis was performed (Fig. 2b). pHEMA/GO composites spectra exhibit the characteristic bands of GO, thus confirming its incorporation in the composites, with CH_2 (2800 cm^{-1}) and C-CH_2 (1700 cm^{-1}) characteristic RAMAN bands of pHEMA appearing only in pHEMA/GO composites with the lower amounts of GO (0.1-0.25%). This is associated with the lower intensity of pHEMA Raman signal compared to the GO.

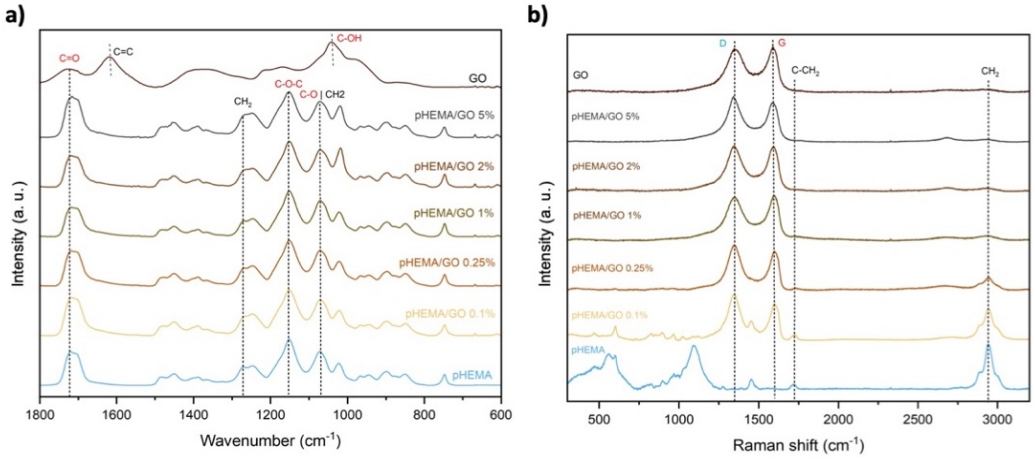

Figure 2 - a) FTIR and b) Raman spectra of GO, pHEMA and pHEMA/GO composites.

Optical microscopy images of pHEMA/GO composites also confirm the presence of GO in the formulations as grey/black spots, with pHEMA/GO 5% being completely opaque due to the high amount of filler (Fig. 3a column 1). For pHEMA/GO 0.1% and 0.25%, GO seems well dispersed, while for 1% and 2% it is possible to identify some aggregates, seen as darker spots. Dispersion of GO in pHEMA matrix was also evaluated through SEM imaging of transversal sections. As clearly shown in Fig. 3a column 2, in the presence of GO, the hydrogel composites show a layered-structure in the cross-section. The formation of this layered-structure could be attributed to the intercalation of GO in the pHEMA matrix. Moreover, it also shows that GO is well distributed and interacts with pHEMA matrix since it is not possible to identify GO sheets in the fracture surface.

Surface features of pHEMA/GO composites were assessed by SEM and contact angle measurements. Fig. 3a (column 3 and 4) shows that GO does not seem to be exposed at the composites surface, but its incorporation increases surface roughness, even at the lowest concentration tested. Other studies also report an increase in surface roughness of sterculia gum [72], poly(lactic acid) [58] and chitosan [73] after GO incorporation. Despite these changes in surface topography, no significant differences were observed in the captive air-bubble contact angle of hydrated composites when compared with pHEMA, maintaining a contact angle of around 28° (Fig. 3b). These results show that the hydrophilic nature of pHEMA surface is not affected by GO incorporation, which is an important feature to preserve in a non-fouling material.

Swelling capacity is an essential condition to define a polymer as a hydrogel. The swelling profile of pHEMA/GO composites was assessed through gravimetric analyses of dehydrated films immersed in water for 4 h, being removed from water in specific time points. The effect of GO incorporation on the swelling of pHEMA is represented in Fig. 3c where it is possible to identify a slight decrease in the swelling rate for all pHEMA/GO composites in the first 30 min. This may be due to GO's presence causing pore blockage or altering the viscoelastic properties of the hydrogels' structure, hindering swelling. However, after 4 h, all materials reach approximately the same swelling value of about 58% of their dry weight, indicating that GO does not affect the equilibrium of water absorption capacity of pHEMA. This is relevant since water absorption capacity plays a crucial role in hydrogel applications considering that it affects their capacity to adsorb dyes or to deliver drugs and their bio/hemocompatibility [74].

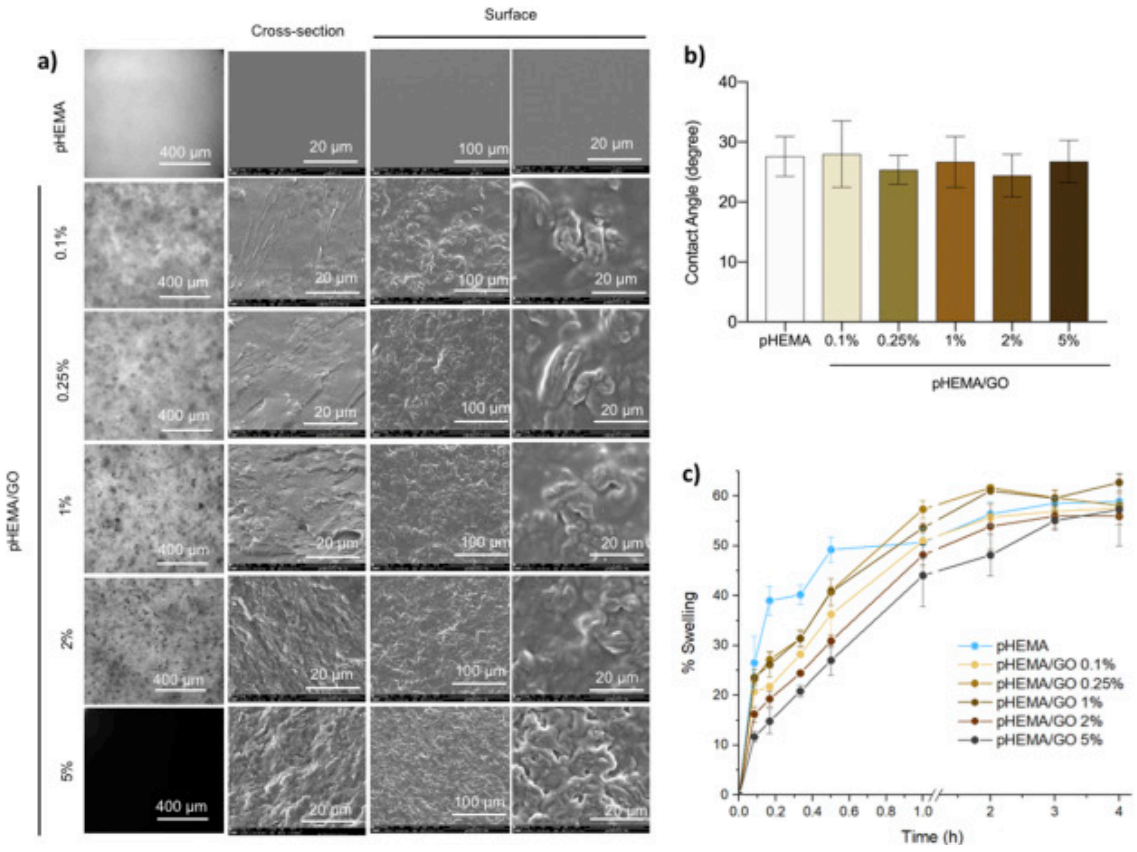

Figure 3 – Characterization of neat pHEMA and pHEMA/GO composites: a) optical microscopy (column 1) and SEM images (column 2-4), b) captive air-bubble contact angles and c) swelling degree in water.

Overall, GO incorporation in pHEMA increases its surface roughness but does not affect its polymerization, surface hydrophilicity, nor swelling capacity.

3.3.3 Mechanical properties of pHEMA/GO composites

Mechanical properties of pHEMA/GO composites were assessed through evaluation of their resistance under tensile and compressive stress. For evaluation of tensile properties, uniaxial tensile tests were proceeded at room temperature using hydrated pHEMA/GO specimens. Fig. S.2 shows the representative tensile stress-strain curves of all pHEMA/GO composites, revealing that they exhibit a linear behavior, indicating an elastic deformation in the entire range of elongation, up to rupture. The obtained curves were analyzed regarding their slope which corresponds to Young's Modulus - YM (stiffness), as well as the maximum values of tensile strength and strain obtained until rupture, which represents the ultimate tensile strength - UTS (tensile resistance) and elongation at break (elasticity), respectively.

Fig. 4a displays the stiffness values of neat pHEMA and pHEMA/GO composites as a function of GO concentration. The YM of pHEMA is around 0.74 MPa. Upon GO incorporation, YM of pHEMA/GO composites shows a quadratic trend as a function of GO concentration.

However, this trend is discontinuous meaning that incorporation of GO even in low amounts (0.1%) has a high impact in stiffness of pHEMA, increasing around 3.1x and allowing YM to achieve 2.1 MPa, above this concentration, YM remains almost unchangeable until 2%. However, for loadings of 5% an abrupt increase in YM is observed reaching values of 6.5 MPa, which are 8.3x higher than neat pHEMA's.

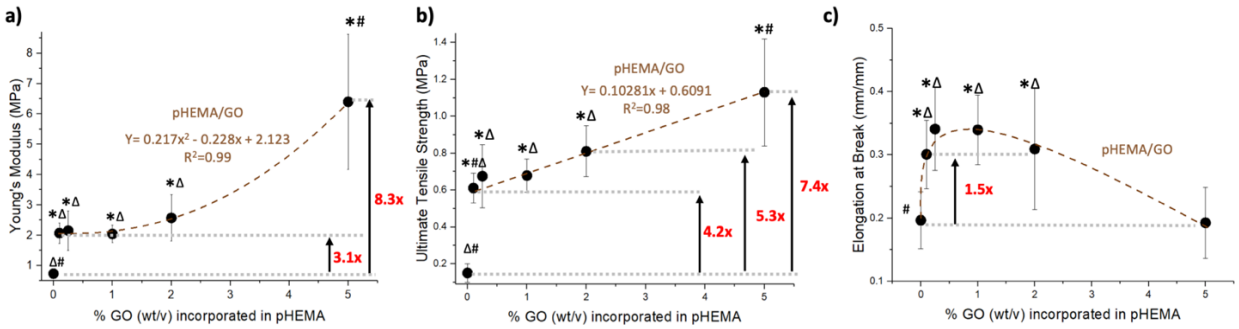

Figure 4 - Mechanical performance of neat pHEMA and pHEMA/GO composites as a function of GO concentration under tensile stress: a) Young's modulus, b) ultimate tensile strength and c) elongation at break. Statistically significantly different from pHEMA (*), pHEMA/GO 2% (#) and pHEMA/GO 5% (Δ) ($p<0.05$ – One Way ANOVA).

Fig. 4b shows the tensile resistance of pHEMA and pHEMA/GO composites. Similar to what was observed for YM, low amounts of GO (0.1–1%) lead to a high increase in UTS from 0.15 MPa to around 0.68 MPa (4.2x). For composites with higher amounts of GO, this effect is surpassed, with the UTS of pHEMA/GO 2% and 5% being 5.3x and 7.4x higher than for pHEMA, respectively.

Contrarily to what was expected, trends of pHEMA/GO YM and UTS as a function of GO concentration are different, revealing that for loadings of GO between 0.1 and 2% the increase in UTS does not reflect an increase in stiffness of composites. This phenomenon can be explained by the rise in polymer elasticity observed for these GO concentrations from 0.2 mm/mm in pHEMA to 0.3 mm/mm in pHEMA/GO (0.1–2%) (Fig. 4c). Such effect was also observed when GO was incorporated in epoxy resin [75], poly(vinyl alcohol) [76] and poly(acrylic acid) [77] matrices. The good dispersion of GO and its interaction with the polymer network have been pointed as the main reasons for this increase in elastic deformation. Thus, we propose that when pHEMA/GO composites are stretched, the GO sheets undergo realignment in the strain direction while maintaining strong attractive interactions with the pHEMA matrix. This allows attaining higher elongations while maintaining the gel's structural integrity. However, for pHEMA/GO 5% the elongation at break is again similar to pHEMA. Despite this considerable improvement of pHEMA elasticity, for some applications such as wearable devices, even higher elasticity may be required [6]. We have shown that decreasing

the concentration of covalent crosslinking agent (TEGDMA) to half in composites with 1% GO (pHEMA/GO ½ TEGDMA) resulted in an elasticity increase of 50% (0.5 mm/mm) with unchanged UTS (0.75) (Table S.1). This effect was reported for poly(acrylic acid) hydrogels, where decreasing the chemical crosslinker in the presence of GO led to an increase in the stretching capability of the hydrogels without affecting their UTS [77].

Several studies have previously reported GBMs as nano-fillers to improve the mechanical properties of materials [6, 33, 61, 78, 79], including hydrogels, as can be seen in Fig. 5. However, the increase found in YM of around 3x upon incorporation of 0.1-2% GO in pHEMA is higher than what was observed for most of GBMs reinforced hydrogels and similar to those reported for GBMs incorporation in polyvinyl alcohol and cellulose (Fig. 5a), despite pHEMA/GO having higher increase in UTS, which could be associated to its rise in elasticity. Moreover, pHEMA/GO (0.1-2%) exhibit the highest relative increase in UTS comparing to all others, except alginate/GO hydrogels, which is similar. For pHEMA/GO 5%, the approximately 8x increase in both YM and UTS are, to our knowledge, unprecedentedly much higher than those obtained for other studies which report GBMs physical incorporation in hydrogels (Fig. 5a). Better compatibility and stronger interaction between oxygen containing functional groups of GO (hydroxyl, ether, ketone and carboxylic) and hydroxyl groups of pHEMA network may explain the notable improvement in the mechanical resistance observed for pHEMA/GO composites. As such, the combined absolute values of YM and UTS of pHEMA/GO 5% hydrogels place them at the top of the most stiff and strong GBMs containing hydrogels, right after chitosan/GO or G, polyacrylamide/GO and cellulose/G or GO (Fig. 5b).

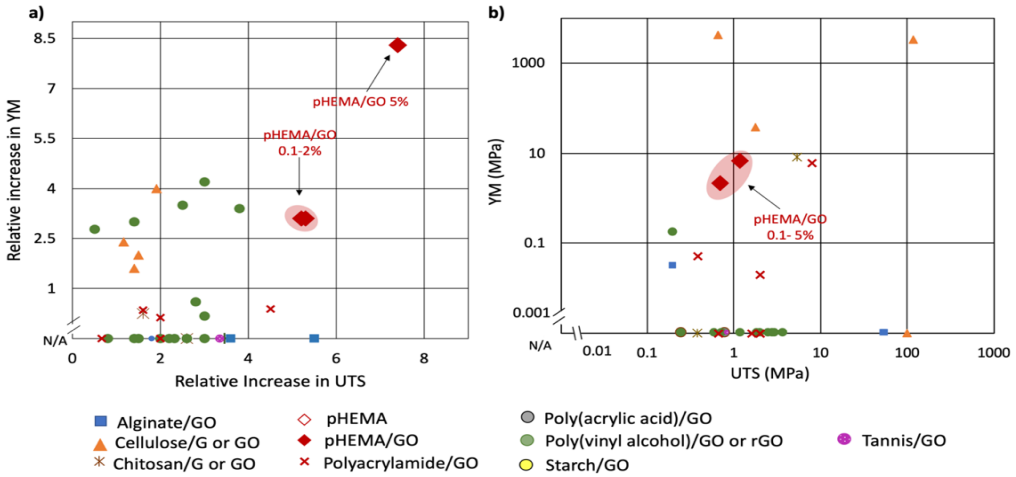

Figure 5 – Comparison of pHEMA/GO hydrogels with previous studies reporting GBMs physical incorporation in hydrogels regarding relative increase towards the neat hydrogel (a) or absolute values of stiffness and tensile strength (b). The polymers used in these studies are alginate [80, 81], bacterial cellulose [82-84], chitosan [85, 86], hydroxyethyl cellulose [87, 88], polyacrylamide [89-93], poly(acrylic acid) [94, 95], polyvinyl alcohol [76, 96-105], tannins [106], silk [107, 108], startch/polyacrylamide [109].

pHEMA/GO specimens with cylindrical shape were used to evaluate their stiffness under compressive stress. Fig. 6 demonstrates that YM of pHEMA/GO composites shows a quadratic trend as a function of GO concentration. This similar behavior is similar to the one obtained for pHEMA/GO YM under tension. However, in this case, incorporation of 0.1% GO did not statistically affect pHEMA's YM. A statistically significant increase in stiffness is observed upon incorporation of at least 2% GO, being the YM 2x higher than in pHEMA, reaching values of 1.60 MPa. For pHEMA/GO 5% the increase in YM is more prominent from 0.90 to 3.79 MPa (4.3x).

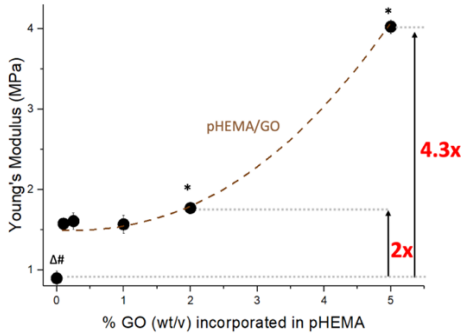

Figure 6 - Young's modulus under compressive stress of neat pHEMA and pHEMA/GO composites as a function of GO concentration. Statistically significantly different from pHEMA (*), pHEMA/GO 2% (#) and pHEMA/GO 5% (Δ) ($p<0.05$ – One Way ANOVA).

As general discussion, the reinforced hydrogels prepared in this work (YM between 2.1 – 6.5 MPa and UTS 0.7-1.2 MPa) are stiffer and stronger than the most commonly used native hydrogels, such as alginate [110], polyvinyl alcohol [111] and acrylamide [112], which have YM and UTS of only around a few hundred kPa [78, 112-115]. pHEMA/GO composites are even stiffer than hydrogels described in literature as having high stiffness, such as most of the nanofillers-reinforced hydrogels (containing TiO_2, nanoclay, silica and carbon nanotubes) [116-119], interpenetrating networking hydrogels (including double networking hydrogels) [109, 120-123], Fe^{3+} crosslinked hydrogels [124], double hydrogen bonding hydrogel [125] and hydrogels with dual physical interactions of dipole–dipole pairings and hydrogen bonding [126], which present YM values between 1-5 MPa. Tensile resistance of pHEMA/GO composites is similar to some double networking hydrogels such as polyacrylamide/alginate-Ca^{2+} [127], hybrid pectin-Fe^{3+}/polyacrylamide [121], gelatin/polyacrylamide [128] and polyacrylic acid-quaternized cellulose/poly(vinyl alcohol) [129]. Although a few other hydrogels exhibiting higher YM and UTS than pHEMA/GO composites (in the order of 10-200 MPa) [130-137], the processes to obtain these materials are much more time consuming, requiring multiple steps and harsher conditions than the simple *in-situ* incorporation of GO as a filler, which would be reflected in production costs. Mechanical properties of pHEMA/GO composites are also

comparable to several well-known materials. The composites with lower amounts of GO (0.1 to 2%) under tensile stress are similar to cork [138], specifically regarding tensile resistance, although elongation at break is 2x higher. pHEMA/GO 5% is stiffer (under compressive and tensile stress) and more resistant to tensile stress, reaching values of YM similar to polydimethylsiloxane (PDMS) [139], cartilage [140], intervertebral disc [141] or arteries walls [140] and UTS similar to polyurethane rigid foams [142].

3.3.4 Cytocompatibility of pHEMA/GO composites

Cytocompatibility of the pHEMA/GO composites was evaluated *in vitro* by measuring the effect of materials' extracts towards a cell line of mouse fibroblasts (NIH 3T3 cells). Fig. 7 displays metabolic activity of NIH 3T3 cells upon 24 h in contact with materials' extracts using cell medium as extraction vehicle. The metabolic activity of cells in contact with pHEMA/GO 0.1% - 5% hydrogels extracts rounds the 100 % and there are no statistically significant differences between these concentrations, nor comparing with the control (cells with extracts without material). As such, these results show that none of the obtained extracts affects the metabolic activity of the cells, confirming the lack of cytotoxicity.

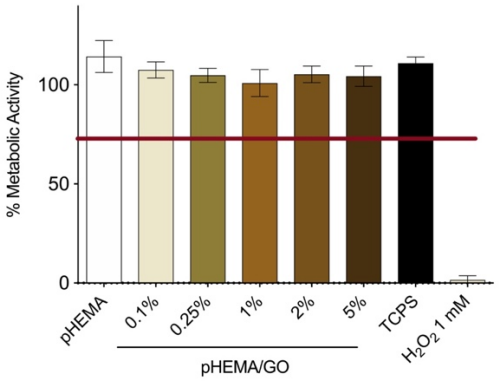

Figure 7 - Metabolic activity of NIH 3T3 cells after incubation with materials extracts (using DMEM+ as extraction vehicle) during 24 h. Metabolic activity is represented as a percentage of the cell metabolic activity of treated cells in relation to cells in DMEM+ only (100%). Extracts of TCPET discs were used as positive control while a solution of 1 mM H_2O_2 in DMEM+ was used as negative control of cell growth. According to ISO 10993-5:2009(E), 70% of metabolic activity is the lower limit to consider the material extracts cytotoxic (red line).

Even though some biological applications are often suggested for several reinforced hydrogels, most of the studies have not performed the necessary biological characterization to validate their use. The herein described *in vitro* biocompatibility of pHEMA/GO hydrogels opens a wide range of possibilities for biomedical applications.

Until now, neat pHEMA has been applied and studied in the development of contact lenses [143], keratoprosthesis [143], drug delivery systems [143], wearable devices to stimulate wound healing [143], soft tissues [143], and coatings for implantable devices (such as orthopedic, catheters, etc) [31]. Taking into account the great improvement in stiffness and tensile resistance, without affecting the intrinsic characteristics of pHEMA, the new composites herein reported will pave the way for new applications of this polymer. Regarding the biomedical field, pHEMA/GO composites could be potentially applied in engineering of load-bearing tissues, such as cartilage, intervertebral disc, blood vessels, cardiac valves and in the design of innovative implantable devices such as catheters, vascular grafts, diaphragm materials in surgeries and hernia repair devices. Uses in other areas can also be envisaged, like in soft robotics, packaging, sealing and even as sensors.

3.4 Conclusions

Incorporation of graphene oxide in pHEMA matrix via *in situ* polymerization produced novel stiff and strong hydrogels with the same swelling capacity and surface chemistry as the pristine polymer. Mechanical properties of these materials depend on GO concentration in the polymer matrix. The most considerable improvements were achieved for 5% GO, with YM and UTS values attaining 6.50 MPa and 1.14 MPa, being 8.3x and 7.4x higher than pristine pHEMA, respectively. This magnitude of improvement was never before described for hydrogels containing GBMs. The elasticity of pHEMA/GO composites can also be tuned through the amount of GO and/or crosslinking agent incorporated in hydrogels formulation. All pHEMA/GO composites were cytocompatible, which opens a wide range of biological applications. Hence, these new materials suppress the mechanical limitations associated to pHEMA, allowing its use in several load-bearing applications that otherwise could not be envisaged.

3.5 Acknowledgements

Authors wish to thank Artur M Pinto from LEPABE for the assistance in tensile mechanical analysis, Maria Lazaro from Bioimaging unit of INEB/i3S, member of the PPBI (PPBI–POCI-01-0145-FEDER-022122) for the assistance in Raman studies, Ricardo Vidal from Biointerfaces and Nanotechnology of INEB/i3S for the assistance in FTIR and contact angle analysis, Rui Fernandes from Histology and Electron Microscopy of IBMC/i3S for the assistance in TEM analysis and Rui Rocha from CEMUP for the assistance in SEM analysis.

Authors acknowledge financial support from Fundação para a Ciência e a Tecnologia (FCT) and Fundo Europeu de Desenvolvimento Regional for PhD grants PD/BD/114156/2016 and SFRH/BD/120154/2016, Research position grant IF/01479/2015, projects POCI-01-0145-FEDER-032431, POCI-01-0145-FEDER-006939, POCI-01-0145-FEDER-007274, NORTE-

01-0145-FEDER-000012, PTDC/CTM-COM/32431/2017 and PTDC/CTM-BIO/4033/2014, and UID/EQU/00511/2019 – LEPABE funded by national funds through FCT/MCTES (PIDDAC).

3.6 References

[1] O. Wichterle, D. LÍM, Hydrophilic Gels for Biological Use, Nature 185(4706) (1960) 117-118.

[2] E. Caló, V.V. Khutoryanskiy, Biomedical applications of hydrogels: A review of patents and commercial products, Eur Polym J 65 (2015) 252-267.

[3] A. Alam, Y.J. Zhang, H.C. Kuan, S.H. Lee, J. Ma, Polymer composite hydrogels containing carbon nanomaterials-Morphology and mechanical and functional performance, Progress in Polymer Science 77 (2018) 1-18.

[4] L. Ionov, Hydrogel-based actuators: possibilities and limitations, Mater Today 17(10) (2014) 494-503.

[5] M.L. Oyen, Mechanical characterisation of hydrogel materials, Int Mat Rev 59(1) (2013) 44-59.

[6] A. Alam, Y. Zhang, H.-C. Kuan, S.-H. Lee, J. Ma, Polymer composite hydrogels containing carbon nanomaterials—Morphology and mechanical and functional performance, Progress in Polymer Science 77 (2018) 1-18.

[7] J.Y. Sun, X. Zhao, W.R. Illeperuma, O. Chaudhuri, K.H. Oh, D.J. Mooney, J.J. Vlassak, Z. Suo, Highly stretchable and tough hydrogels, Nature 489(7414) (2012) 133-6.

[8] M.L. Oyen, Mechanical characterisation of hydrogel materials, Int Mat Rev 59(1) (2014) 44-59.

[9] F.B. Li, G.Z. Zhang, Y.H. Xia, Z.S. Wang, H.Y. Jiang, X.Q. Feng, Y.Q. Zhang, M.J. Liu, H.J. Li, Hierarchically crosslinked ionic nanocomposite hydrogels with ultrahigh mechanical properties for underwater bioinspired capturing device, Compos Sci Technol 165 (2018) 339-346.

[10] J.P. Gong, Y. Katsuyama, T. Kurokawa, Y. Osada, Double-network hydrogels with extremely high mechanical strength, Adv Mater 15(14) (2003) 1155-+.

[11] T. Nonoyama, S. Wada, R. Kiyama, N. Kitamura, M.T. Mredha, X. Zhang, T. Kurokawa, T. Nakajima, Y. Takagi, K. Yasuda, J.P. Gong, Double-Network Hydrogels Strongly Bondable to Bones by Spontaneous Osteogenesis Penetration, Adv Mater 28(31) (2016) 6740-5.

[12] M.L. Oyen, Mechanical characterisation of hydrogel materials, Int Mater Rev 59(1) (2014) 44-59.

[13] Y. Bu, H. Shen, F. Yang, Y. Yang, X. Wang, D. Wu, Construction of Tough, in Situ Forming Double-Network Hydrogels with Good Biocompatibility, Acs Appl Mater Inter 9(3) (2017) 2205-2212.

[14] X. Yan, J. Yang, F. Chen, L. Zhu, Z. Tang, G. Qin, Q. Chen, G. Chen, Mechanical properties of gelatin/polyacrylamide/graphene oxide nanocomposite double-network hydrogels, Compos Sci Technol 163 (2018) 81-88.

[15] C. Sealy, Graphene oxide makes rubber stronger, Mater Today 20(7) (2017) 342-343.

[16] J. Yang, C. Han, Mechanically Viscoelastic Properties of Cellulose Nanocrystals Skeleton Reinforced Hierarchical Composite Hydrogels, Acs Appl Mater Inter 8(38) (2016) 25621-30.

[17] J. Yang, C.R. Han, J.F. Duan, F. Xu, R.C. Sun, Mechanical and viscoelastic properties of cellulose nanocrystals reinforced poly(ethylene glycol) nanocomposite hydrogels, Acs Appl Mater Inter 5(8) (2013) 3199-207.

[18] K. Shi, Z. Liu, Y.Y. Wei, W. Wang, X.J. Ju, R. Xie, L.Y. Chu, Near-Infrared Light-Responsive Poly(N-isopropylacrylamide)/Graphene Oxide Nanocomposite Hydrogels with Ultrahigh Tensibility, Acs Appl Mater Inter 7(49) (2015) 27289-98.

[19] X. Yu, H. Cheng, M. Zhang, Y. Zhao, L. Qu, G. Shi, Graphene-based smart materials, Nature Reviews Materials 2 (2017) 17046.

[20] A. Khoushabi, C.S. Wyss, B. Caglar, D. Pioletti, P.E. Bourbon, Tailoring swelling to control softening mechanisms during cyclic loading of PEG/cellulose hydrogel composites, Compos Sci Technol 168 (2018) 88-95.

[21] A.C. Borges, P.E. Bourban, D.P. Pioletti, J.A.E. Manson, Curing kinetics and mechanical properties of a composite hydrogel for the replacement of the nucleus pulposus, Compos Sci Technol 70(13) (2010) 1847-1853.

[22] K.Y. Lee, Y. Aitomaki, L.A. Berglund, K. Oksman, A. Bismarck, On the use of nanocellulose as reinforcement in polymer matrix composites, Compos Sci Technol 105 (2014) 15-27.

[23] Z.K. Yang, A.D. Qiu, J. Ma, M.Q. Chen, Conducting alpha-Fe2O3 nanorod/polyaniline/CNT gel framework for high performance anodes towards supercapacitors, Compos Sci Technol 156 (2018) 231-237.

[24] M.M. Rahman, A.N. Netravali, Oriented bacterial cellulose-soy protein based fully 'green' nanocomposites, Compos Sci Technol 136 (2016) 85-93.

[25] Z. Zhao, R. Fang, Q. Rong, M. Liu, Bioinspired Nanocomposite Hydrogels with Highly Ordered Structures, Adv Mater 29(45) (2017) 1703045.

[26] A.M.S. Costa, J.F. Mano, Extremely strong and tough hydrogels as prospective candidates for tissue repair – A review, Eur Polym J 72 (2015) 344-364.

[27] G.E. Giammanco, B. Carrion, R.M. Coleman, A.D. Ostrowski, Photoresponsive Polysaccharide-Based Hydrogels with Tunable Mechanical Properties for Cartilage Tissue Engineering, Acs Appl Mater Inter 8(23) (2016) 14423-9.
[28] A. Vedadghavami, F. Minooei, M.H. Mohammadi, S. Khetani, A. Rezaei Kolahchi, S. Mashayekhan, A. Sanati-Nezhad, Manufacturing of hydrogel biomaterials with controlled mechanical properties for tissue engineering applications, Acta Biomater 62 (2017) 42-63.
[29] A.M.S. Costa, J.F. Mano, Extremely strong and tough hydrogels as prospective candidates for tissue repair – A review, European Polymer Journal 72 (2015) 344-364.
[30] J.-P. Montheard, M. Chatzopoulos, D. Chappard, 2-Hydroxyethyl Methacrylate (HEMA): Chemical Properties and Applications in Biomedical Fields, J Macromol Sci R M C 32(1) (1992) 1-34.
[31] L. Indolfi, F. Causa, P.A. Netti, Coating process and early stage adhesion evaluation of poly(2-hydroxy-ethyl-methacrylate) hydrogel coating of 316L steel surface for stent applications, Journal of materials science. Materials in medicine 20(7) (2009) 1541-51.
[32] J.-P. Montheard, M. Chatzopoulos, D. Chappard, 2-Hydroxyethyl Methacrylate (HEMA): Chemical Properties and Applications in Biomedical Fields, J Macromol Sci R M C 32(1) (1992) 1-34.
[33] D.G. Papageorgiou, I.A. Kinloch, R.J. Young, Mechanical properties of graphene and graphene-based nanocomposites, Progress in Materials Science 90 (2017) 75-127.
[34] C. Pan, L. Liu, G. Gai, Recent Progress of Graphene-Containing Polymer Hydrogels: Preparations, Properties, and Applications, Macromol Mater Eng 302(10) (2017) 1700184-n/a.
[35] H. Kim, R. Jalili, G.M. Spinks, G.G. Wallace, S.J. Kim, High-strength graphene and polyacrylonitrile composite fiber enhanced by surface coating with polydopamine, Compos Sci Technol 149 (2017) 280-285.
[36] D. Liu, Q.B. Bian, Y. Li, Y.R. Wang, A.M. Xiang, H.F. Tian, Effect of oxidation degrees of graphene oxide on the structure and properties of poly (vinyl alcohol) composite films, Compos Sci Technol 129 (2016) 146-152.
[37] S.D. Jiang, Z.M. Bai, G. Tang, Y. Hu, L. Song, Fabrication and characterization of graphene oxide-reinforced poly(vinyl alcohol)-based hybrid composites by the sol-gel method, Compos Sci Technol 102 (2014) 51-58.
[38] A. Kumar, K.M. Rao, S.S. Han, Mechanically viscoelastic nanoreinforced hybrid hydrogels composed of polyacrylamide, sodium carboxymethylcellulose, graphene oxide, and cellulose nanocrystals, Carbohyd Polym 193 (2018) 228-238.
[39] A. Kumar, S.M. Zo, J.H. Kim, S.C. Kim, S.S. Han, Enhanced physical, mechanical, and cytocompatibility behavior of polyelectrolyte complex hydrogels by reinforcing halloysite nanotubes and graphene oxide, Compos Sci Technol 175 (2019) 35-45.

[40] Z. Sun, L. Zhao, C. Liu, Y. Zhen, W. Zhang, J. Ma, A novel 3D adsorbent of reduced graphene oxide-β-cyclodextrin aerogel coupled hardness with softness for efficient removal of bisphenol A, Chem Eng J 372 (2019) 896-904.
[41] R. Scaffaro, A. Maio, F. Lopresti, D. Giallombardo, L. Botta, M.L. Bondi, S. Agnello, Synthesis and self-assembly of a PEGylated-graphene aerogel, Compos Sci Technol 128 (2016) 193-200.
[42] F. Xue, X. He, S. Cai, J. Nie, Z. Shi, X. Wang, Synergistic effect of graphene oxide and sodium carboxymethylcellulose on the properties of poly(vinyl alcohol) hydrogels, J Appl Polym Sci 136(24) (2019).
[43] H. Li, C. Sun, H. Liu, J. Li, D. Wang, P. Zhang, T. Liu, A. Yang, Aerogels fabricated with origami graphene part I: Preparation and mechanical behavior, J Alloys Compd 783 (2019) 486-493.
[44] C. Li, M. Ding, B. Zhang, X. Qiao, C.Y. Liu, Graphene aerogels that withstand extreme compressive stress and strain, Nanoscale 10(38) (2018) 18291-18299.
[45] W. Gao, N. Zhao, W. Yao, Z. Xu, H. Bai, C. Gao, Effect of flake size on the mechanical properties of graphene aerogels prepared by freeze casting, Rsc Adv 7(53) (2017) 33600-33605.
[46] A.M. Pinto, I.C. Goncalves, F.D. Magalhaes, Graphene-based materials biocompatibility: a review, Colloids and Surfaces B: Biointerfaces 111 (2013) 188-202.
[47] A.M. Pinto, C. Gonçalves, D.M. Sousa, A.R. Ferreira, J.A. Moreira, I.C. Gonçalves, F.D. Magalhães, Smaller particle size and higher oxidation improves biocompatibility of graphene-based materials, Carbon 99 (2016) 318-329.
[48] B. Fadeel, C. Bussy, S. Merino, E. Vazquez, E. Flahaut, F. Mouchet, L. Evariste, L. Gauthier, A.J. Koivisto, U. Vogel, C. Martin, L.G. Delogu, T. Buerki-Thurnherr, P. Wick, D. Beloin-Saint-Pierre, R. Hischier, M. Pelin, F. Candotto Carniel, M. Tretiach, F. Cesca, F. Benfenati, D. Scaini, L. Ballerini, K. Kostarelos, M. Prato, A. Bianco, Safety Assessment of Graphene-Based Materials: Focus on Human Health and the Environment, ACS Nano 12(11) (2018) 10582-10620.
[49] C.M. Girish, A. Sasidharan, G.S. Gowd, S. Nair, M. Koyakutty, Confocal Raman imaging study showing macrophage mediated biodegradation of graphene in vivo, Adv Healthc Mater 2(11) (2013) 1489-500.
[50] J.H. Liu, S.T. Yang, H. Wang, Y. Chang, A. Cao, Y. Liu, Effect of size and dose on the biodistribution of graphene oxide in mice, Nanomedicine (Lond) 7(12) (2012) 1801-12.
[51] S.P. Mukherjee, A.R. Gliga, B. Lazzaretto, B. Brandner, M. Fielden, C. Vogt, L. Newman, A.F. Rodrigues, W. Shao, P.M. Fournier, M.S. Toprak, A. Star, K. Kostarelos, K. Bhattacharya, B. Fadeel, Graphene oxide is degraded by neutrophils and the degradation products are non-genotoxic, Nanoscale 10(3) (2018) 1180-1188.

[52] D.C. Marcano, D.V. Kosynkin, J.M. Berlin, A. Sinitskii, Z. Sun, A. Slesarev, L.B. Alemany, W. Lu, J.M. Tour, Improved synthesis of graphene oxide, ACS Nano 4(8) (2010) 4806-14.
[53] A.M. Pinto, S. Moreira, I.C. Goncalves, F.M. Gama, A.M. Mendes, F.D. Magalhaes, Biocompatibility of poly(lactic acid) with incorporated graphene-based materials, Colloids Surf B Biointerfaces 104 (2013) 229-238.
[54] I.C. Goncalves, M.C. Martins, M.A. Barbosa, B.D. Ratner, Protein adsorption and clotting time of pHEMA hydrogels modified with C18 ligands to adsorb albumin selectively and reversibly, Biomaterials 30(29) (2009) 5541-51.
[55] S. International, Standard Test Method for Tensile Properties of Thin Plastic Sheeting, (2002).
[56] I.S. Organization, ISO 10993-12:2012: Biological evaluation of medical devices, Part 12: Sample preparation and reference materials, (2012).
[57] I.S. Organization, ISO 10993-5. Biological evaluation of medical devices, Part 5: Tests for in vitro cytotoxicity, (2009).
[58] A.M. Pinto, S. Moreira, I.C. Goncalves, F.M. Gama, A.M. Mendes, F.D. Magalhaes, Biocompatibility of poly(lactic acid) with incorporated graphene-based materials, Colloid Surface B 104 (2013) 229-238.
[59] A. Maio, R. Scaffaro, L. Lentini, A.P. Piccionello, I. Pibiri, Perfluorocarbons-graphene oxide nanoplatforms as biocompatible oxygen reservoirs, Chem Eng J 334 (2018) 54-65.
[60] Y. Wei, X.Y. Hu, Q.R. Jiang, Z.Y. Sun, P.F. Wang, Y.P. Qiu, W.S. Liu, Influence of graphene oxide with different oxidation levels on the properties of epoxy composites, Compos Sci Technol 161 (2018) 74-84.
[61] Y. Wei, X. Hu, Q. Jiang, Z. Sun, P. Wang, Y. Qiu, W. Liu, Influence of graphene oxide with different oxidation levels on the properties of epoxy composites, Compos Sci Technol 161 (2018) 74-84.
[62] A. Maio, R. Scaffaro, L. Lentini, A. Palumbo Piccionello, I. Pibiri, Perfluorocarbons–graphene oxide nanoplatforms as biocompatible oxygen reservoirs, Chemical Engineering Journal 334 (2018) 54-65.
[63] B.D. Ossonon, D. Bélanger, Synthesis and characterization of sulfophenyl-functionalized reduced graphene oxide sheets, Rsc Adv 7(44) (2017) 27224-27234.
[64] R. Scaffaro, A. Maio, G. Lo Re, A. Parisi, A. Busacca, Advanced piezoresistive sensor achieved by amphiphilic nanointerfaces of graphene oxide and biodegradable polymer blends, Compos Sci Technol 156 (2018) 166-176.
[65] A.C. Ferrari, D.M. Basko, Raman spectroscopy as a versatile tool for studying the properties of graphene, Nature Nanotechnology 8(4) (2013) 235-246.

[66] R. Scaffaro, A. Maio, G. Lo Re, A. Parisi, A. Busacca, Advanced piezoresistive sensor achieved by amphiphilic nanointerfaces of graphene oxide and biodegradable polymer blends, Composites Science and Technology 156 (2018) 166-176.
[67] S. Stankovich, D.A. Dikin, R.D. Piner, K.A. Kohlhaas, A. Kleinhammes, Y. Jia, Y. Wu, S.T. Nguyen, R.S. Ruoff, Synthesis of graphene-based nanosheets via chemical reduction of exfoliated graphite oxide, Carbon 45(7) (2007) 1558-1565.
[68] D. Liu, Q.B. Bian, Y. Li, Y.R. Wang, A.M. Xiang, H.F. Tian, Effect of oxidation degrees of graphene oxide on the structure and properties of poly (vinyl alcohol) composite films, Compos Sci Technol 129 (2016) 146-152.
[69] A. Bertoluzza, P. Monti, J.V. Garcia-Ramos, R. Simoni, R. Caramazza, A. Calzavara, Applications of Raman spectroscopy to the ophthalmological field : Raman spectra of soft contact lenses made of poly-2-hydroxyethylmethacrylate (PHEMA), Journal of Molecular Structure 143 (1986) 469-472.
[70] K. Mimura, M. Moriya, W. Sakamoto, T. Yogo, Synthesis of BaTiO3 nanoparticle/poly(2-hydroxyethyl methacrylate) hybrid nanofibers via electrospinning, Compos Sci Technol 70(3) (2010) 492-497.
[71] C.W. Huang, Y.M. Sun, W.F. Huang, Polymerization Kinetics of Poly(2-Hydroxyethyl Methacrylate) Hydrogels and Nanocomposite Materials, J Polym Sci Pol Chem 5(4) (2017) 1873-1889.
[72] B. Singh, B. Singh, Influence of graphene-oxide nanosheets impregnation on properties of sterculia gum-polyacrylamide hydrogel formed by radiation induced polymerization, Int J Biol Macromol 99 (2017) 699-712.
[73] N. Mahmoudi, F. Ostadhossein, A. Simchi, Physicochemical and antibacterial properties of chitosan-polyvinylpyrrolidone films containing self-organized graphene oxide nanolayers, Journal of Applied Polymer Science 133(11) (2016) n/a-n/a.
[74] A.S. Hoffman, Hydrogels for biomedical applications, Ann N Y Acad Sci 944 (2001) 62-73.
[75] S.I. Abdullah, M.N.M. Ansari, Mechanical properties of graphene oxide (GO)/epoxy composites, HBRC Journal 11(2) (2019) 151-156.
[76] J. Chen, X. Shi, L. Ren, Y. Wang, Graphene oxide/PVA inorganic/organic interpenetrating hydrogels with excellent mechanical properties and biocompatibility, Carbon 111 (2017) 18-27.
[77] J. Shen, B. Yan, T. Li, Y. Long, N. Li, M. Ye, Mechanical, thermal and swelling properties of poly(acrylic acid)–graphene oxide composite hydrogels, Soft Matter 8(6) (2012) 1831-1836.
[78] C. Pan, L. Liu, G. Gai, Recent Progress of Graphene-Containing Polymer Hydrogels: Preparations, Properties, and Applications, Macromolecular Materials and Engineering 302(10) (2017) 1700184-n/a.

[79] X. Zhang, J. Zheng, H.M. Fang, Y.F. Zhang, S.L. Bai, G.S. He, Al2O3/graphene reinforced bio-inspired interlocking polyurethane composites with superior mechanical and thermal properties for solid propulsion fuel, Compos Sci Technol 167 (2018) 42-52.
[80] Á. Serrano-Aroca, L. Iskandar, S. Deb, Green synthetic routes to alginate-graphene oxide composite hydrogels with enhanced physical properties for bioengineering applications, Eur Polym J 103 (2018) 198-206.
[81] Q. Huang, S. Liu, K. Li, I. Hussain, F. Yao, G. Fu, Sodium Alginate/Carboxyl-Functionalized Graphene Composite Hydrogel Via Neodymium Ions Coordination, Journal of Materials Science & Technology 33(8) (2017) 821-826.
[82] H. Luo, J. Dong, X. Xu, J. Wang, Z. Yang, Y. Wan, Exploring excellent dispersion of graphene nanosheets in three-dimensional bacterial cellulose for ultra-strong nanocomposite hydrogels, Composites Part A: Applied Science and Manufacturing 109 (2018) 290-297.
[83] H. Si, H. Luo, G. Xiong, Z. Yang, S.R. Raman, R. Guo, Y. Wan, One-step in situ biosynthesis of graphene oxide-bacterial cellulose nanocomposite hydrogels, Macromolecular rapid communications 35(19) (2014) 1706-11.
[84] J.M. Malho, P. Laaksonen, A. Walther, O. Ikkala, M.B. Linder, Facile method for stiff, tough, and strong nanocomposites by direct exfoliation of multilayered graphene into native nanocellulose matrix, Biomacromolecules 13(4) (2012) 1093-9.
[85] S. Sayyar, E. Murray, B.C. Thompson, J. Chung, D.L. Officer, S. Gambhir, G.M. Spinks, G.G. Wallace, Processable conducting graphene/chitosan hydrogels for tissue engineering, Journal of Materials Chemistry B 3(3) (2015) 481-490.
[86] Y. Zhang, M. Zhang, H. Jiang, J. Shi, F. Li, Y. Xia, G. Zhang, H. Li, Bio-inspired layered chitosan/graphene oxide nanocomposite hydrogels with high strength and pH-driven shape memory effect, Carbohyd Polym 177 (2017) 116-125.
[87] Z. Zhang, R. Yang, Novel nanocomposites based on hydroxyethyl cellulose and graphene oxide, Fibers Polym 18(2) (2017) 334-341.
[88] Y. Bai, X. Chen, A fast water-induced shape memory polymer based on hydroxyethyl cellulose/graphene oxide composites, Composites Part A: Applied Science and Manufacturing 103 (2017) 9-16.
[89] P. Zhu, Y. Deng, C. Wang, Graphene/cyclodextrin-based nanocomposite hydrogel with enhanced strength and thermo-responsive ability, Carbohydrate Polymers 174 (2017) 804-811.
[90] R. Liu, S. Liang, X.-Z. Tang, D. Yan, X. Li, Z.-Z. Yu, Tough and highly stretchable graphene oxide/polyacrylamide nanocomposite hydrogels, Journal of Materials Chemistry 22(28) (2012) 14160-14167.

[91] C. Pan, L. Liu, Q. Chen, Q. Zhang, G. Guo, Tough, Stretchable, Compressive Novel Polymer/Graphene Oxide Nanocomposite Hydrogels with Excellent Self-Healing Performance, ACS Applied Materials & Interfaces 9(43) (2017) 38052-38061.

[92] J. Liu, G. Song, C. He, H. Wang, Self-healing in tough graphene oxide composite hydrogels, Macromolecular rapid communications 34(12) (2013) 1002-7.

[93] J.M. Gonzalez-Dominguez, C. Martin, O.J. Dura, S. Merino, E. Vazquez, Smart Hybrid Graphene Hydrogels: A Study of the Different Responses to Mechanical Stretching Stimulus, ACS Appl Mater Interfaces 10(2) (2018) 1987-1995.

[94] M. Zhong, Y.-T. Liu, X.-M. Xie, Self-healable, super tough graphene oxide–poly(acrylic acid) nanocomposite hydrogels facilitated by dual cross-linking effects through dynamic ionic interactions, Journal of Materials Chemistry B 3(19) (2015) 4001-4008.

[95] S. Faghihi, A. Karimi, M. Jamadi, R. Imani, R. Salarian, Graphene oxide/poly(acrylic acid)/gelatin nanocomposite hydrogel: Experimental and numerical validation of hyperelastic model, Materials science & engineering. C, Materials for biological applications 38 (2014) 299-305.

[96] L. Jing, H. Li, R.Y. Tay, B. Sun, S.H. Tsang, O. Cometto, J. Lin, E.H.T. Teo, A.I.Y. Tok, Biocompatible Hydroxylated Boron Nitride Nanosheets/Poly(vinyl alcohol) Interpenetrating Hydrogels with Enhanced Mechanical and Thermal Responses, ACS Nano 11(4) (2017) 3742-3751.

[97] N.-T. Nguyen, J.-H. Liu, A green method for in situ synthesis of poly(vinyl alcohol)/chitosan hydrogel thin films with entrapped silver nanoparticles, J Taiwan Inst Chem E 45(5) (2014) 2827-2833.

[98] Y. Meng, L. Ye, P. Coates, P. Twigg, In Situ Cross-Linking of Poly(vinyl alcohol)/Graphene Oxide–Polyethylene Glycol Nanocomposite Hydrogels as Artificial Cartilage Replacement: Intercalation Structure, Unconfined Compressive Behavior, and Biotribological Behaviors, The Journal of Physical Chemistry C 122(5) (2018) 3157-3167.

[99] B. Zhang, S. Xu, H. Tang, P. Wu, Crosslinked acetylacetonated poly(vinyl alcohol-co-vinyl acetate) nanocomposites with graphene oxide and reduced graphene oxide: a new way to modify the property of nanocomposites, Rsc Adv 3(22) (2013) 8372-8379.

[100] L. Zhang, Z. Wang, C. Xu, Y. Li, J. Gao, W. Wang, Y. Liu, High strength graphene oxide/polyvinyl alcohol composite hydrogels, J Mater Chem 21(28) (2011) 10399-10406.

[101] X. Rui-Hong, R. Peng-Gang, H. Jian, R. Fang, R. Lian-Zhen, S. Zhen-Feng, Preparation and properties of graphene oxide-regenerated cellulose/polyvinyl alcohol hydrogel with pH-sensitive behavior, Carbohydrate Polymers 138 (2016) 222-8.

[102] Q. Luo, Y. Shan, X. Zuo, J. Liu, Anisotropic tough poly(vinyl alcohol)/graphene oxide nanocomposite hydrogels for potential biomedical applications, RSC Advances 8(24) (2018) 13284-13291.

[103] C. Shuai, P. Feng, C. Gao, X. Shuai, T. Xiao, S. Peng, Graphene oxide reinforced poly(vinyl alcohol): nanocomposite scaffolds for tissue engineering applications, Rsc Adv 5(32) (2015) 25416-25423.
[104] Y. Huang, M. Zhang, W. Ruan, High-water-content graphene oxide/polyvinyl alcohol hydrogel with excellent mechanical properties, J. Mater. Chem. A 2(27) (2014) 10508-10515.
[105] Y. Shi, D. Xiong, J. Li, N. Wang, The water-locking and cross-linking effects of graphene oxide on the load-bearing capacity of poly(vinyl alcohol) hydrogel, RSC Adv 6(86) (2016) 82467-82477.
[106] Q. Guo, Z. Shi, H. Xu, X. Ma, J. Yin, M. Tian, Fabrication of Super Extensible and Highly Tough Graphene Composite Hydrogels by Thermal Treatment Strategy for the Mixture of Tannin and Graphene Oxide, Macromolecular Chemistry and Physics 218(6) (2017) 1600549.
[107] L. Wang, C. Lu, B. Zhang, B. Zhao, F. Wu, S. Guan, Fabrication and characterization of flexible silk fibroin films reinforced with graphene oxide for biomedical applications, Rsc Adv 4(76) (2014) 40312-40320.
[108] L. Huang, C. Li, W. Yuan, G. Shi, Strong composite films with layered structures prepared by casting silk fibroin-graphene oxide hydrogels, Nanoscale 5(9) (2013) 3780-6.
[109] A.M. Nzenguet, M. Aqlil, Y. Essamlali, O. Amadine, A. Snik, M. Larzek, M. Zahouily, Novel bionanocomposite films based on graphene oxide filled starch/polyacrylamide polymer blend: structural, mechanical and water barrier properties, J Polym Res 25(4) (2018) 86.
[110] G. Kaklamani, D. Cheneler, L.M. Grover, M.J. Adams, J. Bowen, Mechanical properties of alginate hydrogels manufactured using external gelation, J Mech Behav Biomed 36 (2014) 135-42.
[111] W.K. Wan, G. Campbell, Z.F. Zhang, A.J. Hui, D.R. Boughner, Optimizing the tensile properties of polyvinyl alcohol hydrogel for the construction of a bioprosthetic heart valve stent, J Biomed Mater Res 63(6) (2002) 854-861.
[112] M.L. Oyen, Mechanical characterisation of hydrogel materials, Int Mat Rev 59(1) (2013) 44-59.
[113] J. Li, W.R.K. Illeperuma, Z. Suo, J.J. Vlassak, Hybrid Hydrogels with Extremely High Stiffness and Toughness, ACS Macro Lett 3(6) (2014) 520-523.
[114] L. Zhang, J. Zhao, J. Zhu, C. He, H. Wang, Anisotropic tough poly(vinyl alcohol) hydrogels, Soft Matter 8(40) (2012) 10439-10447.
[115] N. Yuan, L. Xu, H. Wang, Y. Fu, Z. Zhang, L. Liu, C. Wang, J. Zhao, J. Rong, Dual Physically Cross-Linked Double Network Hydrogels with High Mechanical Strength, Fatigue Resistance, Notch-Insensitivity, and Self-Healing Properties, Acs Appl Mater Inter 8(49) (2016) 34034-34044.
[116] T. Wang, Z. Dai, J. Kang, F. Fu, T. Zhang, S. Wang, A TiO 2 nanocomposite hydrogel for Hydroponic plants in efficient water improvement, Mater Chem Phys 215 (2018) 242-250.

[117] F.B. Li, G.Z. Zhang, Y.H. Xia, Z.S. Wang, H.Y. Jiang, X.Q. Feng, Y.Q. Zhang, M.J. Liu, H.J. Li, Hierarchically crosslinked ionic nanocomposite hydrogels with ultrahigh mechanical properties for underwater bioinspired capturing device, Compos Sci Technol 165 (2018) 339-346.

[118] M. Kheirabadi, R. Bagheri, K. Kabiri, Swelling and mechanical behavior of nanoclay reinforced hydrogel: single network vs. full interpenetrating polymer network, Polymer Bulletin 72(7) (2015) 1663-1681.

[119] H. Feng, T. Zheng, X. Wang, H. Wang, Poly(acrylamide)-MWNTs hybrid hydrogel with extremely high mechanical strength, Open Chemistry, 2016, p. 150.

[120] S. Xiang, W. Qian, T. Li, Y. Wang, M. Chen, P. Ma, W. Dong, Hierarchical structural double network hydrogel with high strength, toughness, and good recoverability, New J Chem 41(23) (2017) 14397-14402.

[121] R. Niu, Z. Qin, F. Ji, M. Xu, X. Tian, J. Li, F. Yao, Hybrid pectin-Fe(3+)/polyacrylamide double network hydrogels with excellent strength, high stiffness, superior toughness and notch-insensitivity, Soft Matter 13(48) (2017) 9237-9245.

[122] S. Choi, J. Kim, Designed fabrication of super-stiff, anisotropic hybrid hydrogels via linear remodeling of polymer networks and subsequent crosslinking, J Mat Chem B 3(8) (2015) 1479-1483.

[123] J. Li, W.R.K. Illeperuma, Z. Suo, J.J. Vlassak, Hybrid Hydrogels with Extremely High Stiffness and Toughness, ACS Macro Letters 3(6) (2014) 520-523.

[124] P. Lin, S. Ma, X. Wang, F. Zhou, Molecularly engineered dual-crosslinked hydrogel with ultrahigh mechanical strength, toughness, and good self-recovery, Adv Mater 27(12) (2015) 2054-9.

[125] H. Gao, N. Wang, X. Hu, W. Nan, Y. Han, W. Liu, Double hydrogen-bonding pH-sensitive hydrogels retaining high-strengths over a wide pH range, Macromol Rapid Commun 34(1) (2013) 63-8.

[126] Y.Y. Zhang, Y.M. Li, W.G. Liu, Dipole-Dipole and H-Bonding Interactions Significantly Enhance the Multifaceted Mechanical Properties of Thermoresponsive Shape Memory Hydrogels, Adv Funct Mater 25(3) (2015) 471-480.

[127] B. Zhang, Z. Gao, G. Gao, W. Zhao, J. Li, X. Ren, Highly Mechanical and Fatigue-Resistant Double Network Hydrogels by Dual Physically Hydrophobic Association and Ionic Crosslinking, Macromol Mat Eng 303(7) (2018) 1800072.

[128] X. Yan, Q. Chen, L. Zhu, H. Chen, D. Wei, F. Chen, Z. Tang, J. Yang, J. Zheng, High strength and self-healable gelatin/polyacrylamide double network hydrogels, J Mat Chem B 5(37) (2017) 7683-7691.

[129] Y. Wang, Z. Wang, K. Wu, J. Wu, G. Meng, Z. Liu, X. Guo, Synthesis of cellulose-based double-network hydrogels demonstrating high strength, self-healing, and antibacterial properties, Carbohyd Polym 168 (2017) 112-120.
[130] B. Kurt, U. Gulyuz, D.D. Demir, O. Okay, High-strength semi-crystalline hydrogels with self-healing and shape memory functions, Eur Polym J 81 (2016) 12-23.
[131] S.Y. Zheng, H. Ding, J. Qian, J. Yin, Z.L. Wu, Y. Song, Q. Zheng, Metal-Coordination Complexes Mediated Physical Hydrogels with High Toughness, Stick–Slip Tearing Behavior, and Good Processability, Macromolecules 49(24) (2016) 9637-9646.
[132] P. Lin, T. Zhang, X. Wang, B. Yu, F. Zhou, Freezing Molecular Orientation under Stretch for High Mechanical Strength but Anisotropic Hydrogels, Small 12(32) (2016) 4386-92.
[133] H. Daemi, S. Rajabi-Zeleti, H. Sardon, M. Barikani, A. Khademhosseini, H. Baharvand, A robust super-tough biodegradable elastomer engineered by supramolecular ionic interactions, Biomaterials 84 (2016) 54-63.
[134] X. Hu, M. Vatankhah-Varnoosfaderani, J. Zhou, Q. Li, S.S. Sheiko, Weak Hydrogen Bonding Enables Hard, Strong, Tough, and Elastic Hydrogels, Adv Mater 27(43) (2015) 6899-905.
[135] K.J. Henderson, T.C. Zhou, K.J. Otim, K.R. Shull, Ionically Cross-Linked Triblock Copolymer Hydrogels with High Strength, Macromolecules 43(14) (2010) 6193-6201.
[136] B. Xu, Y. Li, F. Gao, X. Zhai, M. Sun, W. Lu, Z. Cao, W. Liu, High Strength Multifunctional Multiwalled Hydrogel Tubes: Ion-Triggered Shape Memory, Antibacterial, and Anti-inflammatory Efficacies, Acs Appl Mater Inter 7(30) (2015) 16865-72.
[137] P. Lin, S. Ma, X. Wang, F. Zhou, Molecularly engineered dual-crosslinked hydrogel with ultrahigh mechanical strength, toughness, and good self-recovery, Adv Mat 27(12) (2015) 2054-9.
[138] S.P. Silva, M.A. Sabino, E.M. Fernandes, V.M. Correlo, L.F. Boesel, R.L. Reis, Cork: properties, capabilities and applications, Int Mat Rev 50(6) (2013) 345-365.
[139] A.J.T. Teo, A. Mishra, I. Park, Y.J. Kim, W.T. Park, Y.J. Yoon, Polymeric Biomaterials for Medical Implants and Devices, Acs Biomater Sci Eng 2(4) (2016) 454-472.
[140] A.J.T. Teo, A. Mishra, I. Park, Y.-J. Kim, W.-T. Park, Y.-J. Yoon, Polymeric Biomaterials for Medical Implants and Devices, ACS Bio Sci-Eng 2(4) (2016) 454-472.
[141] R.G. Long, O.M. Torre, W.W. Hom, D.J. Assael, J.C. Iatridis, Design Requirements for Annulus Fibrosus Repair: Review of Forces, Displacements, and Material Properties of the Intervertebral Disk and a Summary of Candidate Hydrogels for Repair, J Biomech Eng 138(2) (2016) 021007.
[142] M. Ridha, V.P.W. Shim, Microstructure and Tensile Mechanical Properties of Anisotropic Rigid Polyurethane Foam, Exp Mech 48(6) (2008) 763-776.
[143] A.S. Hoffman, Hydrogels for biomedical applications, Ann NY Acad Sci 64 (2012) 18-23.

3.7 Supporting Information

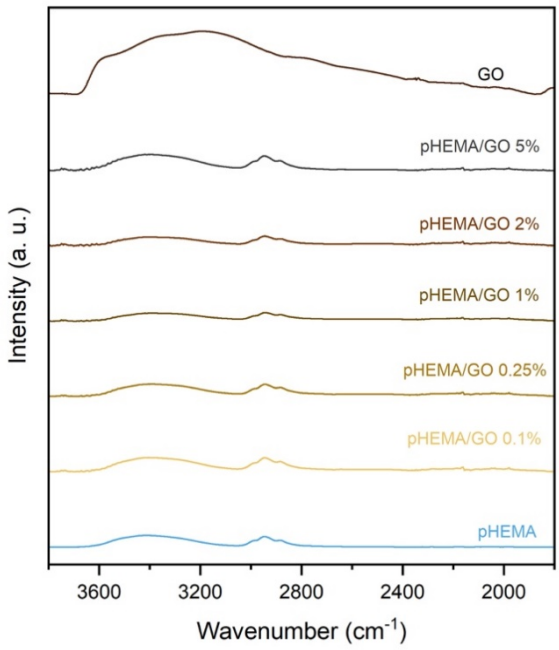

Figure S.1 – FTIR spectra of GO, pHEMA and pHEMA/GO composites in spectral range between 3700-2900 cm^{-1}.

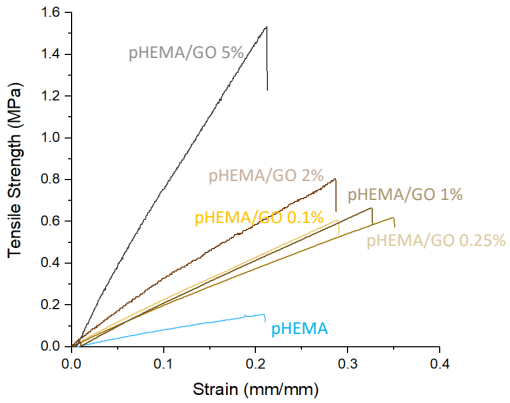

Figure S.2 – Representative Stress/Strain curves of neat pHEMA and pHEMA/GO composites.

Table S.1 - Young's modulus, Ultimate Tensile Strength and Elongation at break of pHEMA, pHEMA/GO 1% and pHEMA/GO 1% with 1/2 TEGDMA.

Material	Young's modulus (MPa)	Ultimate Tensile Strength (MPa)	Elongation at break (mm/mm)
pHEMA	0.80±0.33	0.16±0.04	0.20±0.11
pHEMA/GO 1%	2.05±0.29	0.68±0.09	0.34±0.05
pHEMA/GO 1% (1/2 TEGDMA)	1.50±0.27	0.75±0.15	0.50±0.10

Chapter 4

Graphene-based materials: the key to a successful application of pHEMA as a blood contacting device

Limited performance of blood-contacting devices (BCDs) has high impact on the quality of life and survival of patients, thus having repercussion on the economy. Poly(2-hydroxyethyl methacrylate) (pHEMA), a hydrogel approved by US Food & Drug Administration (FDA), has excellent hemocompatibility, but its poor mechanical properties impair its usage as BCDs. This work evaluates the effect of graphene-based materials (GBMs) thickness, oxidation degree and lateral size in the mechanical reinforcement of pHEMA considering its application as BCDs. Incorporation of five different GBMs in pHEMA, namely graphene oxide (GO), graphene nanoplatelets (GNP-with 5 and 15 μm lateral size) and respective oxidized forms, leads to an increased surface roughness while swelling and surface wettability are not affected for most tested formulations. GBMs oxidation degree and thickness unvail to be crucial factors to improve the tensile properties, being GO the most efficient filler. Biological features are not compromised, as oxidized GBMs do not affect the hemo/cytocompatibility of pHEMA, maintaining the anti-adhesive properties towards endothelial cells, blood platelets and bacteria. Furthermore, 3D pHEMA/GO prototype conduits exhibit low adhesion of blood components in vivo upon contact with non-heparinized circulating blood in a porcine arteriovenous (AV)-shunt model. Our findings reveal that GO is the key to a successful application of pHEMA in several blood contacting medical devices.

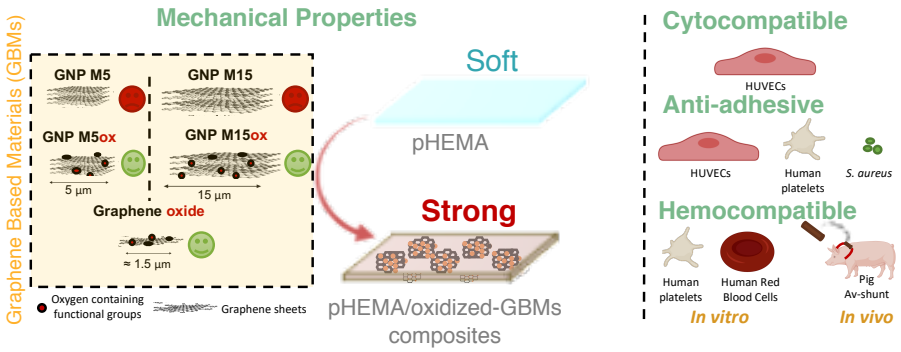

Keywords: Biomaterials, Blood contacting devices, Hemocompatibility, Arteriovenous-shunt, Graphene Based Materials, Tensile tests

This chapter is based on the following paper in preparation:
A.T. Pereira, P.C. Henriques, K. H. Schneider, A. L. Pires, A. M Pereira, M.C.L. Martins, F.D. Magalhães, H. Bergmeister, I.C. Gonçalves, Graphene-based materials: the key to a successful application of pHEMA as a blood contacting device

4.1 Introduction

The design of materials suitable for contact with blood is still a challenge in the biomedical field [1, 2]. Inherent thrombogenicity of the materials has a significant effect on the performance of blood-contacting devices (BCDs) such as catheters, vascular grafts, heart valves, stents, artificial kidneys, artificial lungs, ventricular assist devices [3] and also in intravenous drug delivery systems [4, 5]. Inferior performance of the devices ultimately impacts the quality and life expectancy of patients and has a pronounced negative effect on the worldwide economy [6]. Thrombosis is the major cause for short-term failure of several BCDs. Besides thrombus formation, hemolysis [7, 8] and biomaterials-related infections are complications that make even more demanding the design of efficient materials [9, 10]. Despite several efforts and strategies, such as designing non-fouling, anti-thrombogenic and/or antibacterial surfaces [2, 11-20], the development of new biomaterials for blood contacting applications is still a request in the field of biomaterials [1, 17, 20].

Poly(2-hydroxyethyl methacrylate) (pHEMA) is a synthetic hydrogel produced through *in situ* polymerization of 2-hydroxyethyl methacrylate (HEMA) monomers [21]. Due to its biocompatibility, this material is approved by Food & Drug Administration (FDA) for the production of contact lenses and keratoprosthesis [22, 23]. Described as a non-fouling material, pHEMA has a limited adsorption of blood components (proteins, platelets, red/white blood cells), eukaryotic cells and bacteria on its surface [22, 24]. These non-fouling properties of pHEMA are related with the electrostatically induced hydration that aid in the development of highly protein resistant surfaces [25]. However, the use of neat pHEMA as well as other hydrogels in load-bearing applications, such as BCDs, is limited due to their weak tensile strength, which is in the order of few hundred kPa [26, 27]. As such, for the development of BCDs, pHEMA has been strictly proposed as a surface coating of other mechanically resistant materials (e.g. polyurethane, silicon, steel) [22, 28-30] or as a co-polymer [31]. The requirement of specific chemical or physical properties of substrates and coating stability limit the broad application of this technology [32]. Aiming to surpass these problems and to empower a wide use of pHEMA in load-bearing applications, we previously showed that graphene oxide (GO) incorporation in pHEMA leads to an increase in mechanical properties of around 8.3x in stiffness and 7.4x in tensile resistance, reaching values of around 6.5 MPa and 1.1 MPa, respectively, without affecting most of the physical-chemical features and biocompatibility of neat pHEMA [33]. The stiffness and ultimate tensile strength of these new pHEMA/GO hydrogels are in the range of the mechanical requirements for most BCDs. GO is the oxidized form of graphene, a single-layer sheet of sp^2-bonded carbon atoms in a two-dimensional (2D) honeycomb lattice. Graphene-based materials (GBMs) family comprises a wide range of 2D materials that include multilayered materials (up to 10 layers), several

chemically modified forms (oxidized, covalently or non-covalently modified with small molecules, polymers, biomacromolecules, and inorganic nanoparticles) and materials produced using graphene as precursor [34]. The performance of GBMs in polymers reinforcement strongly depends on their physical-chemical features and/or fabrication techniques [35]. The present study aims to evaluate the effect of GBMs features, such as lateral size, thickness and oxidation degree, on the mechanical reinforcement of pHEMA and also to prospect, for the first time, the application of pHEMA as bulk material in the design of BCDs. To address this, five GBMs differing in oxidation degree or/and lateral size or/and thickness were incorporated in pHEMA. pHEMA/GBMs composites were evaluated regarding physical-chemical and mechanical properties. Furthermore, biocompatibility, hemolysis, platelet adhesion/activation and antimicrobial properties were assessed *in vitro*, and hemocompatibility was evaluated in an (AV-shunt) model in pigs.

4.2 Materials and methods

4.2.1 Materials Synthesis

4.2.1.1 Preparation of Graphene Based-Materials (GBMs)

Graphene Nanoplatelets (GNP) of grade M were purchased from XG Sciences (Lansing, MI, USA) with surface area among 120 - 150 m^2/g, average thickness of 6 nm and an average lateral size of 5 μm (GNP M5) or 15 μm (GNP M15). GO, GNP M5ox and GNP M15ox were prepared by oxidation of carbon graphite (purity: ≥99%, lateral size: 7-11 μm; purchased from American Elements) (Table 1) and GNP M5 or GNP M15, respectively, by modified Hummers' method (MHM) [36]. For this, 3 g of carbon graphite, GNP M5 or GNP M15 were mixed with a H_2SO_4(18.4 M)/H_3PO_4(14.8 M) (4:1) mixture (150 mL), being cooled to 0˚C using an ice bath. After that, 18 g of $KMnO_4$ were gradually added; the mixture was kept for 2 h at 35 ˚C under stirring and afterwards refrigerated to 0˚C and 450 mL of dH_2O added slowly. To eliminate the excess of $KMnO_4$, H_2O_2 was added until oxygen release stopped. After overnight resting, GBMs were washed by consecutively centrifuging at 4000 rpm during 20 min, until pH of supernatant reached the pH of distilled water (pH=5).

The suspension obtained from graphite oxidation was sonicated during 6 h in ultrasonic water bath resulting in GO. GNP M5ox, GNP M15ox and GO suspensions were freeze-dried for 3 days at -80 °C and 0.008 mBar to obtain dry powders.

Table 1 – GBMs used in this work.

GO	GNP M5	GNP M5ox	GNP M15	GNP M15ox
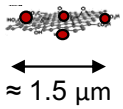 ≈ 1.5 µm	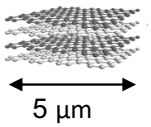 5 µm	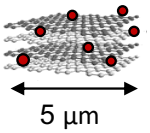 5 µm	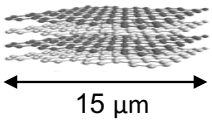 15 µm	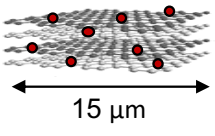 15 µm
Obtained from oxidation of graphite through MHM and exfoliated in ultrasound water bath (6h)	Commercially available	Obtained from oxidation of GNP M5 through MHM.	Commercially available	Obtained from oxidation of GNP M5 through MHM.

4.2.1.2 Production of pHEMA/GBMs composites

Poly(2-hydroxyethyl methacrylate) (pHEMA) was produced by *in situ* polymerization of 2-hydroxyethyl methacrylate (HEMA) monomers, in the absence or presence of GBMs, as described in previous works [37, 38]. Briefly, 7.5 mL of HEMA (>99.5 %, Polysciences, no. 04675) were added to a water/ethylene glycol (Sigma Aldrich, no. 9300) mixture (1.5 mL/2.25 mL) with or without 1% (w/v) GO, GNP M5, GNPox M5, GNP M15 or GNPox M15. The reactional mixture was vortexed for 30 sec and sonicated 5 min in an ultrasound water bath. After that, 0.345 mL of crosslinking agent, tetraethylene glycol dimethacrylate (TEGDMA; Polysciences, no. 02654), and 1.5 mL of mixture containing 1:1 mixture of 40% ammonium persulfate (APS; 98%, Aldrich, no. 24,861-4) and 15% sodium metabisulfite (SMB; 97 %, Aldrich, no. 25.555-6) were added to mixture to initiate the radical polymerization. 2D films or 3D tubes were produced using as a mold two clean glass plates with a 0.54 mm thick teflon or a glass tube and inner glass rod with 6 mm and 4 mm of diameter, respectively. After overnight resting, the hydrogels were released from the molds and rinsed in distilled water for 4 h (water renewed every hour) to leach out initiators, unreacted monomers and oligomer residues.

4.2.2 Materials physical-chemical and mechanical characterization

GBMs were analyzed regarding surface chemical composition by X-ray Photoelectron Spectroscopy (XPS), exfoliation degree by Transmission Electron Microscopy (TEM) and X-Ray Diffraction (XRD) and platelets morphology by Scanning Electron Microscopy (SEM).

pHEMA/GBMs composites were evaluated regarding polymerization by Fourier Transform Infrared Spectroscopy with Attenuated Total Reflectance (FTIR-ATR), GBMs dispersion in the polymer by SEM and TEM, surface topography by SEM, wettability by captive bubble contact angle measurements, swelling capacity by gravimetric analysis and mechanical properties by tensile tests.

4.2.2.1 GBMs

a. XPS

XPS of GO, GNP M5, GNP M5ox, GNP M15 and GNP M15ox powders tablets (prepared in a manual hydraulic press) was obtained using a Kratos Axis Ultra HAS (Kratos Analytical, UK) equipment at "Centro de Materiais da Universidade do Porto" (CEMUP, Porto, Portugal). An Al monochromator with 15 kW was used as X-ray source. The survey spectrum of GBMs was obtained at 80 eV and the C 1s high resolution spectra at 40 eV. All spectra were deconvoluted with CasaXPS processing software version 2.3.16, using Shirley background type. C1s spectral component was set at a binding energy of 284.6 eV to correct the contribution of charge effect. C1s high resolution spectra were fitted into seven peaks being constrained for the following binding energies sp^2 C=C (284.2–284.5 eV), sp^3 C–C (284.8–284.9 eV), C–OH (285.3–286.0 eV), C–O–C (286.1–286.6 eV), C=O (287.5–287.9), O–C=O (288.8–288.9 eV) and π–π (290–292 eV) based on literature data [39-41]. Gaussian–Lorentzian (70:30) function was used to fit all peaks with exception of sp^2 carbon peak, which due to its asymmetric nature was fitted using an asymmetric Lorentzian function (LF) with asymmetry parameter of 0.14 [39].

b. XRD

XRD of GBMs powders was performed in a SmartLab Rigaku® diffractometer that operates with 45 kV and 200 mA and has a Cu-Kα radiation source with a wavelength of λ = 1.540593 Å in a Bragg-Brentano θ/2θ configuration, at room temperature. All the samples were measured in a 2θ range of 5 to 30 with a step of 0.01º in a rotative system (30 Deg/min) that increases the crystallite size statistics. Thickness and crystallites interlayer d-spacing were calculated through Bragg's law equation:

$$n\lambda = 2dsin\theta \qquad \text{Equation 1}$$

where n is a positive integer, λ is the wavelength, d is the interplanar spacing (d-spacing) and θ is the incident angle of the X-ray beam, and Debye-Scherrer equation:

$$\tau = \frac{K\lambda}{\sqrt{B_m^2 - B_s^2}\cos\theta} \qquad \text{Equation 2}$$

where τ corresponds to GBMs crystalline size in the direction perpendicular to the lattice planes, K is the Debye–Scherrer constant (~0.89 for graphitic materials), λ is the incident X-ray wavelength, $\sqrt{B_m^2 - B_s^2}$ is the full width at half-maximum (FWHM) of the XRD peak and θ is

the incident angle. The number of layers was determined dividing the thickness by the d-spacing.

4.2.2.2 pHEMA/GBMs composites

a. SEM

SEM of GBMs powders and pHEMA/GBMs composites were analyzed by FEI QUANTA 400 ESEM (ThermoFischer, USA). Materials were mounted on carbon tape and coated with a thin layer of gold/palladium by sputtering to improve visualization by SEM.

b. TEM

TEM images of GBMs powders and pHEMA/GBMs composites were obtained by JEOL JEM 1400 TEM (Tokyo, Japan) coupled to a digital camera CCD Orious 1100 W (Tokyo, Japan) at Histology and Electron Microscopy Service (HEMS, i3S, Porto, Portugal). Visualization of GBMs was performed after dispersion of a small amount of dry powder in water and dropping the suspension on 200 mesh copper TEM grids. pHEMA/GBMs composites were visualized after preparation of ultrathin sections (40-60 nm thickness) using diamond knives in a Leica Reichert SuperNOVA Ultramicrotome and mounted 200 mesh copper TEM grids.

c. FTIR/ATR

FTIR spectra of dehydrated samples were assessed using a Perkin Elmer Frontier spectrophotometer coupled to a universal Attenuated Total Reflection (ATR) sampling accessory. Spectra were obtained in duplicate using 100 scans and resolution of 2 cm^{-1}. A baseline correction and smooth reduction was performed.

d. Surface Wettability

Inverted drop method was performed with a Data Physics goniometer, model OCA 15 equipped with a video CCD-camera to evaluate the captive-bubble contact angles of hydrated pHEMA and pHEMA/GBMs composites. For this, samples were attached individually to a steel slide and placed into a glass chamber with ultrapure water. To measure the contact angle, a 10 µL air bubble was released from a J-shaped needle on the sample's surface, being the angle measured using the software SCA.

e. Swelling profile

pHEMA and pHEMA/GBMs swelling profile was assessed by gravimetric analysis of dehydrated disc when immersed in water during 4 h. At different time points, 3 replicates of each sample were removed from water, blotted with a kimwipe and weighed. The following equation was used to determinate the swelling degree:

$$Swelling\ degree\ (\%) = \frac{W_S - W_d}{W_d} \times 100 \qquad \text{Equation 3}$$

, where W_s represents the weight swelled and W_d the weight dried.

f. Mechanical Properties

Tensile resistance of hydrated pHEMA and pHEMA/GBMs was evaluated in a Mecmesin Multitest-1d motorized test frame following ASTM D 882-02. Materials were cut (60 mm of length and 15 mm of width) and the loadings recorded at a strain rate of 10 mm.min^{-1} using a digital dynamometer (10N - Mecmesin BF). For each condition at least 6 samples of 2 different batches of materials were tested.

Flexibility of hydrated pHEMA and pHEMA/GBMs was measured according to ASTM F147-87. Briefly, specimens of materials (n=3) were bent 360° around a mandrel with diameter of 3 mm.

4.2.3 Cytocompatibility and cell adhesion capacity of pHEMA/GBMs composites

In vitro biocompatibility of pHEMA and pHEMA/GBMs composites was evaluated using Human Umbilical Vein Endothelial Cells (HUVECs, Sciencell) regarding cytotoxicity of materials extracts (indirect contact assay) by resazurin assay and cell adhesion (direct contact assay) by immunofluorescence. HUVECs were grown at 37 °C under a 5% CO_2 humidified atmosphere, in complete medium (M199+), which consists of M199 medium (Sigma) supplemented with 10% (v/v) inactivated Fetal bovine serum (FBS), 1% (v/v) Penicillin/Streptomicin (Biowest), 90 µg/mL of heparin (Sigma, H3149) and 15 µg/mL of endothelial cell growth supplement (ECGS, Corning, 354480) in 1% (w/v) gelatin coated flasks (Sigma). Cells were used until passage 4.

4.2.3.1 Cytotoxicity assay

For evaluation of cytotoxicity, cells were seeded at a density of 1 × 10^5 cells/mL in a 96-well plate previously coated with 1% (w/v) gelatin and incubated during 24 h in M199+ medium. Materials extracts prepared as described in ISO 0993−12:2004 were added and incubated during 24 h. Briefly, films were cut with Ø = 9 or 13 mm, sterilized with 70% (v/v) ethanol, rinsed with phosphate buffered saline (PBS) and incubated with M199 supplemented with FBS (24 h; 37 ºC; 100 rpm); before incubating with cells, the medium was supplemented with ECGS (15 µg/mL) and heparin (90 µg/mL). Extracts of tissue culture polyethylene terephthalate (TCPET) discs were used as positive control of cell growth, while a solution 1 mM H_2O_2 (in complete medium) was used as negative control. Mitochondrial metabolic activity of cells was quantified by resazurin assay, where the relative fluorescence units of supernatant containing

20% (v/v) resazurin incubated for 3 h were measured using a fluorimeter. Assays were performed with n=5 and repeated twice.

4.2.3.2 Cell adhesion assay

To assess pHEMA and pHEMA/GBMs composites capacity to induce HUVECs adhesion and proliferation, 1.6×10^4 cells (in 50 µL in M199+) were seeded on each material (in 48-well polystyrene plates) and incubated for 4 h. After that, M199+ was added to each material reaching a final volume of 300 µL, and culture was maintaining during 48 h. Metabolic activity was measured at timepoints 24 h and 48 h by the resazurin assay as previously explained. After 48 h, materials were rinsed with PBS and cells fixed using paraformaldehyde 4% (v/v), stained with DAPI (nuclei) and Phalloidin (F-actin in cytoskeleton) and observed in an inverted fluorescence microscope.

4.2.4 Bacterial adhesion to pHEMA/GBMs composites

Multi-resistant *Staphylococcus aureus* (ATCC® MRSA 33591™) was used to evaluate bacterial adhesion at pHEMA and pHEMA/GBMs surface. Bacteria was grown at 37°C in a Tryptic Soy Agar (TSA, Merck Germany) plate overnight and subsequently two colonies were collected and inoculated in 5 mL of liquid Trypticase Soy Broth (TSB, Merck, Germany) at 37 °C and 150 rpm, overnight. After that, *S. aureus* inoculum was rinsed and harvested by centrifugation (2700 rpm for 10 min) being the optical density at 600 nm measured to adjust the concentration of the initial inoculum to 1×10^5 CFU/mL in TSB medium supplemented with 1% (v/v) human plasma. 500 µL of bacteria initial inoculum was added to the surfaces of hydrogels or TCPET control discs and incubated during 24 h at 37 °C in 24-well suspension plates. After rinsing with 0.0859% NaCl adherent bacteria were visualized using syto9 and propidium iodide (PI) live/dead fluorescent staining. 300 µL of a mixture containing syto9 and PI dyes were added to samples and incubated at room temperature for 15 min. After rinsing, materials were transferred to a glass bottom black 24-well µ-Plate (IBIDI, Germany). Images of 9 random fields of view per sample with z-section of around 19 µm (z step = 1 µ) covering area of 1.44 mm^2 were acquired using high-content screening microscope IN Cell Analyzer 2000 (GE Healthcare Life Sciences, UK) with Nikon 40x/0.95 NA Plan Fluor objective. Original images z-sections were projected on one plane using the IN Cell Investigator Developer Toolbox v. 1.9.2 (GE Healthcare, Chicago, IL, USA). For bacteria identification, a software package for image segmentation running a machine-learning algorithm — Ilastik was used [42]. Customized algorithms were generated for each wavelength and individual signal probability images were generated for each projected image. Probabilities images were fed into CellProfiler version 3.1.5 [43] and the number of adhered bacteria was quantified.

4.2.5 Hemocompatibility of pHEMA/GBMs composites

To evaluate the *in vitro* blood compatibility of pHEMA/GBMs composites, materials were incubated with human Red Blood Cells (RBCs) to verify their hemolytic potential or with human platelets to evaluate their capacity to induce platelet adhesion and activation. Before the assays, all materials were cut into discs with 8 mm diameter and sterilized in 70% (v/v) ethanol solution followed by rising with PBS (0.01 M, pH 7.4). The *in vivo* blood compatibility of a 3D tubular prototype of the most promising material (pHEMA/GO) was evaluated through an arteriovenous-shunt (AV-shunt) in non-heparinized pigs.

4.2.5.1 Hemolysis assay

RBCs were isolated from human buffy coats by differential centrifugation at 400 g during 30 min in the presence of Histopaque-1077 (Sigma Aldrich) [36]. After centrifugation, the upper layer (containing plasma components and mononuclear cells) was removed from the lower layer (containing the RBCs). After that, the lower layer was washed three times with PBS and the purified RBCs diluted to a concentration of 2 x 10^8 cells/mL. 300 μL of RBCs were incubated during 3 h at 37 ºC in 48-well polypropylene plates containing pHEMA/GBMs films. Plates were afterwards centrifuged at 4000 rpm for 15 min and 100 mL of supernatant collected from each well to black 96-well polystyrene plates. The absorbance was read at 380, 415, and 450 nm using a micro-plate reader spectrophotometer. The amount of released hemoglobin (Hb) was calculated using the following equation:

$$Hb\ (mg.dL^{-1}) = \frac{(2\times A415-(A380+A450))\times 1000}{E} \qquad \textbf{Equation 4}$$

, where A415, A380, A450 represent the absorbance values at of samples at 415 nm, 380 nm, 450 nm, respectively, and E the molar absorptivity of oxyhemoglobin at 415 nm.
The hemolytic potential of pHEMA/GBMs composites was determined according to the following equation:

$$\%Hemolysis = \frac{Hb\ sample}{total\ Hb} \qquad \textbf{Equation 5}$$

, where total Hb is the correspondent value for 100% hemolysis with Triton 1%. The assay was performed with 5 replicates.

4.2.5.2 Platelets adhesion and activation

Platelets adhesion and activation by pHEMA and pHEMA/GBMs composites were assessed using human platelets concentrate (PC). Briefly, 48-well polystyrene plates were blocked to avoid platelet activation by the wells by incubation in a solution of 1% (w/v) bovine serum albumin (BSA) in PBS (1 h; 37 °C) followed by rinsing with PBS. pHEMA/GBMs films were pre-immersed in pure human plasma (1 h; 37 °C) and then transferred to the BSA-coated plates, incubated with platelets concentrate at 3×10^8 platelet/mL (1 h; 37 °C; 100 rpm). Afterwards, materials were rinsed with PBS and the adhered platelets fixed with 1.5% (v/v) glutaraldehyde in 0.14 M sodium cacodylate buffer (30 min; room temperature). For samples dehydration, materials were incubated with a growing ethanol/water gradient, 50, 60, 70, 80, 90 and 99% (v/v), for 10 min each. Samples were finally dried by critical point (variation of temperature 4°C to 33-38°C maximum pressure of 1000-1400 Psi, 5 cycles of 25 min). Adhered platelets were visualized by SEM, as described in section 4.2.2.2, and evaluated regarding the number of adherent platelets and degree of activation.

4.2.5.3 Arteriovenous shunt (AV-shunt) *in vivo* assay

In vivo blood compatibility of pHEMA/GO was evaluated through arteriovenous-shunt (AV)-shunt assay in non-heparinized pigs. Animal studies were performed in compliance with the protocols approved by the Austrian Federal Ministry of Science and Research, and with the Good Scientific Practice Guidelines of the Medical University of Vienna. Pigs were pre-medicated with ketamine (10 mg/kg, Animedica), midazolam (0.3 mg/kg, Accord) and medetomidin (0.1 mg/kg, Bayer). Anesthesia was introduced using propofol (2.5 mg/kg, Fresenius Kabi), 0.1 mg fentanyl (Hameln Pharma Plus) and 20 mg rocuroniumbromide (Fresenius). After endotracheal intubation, animals were ventilated volume-controlled with 8% desflurane (Baxter). Additionally, 0.01 mg/kg/h fentanyl and 2 mg/kg/h rocuroniumbromide were administered. Animals received continuously ringer lactate (10 ml/kg/h) during the experiment. A blood circuit was established between the right common carotid artery and the left jugular vein using tubes and connectors of a commercially available blood transfusion set (Senso Hem Crystal, Meditrade Medicare). Two different pigs were used to test the conduits. Tubular conduits of pHEMA/GO hydrogels (n=6) with 4 mm inner diameter and 6 mm outer diameter and of ePTFE (Zeus Inc., Orangeburg, SC) with 4 mm inner diameter were attached to the connectors of the circuit, being perfused with circulating blood for 30 min. After blood exposure, each conduit was removed, and the tubes of the blood circuit were flushed with a heparinized saline solution before connection and exposure of a new conduit. After retrieval, the conduits were gently flushed with physiological saline solution, longitudinally opened and fixed in 2.5% (v/v) glutaraldehyde. Thereafter specimens were dehydrated in an ethanol/water

gradient of 50, 60, 70, 80, 90 and 99% (v/v), for 10 min each, and evaluated by SEM as described above.

4.3 Results

4.3.1 Physical and chemical characterization of GBMs

To explore the effect of GBMs features – particles lateral size, thickness and oxidation degree – on the mechanical reinforcement of pHEMA, five different GBMs were tested. Two non-oxidized few layer GBMs – GNP M5 and GNP M15, commercially acquired, differing only in lateral size, 5 μm and 15 μm, respectively – their oxidized forms – GNP M5ox and GNP M15 ox – obtained by oxidation through Modified Hummers' Method (MHM) and GO (used as a reference of a GBMs with thinner and smaller particles (lateral size = 1.5 μm ([38])) synthesized through graphite oxidation by MHM and exfoliation. Surface chemical composition of GBMs powders was evaluated by XPS (Fig. 1A). Non-oxidized GBMs, namely GNP M5 and GNP M15, present a low oxygen content in their composition (<4%). The atomic percentage of oxygen is similar in all oxidized GBMs, ranging from 31% to 34%, which confirms the successful oxidation of the materials by MHM. GBMs C1s high resolution spectra were deconvoluted to determine the contribution of different functional groups in their composition, namely hydroxyl (C–OH), epoxide (C–O–C), carbonyl (C=O) or carboxyl (O–C=O) (Fig. S.1). XPS spectra of non-oxidized GBMs exhibit predominantly one peak corresponding to C=C stretching at 284.5 eV, which is characteristic of sp^2-hybridized carbon atoms present in hexagonal structure of graphene, and a peak that corresponds to π–π interactions. Upon oxidation, the intensity of C=C and π–π peak decreases, and new peaks, characteristic of oxygen-containing functional groups, appear. The most prevalent group was epoxide (C–O–C), while hydroxyl (C–OH), carbonyl (C=O) or carboxyl groups (O–C=O) were in much lower amounts (Fig. S.2).

Crystallinity of dry GBMs was evaluated through XRD (Fig. 1A e 1B). The spectra of non-oxidized GBMs exhibit an intense and narrow peak at 2θ = 26.5°, which corresponds to the reflection plane of (002) associated with the graphene layers planes present in these materials and also in graphite [44]. For oxidized GBMs, the diffraction peak became broader and shifted to a lower position, 2θ around 11.0º for GO and GNP M5ox, and 10.8º for GNP M15ox, which corresponds to the reflection plane of (001) [45]. The thickness (τ) and d-spacing (*d*) of GBMs were determined by Bragg's and Scherrer equation (1,2) (Fig. 1A). Non-oxidized GBMs have thicker and compact crystalline structure (τ =33.4-35.5 nm and *d* = 3.4 Å) than oxidized GBMs (τ = 8.3-11.3 nm and *d* = 8.0-8.2 Å). Oxidized GBMs exhibit a higher d-spacing which is caused by the incorporation of oxygen functional groups between graphene layers during the oxidation process. Among all GBMs, GO is the thinnest material, exhibiting 8.3 nm of thickness. In

agreement with the results obtained by XRD, SEM images reveal that dry GBMs are compacted and agglomerated structures (Fig. 1C). These agglomerates can be redispersed in dH_2O upon sonication, as shown in TEM images (Fig. 1D). As in dry powders, in water suspension GO is the thinnest GBM, being present as a single layer material, while oxidized and non-oxidized GNP exhibit a multilayered structure.

Regarding GBMs sheets morphology, non-oxidized GBMs have planar conformation with sharp edges, while oxidized GBMs platelets show a wrinkled morphology with folded edges (Fig. 1C). The presence of oxygen-containing functional groups in oxidized GBMs promotes these wrinkles through the establishment of intra-sheet hydrogen bonds.

a)

GBMs	XPS Atomic %		XRD		
	C	O	2θ	Thickness (nm)	d-spacing (Å)
GO	66.8	33.2	11.0	8.3	8.0
GNP M5	96.6	3.5	26.5	33.4	3.4
GNP M5ox	66.2	33.8	11.0	11.0	8.0
GNP M15	96.3	3.8	26.5	35.4	3.4
GNP M15ox	66.0	34.0	10.8	11.3	8.2

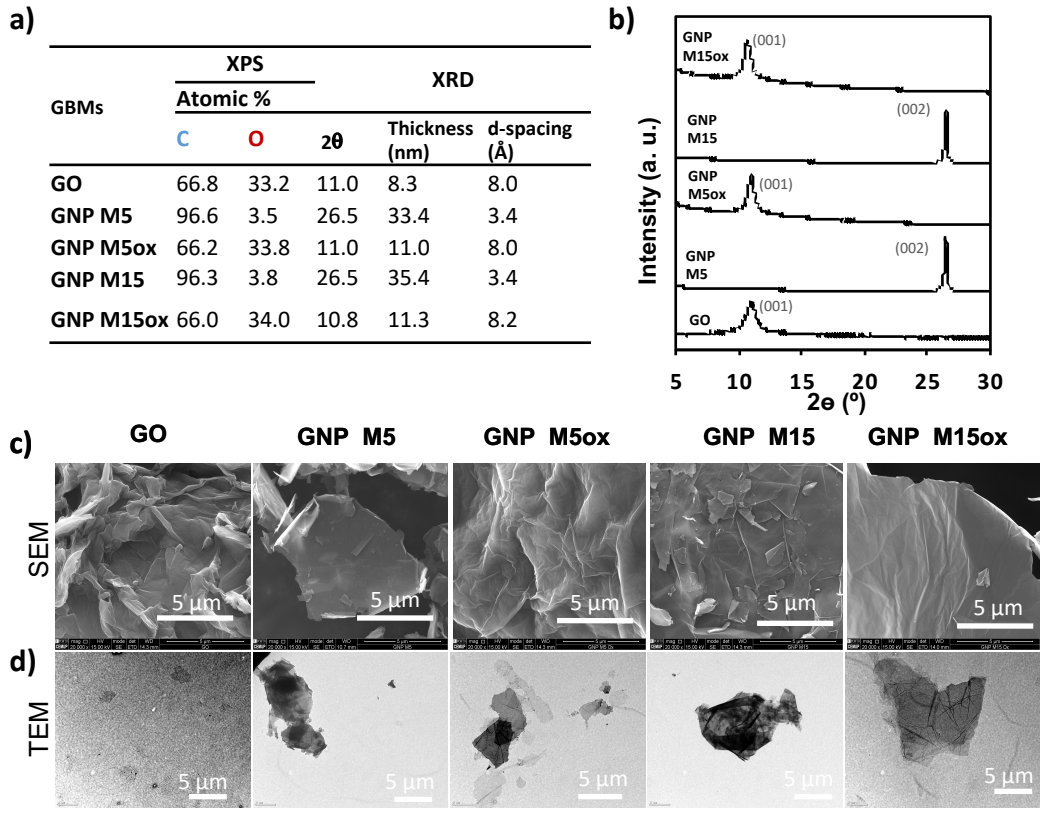

Figure 1 - Characterization of GBMs: a) atomic percentage taken from XPS survey spectra and thickness and d-spacing obtained from b) XRD spectra and c) SEM images of GBMs powders and d) TEM images of GBMs suspension

4.3.2 Physical, chemical and mechanical Properties of pHEMA/GBMs composites

To confirm pHEMA polymerization in the presence of GBMs, FTIR spectra of neat-pHEMA and composites were acquired (Fig. S.3). All the pHEMA/GBMs spectra show the characteristic stretching bands of the neat polymer, namely C=O (1727 cm^{-1}), CH_2 (1277 cm^{-1}), COC (1158 cm^{-1}) and CO or CH_2 (1079 cm^{-1}). None of the spectra exhibit the characteristic band of HEMA monomers, C=C (1635 cm^{-1}) [46], demonstrating that pHEMA polymerization

occurs even in the presence of GBMs, as shown before for GO [38]. Moreover, incorporation of GBMs did not induce the appearance of new absorbance peaks suggesting that no new functional groups were formed during the preparation of these composites.

SEM and TEM images of materials cross-section were acquired to visualize GBMs platelets distribution in pHEMA (Fig. 2A). Cross-sectional surface topographies depend on the type of GBM used. Individualized platelets can be identified for non-oxidized GBMs, surrounded by a smooth surface similar to neat-pHEMA. A homogeneously rough surface is visible in the cross-sections containing oxidized GNPs. This suggests better distribution and interaction of oxidized platelets within the polymeric network of pHEMA. TEM images concur these observations, showing that oxidized GBMs appear well dispersed in the pHEMA network, without being possible to visualize platelets edges, while non-oxidized GBMs particles tend to agglomerate, and platelet edges are identifiable.

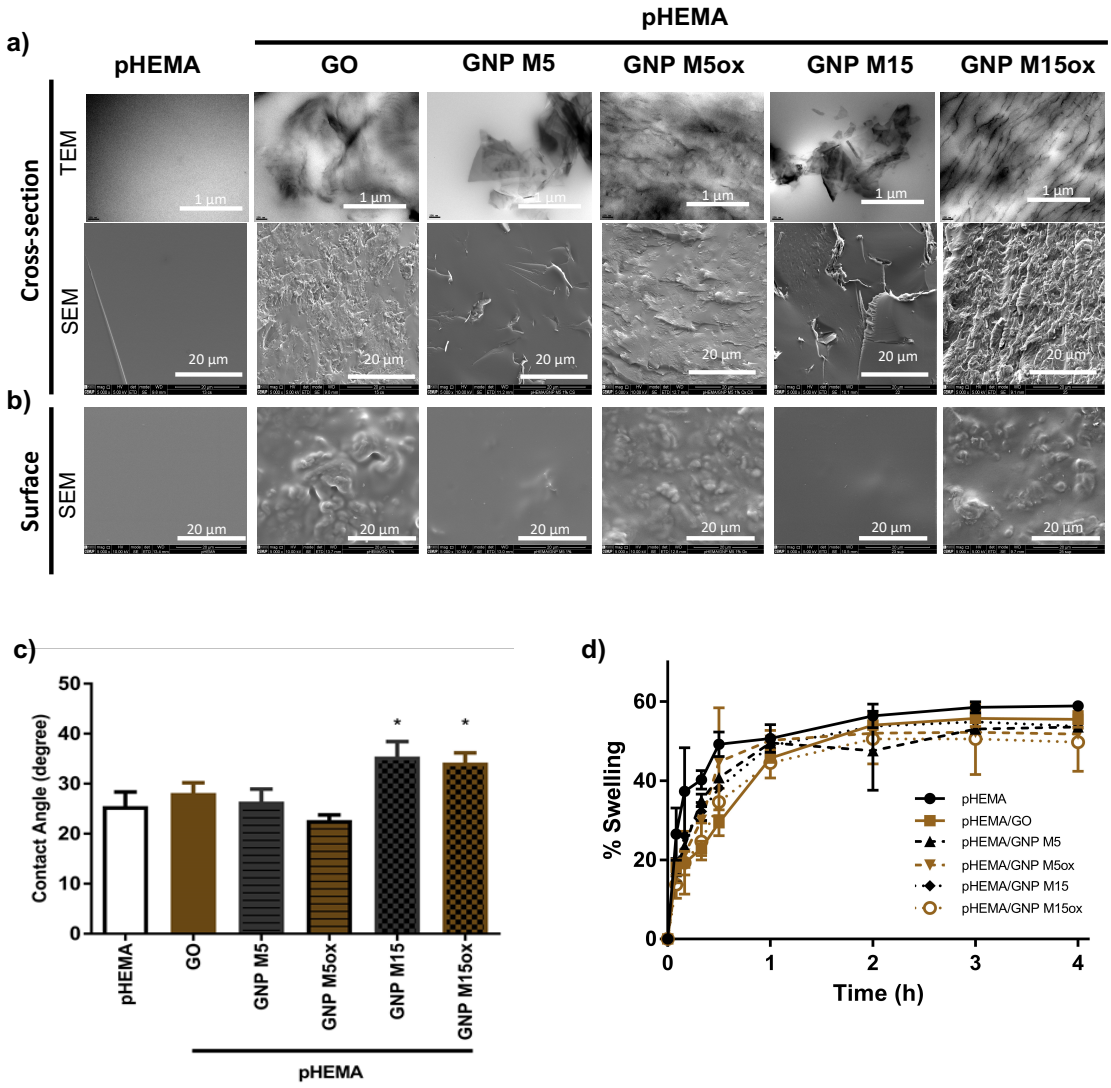

Figure 2 - Characterization of pHEMA and pHEMA/GBMs: a) GBMs dispersion in pHEMA evaluated by TEM and SEM images of ultrathin sections and fracture cross-sections,

respectively, b) surface topography assessed by SEM, c) captive air-bubble contact angles and d) swelling degree in water.

Surface topography of pHEMA/GBMs composites was evaluated by SEM, revealing that incorporation of GBMs increased surface roughness of pHEMA (Fig. 2A). This effect is emphasized when oxidized forms of GBMs are incorporated. In the case of pHEMA/GNP M5 and pHEMA/GNP M15 composites, some GBMs platelets seem to be exposed at the surface, while in pHEMA/GO, pHEMA/GNP M5ox and pHEMA/GNP M15ox composites, GBMs seem to be completely embedded within the polymer.

Surface wettability of pHEMA/GBMs composites was assessed by evaluation of the captive air-bubble contact angle. Fig. 2C shows that the incorporation of GBMs with smaller lateral size (GO, GNP M5 and GNP M5ox) did not induce a significant alteration in surface wettability of pHEMA, which is approximately 25º. Larger GNPs (GNP M15 and GNP M15ox) decrease surface hydrophilicity by around 10º, presenting a contact angle of approximately 35º.

Swelling profile of pHEMA/GBMs composites was assessed through gravimetric analysis of dehydrated films in water for 4 h (Fig. 2D). As shown before for GO [38], incorporation of GBMs decreases slightly the swelling rate of pHEMA in the first 1 h. However, after 4 h none of the incorporated GBMs affected significantly the swelling profile and total water absorption capacity of pHEMA, which is around 55%.

Mechanical properties of hydrated pHEMA/GBMs composites were assessed through uniaxial tensile testing. The obtained stress–strain curves of neat pHEMA and composites are linear (Fig. 3A), which is a characteristic behavior of elastic materials. The stress–strain curves were used to determine the Young's Modulus - YM (stiffness), which corresponds to the slope of curves and evaluates stiffness, the ultimate tensile strength – UTS (tensile), which is the maximum tensile stress that the material can withstand until rupture, and the elongation at break, which is the maximum strain and a measurement of the material's elasticity when rupture occurs before yield, as in this case. Fig. 3 shows these properties for neat pHEMA and pHEMA/GBMs composites. Incorporation of each oxidized GBMs leads to an increase of 2.5x in pHEMA YM, changing from 0.744 to 1.80 $\times 10^3$ kPa, while non-oxidized GBMs do not show any effect (Fig. 3B). As observed for stiffness, incorporation of non-oxidized GBMs does not affect the tensile resistance of pHEMA, maintaining its UTS at around 150 kPa (Fig. 3C). Oxidized GBMs, on the other hand, have a strong influence in UTS, the most effective being GO, which shows an increase in UTS of 4.4×, reaching 678 kPa. GNP M5ox and GNP M15ox show an increase of 3.4× and 2.8× in UTS, respectively.

As shown in our previous work for pHEMA/GO (for concentrations ranging 0.1-2%) [38], the increase in UTS of pHEMA/oxidized GBMs is higher than the increase in YM. This is due to

the simultaneous increase in elasticity observed when these oxidized GBMs are used. pHEMA elasticity is higher when the filler is GO, reaching 0.37 (mm/mm) (Fig. 3D). As observed for the other properties, pHEMA/non-oxidized GBMs composites exhibit the same elasticity of neat pHEMA.

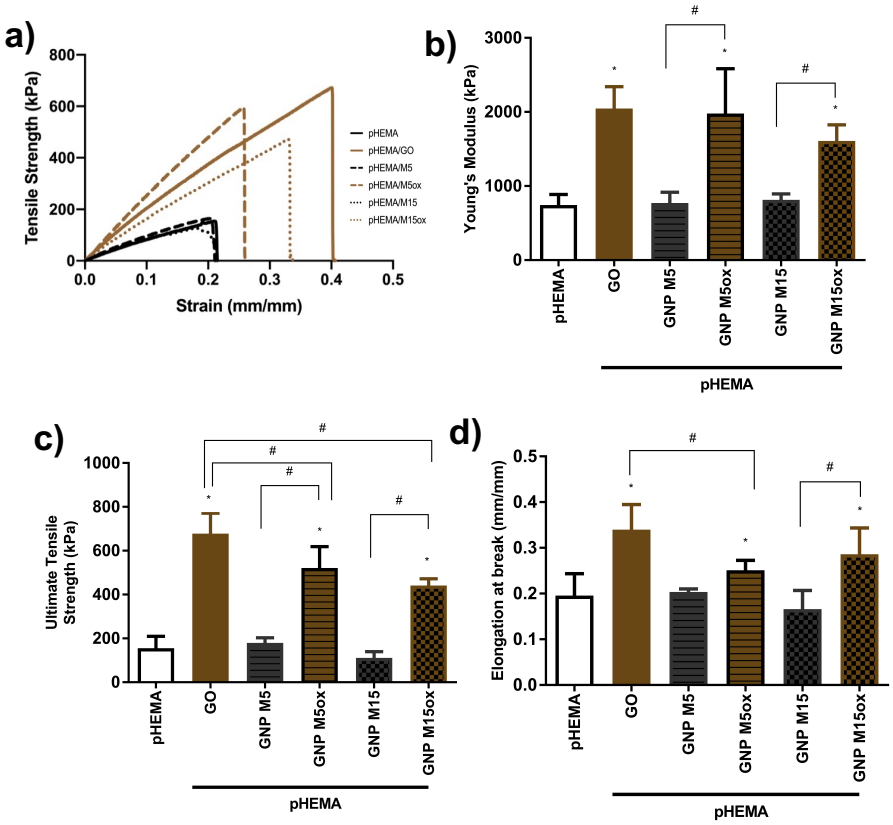

Figure 3 – Tensile Properties of pHEMA and pHEMA/GBMs composites: a) Representative stress/strain curves b) Young's Modulus, c) Ultimate Tensile Strength, d) Elongation at break. Statistically significantly different from pHEMA (*) and different between each sample (#) ($P<0.05$; One Way ANOVA).

pHEMA and pHEMA/GBMs composites flexibility (hydrated) was measured according to ASTM F147-87. Specimens of materials (n=3) were bent 360° around a mandrel with diameter of 3 mm without break.

4.3.3 Biocompatibility of pHEMA/GBMs composites

The cytocompatibility of pHEMA/GBMs hydrogels was evaluated by the contacting of materials extracts with endothelial cell line (Human Umbilical Vein Endothelial Cells-HUVECs) during 24 h. Results showed that none of the obtained extracts affects the metabolic activity of the endothelial cells (Fig. 4), confirming lack of cytotoxicity.

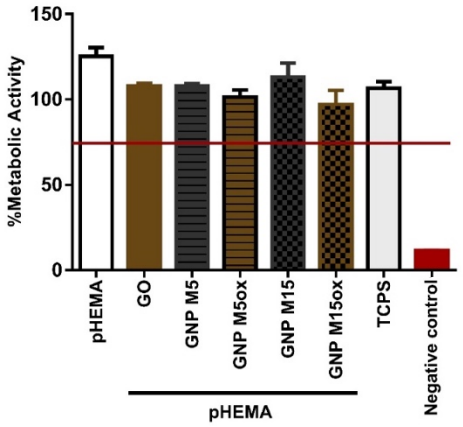

Figure 4 – Metabolic activity of HUVECs after 24 h incubation with materials extracts (M199+ as extraction vehicle). The metabolic activity of cells is represented in percentage in comparison to cells growing in M199+ (100 %). Extracts of TCPS discs were used as positive control and 1 mM H_2O_2 (in M199+) was used as negative control. According to ISO 10993-5:2009(E), 70% of metabolic activity is the lower limit to consider the material extracts cytotoxic (red line).

Fig. 5 shows inverted fluorescence microscopy images of pHEMA and pHEMA/GBMs hydrogels surfaces after 24h incubation with HUVECs. pHEMA, as non-fouling material, does not exhibit any cells at its surface. Incorporation of GBMs did not promote the adhesion of cells on the surface of pHEMA.

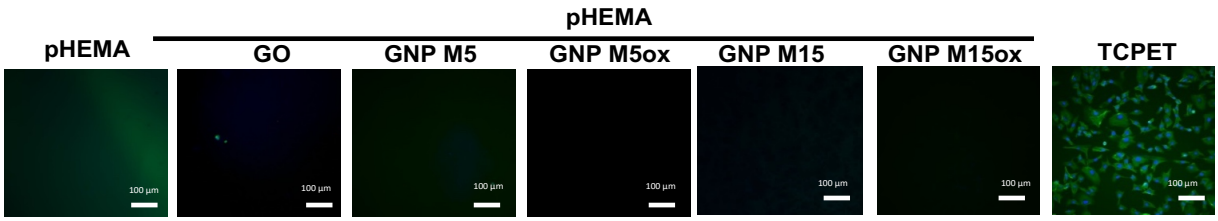

Figure 5 - Visualization of adhered HUVECs to pHEMA and pHEMA/GBMs surfaces upon 48 h incubation. Cells were stained with DAPI (nuclei) in blue and with phalloidin (F-actin in cytoskeleton) in green.

4.3.4 Bacterial adhesion at pHEMA/GBMs composites

Non-fouling properties of pHEMA and pHEMA/GBMs were also evaluated regarding bacterial adhesion at their surface. Fig. 6 shows that pHEMA has low *S. aureus* adhesion when comparing with TCPET, a positive control surface of bacterial adhesion. Incorporation of oxidized GBMs does not affect significantly this feature while non-oxidized GBMs promote

bacterial adhesion at pHEMA surface being this effect more prevailing when larger particles are used (GNP M15).

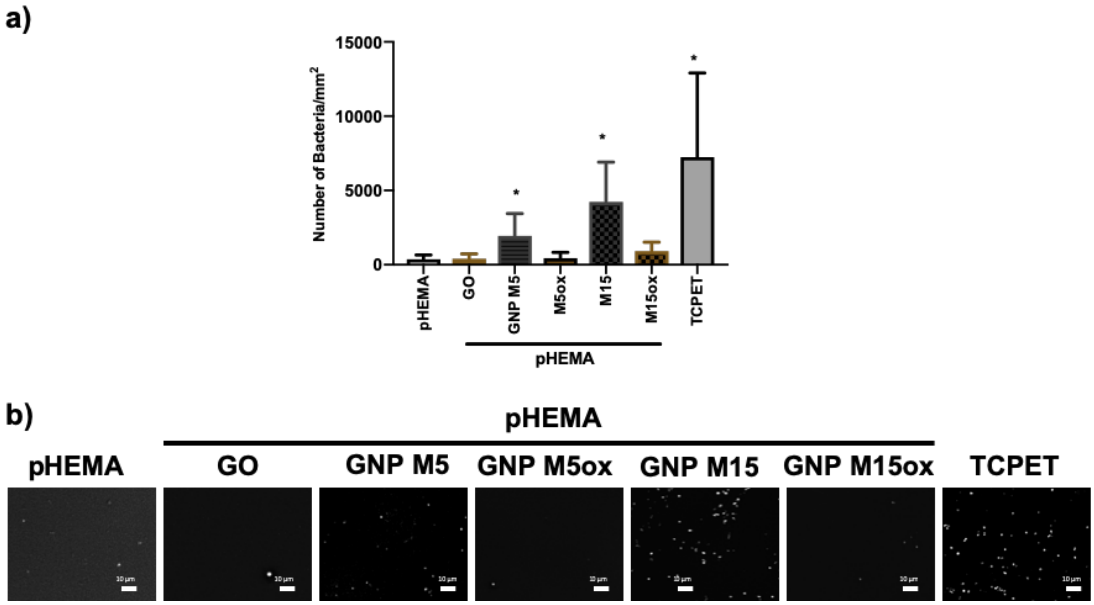

Figure 6 – Quantification and visualization of adhered bacteria to pHEMA and pHEMA/GBMs surfaces: a) Number of bacteria adhered to pHEMA and pHEMA/GBMs surface per mm^2 upon 24 h of incubation with *S. aureus* ATCC® MRSA 33591™ Statistically significantly different from pHEMA, pHEMA/GO, pHEMA/GNP M5ox and pHEMA/GNP M15ox (*) ($P<0.05$; One Way ANOVA) and b) representative images of adhered bacteria.

4.3.5 Blood compatibility of pHEMA/GBMs composites

Fig. 7A shows the hemolysis potential of pHEMA and pHEMA/GBMs composites. Hemolytic ratio of all tested materials was lower than 1% which is below the permissible limit set by ISO 10993-4 standard for hemocompatible materials (≤ 5%) [47].

Platelets adhesion and activation to pHEMA/GBMs surface was evaluated *in vitro* through the incubation of materials with human platelets (Fig. 7B). pHEMA revealed to be a non-fouling material, with no platelets adhered. Furthermore, none of the incorporated GBMs influenced platelets adhesion and activation on pHEMA, even when surfaces are pre-incubated with plasma proteins that could promote platelet adhesion and activation to the surface.

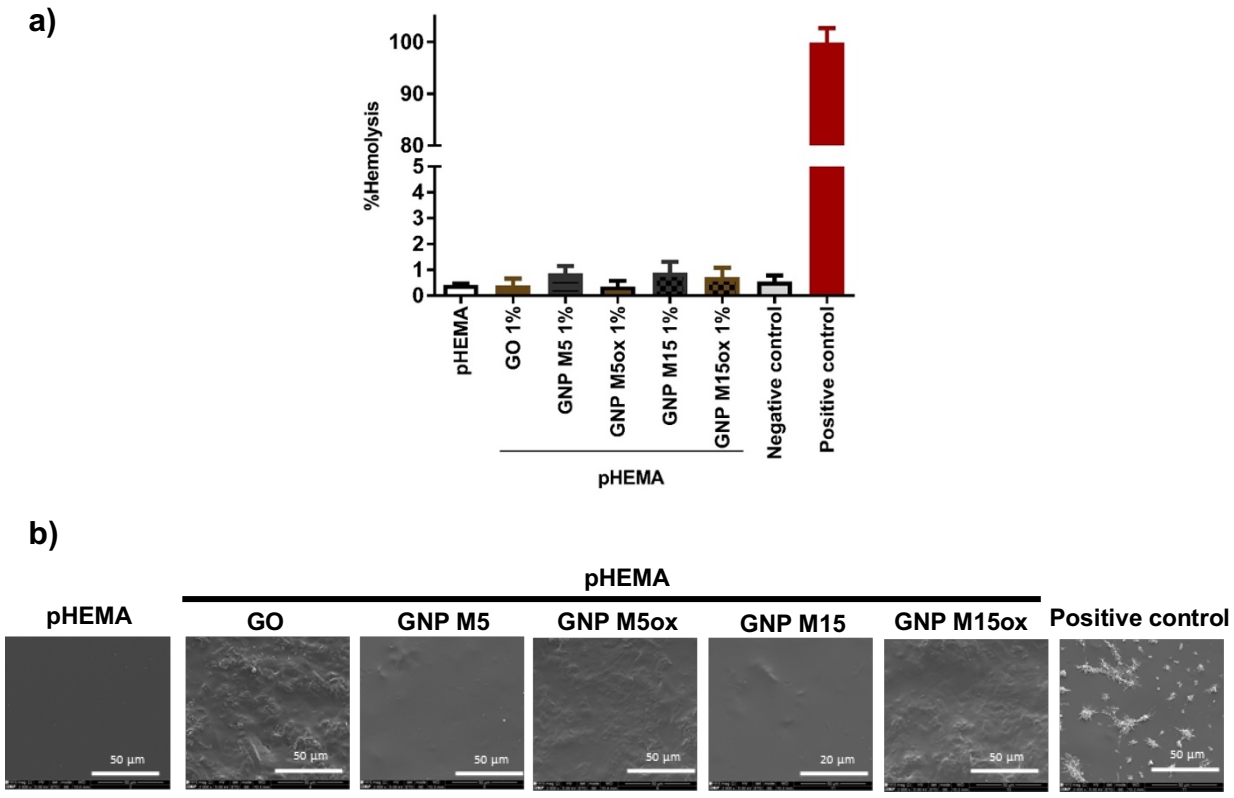

Figure 7 - *In vitro* hemocompatibility of pHEMA and pHEMA/GBMs composites: a) Hemolytic potential. PBS and 1% Triton were used as negative and positive control of lysis, respectively, b) SEM images of pHEMA and pHEMA/GBMs composites surface after 1 h incubation with human platelets at 37° C.

The promising mechanical and biological properties (*in vitro)* of pHEMA/GO, (highest resistant to tensile stress and its non-fouling properties) driven us to test its blood compatibility *in vivo*. A tubular prototype of pHEMA/GO was produced by molding and evaluated through the exposure of their luminal surface to arterial blood flow for 30 min by AV-shunt in non-heparinized pigs (Fig. S.1). As control, ePTFE grafts were also exposed to the same conditions, as they are the commercially available and currently used material for vascular access and the replacement of vessels. The established blood circuit between the right common carotid artery and the left jugular vein allowed to test several conduits using the same set up without thrombus formation in connectors. All conduits resist to blood flow and does not clot during incubation time. Fig. 8 shows SEM images of the luminal surface of both graft types after 30 min blood flow exposure. pHEMA/GO grafts do not exhibit adhered platelets while ePTFE grafts show several adhered/activated platelets on its surface. Regarding the systemic blood parameters, all the animals exhibit normal number of white blood cells, platelets, red blood cells before and after exposure to ePTFE or pHEMA/GO (Table S.1.).

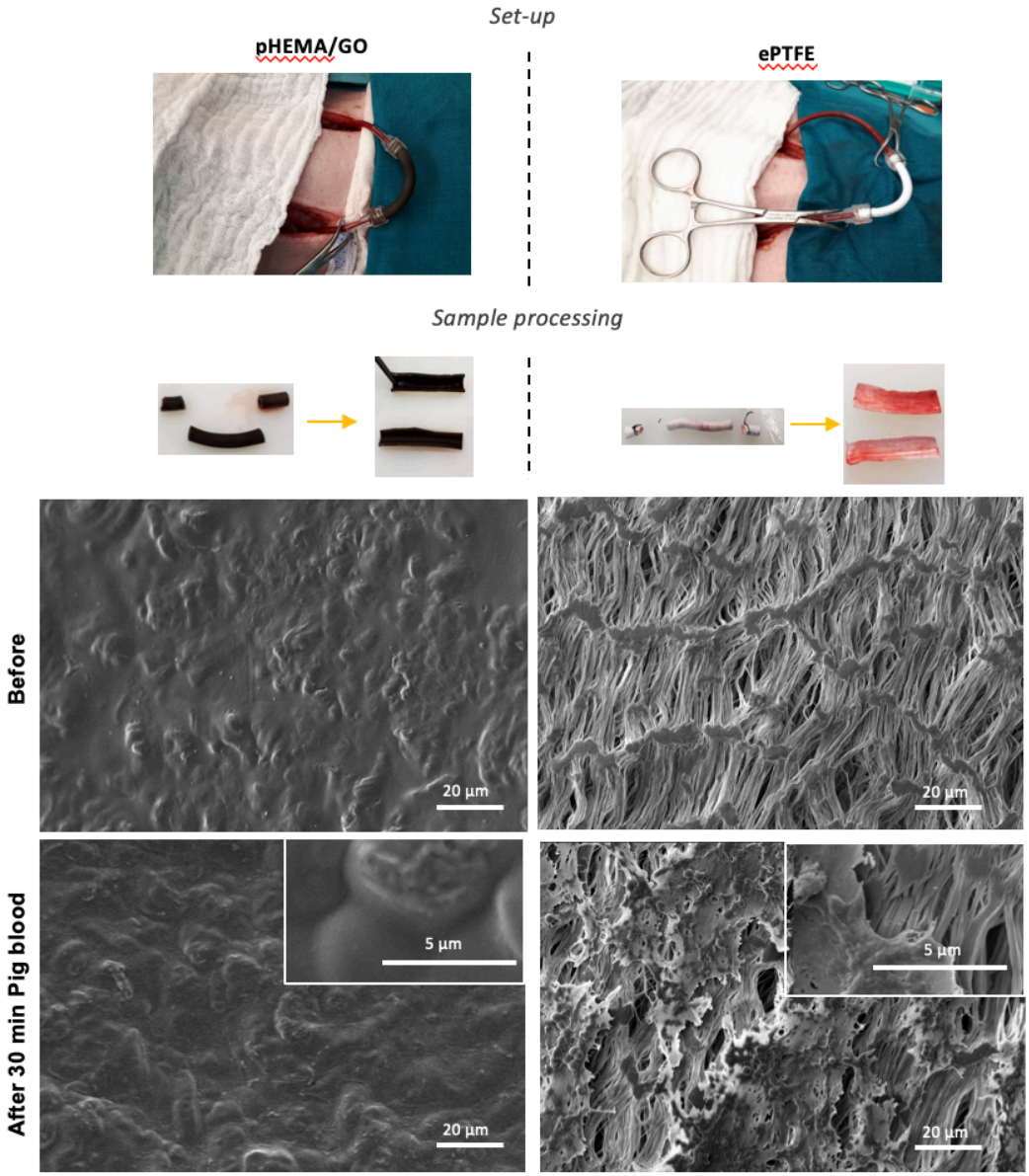

Figure 8 – *In vivo* hemocompatibility of pHEMA/GO composites: SEM images of the luminal surface of pHEMA/GO 1% and ePTFE grafts before and after 30 min blood exposure in an AV-shunt model in pigs.

4.4 Discussion

Five different GBMs which varying in oxidation degree, lateral size and thickness were incorporated in pHEMA to improve its mechanical properties aiming to enable its application in design for blood contacting devices. pHEMA/GBMs composites were produced by *in situ* polymerization, an effective method to achieve a good dispersion and strong interactions between the polymer matrix and GBMs [48-52]. Pre-mixing of monomers or pre-polymers with GBMs allows the polymer grafting (covalent or non-covalent) [35]. In pHEMA/GBMs composites, GBMs seems to interact non-covalently with HEMA monomers since FTIR spectra

of composites and neat pHEMA are similar as observed for GO interaction with other acrylate monomers after radical polymerization [53].

From all tested GBMs, only the oxidized GBMs were efficient in the mechanical reinforcement of pHEMA despite being conceptual that non-oxidized GBMs have a higher mechanical resistance than the oxidized GBMs (YM = 1 TPa and 40 GPa and UTS = 130 GPa and 120 MPa for graphene [54] and graphene oxide [55], respectively). This may be due to the high stability of sp^2 bonds that form the honey-comb structure which exhibit several defects as consequence of oxidation process. The better interaction and dispersion of oxidized GBMs allows their uniform distribution within pHEMA, exhibiting less rupture points than non-oxidized GBMs, which tend to agglomerate in spots leaving a lot of area in pHEMA without reinforcement. This stronger interaction of oxidized GBMs with polymer hydrogel networks has also been reported for polyacrylamide and polyvinyl alcohol [56], as reviewed by *Papageorgiou et al. [35]*. Besides the oxidation degree, the lateral size of GBMs platelets is also known to play a critical role in the mechanical reinforcement of polymers [35]. It has been suggested that graphene with lateral size higher than 8 μm induces a better reinforcement in composites [35, 57]. However, we saw no significant differences between GNP with 5 and 15 μm in terms of the tested mechanical features (neither between pHEMA/GNP M5 and pHEMA/GNP M15 nor between pHEMA/GNP M5ox and pHEMA/GNP M15ox). Gong *et al.* showed that GBMs thickness impacts on effective modulus of the flakes, single and bilayer graphene, which decreases by 15% for tri-layer graphene and by 50% when the number of layers is higher than seven [58]. Our results show that the UTS of pHEMA/oxidized-GBMs composites seems to depend on GBMs layers, being the thinner GBM (GO) the most efficient filler. However, this is still contradictory, since Li *et al.* showed that polymers reinforcement using GO is independent of its number of layers and stacking configurations [59].

Due to its hydrophilicity, pHEMA is a non-fouling material that prevents the adhesion of cells, bacteria and blood-components on its surface [22, 24]. Most of the times, mechanical reinforcement of hydrogels, by using fillers or increasing crosslinking agent [52, 60, 61], changes their surface chemistry and swelling capacity, which may compromise the interactions with biological systems. In the present case, incorporation of GBMs does not change its pHEMA's hydrophilic surface but increased surface roughness, especially for the oxidized forms.

Rougher surfaces have been associated with higher adhesion of bacteria, cells and platelets [16, 17, 62, 63]. Despite presenting higher roughness, pHEMA/oxidized-GBMs composites kept the non-fouling properties against bacteria, endothelial cells and platelets of pHEMA, indicating that surface chemistry prevails over topography for pHEMA. According to ISO 10993-5:2009 pHEMA/GBMs are non-cytotoxic towards HUVECs.

Besides cytocompatibility, the design of BCDs requires a further step of complexity that is stills an open question in the field, which is to provide an appropriate interface for contact with blood. In this study, we show that GBMs incorporation in pHEMA does not affect its intrinsic hemocompatibility. Previous studies also reported that incorporation of GBMs in other polymers did not promote hemolysis [64-66] or platelets adhesion/activation, being observed a decrease in platelets adhesion and activation when they are incorporated in some polymers such as PLA (associated to an increase in surface hydrophobicity) [65] or polyetherimide (associated to an increase in surface hydrophilicity) [67]. Blood compatibility and non-fouling features were even confirmed *in vivo* when the 3D conduits of pHEMA/GO composites (the formulation with best mechanical performance among all pHEMA/GBMs) were exposed to blood flow. pHEMA/GO surfaces show good hemocompatibility *in vivo* exhibiting lower adhesion of platelets than ePTFE, a material commercially available for vascular access and replacement. Nojiri *et al.* also showed that inner membrane coating of Dacron/polyurethane vascular graft with HEMA and styrene block copolymer exhibits good hemocompatibility *in vivo [68]*. Moreover, the *in vivo* AV-shunt model here established to promote arteriovenous circulation showed high potential to be applied in the evaluation of other materials.

Considering the mechanical features and bio/hemocompatible properties of the pHEMA/GO composites developed in this work, these new materials have a high potential for use in the design of many well-known blood contacting biomaterials [69-73] (Table 1).

Table 1 - Comparison between mechanical features of pHEMA/GO 1% and blood contacting devices

Material	Young's Modulus (kPa)	Ultimate Tensile Strength (kPa)	Elongation at Break (mm/mm)	References
pHEMA/GO 1%	2100	689	0.30	This study
Porcine aortic valve	-	1000	0.23	[71]
Human aortic valve	-	[750 – 2500]	[0.10 – 0.17]	[71]
Tissue engineered heart valves	3000	700	0.33	[71, 73]
Native saphenous vein	-	1000	0.50	[69]
Internal thoracic artery	-	1000	1.5	[69]
Silicon Catheter	1000-2000	2000-3000	4.0	[74]

A human aortic valve has UTS (circumferential) of 750 – 2500 kPa and elongation at break of 0.10 – 0.17 mm/mm [71]. The mechanical properties obtained for pHEMA/GO composites (YM ≅ 2100 kPa, UTS ≅ 680 kPa and elongation at break ≅ 0.30 mm/mm) are very similar to these, to currently used porcine aortic valves (UTS (circumferential) ≅ 1000 kPa and elongation

at break ≅ 0.23 mm/mm) [71] and to other materials under research like tissue engineered fabricated porous polyhydroxyalkanoate heart valves (YM ≅ 3 000 kPa, UTS (circumferential) ≅ 700 kPa and elongation at break ≅ 0.33 mm/mm) [71, 73]. The design of vascular grafts could be another future application for these pHEMA/GBMs hydrogels. Tensile resistance of native veins and arteries is about 1000 kPa while elongation at break rounds the 0.50 mm/mm for saphenous vein. However, blood vessels display a J-shaped stress–strain curve that is essential for their compliance. This should be taken into consideration in further optimizations of pHEMA/GBMs composites for this application, as well as the achievement of sufficient suture retention strength. Catheters are another potential application of pHEMA/GO hydrogels. The YM of silicon catheters is 1000-2000 kPa, very similar to the obtained for our composites, despite silicon catheters having higher resistance to tensile stress (2000-3000 kPa) and elasticity (4 mm/mm) [74]. Nevertheless, the lower elasticity of our composites may not be an issue for this application, since catheters made from other polymers such as polyurethane have elasticity in the elastic part of tensile resistance similar to obtained values for pHEMA/GO [74].

In this study, it was demonstrated that oxidized GBMs can effectively increase the mechanical properties of pHEMA without affecting its bio/hemocompatibility (*in vitro* and *in vivo*), showing great potential for use in several blood contacting devices, with better performance than the materials available nowadays. Its usage could avoid numerous problems associated with BCDs, such as thrombosis and infection occurrence, as recently review by Jaffer *et al.* [20]. A future application of these composites in clinics demands further studies that are beyond the scope of this paper, namely the production and optimization of a specific BCDs, and *in vivo* implantation in order to evaluate long-term performance.

4.5 Conclusion

Five different types of GBMs, varying in oxidation degree, thickness and lateral size, were successfully incorporated in pHEMA by *in situ* polymerization. In spite of the increase in surface roughness of pHEMA, more predominant when the oxidized GBMs were incorporated, wettability of pHEMA is only affected when GNP M15 and GNP M15ox were used, while swelling capacity of pHEMA/GBMs is maintained for all composites. Regarding the mechanical reinforcement of pHEMA, oxidation degree and lower thickness of GBMs revealed to be crucial factors in order to achieve higher improvements (2.5× in YM and 4.4× in UTS, reaching 1800 kPa and 680 kPa, respectively) in the mechanical properties of pHEMA, while particles lateral size had a minor effect. As such, GO was the most efficient filler concerning pHEMA's increase in stiffness and tensile resistance. Incorporation of oxidized GBMs did not affect bacterial adhesion to pHEMA, keeping its non-fouling properties. All the pHEMA/GBMs composites

exhibited negligible levels of blood platelets adhesion and activation, and had non-hemolytic potential and were non-cytotoxic. The hemocompatibility of pHEMA/GO was confirmed *in vivo* when a 3D tubular prototype was evaluated in an AV-shunt acute model in pigs. Thus, materials developed in this study revealed to be promising for application in the design of BCDs.

4.6 Acknowledgements

The authors acknowledge the support of the i3S Scientific Platform specifically André Maia from BioSciences Screening for and Rui Fernandes from Histology and Electron Microscopy Service, member of the PPBI (PPBI-POCI-01-0145-FEDER-022122), Ricardo Vidal from Biointerfaces and Nanotechnology of INEB/i3S for the assistance in FTIR and contact angle analysis. The authors would like to thank Rui Rocha and Daniela Silva for the assistance in SEM analysis at CEMUP, Porto, Eng. Carlos Sá for XPS analysis at CEMUP, Porto and i3S and serviço de Imunohemoterapia of Centro Hospitalar Universitário de São João (CHUSJ) for platelets donating.

Andreia T. Pereira and P. C. Henriques wish to thank FCT for PhD grant PD/BD/114156/2016 and SFRH/BD/120154/2016, respectively, funded by European Social Fund and Portuguese Ministry of Education and Science through Programa Operacional Capital Humano. This work was financially supported by project POCI-01-0145-FEDER-032431, POCI-01-0145-FEDER-006939, POCI-01-0145-FEDER-007274, PTDC/CTM-COM/32431/2017 and PTDC/CTM-BIO/4033/2014, and UID/EQU/00511/2019 – LEPABE funded by national funds through FCT/MCTES (PIDDAC).

4.7 References

[1] B.D. Ratner, The catastrophe revisited: blood compatibility in the 21st Century, Biomaterials 28(34) (2007) 5144-7.

[2] B.D. Ippel, P.Y.W. Dankers, Introduction of Nature's Complexity in Engineered Blood-compatible Biomaterials, Adv Healthc Mater 7(1) (2018).

[3] A.S.H. B. D. Ratner, F. J. Schoen, J. E. Lemons, Application of Materials in Medicine and Dentisty, in: E. Science (Ed.), Biomaterials Science: An Introduction to Materials in Medicine, Oxford2012, pp. 283-375.

[4] M.A. Shahbazi, M. Hamidi, E.M. Makila, H. Zhang, P.V. Almeida, M. Kaasalainen, J.J. Salonen, J.T. Hirvonen, H.A. Santos, The mechanisms of surface chemistry effects of mesoporous silicon nanoparticles on immunotoxicity and biocompatibility, Biomaterials 34(31) (2013) 7776-89.

[5] Z. He, Z. Shi, W. Sun, J. Ma, J. Xia, X. Zhang, W. Chen, J. Huang, Hemocompatibility of folic-acid-conjugated amphiphilic PEG-PLGA copolymer nanoparticles for co-delivery of cisplatin and paclitaxel: treatment effects for non-small-cell lung cancer, Tumour biology : the journal of the International Society for Oncodevelopmental Biology and Medicine 37(6) (2016) 7809-21.
[6] M. Weber, H. Steinle, S. Golombek, L. Hann, C. Schlensak, H.P. Wendel, M. Avci-Adali, Blood-Contacting Biomaterials: In Vitro Evaluation of the Hemocompatibility, Front Bioeng Biotechnol 6 (2018) 99.
[7] H. Yu, S. Engel, G. Janiga, D. Thevenin, A Review of Hemolysis Prediction Models for Computational Fluid Dynamics, J Art Org 41(7) (2017) 603-621.
[8] Y. Shapira, M. Vaturi, A. Sagie, Hemolysis Associated With Prosthetic Heart Valves: A Review, Cardiol Rev 17(3) (2009) 121-124.
[9] J. Sjollema, S.A.J. Zaat, V. Fontaine, M. Ramstedt, R. Luginbuehl, K. Thevissen, J. Li, H.C. van der Mei, H.J. Busscher, In vitro methods for the evaluation of antimicrobial surface designs, Acta Biomater 70 (2018) 12-24.
[10] W.F. Oliveira, P.M.S. Silva, R.C.S. Silva, G.M.M. Silva, G. Machado, L. Coelho, M.T.S. Correia, Staphylococcus aureus and Staphylococcus epidermidis infections on implants, J Hosp Infect 98(2) (2018) 111-117.
[11] S. Schopka, T. Schmid, C. Schmid, K. Lehle, Current Strategies in Cardiovascular Biomaterial Functionalization, Materials 3(1) (2010) 638.
[12] I. Reviakine, F. Jung, S. Braune, J.L. Brash, R. Latour, M. Gorbet, W. van Oeveren, Stirred, shaken, or stagnant: What goes on at the blood-biomaterial interface, Blood reviews 31(1) (2017) 11-21.
[13] A. Wallace, H. Albadawi, N. Patel, A. Khademhosseini, Y.S. Zhang, S. Naidu, G. Knuttinen, R. Oklu, Anti-fouling strategies for central venous catheters, Cardiovasc Diagn Ther 7(Suppl 3) (2017) S246-S257.
[14] D. Campoccia, L. Montanaro, C.R. Arciola, A review of the biomaterials technologies for infection-resistant surfaces, Biomaterials 34(34) (2013) 8533-54.
[15] S. Movafaghi, V. Leszczak, W. Wang, J.A. Sorkin, L.P. Dasi, K.C. Popat, A.K. Kota, Hemocompatibility of Superhemophobic Titania Surfaces, Adv Healthc Mater 6(4) (2017).
[16] X. Liu, L. Yuan, D. Li, Z. Tang, Y. Wang, G. Chen, H. Chen, J.L. Brash, Blood compatible materials: state of the art, J Mater Chem B 2(35) (2014) 5718-5738.
[17] L. Pocivavsek, S.H. Ye, J. Pugar, E. Tzeng, E. Cerda, S. Velankar, W.R. Wagner, Active wrinkles to drive self-cleaning: A strategy for anti-thrombotic surfaces for vascular grafts, Biomaterials 192 (2019) 226-234.

[18] X. Dong, X. Yuan, L. Wang, J. Liu, A.C. Midgley, Z. Wang, K. Wang, J. Liu, M. Zhu, D. Kong, Construction of a bilayered vascular graft with smooth internal surface for improved hemocompatibility and endothelial cell monolayer formation, Biomaterials 181 (2018) 1-14.

[19] R.A. Hoshi, R. Van Lith, M.C. Jen, J.B. Allen, K.A. Lapidos, G. Ameer, The blood and vascular cell compatibility of heparin-modified ePTFE vascular grafts, Biomaterials 34(1) (2013) 30-41.

[20] I.H. Jaffer, J.I. Weitz, The blood compatibility challenge. Part 1: Blood-contacting medical devices: The scope of the problem, Acta Biomater 94 (2019) 2-10.

[21] O. Wichterle, D. LÍM, Hydrophilic Gels for Biological Use, Nature 185 (1960) 117.

[22] L. Indolfi, F. Causa, P.A. Netti, Coating process and early stage adhesion evaluation of poly(2-hydroxy-ethyl-methacrylate) hydrogel coating of 316L steel surface for stent applications, J Mater Sci Mater Med 20(7) (2009) 1541-51.

[23] J. Montheard, M. Chatzopoulos, D. Chappard, 2-Hydroxyethyl Methacrylate (HEMA): Chemical Properties and Applications in Biomedical Fields, J Macromol Sci R M C 32(1) (1992) 1-34.

[24] J. Montheard, M. Chatzopoulos, D. Chappard, 2-Hydroxyethyl Methacrylate (HEMA): Chemical Properties and Applications in Biomedical Fields, J Macromol Sci C: Polymer Reviews 32(1) (1992) 1-34.

[25] N.Y. Kostina, C. Rodriguez-Emmenegger, M. Houska, E. Brynda, J. Michalek, Non-fouling hydrogels of 2-hydroxyethyl methacrylate and zwitterionic carboxybetaine (meth)acrylamides, Biomacromolecules 13(12) (2012) 4164-70.

[26] A. Dixit, D.S. Bag, S.J.S. Kalra, Synthesis of strong and stretchable double network (DN) hydrogels of PVA-borax and P(AM-co-HEMA) and study of their swelling kinetics and mechanical properties, Polymer 119 (2017) 263-273.

[27] S. Atzet, S. Curtin, P. Trinh, S. Bryant, B. Ratner, Degradable poly(2-hydroxyethyl methacrylate)-co-polycaprolactone hydrogels for tissue engineering scaffolds, Biomacromolecules 9(12) (2008) 3370-7.

[28] K. Chen, S. Zhou, L. Wu, Self-repairing nonfouling polyurethane coatings via 3D-grafting of PEG-b-PHEMA-b-PMPC copolymer, Rsc Adv 5(127) (2015) 104907-104914.

[29] Y.Y. Liu, D.M. Liu, S.Y. Chen, T.H. Tung, T.Y. Liu, In situ synthesis of hybrid nanocomposite with highly order arranged amorphous metallic copper nanoparticle in poly(2-hydroxyethyl methacrylate) and its potential for blood-contact uses, Acta Biomater 4(6) (2008) 2052-8.

[30] B.W. Hanak, C.Y. Hsieh, W. Donaldson, S.R. Browd, K.K.S. Lau, W. Shain, Reduced cell attachment to poly(2-hydroxyethyl methacrylate)-coated ventricular catheters in vitro, J Biomed Mater Res B Appl Biomater 106(3) (2018) 1268-1279.

[31] N.Y. Kostina, C. Rodriguez-Emmenegger, M. Houska, E. Brynda, J. Michálek, Non-fouling Hydrogels of 2-Hydroxyethyl Methacrylate and Zwitterionic Carboxybetaine (Meth)acrylamides, Biomacromolecules 13(12) (2012) 4164-4170.
[32] Q. Wei, R. Haag, Universal polymer coatings and their representative biomedical applications, Mater Horiz 2(6) (2015) 567-577.
[33] A.T. Pereira, P.C. Henriques, P.C. Costa, M.C.L. Martins, F.D. Magalhaes, I.C. Goncalves, Graphene oxide-reinforced poly(2-hydroxyethyl methacrylate) hydrogels with extreme stiffness and high-strength, Compos Sci Technol 184 (2019) 107819.
[34] A. Bianco, H.-M. Cheng, T. Enoki, Y. Gogotsi, R.H. Hurt, N. Koratkar, T. Kyotani, M. Monthioux, C.R. Park, J.M.D. Tascon, J. Zhang, All in the graphene family – A recommended nomenclature for two-dimensional carbon materials, Carbon 65 (2013) 1-6.
[35] D.G. Papageorgiou, I.A. Kinloch, R.J. Young, Mechanical properties of graphene and graphene-based nanocomposites, Prog Mater Sci 90 (2017) 75-127.
[36] A.M. Pinto, C. Gonçalves, D.M. Sousa, A.R. Ferreira, J.A. Moreira, I.C. Gonçalves, F.D. Magalhães, Smaller particle size and higher oxidation improves biocompatibility of graphene-based materials, Carbon 99(Supplement C) (2016) 318-329.
[37] I.C. Goncalves, M.C. Martins, M.A. Barbosa, B.D. Ratner, Protein adsorption and clotting time of pHEMA hydrogels modified with C18 ligands to adsorb albumin selectively and reversibly, Biomaterials 30(29) (2009) 5541-51.
[38] A.T. Pereira, P.C. Henriques, P.C. Costa, M.C.L. Martins, F.D. Magalhães, I.C. Gonçalves, Graphene oxide-reinforced poly(2-hydroxyethyl methacrylate) hydrogels with extreme stiffness and high-strength, Compos Sci Technol 184 (2019) 107819.
[39] A. Kovtun, D. Jones, S. Dell'Elce, E. Treossi, A. Liscio, V. Palermo, Accurate chemical analysis of oxygenated graphene-based materials using X-ray photoelectron spectroscopy, Carbon 143 (2019) 268-275.
[40] K. Krishnamoorthy, M. Veerapandian, K. Yun, S.J. Kim, The chemical and structural analysis of graphene oxide with different degrees of oxidation, Carbon 53 (2013) 38-49.
[41] S. Vranic, A.F. Rodrigues, M. Buggio, L. Newman, M.R.H. White, D.G. Spiller, C. Bussy, K. Kostarelos, Live Imaging of Label-Free Graphene Oxide Reveals Critical Factors Causing Oxidative-Stress-Mediated Cellular Responses, ACS Nano 12(2) (2018) 1373-1389.
[42] C. Sommer, C. Straehle, U. Kothe, F.A. Hamprecht, Ilastik: Interactive Learning and Segmentation Toolkit, I S Biomed Imaging (2011) 230-233.
[43] A.E. Carpenter, T.R. Jones, M.R. Lamprecht, C. Clarke, I.H. Kang, O. Friman, D.A. Guertin, J.H. Chang, R.A. Lindquist, J. Moffat, P. Golland, D.M. Sabatini, CellProfiler: image analysis software for identifying and quantifying cell phenotypes, Genome Biol 7(10) (2006) R100.

[44] P. Trucano, R. Chen, Structure of graphite by neutron diffraction, Nature 258(5531) (1975) 136-137.
[45] L. Stobinski, B. Lesiak, A. Malolepszy, M. Mazurkiewicz, B. Mierzwa, J. Zemek, P. Jiricek, I. Bieloshapka, Graphene oxide and reduced graphene oxide studied by the XRD, TEM and electron spectroscopy methods, J Electron Spectros Relat Phenomena 195 (2014) 145-154.
[46] C.W. Huang, Y.M. Sun, W.F. Huang, Polymerization Kinetics of Poly(2-Hydroxyethyl Methacrylate) Hydrogels and Nanocomposite Materials, J Polym Sci Pol Chem 5(4) (2017) 1873-1889.
[47] Z.Y. Cheng, S.H. Teoh, Surface modification of ultra thin poly (epsilon-caprolactone) films using acrylic acid and collagen, Biomaterials 25(11) (2004) 1991-2001.
[48] Z. Xu, C. Gao, In situ Polymerization Approach to Graphene-Reinforced Nylon-6 Composites, Macromolecules 43(16) (2010) 6716-6723.
[49] J.R. Potts, S.H. Lee, T.M. Alam, J. An, M.D. Stoller, R.D. Piner, R.S. Ruoff, Thermomechanical properties of chemically modified graphene/poly(methyl methacrylate) composites made by in situ polymerization, Carbon 49(8) (2011) 2615-2623.
[50] N.D. Luong, U. Hippi, J.T. Korhonen, A.J. Soininen, J. Ruokolainen, L.-S. Johansson, J.-D. Nam, L.H. Sinh, J. Seppälä, Enhanced mechanical and electrical properties of polyimide film by graphene sheets via in situ polymerization, Polymer 52(23) (2011) 5237-5242.
[51] J.-Y. Wang, S.-Y. Yang, Y.-L. Huang, H.-W. Tien, W.-K. Chin, C.-C.M. Ma, Preparation and properties of graphene oxide/polyimide composite films with low dielectric constant and ultrahigh strength via in situpolymerization, J Mater Chem A 21(35) (2011) 13569-13575.
[52] X. Wang, Y. Hu, L. Song, H. Yang, W. Xing, H. Lu, In situ polymerization of graphene nanosheets and polyurethane with enhanced mechanical and thermal properties, J Mat Chem 21(12) (2011) 4222-4227.
[53] I.S. Tsagkalias, T.K. Manios, D.S. Achilias, Effect of Graphene Oxide on the Reaction Kinetics of Methyl Methacrylate In Situ Radical Polymerization via the Bulk or Solution Technique, Polymers (Basel) 9(9) (2017).
[54] C. Lee, X. Wei, J.W. Kysar, J. Hone, Measurement of the elastic properties and intrinsic strength of monolayer graphene, Science 321(5887) (2008) 385-8.
[55] D.A. Dikin, S. Stankovich, E.J. Zimney, R.D. Piner, G.H.B. Dommett, G. Evmenenko, S.T. Nguyen, R.S. Ruoff, Preparation and characterization of graphene oxide paper, Nature 448 (2007) 457.
[56] Y. Huang, M. Zhang, W. Ruan, High-water-content graphene oxide/polyvinyl alcohol hydrogel with excellent mechanical properties, J. Mater. Chem. A 2(27) (2014) 10508-10515.
[57] G. Anagnostopoulos, C. Androulidakis, E.N. Koukaras, G. Tsoukleri, I. Polyzos, J. Parthenios, K. Papagelis, C. Galiotis, Stress transfer mechanisms at the submicron level for graphene/polymer systems, Acs Appl Mater Inter 7(7) (2015) 4216-23.

[58] L. Gong, R.J. Young, I.A. Kinloch, I. Riaz, R. Jalil, K.S. Novoselov, Optimizing the reinforcement of polymer-based nanocomposites by graphene, ACS Nano 6(3) (2012) 2086-95.
[59] Z. Li, I.A. Kinloch, R.J. Young, The role of interlayer adhesion in graphene oxide upon its reinforcement of nanocomposites, Philosophical transactions. Series A, Mathematical, physical, and engineering sciences 374(2071) (2016) 20150283.
[60] E.Z. Zhang, T. Wang, C.X. Lian, W.X. Sun, X.X. Liu, Z. Tong, Robust and thermo-response graphene-PNIPAm hybrid hydrogels reinforced by hectorite clay, Carbon 62 (2013) 117-126.
[61] O. Okay, General Properties of Hydrogels, in: G. Gerlach, Arndt, K.-F. (Ed.), Hydrogel Sensors and Actuators 2010, pp. 1-14.
[62] R.L. Taylor, J. Verran, G.C. Lees, A.J.P. Ward, The influence of substratum topography on bacterial adhesion to polymethyl methacrylate, J Mater Sci-Mater M 9(1) (1998) 17-22.
[63] V. Vadillo-Rodriguez, A.I. Guerra-Garcia-Mora, D. Perera-Costa, M.L. Gonzalez-Martin, M.C. Fernandez-Calderon, Bacterial response to spatially organized microtopographic surface patterns with nanometer scale roughness, Colloids Surf B Biointerfaces 169 (2018) 340-347.
[64] B. Singh, B. Singh, Influence of graphene-oxide nanosheets impregnation on properties of sterculia gum-polyacrylamide hydrogel formed by radiation induced polymerization, Int J Biol Macromol 99 (2017) 699-712.
[65] A.M. Pinto, S. Moreira, I.C. Goncalves, F.M. Gama, A.M. Mendes, F.D. Magalhaes, Biocompatibility of poly(lactic acid) with incorporated graphene-based materials, Colloids and Surf B, Biointerfaces 104 (2013) 229-38.
[66] S. Thampi, V. Muthuvijayan, R. Parameswaran, Mechanical characterization of high-performance graphene oxide incorporated aligned fibroporous poly(carbonate urethane) membrane for potential biomedical applications, J Appl Polym Sci 132(16) (2015) n/a-n/a.
[67] A. Modi, S.K. Verma, J. Bellare, Graphene oxide-doping improves the biocompatibility and separation performance of polyethersulfone hollow fiber membranes for bioartificial kidney application, J Colloid Interface Sci 514 (2017) 750-759.
[68] C. Nojiri, K. Senshu, T. Okano, Nonthrombogenic polymer vascular prosthesis, J Art Org 19(1) (1995) 32-8.
[69] S. Pashneh-Tala, S. MacNeil, F. Claeyssens, The Tissue-Engineered Vascular Graft-Past, Present, and Future, Tissue Eng Part B Rev 22(1) (2016) 68-100.
[70] S. Aslam, R.O. Darouiche, Mechanical Integrity of Hemodialysis Catheters is Maintained After Exposure to a Novel Catheter Lock Solution, Infect Control Hosp Epidemiol 31(11) (2010) 1124-1129.
[71] A. Hasan, K. Ragaert, W. Swieszkowski, S. Selimovic, A. Paul, G. Camci-Unal, M.R. Mofrad, A. Khademhosseini, Biomechanical properties of native and tissue engineered heart valve constructs, J Biomec 47(9) (2014) 1949-63.

[72] A. Balguid, M.P. Rubbens, A. Mol, R.A. Bank, A.J. Bogers, J.P. van Kats, B.A. de Mol, F.P. Baaijens, C.V. Bouten, The role of collagen cross-links in biomechanical behavior of human aortic heart valve leaflets--relevance for tissue engineering, Tiss Eng 13(7) (2007) 1501-11.

[73] R. Sodian, S.P. Hoerstrup, J.S. Sperling, S. Daebritz, D.P. Martin, A.M. Moran, B.S. Kim, F.J. Schoen, J.P. Vacanti, J.E. Mayer, Jr., Early in vivo experience with tissue-engineered trileaflet heart valves, Circulation 102(19 Suppl 3) (2000) Iii22-9.

[74] S. Aslam, R.O. Darouiche, Mechanical Integrity of Hemodialysis Catheters is Maintained After Exposure to a Novel Catheter Lock Solution, Infection control and hospital epidemiology : the official journal of the Society of Hospital Epidemiologists of America 31(11) (2010) 1124-1129.

4.8 Supporting Information

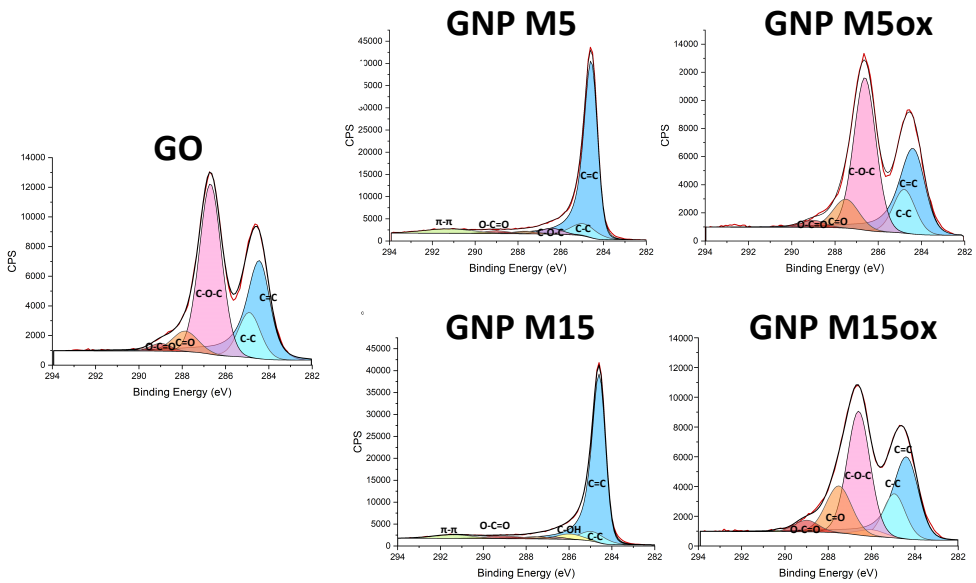

GBMs	Chemical group (%)						
	C sp2 (284.2–284.5 eV)	C sp3 (284.8–284.9 eV)	C-OH (285.3–286.0 eV)	C-O-C (286.1–286.6 eV)	C=O (287.5–287.9 eV)	O-C=O (288.8–288.9 eV)	π-π (290.0–292.0 eV)
GO	34.0	12.0	-	45.4	6.4	1.9	0.3
GNP M5	77.6	8.5	0.5	3.6	1.8	2.0	6.1
GNP M5ox	32.9	12.3	-	43.0	9.5	2.1	0.3
GNP M15	78.4	7.1	4.0	1.4	1.8	3.2	4.1
GNP M15ox	31.1	12.2	2.2	35.8	15.2	3.4	0.1

Figure. S.1 – C1s high resolution spectra of GO, GNP M5, GNP M5ox, GNP M15 and GNP M15ox.

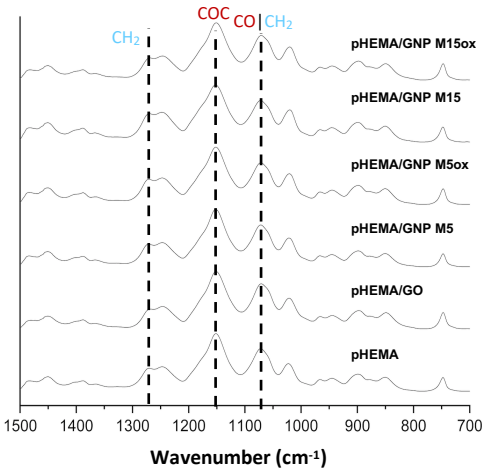

Figure S.2 - Infrared spectra of pHEMA and pHEMA/GBMs composites.

Table S.1 – Pig information, blood profiles evaluated by a hematology analyzer (Advia 2120, Siemens Healthineers)

Weight	Pig 1 57 kg		Pig 2 55 kg	
	Before	After	Before	After
Body temperature	38.9	39.8	39	39.5
White Blood Cells (cells/μL)	11.91 x 10^3	12.58 x 10^3	20.02 x 10^3	18.87 x 10^3
Red Blood Cells (cells/μL)	5.40 x 10^6	6.15 x 10^6	5.96 x 10^6	5.86 x 10^6
Platelets (cells/μL)	221 x 10^3	242 x 10^3	386 x 10^3	368 x 10^3
Platelets clumps	No	No	No	No
Blood pressure (mmHg)	100/70	99/78	99/78	97/70
Blood flow Carotid Artery (mL/min)	201	-	200 (mL/min)	-

Chapter 5

GO-coated decellularized arteries with improved mechanical and biological performance

The lack of an effective alternative to autologous graft in the replacement of small diameter vessels (inner diameter < 5 mm) has a huge impact in the prognostic and progression of cardiovascular diseases, the major cause of death globally. Decellularized arteries have been proposed as alternative but their performance is still not enough for a successful application in the market. In this study, GO was proposed as coating of decellularized umbilical cord and placenta chorion arteries, aiming to suppress their poor mechanical properties and to promote their hemocompatibility. In decellularized umbilical cord arteries an increase of 27%, 29% and 25% was observed for maximum force, burst pressure and strain, respectively, reaching values similar to human saphenous vein, that is used nowadays for vessels replacement. Besides the increase in mechanical properties, GO coatings reduced platelets adhesion in decellularized artery without compromising endothelial cells adhesion. In vivo pig arteriovenous-shunt revealed that successful implantation can be achieved after a heparinization step. Overall, our results show that GO-coating has an effective role in the improvement of decellularized umbilical cord arteries performance which is a step forward on the transition from lab bench to market of these grafts.

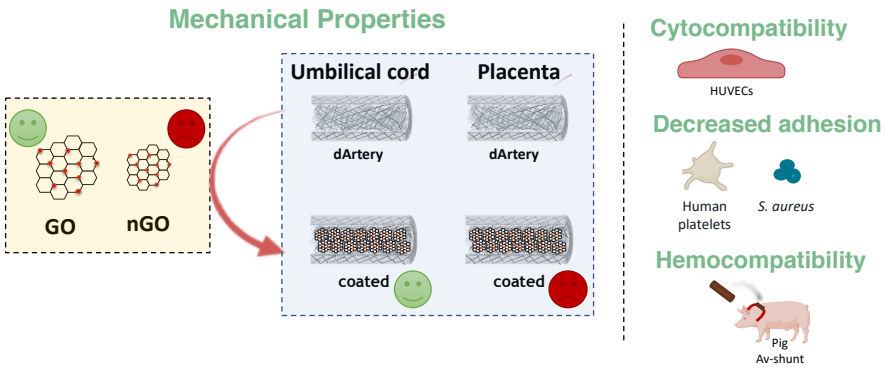

Keywords: Arteriovenous-shunt, coating, Decellularized Arteries, Graphene oxide, Hemocompatibility, Mechanical properties

This chapter is based on the following paper in preparation:

A.T. Pereira, K. H. Schneider, P.C. Henriques, S. Melo, C. Grasl, A. L. Pires, A. M Pereira, M.C.L. Martins, H. Bergmeister, I.C. Gonçalves, GO-coated decellularized arteries with improved mechanical and biological performance

5.1 Introduction

Every year approximately 400 000 arterial bypass surgeries are performed only in the US. For the reconstruction of large caliber vessels (inner diameter - i.d. > 5 mm), there are commercially available synthetic grafts that show excellent outcomes. However, for the replacement of small-diameter vessels (< 5 mm), such as coronary arteries and below-knee vessels, these materials exhibit low patency rates due to the occurrence of thrombosis, intimal hyperplasia and/or chronic inflammation. Despite the several efforts for the development of new strategies [1-4], the use of autologous grafts (e.g. saphenous vein) is still the gold standard for the reconstruction of small-diameter vessels [5, 6]. This approach is associated to several limitations such as high failure rate (40-50%) after ten years for coronary arteries replacement, the requirement of multiple surgical interventions and, in 30% of the cases, this vein is not available due to previous harvest, anatomical limitations or disease progression [6, 7]. All these facts highlight an urgent need for new prosthesis to substitute small-diameter vascular vessels.

The use of decellularized arteries derived from several sources has been extensively explored for the replacement of small diameter vessels [8-47] since they are naturally derived and preserve the architecture and molecular cues to support cell recruitment and adhesion [48, 49]. However, the collagen exposure, which promotes thrombosis and infection occurrence, the mismatch in mechanical properties and the late endothelialization of the luminal surface are some problems associated with the use of decellularized matrices as an acellular scaffold for the reconstruction of small caliber vessels [1, 10, 50]. Some strategies have been adopted to improve their performance such as promoting reendothelialization before implantation [38, 39, 45, 51-56], using chemical crosslinkers [20, 57, 58], combination with other polymers [59], modifying their surface lumen with endothelial growth factors [60, 61], peptides (that stimulate cell adhesion) [62], heparin [40-42, 63-68] or others sulfated polysaccharides [19]. Despite the observed better outcomes, most of these grafts are complex to produce involving several steps and/or are not off-the shelf available, which demands better solutions.

Graphene is a 2D material that consists in a single layer of sp^2-bonded carbon atoms organized in a crystalline honeycomb lattice. This structure confers unique properties to graphene and also graphene-based materials (GBMs), such as graphene oxide, making them attractive for several applications, including in the biomedical field. From all GBMs features is important to highlight their exceptional mechanical properties, being described as the strongest material in the world [69, 70], antimicrobial features [71, 72], namely when exposed at the surface. Despite several studies focus on the mechanical properties of GBMs nanocomposites, as reviewed by Papageorgiou *et al.* [70], only some studies point out the effect of GBMs coating, which showed to improve the filler performance of glasses [73, 74] and carbon fibers

[75, 76] and acellular dermal matrix [77]. At our knowledge, coatings of decellularized matrices with GBMs are poorly explored in literature being reported for acellular dermal matrix exhibiting a better mechanical performance [77], decellularized sciatic nerve matrices showing a benefic effect in its regeneration [78], for decellularized pulmonary valve not exhibiting a specific advantage for hemocompatibility [79] and as a support platform for a dual enzymatic system that promotes anti-coagulation [80].

The ideal vascular graft should be available off-the shelf, exhibit a good performance upon long-time implantation, show low inflammatory, thrombogenic and infectious potential and match the mechanical properties of recipient's vessel. We herein propose the coating of decellularized arteries with GO materials aiming to improve the mechanical performance, hemocompatibility and also to confer them an anti-infective potential. For this, arteries from two different human sources with distinct vascular anatomy were used. Umbilical cord exhibits in all its extension (20-80 cm) two long arteries (inner diameter (i.d.) 1.5 mm under collapsed conditions and 4.5-5.5 mm under physiological pressure) which form a cylindrical helix around the umbilical vein (i.d. 4 mm) [81, 82] while vessels of chorion placenta are highly ramified with a shorter length 1-2 cm and a variable i.d. (0.55-3.2 mm) [83]. This heterogeneity in the placenta chorion arteries could enable the obtention of grafts that perfectly match the host vessel, but their short length, the presence of some microvasculature and isolation procedure (which sometimes induces some leaks) could unfeasible their usage. Upon arteries isolation and decellularization, a coating with graphene oxide was performed.

After this, a deep characterization was carried out being the grafts analyzed regarding coating homogeneity, mechanical properties, cytocompatibility, bacterial adhesion and hemocompatibility. The *in vivo* hemocompatibility of the most promising graft was evaluated through arteriovenous shunt in the pig model.

5.2 Methods

5.2.1 Decellularized arteries

5.2.1.1 Isolation and decellularization

Human placenta and umbilical cord tissues of caesarian births were either obtained from the Vienna General Hospital, Austria or Centro Hospitalar de S. João, Porto, Portugal with the approval of the ethical committee and informed consent of the donors. Umbilical cord and placenta vasculature were rinsed with PBS to remove the remaining blood in the vessels being isolated and connected to a surgical thread to a 14GA BD Venflon™. After the isolation, arteries were decellularized as previously described [10, 68]. Briefly, the arteries were frozen at -80 °C during at least 18 h and thawed in PBS at room temperature. The arteries were connected through the Venflon to a recirculating perfusion system being perfused with

hypertonic solution (1.4% NaCl, 1 h), followed by dH_2O (20 min), PBS (10 min), 1% Triton X-100 and 0.02% w/w ethylene-diamine-tetra acetic acid (EDTA) in phosphate buffered saline (PBS) (20 h) at room temperature. To eliminate the detergent, arteries were afterwards perfused with PBS for 24 h, being PBS exchanged several times. DNase enzymatic treatment (200 IU/ml, Roche) was performed overnight at 4 °C under static conditions followed by PBS rinsing during 3h. For chemical sterilization, decellularized arteries (dArteries) were incubated with an aqueous solution of 0.18% (w/v) peracetic acid containing 4.8% ethanol (v/v) for 90 minutes, followed by rinsing with sterile PBS (3 x 10 min).

5.2.1.2 Characterization

a) Histology

Native and decellularized arteries were cut with 5 mm length and fixed in formaldehyde solution 4%, buffered, pH 6.9 (Sigma-Aldrich) for 24 h, at 4 ºC. The samples were washed with water and transferred to 70% ethanol and dehydrated in an ethanol ascending series. The specimens were embedded in paraffin and cut into 5-μm sections. After slides deparaffinization, they were stained with H&E and scanned in light microscope to visualize nuclear material.

b) DNA identification and quantification

DNA remnants in tissue were evaluated through propidium iodide (PI) staining of arteries lumen. The tissue was incubated with 3 nM PI solution for 15 min at 37 °C being evaluated in a fluorescence microscope.

DNA content of native and decellularized arteries was determined using the AccuBlue® High Sensitivity dsDNA Quantitation Kit. Arteries segments were freeze-dried, weighed and digested in papain buffer (papain 250 μg/mL, 1.57 mg/L cysteine, 5 mM NaCl, 22.5 mM Na citrate, 15 mM EDTA, 0.1 M NaH_2PO_4, pH 6.0) at 60 °C overnight [17]. The papain sample solution was incubated with a solution kit being the DNA amount quantified measuring the fluorescence at an excitation wavelength of 485 nm and an emission wavelength of 530 nm. DNA from calf thymus (Invitrogen) was used as standard.

c) SEM

Scanning Electron Microscopy images were acquired after arteries fixation in 2.5% glutaraldehyde (Sigma-Aldrich) in PBS overnight at 4 °C, being the samples dried in graded ethanol series (50%, 60%, 70%, 80%, 90%, 99%; 10 min each), with hexamethyldisilazane (HMDS) used as drying agent evaporating overnight. All samples were coated with a thin layer of gold/palladium by sputtering. A FEI Quanta 400FEG ESEM / EDAX Genesis X4M SEM and

Zeiss EVO 10 with an accelerating voltage of 5, 10 or 15 kV, were used to visualize the samples.

5.2.2 Graphene Oxide (GO) synthesis and characterization

5.2.2.1 Graphene Oxide (GO) synthesis

GO used for incorporation in decellularized matrices were obtained by graphite oxidation and exfoliation through modified Hummers method, as previously described – GO [84] or commercially available (795534, Aldrich) - nGO. Briefly, carbon graphite micropowder (purity: ≥99% and laterla size: 7-11 μm, American Elements) was added to a mixture containing H2SO4/H3PO4 (4:1) followed by cooling to 0 °C and addition of KMnO4. After that, the reaction was kept at 35 °C and stirred for 2 h followed by cooling to 0 °C and addition of 450 mL of distilled water. To eliminate the excess of $KMnO_4$, H_2O_2 was added until oxygen release stopped. After overnight resting, the material was consecutively centrifuged at 4000 rpm for 20 min, until pH of supernatant reached the pH of distilled water. The suspension was sonicated during 6 h in an ultrasonic bath to obtain GO. Both GO materials were sterilized with 70% ethanol.

5.2.2.2 GO characterization

a) XPS

X-ray photoelectron spectroscopy (XPS) was performed to evaluate the oxidation degree of GO and nGO using a Kratos Axis Ultra HAS (Kratos Analytical, UK) equipment. An Al monochromator with 15 kW was used as X-ray source. The survey spectrum of GBMs was obtained at 80 eV and the C 1s high resolution spectra at 40 eV. CasaXPS processing software version 2.3.16 was used to deconvolute the C 1s high resolution spectra. After a Shirley background type subtraction, the C1s spectral component was set at a binding energy of 284.6 eV to correct the contribution of charge effect. C1s high resolution spectra were fitted into seven peaks being constrained for the following binding energies sp^2 C=C (284.2–284.5 eV), sp^3 C–C (284.8–284.9 eV), C–OH (285.3–286.0 eV), C–O–C (286.1–286.6 eV), C=O (287.5–287.9), O–C=O (288.8–288.9 eV) and π–π (290–292 eV) based on literature data [85-87]. sp^2 carbon peak due to its asymmetric nature was fitted using an asymmetric Lorentzian function (LF) with an asymmetry parameter of 0.14 [85] while a Gaussian–Lorentzian (70:30) function was used to fit the remaining peaks.

b) XRD

X-ray powder diffraction were performed to determine the thickness and interlayer spacing of GO and nGO particles crystallinity. GO and nGO were dried in a vacuum oven 60º overnight being XRD performed, at room temperature, in a SmartLab Rigaku® diffractometer that operates with 45 kV and 200 mA and have a Cu-Kα radiation source with a wavelength of λ = 1.540593 Å in a Bragg-Brentano θ/2θ configuration. All the samples were measured with step size of 0.01º in a range of 5 to 30 theta (2θ) using a rotative system (30 Deg/min) which increases. Thickness and crystallites interlayer d-spacing were calculated through Bragg's law equation:

$$n\lambda = 2dsin\theta \qquad \text{Equation 1}$$

where n is a positive integer, λ is the wavelength, d is the interplanar spacing and θ is the incident angle of the X-ray beam

and Debye-Scherrer equation:

$$\tau = \frac{K\,\lambda}{\sqrt{B_m^2 - B_s^2}\cos\theta} \qquad \text{Equation 2}$$

where τ corresponds to GBMs crystalline size in the direction perpendicular to the lattice planes, K is the Debye–Scherrer constant (~0.89 for graphitic materials), λ is the incident X-ray wavelength, $\sqrt{B_m^2 - B_s^2}$ is the full width at half-maximum (FWHM) of the XRD peak and θ is the diffraction angle. The number of layers was determined by dividing the thickness by the d-SEM images of GO and nGO were acquired to evaluate their surface morphology.

c) TEM

Transmission electron microscopy (TEM) images of GO and nGO water dispersions were acquired to evaluate the lateral size, thickness and morphology of GO and nGO sheets. The images were obtained on JEOL JEM 1400 TEM (Tokyo, Japan) coupled to a digital camera CCD Orious 1100 W (Tokyo, Japan).

d) DLS

Dynamic light scattering (DLS) particle size analysis measurements were performed to evaluate the lateral size of GO and nGO water colloids in a Zetasizer Nano ZS instrument

(Malvern Instruments Ltd., Worcestershire, UK). Previously, the colloids was homogenized using an ultrasonication bath for 10 min.

5.2.3 Coating of decellularized arteries with GO and nGO

5.2.3.1 Preparation

The inner lumen of the decellularized arteries were perfused using a recirculating perfusion system being perfused overnight with GO or nGO suspensions (0.5 mg/mL in H_2O) at 10 rpm, followed by a PBS washing step (1h), to remove poorly adhered particles. The coated grafts were preserved at 4ºC until further use. Coating stability was evaluated by SEM images of coated decellularized arteries surface after 3h of PBS perfusion in the maximum flow of the peristaltic pump (60 rpm).

5.2.3.2 Characterization

a) SEM

Scanning electron microscopy (SEM) was performed to visualize GO and nGO coatings of the lumen of decellularized arteries, as described in section 5.2.1.2 c.

b) Mechanical Properties

Mechanical properties of the grafts, namely maximal loaded radial force (Fmax), elongation (strain) and pressure (burst pressure) at rupture, ability to distend and contract with pressure variations (compliance) and suture retention were evaluated as previously described [9, 88]. The mechanical properties of uncoated and GO-coated decellularized arteries were evaluated within the same artery to minimize differences associated with artery variability. For this, 3.0 mm long ring segments were cut for each condition (n = 4-10 per condition per vessel) and loaded into the uniaxial BOSE electroforce LM1 test bench system (Bose corp, MN, USA), being the Fmax and strain evaluated. Theorical burst pressure was calculated using Laplace's Law:

$$p = \frac{F}{2 \times l \times r} \qquad \text{Equation 1}$$

F is the load (for burst pressure is Fmax), l is length and r is the luminal radius. Compliance (% diameter change/100mmHg) was determined through the equation:

$$\frac{\frac{D_{120} - D_{80}}{D_{80}}}{\Delta p} \times 10^4 \qquad \text{Equation 2}$$

where D_{120} is the systolic diameter at 120 mmHg, D_{80} is the diastolic diameter at 80 mmHg and Δp is the pressure difference [88].

For the suture retention measurements, a loop of a 7.0 polypropylene suture (Prolene, BV 176-8, Ethicon, USA) was placed 2 mm from the edge of the free end of the decellularized arteries and clamped to the other arm which was moving at a constant speed of 120 mm/min until failure. The test was repeated on the same sample at the opposite end of the graft (n = 5 for each graft type).

5.2.4 Biological features

5.2.4.1 *In vitro* biocompatibility

Human umbilical vein endothelial cells (HUVECs) were grown at 37 °C under a 5% CO_2 humidified atmosphere, in complete medium (M199+) which consists in M199 medium (Sigma) supplemented with 10% v/v inactivated FBS, 1% v/v Penicillin/Streptomycin (Biowest), 90 $\mu g.mL^{-1}$ of heparin (Sigma, H3149) and 15 $\mu g.mL^{-1}$ of endothelial cell growth supplement (ECGS, Corning, 354480) in 1% w/v gelatin coated flasks (Sigma). 1 $x10^5$ cells (in a volume of 10 µL in complete medium) were seeded on the lumen of uncoated and coated decellularized arteries lumen (in 48-well suspension plate) and incubated for 1 h. After that, M199+ was added to each material reaching a final volume of 300 µL and culture was maintaining for 1 day and 7 days. The grafts were rinsed in PBS and the cells stained with Live/Dead Viability/Cytotoxicity kit (L-3224, Thermo Fisher Scientific), which is composed of Calcein-AM (1 µM) and Ethidium-1 (4 µM) and Hoechst 33342 stain (5 µL/10 000 µL PBS, Thermo Fisher 365 Scientific) for visualization by confocal microscopy.

5.2.4.2 Antimicrobial activity

Multi-resistant *Staphylococcus aureus* (ATCC® MRSA 33591™) was used to evaluate bacterial adhesion to uncoated and GO/nGO-coated surface. Bacteria was grown at 37°C in a Tryptic Soy Agar (TSA, Merck Germany) plate overnight and subsequently two colonies were collected and inoculated in 5 mL of liquid Trypticase Soy Broth (TSB, Merck, Germany) at 37 °C and 150 rpm, overnight. After that, *S. aureus* inoculum was rinsed and harvested by centrifugation (2700 rpm for 10 min) being the optical density at 600 nm measured to adjust the concentration of the initial inoculum to $1x10^6$ CFU/mL in TSB medium supplemented with 1% (v/v) human plasma. 300 µL of bacteria initial inoculum was added to the lumen of uncoated and coated dArteries and incubated during 24 h at 37 °C. Samples were rinsed 2 times with PBS and fixed for visualization by SEM. The samples were prepared as described in section 5.2.1.2 c).

5.2.4.3 Hemocompatibility

a) Platelets adhesion

Platelets adhesion and activation by uncoated and coated decellularized arteries was assessed *in vitro* using human platelets concentrate (PC). Briefly, 24-well polystyrene plates were blocked to avoid platelet activation by the wells by incubation in a solution of 1% (w/v) bovine serum albumin (BSA) in PBS (1 h; 37 °C) followed by rising with PBS. The samples were incubated with PC at 3×10^8 platelet/mL (1 h; 37 °C; 100 rpm). Afterwards, materials were rinsed with PBS and the adhered platelets fixed with 1.5% (v/v) glutaraldehyde in 0.14 M sodium cacodylate buffer for 30 min at RT. Dehydration and visualization of adhered platelets by SEM was performed as described in section 1.2.1.2 c).

b) Thrombogenic potential

Thrombogenic potential of uncoated and coated decellularized arteries was evaluated *in vitro* through coagulation test and *in vivo* through a pig AV-shunt model. Since the use of decellularized vessels requires their heparinization before *in vivo* implantation [8, 68], several procedures were evaluated to incorporate heparin in GO-coated dArteries, as summarized in Table 1. Heparin was covalently bound to uncoated decellularized arteries, (dArteries)covHep, and in the case of GO-coated dArteries, it was either performed before or after the GO coating: (dArteries)covHep+GO and (dArteries+GO)covHep, respectively. Briefly, the uncoated and GO-coated decellularized arteries were manually perfused, incubated with 1 M hydroxylamine sulfate (Sigma) solution (18h; RT), rinsed in water and incubated with heparin (25 IU/mL)/1-ethoxy-3(3-dimethylaminopropyl)carbodiimide (EDC, 84 mg/mL) solution at pH 1.5 (48 h) in an orbital shaker [89]. The grafts were then washed with water renewing during 5 h and preserved in PBS at 4ºC until use. Physical incorporation of heparin through GO was also attempted, and in the condition dArteries+(GO)adsHep, decellularized arteries were coated with GO containing previously adsorbed heparin, (GO)adsHep. For that, GO was incubated overnight with a heparin solution of 3600 U and afterwards rinsed twice with PBS by ultracentrifugation (14 000 rpm, 15 min) to obtain (GO)adsHep [90].

Table 1 – Heparin modification of uncoated and GO coated decellularized arteries.

Condition	Schematic representation
(dArteries)covHep	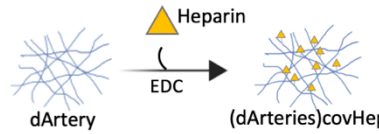
dArteries+(GO)adsHep	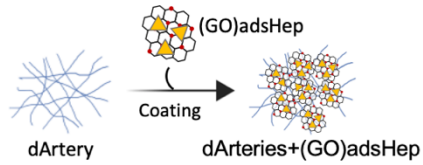
(dArteries)covHep+GO	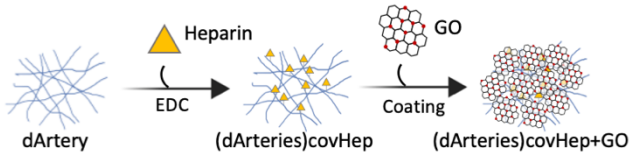
(dArteries+GO)covHep	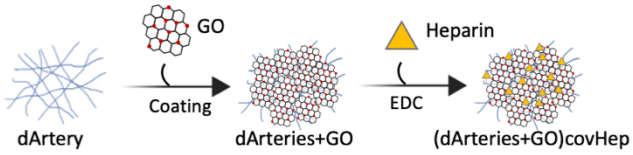
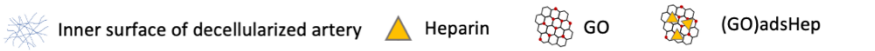	

i) In vitro coagulation time

Human whole blood without anticoagulants was incubated with uncoated, GO-coated, nGO-coated and heparin modified dArteries to evaluate their thrombogenicity. Briefly, the grafts were placed in 5 mL cryovials and incubated with 750 μL of blood at 200 rpm (24 h; RT). Clot formation was evaluated through blood gelation, detected by loss of movement of the blood in response to rotation and shaking.

ii) In vivo arteriovenous shunt (AV-shunt)

Animal studies were performed in compliance with protocols approved by the Austrian Federal Ministry of Science and Research and the Good Scientific Practice Guidelines of the Medical University of Vienna. Blood compatibility of, uncoated, GO-coated and heparinized arteries was evaluated through arteriovenous-shunt (AV)-shunt acute assay in non-heparinized pigs. Pigs were pre-medicated with ketamine (10mg/kg, Animedica), midazolam (0.3 mg/kg, Accord) and medetomidin (0.1mg/kg, Bayer). Anesthesia was introduced using propofol (2.5 mg/kg, Fresenius Kabi), fentanyl 0.1 mg (Hameln Pharma Plus) and 20 mg rocuroniumbromide (Fresenius). After endotracheal intubation, animals were ventilated volume-controlled with 8% desflurane (Baxter). Additionally, 0.01 mg/kg/h and fentanyl 2

mg/kg/h rocuroniumbromide were administered. Animals received ringer lactate (10 $ml.kg^{-1}.h^{-1}$) continuously during the experiment. A blood circuit was established between the right common carotid artery and the left jugular vein using tubes and connectors of a commercially available blood transfusion set (Senso Hem Crystal, Meditrade Medicare). The grafts were attached to the circuit using 14GA BD Venflon™ being perfused with circulating blood for 30 min. Upon blood exposure, each graft was removed being opened and fixed in 2.5% glutaraldehyde for evaluation by SEM, as described in section 5.2.1.2. a).

5.3 Results

5.3.1 Characterization of native and decellularized arteries

Arteries from human placenta chorion and umbilical cord were isolated and decellularized. Hematoxylin/Eosin (H&E) and propidium Iodide (PI) staining reveal that after the decellularization process there are no detectable cell nucleus or DNA residues in the arteries (Fig. 1A and 1B).

H&E staining also shows that the umbilical cord artery exhibits a thicker wall than the placenta artery. SEM images show that both decellularized arteries exhibit an intact hierarchical collagen fiber structure characteristic of extracellular matrices. Cells or cell debris were not identified in SEM images, which corroborates with results from H&E and PI staining (Fig 1C). DNA content of native and decellularized arteries were evaluated to confirm the DNA removal after decellularization process. DNA amounts of the native placenta chorion artery (1.6 ± 0.04 μg/mg of dry weight) and umbilical cord artery (2.0 ± 0.03 μg/mg of dry weight) were reduced after decellularization (0.23 ± 0.13 μg/mg dry weight and 0.6 ± 0.06 μg/mg, respectively) (Fig. 1D).

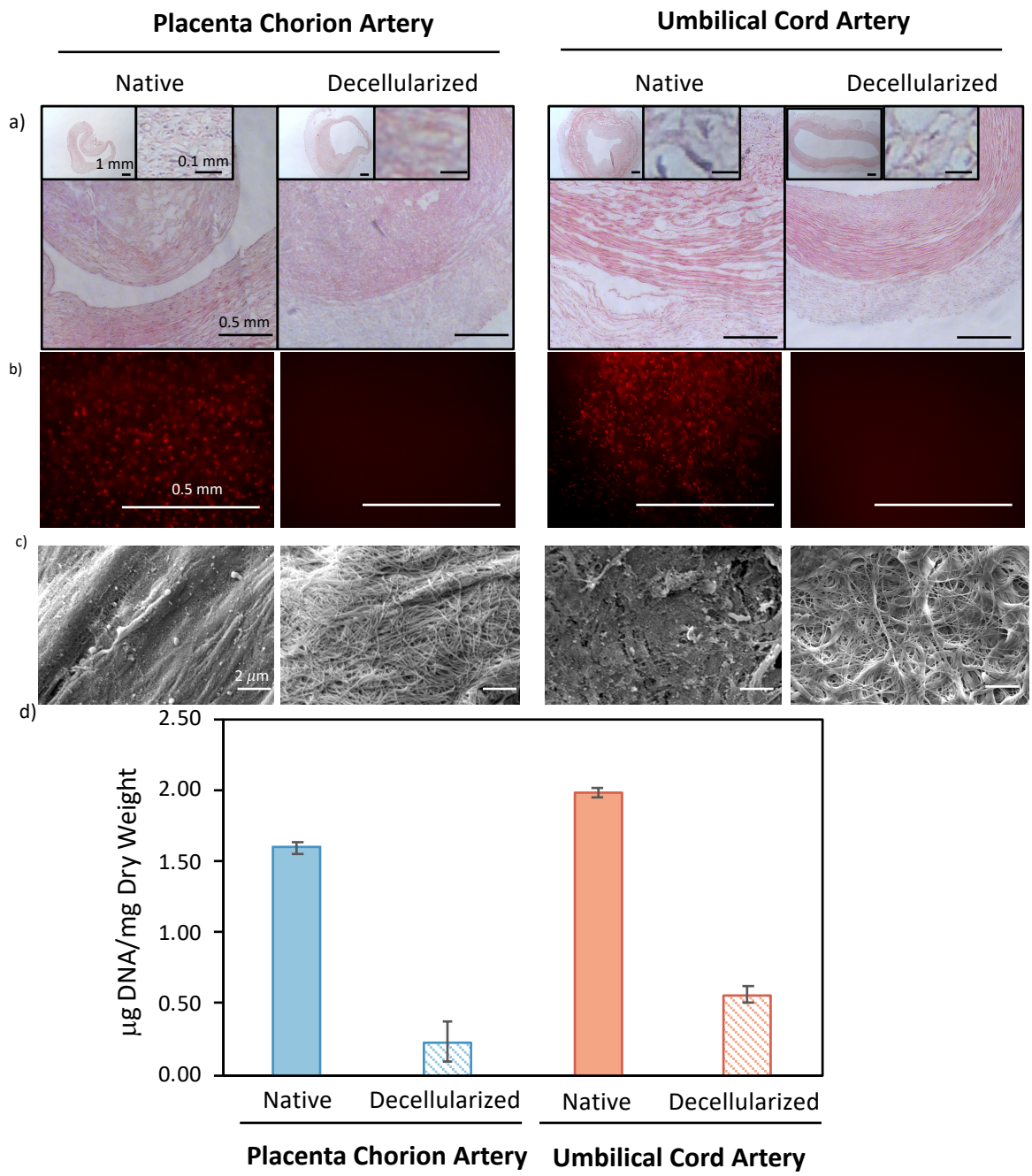

Figure 1 - Characterization of native and decellularized placenta chorion and umbilical cord arteries. A) Hematoxylin/Eosin staining of arteries cross-sections, insets show areas with lower (10x) and higher (40x) magnification, b) Propidium Iodide (PI) staining, c) SEM images of the luminal surfaces of the arteries and d) Amount of DNA in dried tissue

5.3.2 Characterization of graphene oxide materials

Two different graphene oxides, one obtained by graphite oxidation through modified Hummers' method (MHM), (GO), and the other purchased, graphene oxide nanocolloids (nGO), were explored to coat the decellularized arteries. XPS analysis of GO and nGO shows that both materials exhibit a similar sp^2 and sp^3 carbon ratio and atomic percentage of oxygen

around 33%, being the epoxides (45.5%) the most prevalent groups while carbonyl (6.4-7.4%) and carboxyl groups (1.7-1.9%) were in much lower amounts (Fig. 2A). XRD spectra show that composition of nGO is heterogeneous while GO is homogenous. Both materials exhibit a broad peak at 2θ=11.0º in the reflection plane of 001, which is characteristic of oxidized forms of graphene-based materials [91]. nGO also exhibits 2 other peaks at 2θ=20.0º in the reflection plane of 111, which is characteristic of T-carbon, a carbon allotrope [92], and at 2θ=24.0º in the reflection plane of 002, which is characteristic of reduced forms of graphene based materials [93]. This means that nGO is constituted by oxidized and reduced graphene particles and another carbon material. The thickness, d-spacing and the number of layers of GO and nGO were determined through the Scherrer and Bragg's equations (Fig 2B) using the peaks of 2θ=11.0º and 2θ=24.0º. GO exhibits a crystallite size of 8.3 nm (thickness) and d-spacing of 8.0 Å, which corresponds to 11 graphene layers in a stacked nanostructure. nGO comprises particles crystallite size of 7.0 and 5.9 nm and d-spacing of 7.9 and 3.6 Å, which correspond to 10 and 17 layers.

TEM images show the exfoliation degree and lateral size of GO and nGO. Both materials exhibit good dispersion in water (Fig. 2C), always presenting as a single layer in TEM images. This could be associated with the presence of oxygen functional groups in their structure, which confers them a hydrophilic character. The evaluation of several TEM images indicates that the lateral size of GO is around 1.5 (± 0.5) µm while nGO exhibit smaller sheets 1.2 (± 0.6) µm (Fig. 2D). GO and nGO materials were also evaluated by dynamic light scattering (DLS) to infer their lateral size. Despite this method considers all materials as spherical particles, which is not valid for GBMs, GO and nGO exhibit the same thickness that allows the direct comparison between them. Fig. 2D exhibits the PDS intensity in the function of particle lateral size. nGO material exhibits a broader peak than GO, which shows a more heterogeneous distribution of particle lateral size. Although DLS software computes the averaged particles size "average lateral size", the average lateral size of GO and nGO particles were determined using the position of the primary peak from the intensity PDS, α_{DLS} using a previously described approximation: Lateral size = $(0.07 \pm 0.03)\alpha_{DLS}^{(1.5\pm0.15)}$ for GBMs [94]. nGO lateral size (1.3 µm) is lower than GO (1.9 µm), but not in the nanometric dimensions as described by the supplier.

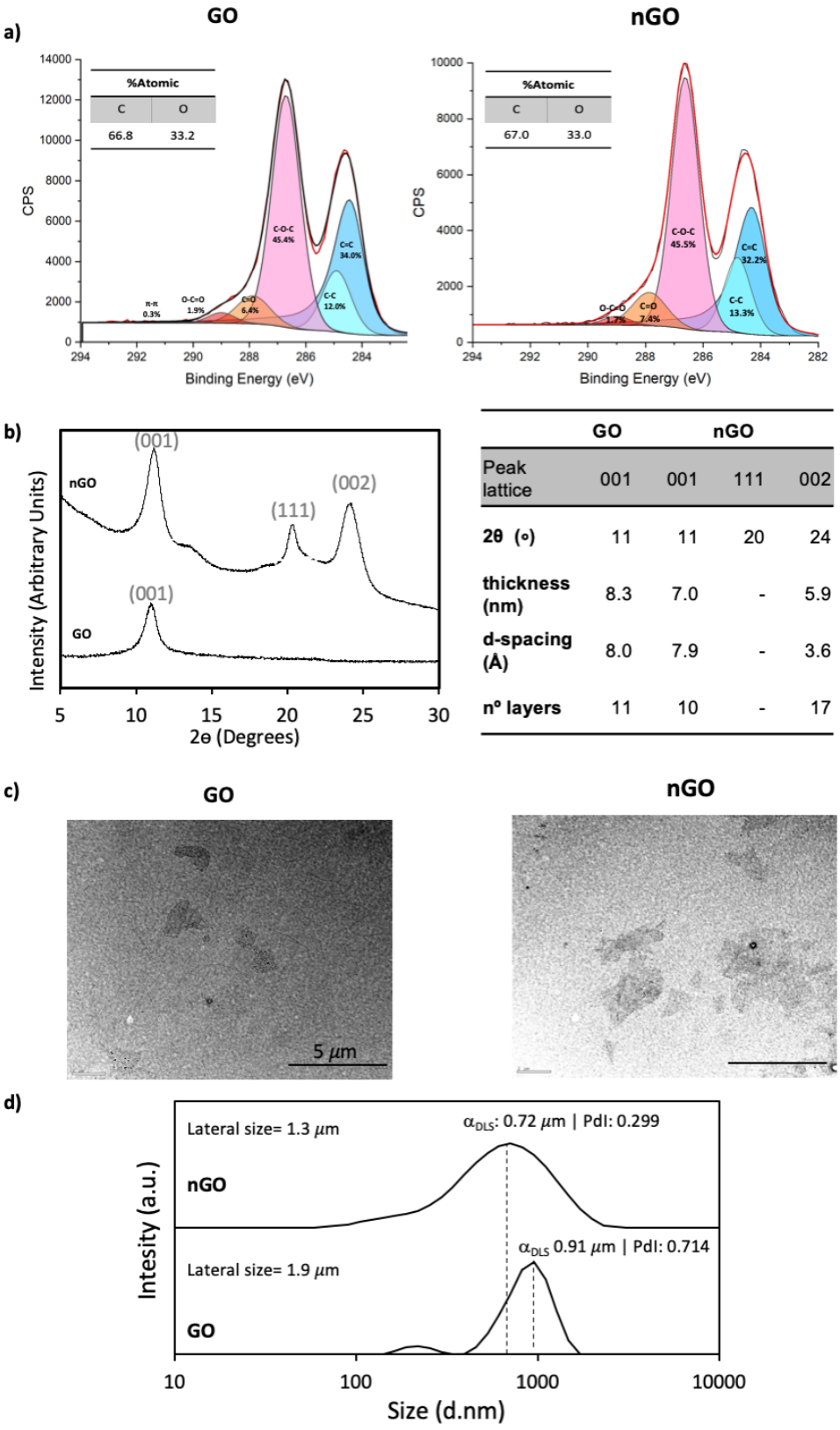

	GO	nGO		
Peak lattice	001	001	111	002
2θ (°)	11	11	20	24
thickness (nm)	8.3	7.0	-	5.9
d-spacing (Å)	8.0	7.9	-	3.6
nº layers	11	10	-	17

Figure 2 – Characterization of GO and nGO: a) elemental composition (Atomic %) and C1s high resolution spectrum obtained by XPS, b) XRD spectra, c) TEM images and d) particle size distribution obtained by DLS.

5.3.3 Coating of decellularized arteries with GO and nGO

5.3.3.1 Surface characterization

Decellularized arteries were automatically perfused with GO and nGO colloids (Fig. 3). SEM images show that GO and nGO-coated decellularized placenta and umbilical cord arteries exhibit a homogeneous coating that covers all the collagen fibers. These coatings showed to be stable after strong perfusion with PBS (Fig. S.1).

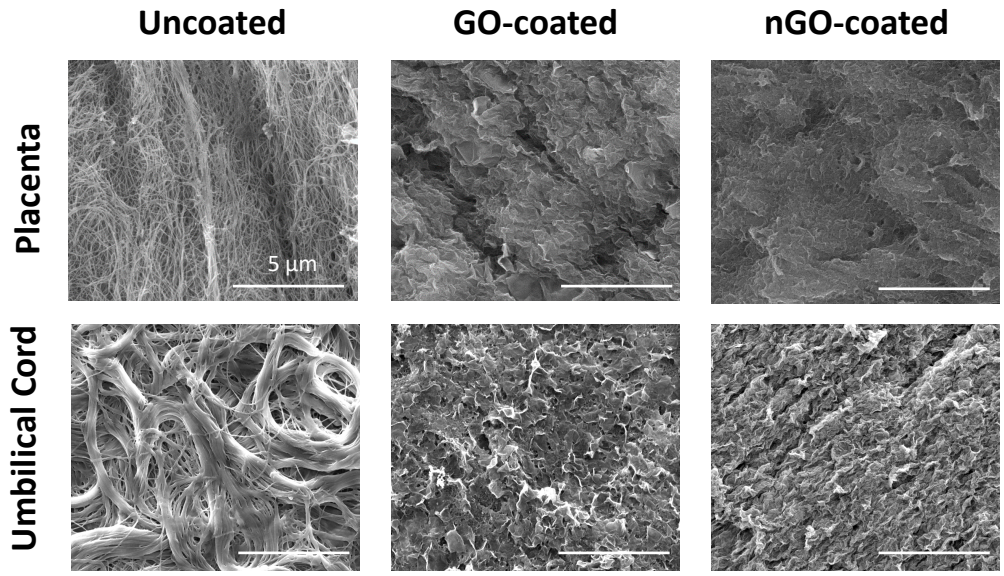

Figure 3 – SEM images of GO and nGO coated decellularized placenta and umbilical cord arteries.

5.3.3.2 Mechanical properties of decellularized arteries coating

Mechanical properties of uncoated and GO/nGO-coated decellularized placenta and umbilical cord arteries were assessed through evaluation of Fmax, strain, compliance, burst pressure and suture retention. Fmax of decellularized placenta and umbilical cord arteries exhibits a high variety ranging between 0.4-4.9 N and 1.3-5.9 N, respectively (Fig. S.2.). However, Fmax variability is lower within the same arteries (Fig. S.2.), being all the comparisons between GO/nGO-coatings and uncoated performed into the same decellularized artery. For decellularized placenta chorion arteries, GO and nGO-coatings do not have a significant effect on the mechanical features (Fig. 4 and S. 3 with exception of compliance, which GO coating improves 10%. However, for umbilical cord arteries, GO coating leads to an increase in Fmax of around 27% (Fig. 4 and S.4). Since theoretical burst pressure depends on Fmax, the observed pattern for burst pressure is similar to Fmax (Fig. 4, Fig. S.3 and S. 5). Thus, GO-coating increases 29% of burst pressure of umbilical cord decellularized arteries.

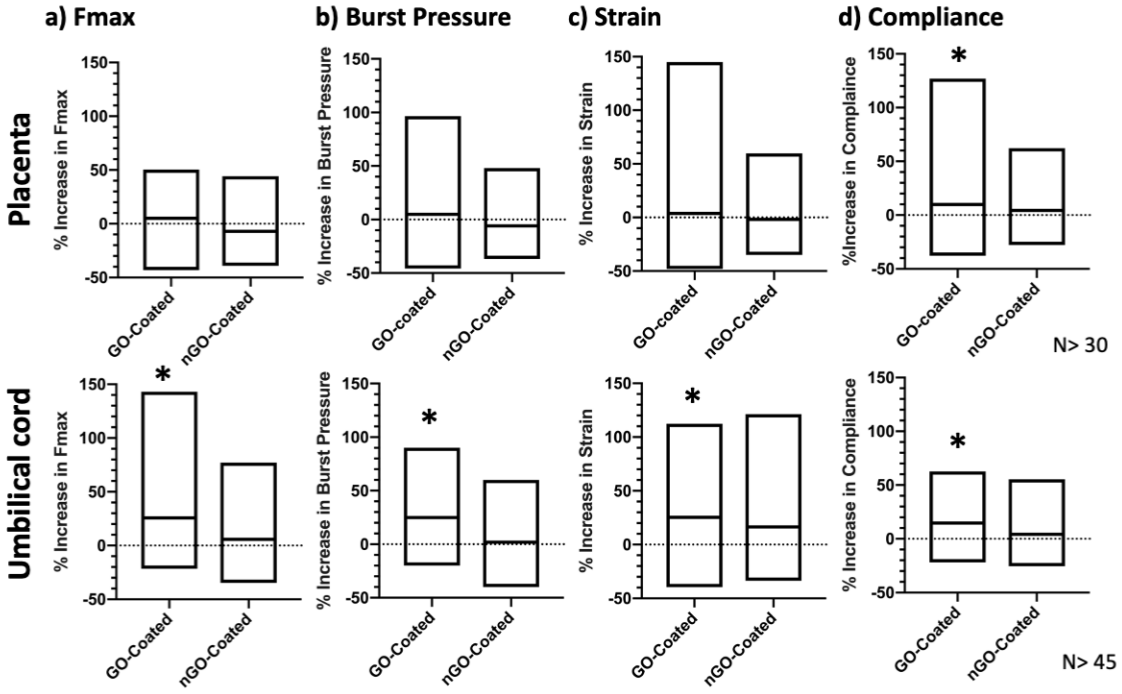

Figure 4 – Mechanical properties of uncoated and GO/nGO-coated decellularized placenta and umbilical cord arteries. Box plot graphs containing average, min and max values of % increase in Fmax a) burst pressure b), %maximum strain d), compliance e) comparing to uncoated. Statistically significantly different from uncoated decellularized artery (*) ($p < 0.05$ – One Way ANOVA).

Despite these increases in Fmax and burst pressure, GO coating promotes an increase in arteries strain of around 25%, without compromising the compliance. As observed for decellularized placenta chorion arteries, nGO coating does not have a significant effect in the mechanical properties of umbilical cord arteries.

Regarding suture retention, all the grafts exhibit good suture retention capacity ranging between 80-100 g (Fig. S. 5).

5.3.4 Biological Features

5.3.4.1 *In vitro* biocompatibility

Human umbilical vein endothelial cells (HUVECs) were incubated during 1 day with uncoated and coated decellularized arteries being their lumen visualized by confocal microscopy upon Ethidium-1/Hoechst/Calcein AM staining (Fig. 5). HUVECs have the capacity to adhere in all decellularized arteries being most of cells viable. Preliminary results showed that uncoated and coated chorion placenta arteries exhibit capacity to sustain viability and growth of HUVECs up to 7 days (Fig. S.6).

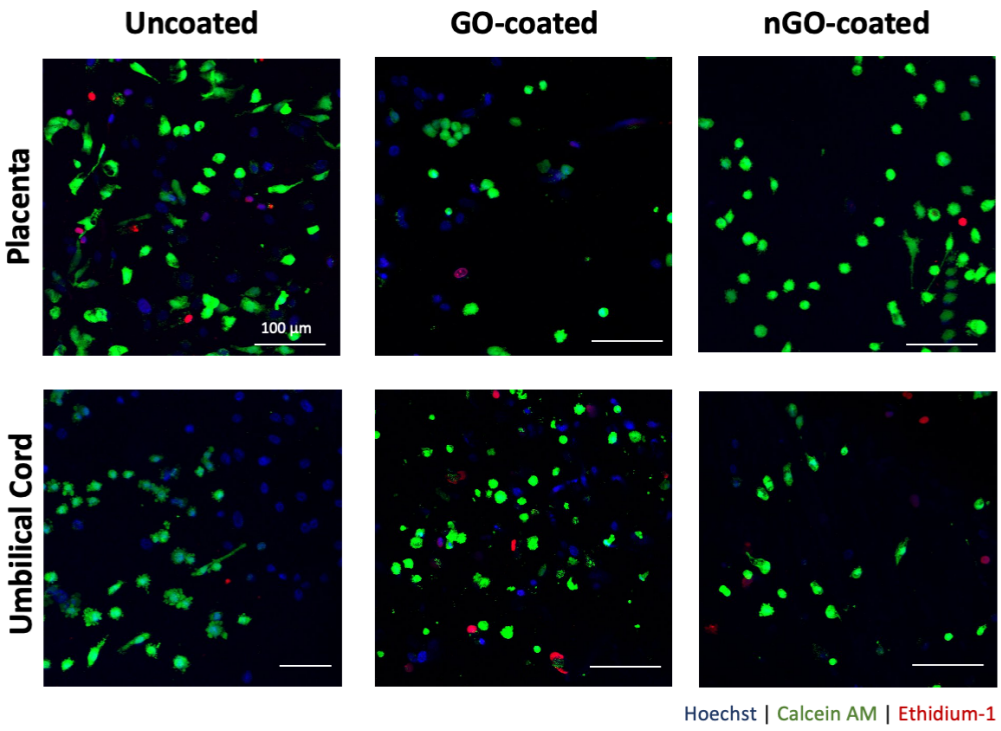

Figure 5 - Immunofluorescence images of HUVECs adherent to uncoated, GO- and nGO-coated decellularized placenta chorion and umbilical cord artery surface after 1 day of incubation. Cells stained with Hoechst (DNA) in blue, calcein-AM (live cells) in green and ethidium-1 (dead cells) in red.

5.3.4.2 Antimicrobial activity

The lumen of uncoated and coated decellularized arteries was challenged regarding antimicrobial features against *S. aureus*. SEM images of materials surface reveal that bacteria adhere in higher amounts to decellularized placenta arteries than to decellularized umbilical cord arteries (Fig. 6).

For placenta decellularized arteries, bacteria are homogenously distributed through all the surface. Upon coating with GO and nGO, bacterial adhesion is reduced, only appearing in some areas mainly associated with valleys characteristic of decellularized arteries topography (Fig. 6).

As decellularized umbilical cord arteries exhibit a lower adhesion of bacteria at their surface, GO and nGO coating effect is not as noticeable as observed for decellularized placenta arteries, being more evident only in the nGO coating.

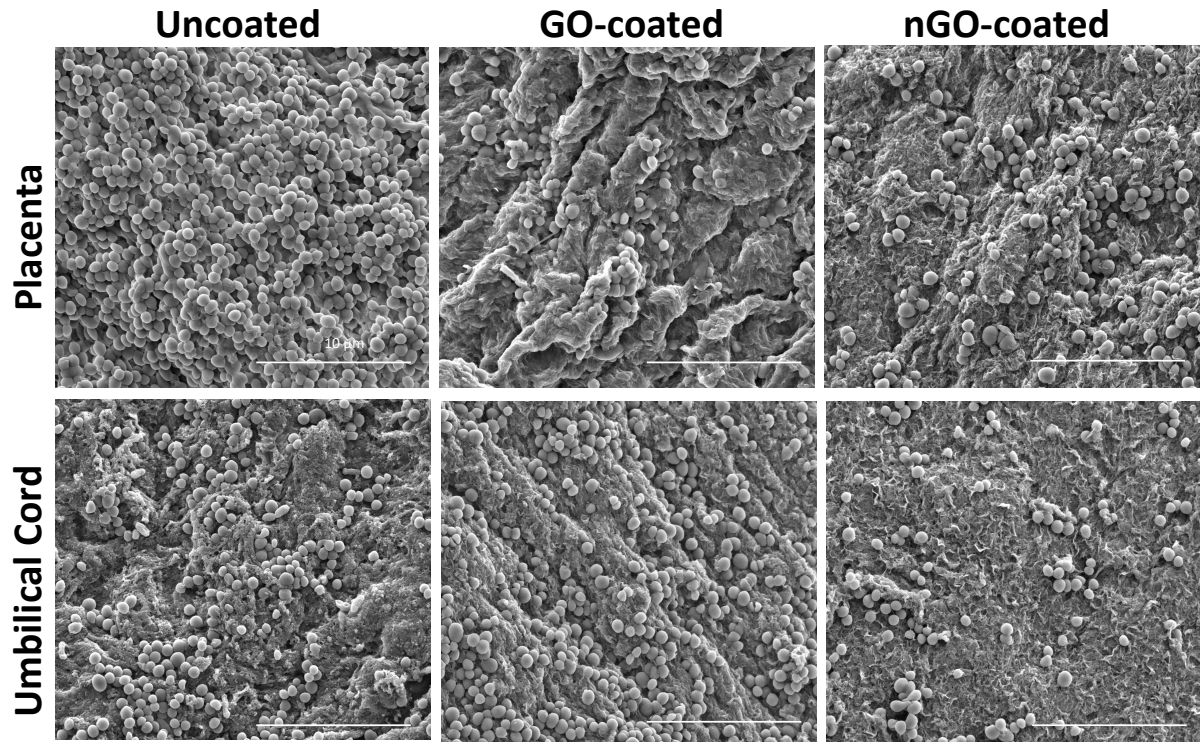

Figure 6 - SEM images of *S. aureus* adhered to uncoated, GO- and nGO-coated decellularized placenta artery surface after 24 h of incubation.

5.3.4.3 Hemocompatibility

a) Platelets adhesion

Uncoated and coated decellularized arteries were evaluated regarding human platelets adhesion to their surface lumen. Both placenta and umbilical cord uncoated decellularized arteries exhibit high adhesion of platelets. Upon GO and nGO coating, there is a decrease in adhered platelets (Fig. 7).

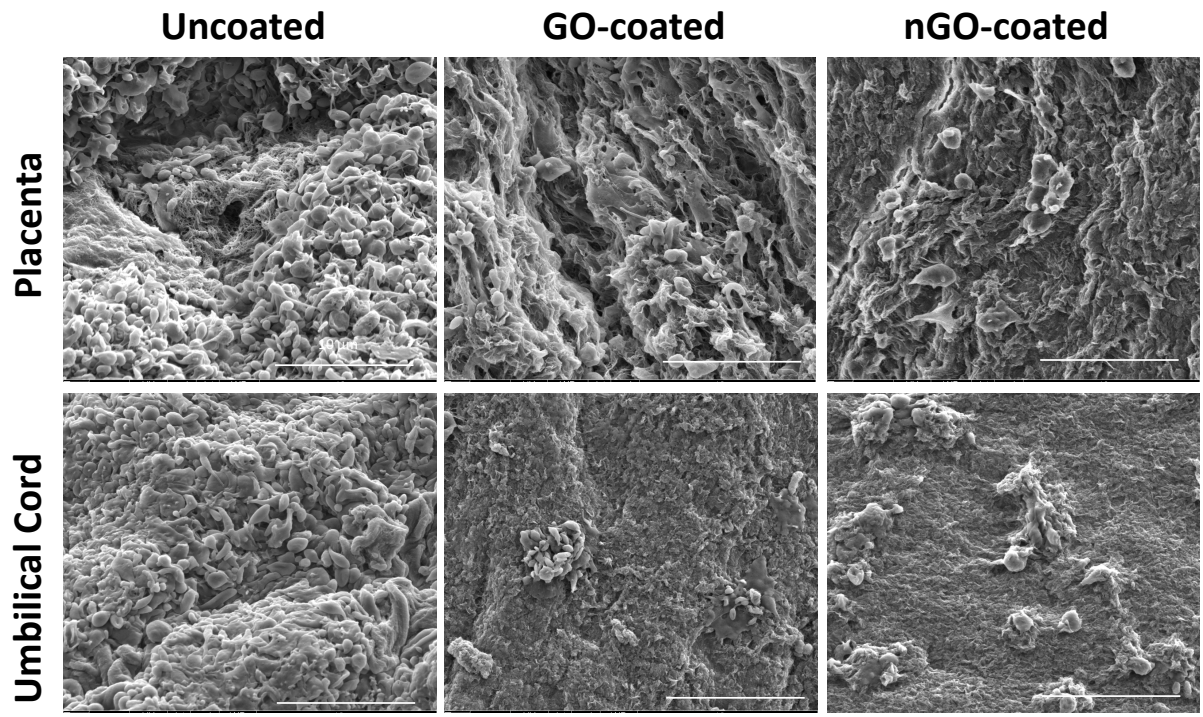

Figure 7 - SEM images of human platelets adhered to uncoated, GO- and nGO-coated decellularized placenta chorion and umbilical cord arteries surface after 1 h of incubation.

b) *In vitro* coagulation

Thrombogenic potential of uncoated and GO/nGO coated decellularized arteries was evaluated *in vitro* through their exposure to human blood without anticoagulants. When in contact with uncoated decellularized arteries, blood coagulates in approximately 5 min (Table 2). GO and nGO coating do not affect the blood coagulation time being similar to uncoated decellularized arteries (< 5 min).

To achieve better performance, heparin was conjugated with uncoated and coated decellularized arteries. As the mechanical improvements were only observed in GO-coated decellularized umbilical cord arteries, heparin incorporation was only performed in these grafts. Heparin was conjugated in three different ways, namely previously adsorbed to GO and only afterwards used to coat decellularized arteries (dArteries+GO(adsHep)), covalently linked to decellularized arteries which are then coated with GO (d(dArteries)covHep+GO) and covalently linked to decellularized arteries already coated with GO (dArteries+GO)covHep (Table 2). Decellularized umbilical cord arteries coated with GO containing adsorbed heparin (dArteries+(GO)adsHep) or covalently linked to heparin and afterwards coated with GO ((dArteries)covHep+GO) behave similarly to uncoated decellularized arteries, clotting after 5 min. The two grafts that were covalently heparinized as the last step, (dArteries)covHep and (dArteries+GO)covHep, do not induce blood coagulation during at least during 24h.

Artery Source	Condition	Clotting time
Placenta	Uncoated	< 5 min
	GO-coated	< 5 min
	nGO-coated	< 5 min
Umbilical cord	Uncoated	< 5 min
	GO-coated	< 5 min
	nGO-coated	< 5 min
	(dArteries)covHep	>24 h
	dArteries+(GO)adsHep	< 5 min
	(dArteries)covHep+GO	< 5 min
	(dArteries+GO)covHep	>24 h

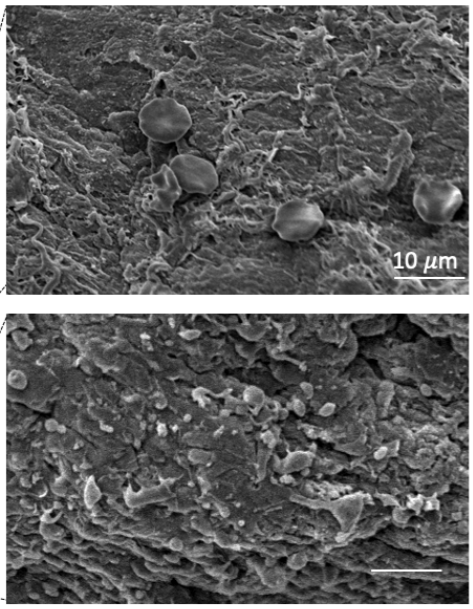

Table 2 – Clotting time of human whole blood without anticoagulants upon exposure to uncoated and GO and nGO-coated placenta and umbilical cord arteries. Furthermore, specimens with additional heparin modification were investigated.

c) *In vivo* arteriovenous shunt *in vivo* assay

AV-shunt set-up was performed to evaluate the grafts acute hemocompatibility *in vivo* (Table 3). As observed for *in vitro* human whole blood exposure, decellularized arteries coated with GO with adsorbed heparin (dArteries)covHep or heparinized decellularized arteries with GO coating (dArteries)covHep+GO induce graft occlusion in the first 15 min, while (dArteries)covHep and (dArteries+GO)covHep stayed patent during whole the exposure time (30 min). SEM images of grafts inner lumen reveal that dArteries+(GO)adsHep and (dArteries)covHep+GO exhibit huge clots but covHepdArteries and covHep(dArteries+GO) have few platelets adhered, suggesting that anticoagulant properties can only be achieved when heparinization is performed as last step, and when heparin is covalently immobilized.

Table 3 – Occlusion time and SEM images of surface lumen of (dArteries)covHep, dArteries+(GO)adsHep, (dArteries)covHep+GO, and (dArteries+GO)covHep after 30 min of contact with blood from pig AV-shunt.

AV-Shunt Set-up

Condition	Occlusion time	SEM image of surface lumen
(dArteries)covHep	Did not occlude Up to 30 min	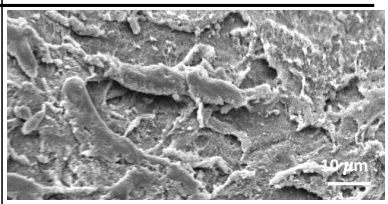
dArteries+(GO)adsHep	<15 min	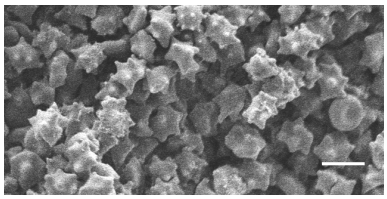
(dArteries)covHep+GO	< 15 min	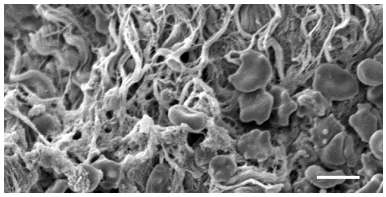
(dArteries+GO)covHep	Did not occlude Up to 30 min	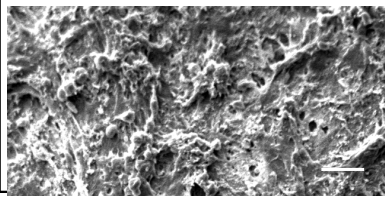

5.4 Discussion

In this study, a novel coating comprising GO materials was developed to improve the outcomes of decellularized arteries' performance as small diameter vascular graft. Arteries from two different sources with completely distinct vascular anatomy were adopted, namely from human placenta chorion and umbilical cord. Besides the source of the raw material, the features of the decellularized matrices highly depend on the adopted decellularization protocol, namely the use of a static treatment vs a perfusion system, the adopted enzymatic treatments and detergent, etc. [95]. To decrease the variables of this study, arteries from placenta chorion and umbilical cord were decellularized using the same protocol, which was previously established [68], consisting in an automatic perfusion of the arteries with a hypertonic/hypotonic solution followed by treatment with 1% Triton X-100 during more than 18h and an overnight DNase digestion. Comparing to the use of SDS the use of Triton X-100 as detergent is less harsh for extracellular matrix (ECM) constituents showing higher preservation of its components, namely glycosaminoglycans (GAGs), proteins, proteoglycans

[68, 96]. For both grafts, this decellularization protocol was efficient in removing cells and cell remnants as shown by H&E, PI staining, as well as DNA quantification and SEM images. Still, umbilical cord arteries exhibit a higher amount of residual DNA than placenta arteries, which could be explained by the thicker wall that these arteries display. In spite of this, the amount of DNA present in umbilical cord decellularized arteries is similar to the reported for decellularization protocols previously established by others [15].

GO and nGO exhibit a similar oxidation degree, around 34% of oxygen atoms containing a similar amount of oxygen-containing functional groups. nGO exhibits a heterogenous composition having oxidized and non-oxidized graphene sheets and T-carbon allotrope while GO is only constituted by oxidized graphene sheets. Despite being smaller than GO, nGO did not exhibit the nanometric dimensions described by the supplier.

In this work, a homogeneous coating that covers the collagen fibers was obtained through the automatic perfusion of GO or nGO inside of the decellularized lumen. Mechanical properties of grafts play a critical role in their patency rates since they have to be sufficiently strong to resist and retain the integrity within the blood pressure and at the same time, should have the same compliance and strain of native recipient vessel [97]. Mismatch of the compliance and/or strain perturbs the hemodynamic flow inducing turbulence which promotes thrombus formation, injures the endothelial cells and stimulates vascular smooth muscle cells to differentiate and migrate resulting in intimal hyperplasia development [98, 99], one of the common cause for vascular graft failure [100]. Thus, mechanical properties of graft must mimic as much as possible the vessel to be replaced. Moreover, the graft should be capable to retain sutures to enable its implantation. Mechanical properties of the saphenous vein (SV) and internal thoracic artery (ITA) have often been used as standard since, when available, these materials are currently the gold standard for small diameter vascular replacement. For these arteries, the burst pressure, suture retention strength, and compliance are 2134 mmHg and 25.6%/100 mmHg for the SV and 3073 mmHg and 11.5%/100 mmHg for the ITA [1, 101, 102]. Most of the uncoated arteries did not reach values of this order of magnitude but GO-coated decellularized umbilical cord arteries exhibit a mean burst pressure and compliance of around 1960 mmHg and 13.9%/100 mmHg, respectively, which are values similar to SV burst pressure and ITA compliance. Comparing the compliance and burst pressure of these GO-coated decellularized grafts with the literature [1] it is possible to place them in the top of the most compliant and strong grafts. The observed effect of mechanical reinforcement of decellularized umbilical cord arteries was not visible in decellularized placenta chorion arteries, possibly due to the high variability of Fmax values within the same artery that cloak the GO-coating effect (Fig. S.1). These differences could be associated with the natural heterogeneity of placenta arteries, or to the isolation process, which could damage the arteries in some parts of their

extension. nGO coating does not show a clear impact on the mechanical properties of decellularized arteries, suggesting that larger GO particles have a higher efficacy.

Upon GO/nGO-coating, the luminal surface of decellularized arteries keeps its capacity to promote adhesion of endothelial cells. Seeded endothelial cells also exhibit high viability for all the tested condition, confirming the lack of toxicity of all potential grafts. Longer incubation time points should be assessed to evaluate the potential of graft to sustain cells proliferation. The lack of cytotoxicity of GO integrating surfaces towards endothelial cells had also been described for collagen/GO composites [103], electrospun polyurethane/GO fibers [104], polycaprolactone/GO [105], and for GO coatings on titanium [90] or nitinol [106] surfaces; with GO being responsible for promoting cell proliferation in these last three studies. In a chicken embryo angiogenesis model, GO powders also showed to induce an increase in endothelial cells proliferation through the intracellular formation of reactive oxygen and nitrogen species and also by the activation of phospho-eNOS and phospho-Akt [107]. Besides these intracellular effects, GBMs have been reported to influence cell attachment, growth, proliferation and phenotypes due to their high capacity to recruit and adsorb nutrients and cell growth and differentiation factors on their surface [108].

Infection is a common failure cause to all implantable devices and vascular grafts are not an exception [109-112]. In this study, we show that decellularized matrices adhere high amount of *S. aureus*, one of the most prevalent infection agents for vascular grafts [112], on their surface. This effect could be explained by the high capacity of *S. aureus* to adhere to several extracellular matrix proteins, including collagen [113], fibronectin [114], elastin [115], laminin [116], vitronectin [117] and fibrinogen [118]. Moreover, rough surfaces, such as the luminal surface of the decellularized matrix graft, could also potentiate the adherence, viability and proliferation of small bacteria such as *S. aureus* since they can fit in the lumen wrinkles. Despite being more noticeable in decellularized placenta arteries than in decellularized umbilical cord arteries, GO or nGO coatings decreased bacterial adhesion at their surface. The limited exposure of ECM factors as well as the smoother surface obtained after GO or nGO coatings could explain this decrease in bacterial adhesion. This preventive effect of GO was also shown before for GO coatings 96-well microtiter [119] or silicon surfaces (when in low amounts) [72], polycaprolactone/GO fibrous scaffolds [105] and electrospun fibroporous polycarbonate urethane [120].

A similar effect was also observed for human platelets adhesion, where GO/nGO coated decellularized arteries exhibit lower adhesion of platelets at their surface. This could be also explained by the decreased exposition of RGD motifs, highly expressed in ECM components, as well as from a decrease in surface roughness. In previous studies, GO coatings also showed a successful effect in decreasing platelets adhesion to titanium [90], electrospun fibroporous polycarbonate urethane [120], nitinol [106], polyether-sulfone hollow fiber

membranes [121] and poly(lactic acid) [122]. *Wilczek et al.* did not find a significant difference in platelet activation and adhesion upon reduced graphene oxide (rGO) coating of decellularized heart valves [79]. The higher hydrophilicity of GO comparing to rGO could explain these differences, since low-fouling features are associated with hydrophilic surfaces. *In vivo* results show that despite the improvement in surface blood compatibility *in vitro*, this is not enough for the graft implantation without any further treatment. Following the strategy of heparinization described for *in vivo* implantation of decellularized vessels [8, 68], three different approaches were adopted to improve their *in vivo* outcome. The only materials that did not clot upon acute exposure to non-heparinized pig blood through an AV-shunt were the decellularized arteries covalently immobilized with heparin, either uncoated or GO-coated before heparinization. Overall, heparinized GO-coated decellularized umbilical cord arteries exhibit a high potential to be applied in development of small diameter vascular grafts.

5.5 Conclusion

GO materials were used to coat decellularized matrices aiming to improve their mechanical and biological performance. Automatic perfusion of GO and nGO colloids allowed to obtain a smooth surface in the lumen of decellularized placenta chorion and umbilical cord arteries, covering the exposed fibers of the decellularized matrices. Although no mechanical reinforcement is observed in decellularized placenta chorion arteries, GO-coating improves the maximum force, burst pressure and compliance of decellularized umbilical cord arteries. These GO-coated grafts reach similar mechanical features of human saphenous vein, the current gold standard for vascular replacement. All GO or nGO coated decellularized arteries show endothelial cells adhesion, with reduced human platelets adhesion. *In vitro* and *in vivo* acute thrombogenicity studies reveal that the covalent binding of heparin to both uncoated and GO coated decellularized umbilical cord arteries prevents clotting of the arteries when exposed to non-heparinized blood. In summary, GO-coated decellularized umbilical cord arteries emerge as a promising possibility for a novel ‘‘off-the-shelf” small diameter vascular grafts.

5.6 Acknowledgements

Daniela Silva for the assistance in SEM analysis at CEMUP, Porto, Eng. Carlos Sá for XPS analysis at CEMUP, Porto and Rui Fernandes from Histology and Electron Microscopy Service for TEM analysis at HEMS, i3S.

Authors acknowledge financial support from Fundação para a Ciência e a Tecnologia (FCT) and Fundo Europeu de Desenvolvimento Regional for PhD grants PD/BD/114156/2016, Research position grant IF/01479/2015, projects POCI-01-0145- FEDER-032431, POCI-01-0145-FEDER-006939, POCI-01-0145-FEDER- 007274, NORTE-01-0145-FEDER-000012

and PTDC/CTM-COM/32431/ 2017, and UID/EQU/00511/2019 – LEPABE funded by national funds through FCT/MCTES (PIDDAC).[123]

5.7 References

[1] S. Pashneh-Tala, S. MacNeil, F. Claeyssens, The Tissue-Engineered Vascular Graft-Past, Present, and Future, Tissue Eng Part B Rev 22(1) (2016) 68-100.

[2] V. Catto, S. Farè, G. Freddi, M.C. Tanzi, Vascular Tissue Engineering: Recent Advances in Small Diameter Blood Vessel Regeneration, Vasc Med 2014 (2014) 1-27.

[3] H. Bergmeister, M. Strobl, C. Grasl, R. Liska, H. Schima, Tissue engineering of vascular grafts, Eur Surg 45(4) (2013) 187-193.

[4] D.G. Seifu, A. Purnama, K. Mequanint, D. Mantovani, Small-diameter vascular tissue engineering, Nat Rev Cardiol 10(7) (2013) 410-21.

[5] H. Bergmeister, M. Strobl, C. Grasl, R. Liska, H. Schima, Tissue engineering of vascular grafts, Europ Surg 45(4) (2013) 187-193.

[6] E. Caliskan, D.R. de Souza, A. Boning, O.J. Liakopoulos, Y.H. Choi, J. Pepper, C.M. Gibson, L.P. Perrault, R.K. Wolf, K.B. Kim, M.Y. Emmert, Saphenous vein grafts in contemporary coronary artery bypass graft surgery, Nat Rev Cardiol (2019).

[7] M.A. Hiob, S. She, L.D. Muiznieks, A.S. Weiss, Biomaterials and Modifications in the Development of Small-Diameter Vascular Grafts, ACS Biomater-Sci Eng 3(5) (2016) 712-723.

[8] H. Bergmeister, R. Plasenzotti, I. Walter, C. Plass, F. Bastian, E. Rieder, W. Sipos, A. Kaider, U. Losert, G. Weigel, Decellularized, xenogeneic small-diameter arteries: transition from a muscular to an elastic phenotype in vivo, J Biomed Mater Res B Appl Biomater 87(1) (2008) 95-104.

[9] K.H. Schneider, M. Enayati, C. Grasl, I. Walter, L. Budinsky, G. Zebic, C. Kaun, A. Wagner, K. Kratochwill, H. Redl, A.H. Teuschl, B.K. Podesser, H. Bergmeister, Acellular vascular matrix grafts from human placenta chorion: Impact of ECM preservation on graft characteristics, protein composition and in vivo performance, Biomaterials 177 (2018) 14-26.

[10] K.H. Schneider, P. Aigner, W. Holnthoner, X. Monforte, S. Nurnberger, D. Runzler, H. Redl, A.H. Teuschl, Decellularized human placenta chorion matrix as a favorable source of small-diameter vascular grafts, Acta Biomater 29 (2016) 125-134.

[11] V.E. Rodriguez-Rodriguez, B. Martinez-Gonzalez, A. Quiroga-Garza, C.G. Reyes-Hernandez, D. de la Fuente-Villarreal, O. de la Garza-Castro, S. Guzman-Lopez, R.E. Elizondo-Omana, Human Umbilical Vessels: Choosing the Optimal Decellularization Method, Asaio J 64(5) (2018) 575-580.

[12] P. Mallis, E. Michalopoulos, A. Dinou, M.S. Vlachou, E. Panagouli, A. Papapanagiotou, E. Kassi, C.S. Giokas, Development of HLA-matched vascular grafts utilizing decellularized human umbilical artery, Hum Immunol 79(12) (2018) 855-860.
[13] S. Mangold, S. Schrammel, G. Huber, M. Niemeyer, C. Schmid, M. Stangassinger, M. Hoenicka, Evaluation of decellularized human umbilical vein (HUV) for vascular tissue engineering - comparison with endothelium-denuded HUV, J Tissue Eng Regen Med 9(1) (2015) 13-23.
[14] H.Y. Tuan-Mu, C.H. Yu, J.J. Hu, On the decellularization of fresh or frozen human umbilical arteries: implications for small-diameter tissue engineered vascular grafts, Ann Biomed Eng 42(6) (2014) 1305-18.
[15] P. Mallis, I. Gontika, T. Poulogiannopoulos, J. Zoidakis, A. Vlahou, E. Michalopoulos, T. Chatzistamatiou, A. Papassavas, C. Stavropoulos-Giokas, Evaluation of decellularization in umbilical cord artery, Transplant Proc 46(9) (2014) 3232-9.
[16] S.J. Chen, J.X. Li, P.Q. Dong, Utilization of Pulsatile flow to Decellularize the Human Umbilical Arteries to Make Small-Caliber Blood Vessel Scaffolds, Acta Cardiol Sin 29(5) (2013) 451-456.
[17] L. Gui, A. Muto, S.A. Chan, C.K. Breuer, L.E. Niklason, Development of decellularized human umbilical arteries as small-diameter vascular grafts, Tissue Eng Part A 15(9) (2009) 2665-76.
[18] A.M. Kajbafzadeh, R. Khorramirouz, S.M. Kameli, K. Fendereski, S.S. Daryabari, S.M. Tavangar, B. Azizi Garajegayeh, Three-year efficacy and patency follow-up of decellularized human internal mammary artery as a novel vascular graft in animal models, J Thorac Cardiov Sur 157(4) (2019) 1494-1502.
[19] S. Ilanlou, M. Khakbiz, G. Amoabediny, J. Mohammadi, H. Rabbani, Carboxymethyl kappa carrageenan-modified decellularized small-diameter vascular grafts improving thromboresistance properties, J Biomed Mater Res A 107(8) (2019) 1690-1701.
[20] H. Qi, C. Cheng, X. Wang, X. Yu, Preparation and investigation of novel SrCl2/DCMC-modified (via DOPA) decellularized arteries with excellent physicochemical properties and cytocompatibility for vascular scaffolds, RSC Adv 8(53) (2018) 30098-30105.
[21] N. Jeinsen, L. Magel, D. Jonigk, M. Klingenberg, A. Haverich, M. Wilhelmi, U. Boer, Biocompatibility of Intensified Decellularized Equine Carotid Arteries in a Rat Subcutaneous Implantation Model and in a Human In Vitro Model, Tissue Eng Part A 24(3-4) (2018) 310-321.
[22] S. Xu, F. Lu, L. Cheng, C. Li, X. Zhou, Y. Wu, H. Chen, K. Zhang, L. Wang, J. Xia, G. Yan, Z. Qi, Preparation and characterization of small-diameter decellularized scaffolds for vascular tissue engineering in an animal model, Biomed Eng Online 16(1) (2017) 55.

[23] A. Porzionato, M.M. Sfriso, A. Pontini, V. Macchi, M.I. Buompensiere, L. Petrelli, F. Bassetto, V. Vindigni, R. De Caro, Development of Small-Diameter Vascular Grafts Through Decellularization of Human Blood Vessels, J Biomater Tiss Eng 7(2) (2017) 101-110.
[24] J. Negishi, Y. Hashimoto, A. Yamashita, Y. Zhang, T. Kimura, A. Kishida, S. Funamoto, Evaluation of small-diameter vascular grafts reconstructed from decellularized aorta sheets, J Biomed Mater Res A 105(5) (2017) 1293-1298.
[25] N.J. Kristofik, L. Qin, N.E. Calabro, S. Dimitrievska, G. Li, G. Tellides, L.E. Niklason, T.R. Kyriakides, Improving in vivo outcomes of decellularized vascular grafts via incorporation of a novel extracellular matrix, Biomaterials 141 (2017) 63-73.
[26] A.M. Kajbafzadeh, R. Khorramirouz, S.M. Kameli, J. Hashemi, A. Bagheri, Decellularization of Human Internal Mammary Artery: Biomechanical Properties and Histopathological Evaluation, Biores Open Access 6(1) (2017) 74-84.
[27] A. Daugs, B. Hutzler, M. Meinke, C. Schmitz, N. Lehmann, A. Markhoff, O. Bloch, Detergent-Based Decellularization of Bovine Carotid Arteries for Vascular Tissue Engineering, Ann Biomed Eng 45(11) (2017) 2683-2692.
[28] N. Dahan, U. Sarig, T. Bronshtein, L. Baruch, T. Karram, A. Hoffman, M. Machluf, Dynamic Autologous Reendothelialization of Small-Caliber Arterial Extracellular Matrix: A Preclinical Large Animal Study, Tissue Eng Pt A 23(1-2) (2017) 69-79.
[29] D.K. Li, Z.F. Xin, J.Y. Wan, X.L. Ma, Y. Xin, D. Gong, Z.F. Zhou, W.B. Li, X.F. Xu, Decellularized sheep internal carotid arteries as a tissue-engineered small-diameter vascular scaffold, Int J Clin Exp Med 9(6) (2016) 9983-9991.
[30] T. Pennel, G. Fercana, D. Bezuidenhout, A. Simionescu, T.H. Chuang, P. Zilla, D. Simionescu, The performance of cross-linked acellular arterial scaffolds as vascular grafts; pre-clinical testing in direct and isolation loop circulatory models, Biomaterials 35(24) (2014) 6311-22.
[31] M.T. Koobatian, S. Row, R.J. Smith, Jr., C. Koenigsknecht, S.T. Andreadis, D.D. Swartz, Successful endothelialization and remodeling of a cell-free small-diameter arterial graft in a large animal model, Biomaterials 76 (2016) 344-58.
[32] L. Mancuso, A. Gualerzi, F. Boschetti, F. Loy, G. Cao, Decellularized ovine arteries as small-diameter vascular grafts, Biomed Mater 9(4) (2014) 045011.
[33] S.G. Jones, Y. Hu, Q. Xu, M. Jahangiri, Stem cells accumulate on a decellularized arterial xenograft in vivo, Ann Thorac Surg 97(6) (2014) 2104-10.
[34] L. Dall'Olmo, I. Zanusso, R. Di Liddo, T. Chioato, T. Bertalot, E. Guidi, M.T. Conconi, Blood vessel-derived acellular matrix for vascular graft application, Biomed Res Int 2014 (2014) 685426.
[35] J.A. Brennan, J.H. Arrizabalaga, M.U. Nollert, Development of a Small Diameter Vascular Graft Using the Human Amniotic Membrane, Cardiovasc Eng and Techn 5(1) (2013) 96-109.

[36] Y. Xiong, W.Y. Chan, A.W. Chua, J. Feng, P. Gopal, Y.S. Ong, C. Song, Decellularized porcine saphenous artery for small-diameter tissue-engineered conduit graft, Art Organs 37(6) (2013) E74-87.
[37] S.P. Wilshaw, P. Rooney, H. Berry, J.N. Kearney, S. Homer-Vanniasinkam, J. Fisher, E. Ingham, Development and characterization of acellular allogeneic arterial matrices, Tissue Eng Pt A 18(5-6) (2012) 471-83.
[38] J. Heine, A. Schmiedl, S. Cebotari, M. Karck, H. Mertsching, A. Haverich, K. Kallenbach, Tissue engineering human small-caliber autologous vessels using a xenogenous decellularized connective tissue matrix approach: preclinical comparative biomechanical studies, Art Organs 35(10) (2011) 930-40.
[39] Y. Zhao, S. Zhang, J. Zhou, J. Wang, M. Zhen, Y. Liu, J. Chen, Z. Qi, The development of a tissue-engineered artery using decellularized scaffold and autologous ovine mesenchymal stem cells, Biomaterials 31(2) (2010) 296-307.
[40] M. Zhou, Z. Liu, Z. Wei, C. Liu, T. Qiao, F. Ran, Y. Bai, X. Jiang, Y. Ding, Development and validation of small-diameter vascular tissue from a decellularized scaffold coated with heparin and vascular endothelial growth factor, Art Organs 33(3) (2009) 230-9.
[41] D. Liao, X. Wang, P.H. Lin, Q. Yao, C.J. Chen, Covalent linkage of heparin provides a stable anti-coagulation surface of decellularized porcine arteries, J Cell Mol Med 13(8B) (2009) 2736-43.
[42] X.N. Wang, C.Z. Chen, M. Yang, Y.J. Gu, Implantation of decellularized small-caliber vascular xenografts with and without surface heparin treatment, Art Organs 31(2) (2007) 99-104.
[43] Z. Wang, Y. He, X. Yu, W. Fu, W. Wang, H. Huang, Rapid vascularization of tissue-engineered vascular grafts in vivo by endothelial cells in co-culture with smooth muscle cells, Journal of materials science. Materials in medicine 23(4) (2012) 1109-17.
[44] N.D. Martin, P.J. Schaner, T.N. Tulenko, I.M. Shapiro, C.A. Dimatteo, T.K. Williams, E.S. Hager, P.J. DiMuzio, In vivo behavior of decellularized vein allograft, J Surg Res 129(1) (2005) 17-23.
[45] A. Ketchedjian, A.L. Jones, P. Krueger, E. Robinson, K. Crouch, L. Wolfinbarger, Jr., R. Hopkins, Recellularization of decellularized allograft scaffolds in ovine great vessel reconstructions, Ann Thorac Surg 79(3) (2005) 888-96; discussion 896.
[46] P.J. Schaner, N.D. Martin, T.N. Tulenko, I.M. Shapiro, N.A. Tarola, R.F. Leichter, R.A. Carabasi, P.J. Dimuzio, Decellularized vein as a potential scaffold for vascular tissue engineering, J Vasc Surg 40(1) (2004) 146-53.
[47] B.S. Conklin, E.R. Richter, K.L. Kreutziger, D.S. Zhong, C. Chen, Development and evaluation of a novel decellularized vascular xenograft, Med Eng Phys 24(3) (2002) 173-83.

[48] D. Rana, H. Zreiqat, N. Benkirane-Jessel, S. Ramakrishna, M. Ramalingam, Development of decellularized scaffolds for stem cell-driven tissue engineering, J Tissue Eng Regen Med 11(4) (2017) 942-965.
[49] T. Hoshiba, H. Lu, N. Kawazoe, G. Chen, Decellularized matrices for tissue engineering, Expert Opin Biol Ther 10(12) (2010) 1717-28.
[50] C.H. Lin, K. Hsia, H. Ma, H. Lee, J.H. Lu, In Vivo Performance of Decellularized Vascular Grafts: A Review Article, I J Mol Science 19(7) (2018).
[51] H. Kerdjoudj, C. Boura, V. Moby, K. Montagne, P. Schaaf, J.C. Voegel, J.F. Stoltz, P. Menu, Re-endothelialization of human umbilical arteries treated with polyelectrolyte multilayers: A tool for damaged vessel replacement, Adv Funct Mater 17(15) (2007) 2667-2673.
[52] Q.F. Tu, Y. Zhang, D.X. Ge, J. Wu, H.Q. Chen, Novel tissue-engineered vascular patches based on decellularized canine aortas and their recellularization in vitro, Appl Surf Sci 255(2) (2008) 282-285.
[53] Z. Tosun, P.S. McFetridge, Improved recellularization of ex vivo vascular scaffolds using directed transport gradients to modulate ECM remodeling, Biotechnol Bioeng 110(7) (2013) 2035-45.
[54] S.W. Cho, S.H. Lim, I.K. Kim, Y.S. Hong, S.S. Kim, K.J. Yoo, H.Y. Park, Y. Jang, B.C. Chang, C.Y. Choi, K.C. Hwang, B.S. Kim, Small-diameter blood vessels engineered with bone marrow-derived cells, Ann Surg 241(3) (2005) 506-15.
[55] B.W. Tillman, S.K. Yazdani, L.P. Neff, M.A. Corriere, G.J. Christ, S. Soker, A. Atala, R.L. Geary, J.J. Yoo, Bioengineered vascular access maintains structural integrity in response to arteriovenous flow and repeated needle puncture, J Vasc Surg 56(3) (2012) 783-93.
[56] M. Olausson, P.B. Patil, V.K. Kuna, P. Chougule, N. Hernandez, K. Methe, C. Kullberg-Lindh, H. Borg, H. Ejnell, S. Sumitran-Holgersson, Transplantation of an allogeneic vein bioengineered with autologous stem cells: a proof-of-concept study, Lancet 380(9838) (2012) 230-7.
[57] A. Porzionato, E. Stocco, S. Barbon, F. Grandi, V. Macchi, R. De Caro, Tissue-Engineered Grafts from Human Decellularized Extracellular Matrices: A Systematic Review and Future Perspectives, I J Mol Science 19(12) (2018).
[58] Y. Gu, F. Wang, R. Wang, J. Li, C. Wang, L. Li, Z. Xu, J. Zhang, Preparation and evaluation of decellularized porcine carotid arteries cross-linked by genipin: the preliminary results, Cell Tissue Bank 19(3) (2018) 311-321.
[59] E. Lopez-Ruiz, S. Venkateswaran, M. Peran, G. Jimenez, S. Pernagallo, J.J. Diaz-Mochon, O. Tura-Ceide, F. Arrebola, J. Melchor, J. Soto, G. Rus, P.J. Real, M. Diaz-Ricart, A. Conde-Gonzalez, M. Bradley, J.A. Marchal, Poly(ethylmethacrylate-co-diethylaminoethyl acrylate) coating improves endothelial re-population, bio-mechanical and anti-thrombogenic

properties of decellularized carotid arteries for blood vessel replacement, Sci Rep 7(1) (2017) 407.
[60] M. Iijima, H. Aubin, M. Steinbrink, F. Schiffer, A. Assmann, R.D. Weisel, Y. Matsui, R.K. Li, A. Lichtenberg, P. Akhyari, Bioactive coating of decellularized vascular grafts with a temperature-sensitive VEGF-conjugated hydrogel accelerates autologous endothelialization in vivo, J Tissue Eng Regen Med 12(1) (2018) e513-e522.
[61] R.J. Smith, Jr., M.T. Koobatian, A. Shahini, D.D. Swartz, S.T. Andreadis, Capture of endothelial cells under flow using immobilized vascular endothelial growth factor, Biomaterials 51 (2015) 303-312.
[62] J.S. Lee, K. Lee, S.H. Moon, H.M. Chung, J.H. Lee, S.H. Um, D.I. Kim, S.W. Cho, Mussel-inspired cell-adhesion peptide modification for enhanced endothelialization of decellularized blood vessels, Macromol Biosci 14(8) (2014) 1181-9.
[63] W.W. Cai, Y.J. Gu, X.N. Wang, C.Z. Chen, Heparin coating of small-caliber decellularized xenografts reduces macrophage infiltration and intimal hyperplasia, Art Org 33(6) (2009) 448-55.
[64] Z. Cai, Y. Gu, J. Cheng, J. Li, Z. Xu, Y. Xing, C. Wang, Z. Wang, Decellularization, cross-linking and heparin immobilization of porcine carotid arteries for tissue engineering vascular grafts, Cell Tissue Bank 20(4) (2019) 569-578.
[65] X. Zhou, B. Zhao, J. Wang, Y. Zhou, J. Chai, H. Liu, Y. Zheng, Y. Zhang, G. Xu, H. Pan, H. Zhang, J. Zhou, Y. Liu, M. Zhen, Y. Zhao, Engineered Vascular Graft Using Nanoscale Decellularized Arteries Modified with Controlled-Release Heparin and Vascular Endothelial Growth Factor, J Biomater Tiss Eng 6(11) (2016) 870-882.
[66] X.F. Xu, H.P. Guo, X.J. Ren, D. Gong, J.H. Ma, A.P. Wang, H.F. Shi, Y. Xin, Y. Wu, W.B. Li, Effect of carbodiimide cross-linking of decellularized porcine pulmonary artery valvular leaflets, Int J Clin Exp Med 7(3) (2014) 649-56.
[67] M. Zhou, Z. Liu, C. Liu, X. Jiang, Z. Wei, W. Qiao, F. Ran, W. Wang, T. Qiao, C. Liu, Tissue engineering of small-diameter vascular grafts by endothelial progenitor cells seeding heparin-coated decellularized scaffolds, J Biomed Mater Res B Appl Biomater 100(1) (2012) 111-20.
[68] K. Schneider, M. Enayati, C. Grasl, I. Walter, L. Budinsky, G. Zebic, C. Kaun, A. Wagner, K. Kratochwill, H. Redl, A. Teuschl, B. K. Podesser, H. Bergmeister, Acellular vascular matrix grafts from human placenta chorion: Impact of ECM preservation on graft characteristics, protein composition and in vivo performance, Biomaterials, 2018.
[69] A.T. Pereira, P.C. Henriques, P.C. Costa, M.C.L. Martins, F.D. Magalhães, I.C. Gonçalves, Graphene oxide-reinforced poly(2-hydroxyethyl methacrylate) hydrogels with extreme stiffness and high-strength, Compos Sci Technol 184 (2019) 107819.

[70] D.G. Papageorgiou, I.A. Kinloch, R.J. Young, Mechanical properties of graphene and graphene-based nanocomposites, Prog Mater Science 90 (2017) 75-127.
[71] P.C. Henriques, I. Borges, A.M. Pinto, F.D. Magalhães, I.C. Gonçalves, Fabrication and antimicrobial performance of surfaces integrating graphene-based materials, Carbon 132 (2018) 709-732.
[72] R.N. Gomes, I. Borges, A.T. Pereira, A.F. Maia, M. Pestana, F.D. Magalhães, A.M. Pinto, I.C. Gonçalves, Antimicrobial graphene nanoplatelets coatings for silicone catheters, Carbon 139 (2018) 635-647.
[73] M.A. Raza, M. Mujddid, M. Hussain, H.Q. Ali, Z.U. Rehman, A. Inam, Mechanical properties of graphene oxide coated-glass fiber reinforced unsaturated polyester composites, Mater Res Express 6(11) (2019).
[74] H. Mahmood, L. Vanzetti, M. Bersani, A. Pegoretti, Mechanical properties and strain monitoring of glass-epoxy composites with graphene-coated fibers, Compos Part A Appl Sci Manuf 107 (2018) 112-123.
[75] F. Li, Y. Hua, C.-B. Qu, H.-M. Xiao, S.-Y. Fu, Greatly enhanced cryogenic mechanical properties of short carbon fiber/polyethersulfone composites by graphene oxide coating, Compos Part A Appl Sci Manuf 89 (2016) 47-55.
[76] L. Bhanuprakash, S. Parasuram, S. Varghese, Experimental investigation on graphene oxides coated carbon fibre/epoxy hybrid composites: Mechanical and electrical properties, Compos Sci Technol 179 (2019) 134-144.
[77] J. Fu, Y. Zhang, J. Chu, X. Wang, W. Yan, Q. Zhang, H. Liu, Reduced Graphene Oxide Incorporated Acellular Dermal Composite Scaffold Enables Efficient Local Delivery of Mesenchymal Stem Cells for Accelerating Diabetic Wound Healing, ACS Biomater-Sci Eng 5(8) (2019) 4054-4066.
[78] Q. Wang, J. Chen, Q. Niu, X. Fu, X. Sun, X. Tong, The application of graphene oxidized combining with decellularized scaffold to repair of sciatic nerve injury in rats, Saudi Pharm J 25(4) (2017) 469-476.
[79] P. Wilczek, R. Major, L. Lipinska, J. Lackner, A. Mzyk, Thrombogenicity and biocompatibility studies of reduced graphene oxide modified acellular pulmonary valve tissue, Mat Sci Eng C-Mater 53 (2015) 310-21.
[80] D. Huo, G. Liu, Y. Li, Y. Wang, G. Guan, M. Yang, K. Wei, J. Yang, L. Zeng, G. Li, W. Zeng, C. Zhu, Construction of Antithrombotic Tissue-Engineered Blood Vessel via Reduced Graphene Oxide Based Dual-Enzyme Biomimetic Cascade, ACS Nano 11(11) (2017) 10964-10973.
[81] S. Bimpong, C.S. Abaidoo, O.O.-D. Atuahene, J. Tetteh, Morphometric Characterization of Umbilical Cord Vessels and Neonatal Outcome, J Anat 7(1.1) (2019) 6050-6058.

[82] C.B. H. Kerdjoudj, L. Marchal, D. Dumas, P. Schaff, J.-C. Voegel, J.-F. Stoltz and P. Menu Decellularized umbilical artery treated with thin polyelectrolyte multilayer films: Potential use in vascular engineering, Bio-Med Mater Eng 16 (2016).
[83] Z. Gordon, D. Elad, R. Almog, Y. Hazan, A.J. Jaffa, O. Eytan, Anthropometry of fetal vasculature in the chorionic plate, J Anat 211(6) (2007) 698-706.
[84] A.M. Pinto, C. Gonçalves, D.M. Sousa, A.R. Ferreira, J.A. Moreira, I.C. Gonçalves, F.D. Magalhães, Smaller particle size and higher oxidation improves biocompatibility of graphene-based materials, Carbon 99(Supplement C) (2016) 318-329.
[85] A. Kovtun, D. Jones, S. Dell'Elce, E. Treossi, A. Liscio, V. Palermo, Accurate chemical analysis of oxygenated graphene-based materials using X-ray photoelectron spectroscopy, Carbon 143 (2019) 268-275.
[86] K. Krishnamoorthy, M. Veerapandian, K. Yun, S.J. Kim, The chemical and structural analysis of graphene oxide with different degrees of oxidation, Carbon 53 (2013) 38-49.
[87] S. Vranic, A.F. Rodrigues, M. Buggio, L. Newman, M.R.H. White, D.G. Spiller, C. Bussy, K. Kostarelos, Live Imaging of Label-Free Graphene Oxide Reveals Critical Factors Causing Oxidative-Stress-Mediated Cellular Responses, ACS Nano 12(2) (2018) 1373-1389.
[88] H. Bergmeister, C. Schreiber, C. Grasl, I. Walter, R. Plasenzotti, M. Stoiber, D. Bernhard, H. Schima, Healing characteristics of electrospun polyurethane grafts with various porosities, Acta Biomater 9(4) (2013) 6032-40.
[89] H. Bergmeister, F. Bastian, C. Plass, E. Rieder, U. Losert, G. Weigel, 563: In vivo remodeling of decellularized xenogeneic arteries: Impact of heparin-crosslinking on graft stability, J Heart Lung Transp 26(2) (2007) S262-S262.
[90] C.J. Pan, L.Q. Pang, F. Gao, Y.N. Wang, T. Liu, W. Ye, Y.H. Hou, Anticoagulation and endothelial cell behaviors of heparin-loaded graphene oxide coating on titanium surface, Materials science & engineering. C, Mat Sci Eng C-Mater 63 (2016) 333-40.
[91] L. Stobinski, B. Lesiak, A. Malolepszy, M. Mazurkiewicz, B. Mierzwa, J. Zemek, P. Jiricek, I. Bieloshapka, Graphene oxide and reduced graphene oxide studied by the XRD, TEM and electron spectroscopy methods, J Electron Spectros Relat Phenomena 195 (2014) 145-154.
[92] X.L. Sheng, Q.B. Yan, F. Ye, Q.R. Zheng, G. Su, T-carbon: a novel carbon allotrope, Phys Rev Lett 106(15) (2011) 155703.
[93] P. Trucano, R. Chen, Structure of graphite by neutron diffraction, Nature 258(5531) (1975) 136-137.
[94] M. Lotya, A. Rakovich, J.F. Donegan, J.N. Coleman, Measuring the lateral size of liquid-exfoliated nanosheets with dynamic light scattering, Nanotechnology 24(26) (2013) 265703.
[95] S.F. Badylak, D.O. Freytes, T.W. Gilbert, Extracellular matrix as a biological scaffold material: Structure and function, Acta Biomater 5(1) (2009) 1-13.

[96] P.M. Crapo, T.W. Gilbert, S.F. Badylak, An overview of tissue and whole organ decellularization processes, Biomaterials 32(12) (2011) 3233-43.
[97] V. Catto, S. Farè, G. Freddi, M.C. Tanzi, Vascular Tissue Engineering: Recent Advances in Small Diameter Blood Vessel Regeneration, ISRN Vascular Medicine 2014 (2014) 1-27.
[98] H. Haruguchi, S. Teraoka, Intimal hyperplasia and hemodynamic factors in arterial bypass and arteriovenous grafts: a review, J Artif Organs 6(4) (2003) 227-35.
[99] A.C. Newby, A.B. Zaltsman, Molecular mechanisms in intimal hyperplasia, J Pathol 190(3) (2000) 300-9.
[100] M.S. Lemson, J.H. Tordoir, M.J. Daemen, P.J. Kitslaar, Intimal hyperplasia in vascular grafts, Eur J Vasc Endovasc Surg 19(4) (2000) 336-50.
[101] G. Konig, T.N. McAllister, N. Dusserre, S.A. Garrido, C. Iyican, A. Marini, A. Fiorillo, H. Avila, W. Wystrychowski, K. Zagalski, M. Maruszewski, A.L. Jones, L. Cierpka, L.M. de la Fuente, N. L'Heureux, Mechanical properties of completely autologous human tissue engineered blood vessels compared to human saphenous vein and mammary artery, Biomaterials 30(8) (2009) 1542-50.
[102] P. Lamm, G. Juchem, S. Milz, M. Schuffenhauer, B. Reichart, Autologous endothelialized vein allograft: a solution in the search for small-caliber grafts in coronary artery bypass graft operations, Circulation 104(12 Suppl 1) (2001) I108-14.
[103] M.H. Norahan, M. Amroon, R. Ghahremanzadeh, M. Mahmoodi, N. Baheiraei, Electroactive graphene oxide-incorporated collagen assisting vascularization for cardiac tissue engineering, J Biomed Mater Res A 107(1) (2019) 204-219.
[104] X. Jing, H.Y. Mi, M.R. Salick, T.M. Cordie, X.F. Peng, L.S. Turng, Electrospinning thermoplastic polyurethane/graphene oxide scaffolds for small diameter vascular graft applications, Mat Sci Eng C-Mater 49 (2015) 40-50.
[105] S.N. Sofia Melo, Andreia T Pereira, Inês Borges, Pedro Granja, Fernão Magalhães, Incorporation of graphene oxide into poly(ε-caprolactone) 3D printed fibrous scaffolds improves their antimicrobial properties, Mat Sci Eng C-Mater (2020).
[106] R. Podila, T. Moore, F. Alexis, A.M. Rao, Graphene coatings for enhanced hemo-compatibility of nitinol stents, RSC Adv. 3(6) (2013) 1660-1665.
[107] S. Mukherjee, P. Sriram, A.K. Barui, S.K. Nethi, V. Veeriah, S. Chatterjee, K.I. Suresh, C.R. Patra, Graphene Oxides Show Angiogenic Properties, Adv Healthc Mater 4(11) (2015) 1722-32.
[108] Kenry, W.C. Lee, K.P. Loh, C.T. Lim, When stem cells meet graphene: Opportunities and challenges in regenerative medicine, Biomaterials 155 (2018) 236-250.
[109] A. Kilic, D.J. Arnaoutakis, T. Reifsnyder, J.H. Black, 3rd, C.J. Abularrage, B.A. Perler, Y.W. Lum, Management of infected vascular grafts, Vasc Med 21(1) (2016) 53-60.

[110] M. Revest, F. Camou, E. Senneville, J. Caillon, F. Laurent, B. Calvet, P. Feugier, M. Batt, C. Chidiac, v. Groupe de Reflexion sur les Infections de Protheses, Medical treatment of prosthetic vascular graft infections: Review of the literature and proposals of a Working Group, Int. J Antimicrob Agents 46(3) (2015) 254-65.
[111] C.N. Antonopoulos, N.A. Papakonstantinou, D. Hardy, S.P. Lyden, Editor's Choice - Cryopreserved Allografts for Arterial Reconstruction after Aorto-Iliac Infection: A Systematic Review and Meta-Analysis, Eur J Vasc Endovasc Surg 58(1) (2019) 120-128.
[112] A. Gharamti, Z.A. Kanafani, Vascular Graft Infections: An update, Infect Dis Clin North Am 32(4) (2018) 789-809.
[113] D. Holderbaum, G.S. Hall, L.A. Ehrhart, Collagen binding to Staphylococcus aureus, Infect Immun 54(2) (1986) 359-64.
[114] P. Kuusela, Fibronectin binds to Staphylococcus aureus, Nature 276(5689) (1978) 718-20.
[115] P.W. Park, D.D. Roberts, L.E. Grosso, W.C. Parks, J. Rosenbloom, W.R. Abrams, R.P. Mecham, Binding of elastin to Staphylococcus aureus, J Biol Chem 266(34) (1991) 23399-406.
[116] J.D. Lopes, M. dos Reis, R.R. Brentani, Presence of laminin receptors in Staphylococcus aureus, Science 229(4710) (1985) 275-7.
[117] G.S. Chhatwal, K.T. Preissner, G. Muller-Berghaus, H. Blobel, Specific binding of the human S protein (vitronectin) to streptococci, Staphylococcus aureus, and Escherichia coli, Infect Immun 55(8) (1987) 1878-83.
[118] J. Hawiger, S. Timmons, D.D. Strong, B.A. Cottrell, M. Riley, R.F. Doolittle, Identification of a region of human fibrinogen interacting with staphylococcal clumping factor, Biochem 21(6) (1982) 1407-13.
[119] N. Yadav, A. Dubey, S. Shukla, C.P. Saini, G. Gupta, R. Priyadarshini, B. Lochab, Graphene Oxide-Coated Surface: Inhibition of Bacterial Biofilm Formation due to Specific Surface-Interface Interactions, ACS Omega 2(7) (2017) 3070-3082.
[120] S. Thampi, A.M. Nandkumar, V. Muthuvijayan, R. Parameswaran, Differential Adhesive and Bioactive Properties of the Polymeric Surface Coated with Graphene Oxide Thin Film, Acs Appl Mater Inter 9(5) (2017) 4498-4508.
[121] A. Modi, S.K. Verma, J. Bellare, Graphene oxide-doping improves the biocompatibility and separation performance of polyethersulfone hollow fiber membranes for bioartificial kidney application, J Colloid Interface Sci 514 (2018) 750-759.
[122] L. Ma, L. Huang, Y. Zhang, L. Zhao, Q. Xin, H. Ye, H. Li, Hemocompatible poly(lactic acid) membranes prepared by immobilizing carboxylated graphene oxide via mussel-inspired method for hemodialysis, Rsc Adv 8(1) (2018) 153-161.

[123] S.N. Sofia Melo, Andreia T Pereira, Inês Borges, Pedro Granja, Fernão Magalhães, Inês Gonçalves, Incorporation of graphene oxide into poly(ε-caprolactone) 3D printed fibrous scaffolds improves their antimicrobial properties, Mat Sci Eng C-Bio S (2019).

5.8 Supporting Information

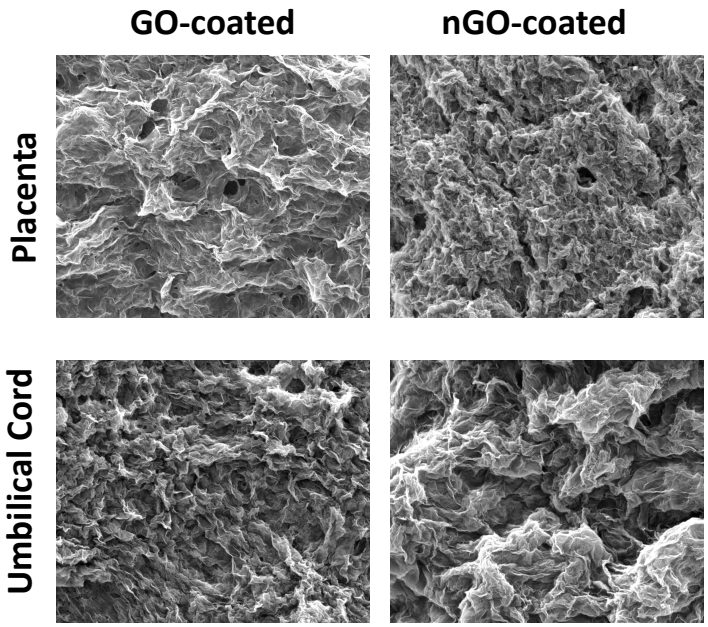

Figure S.1 – Coating stability upon 3h perfusion with PBS at 60 rpm

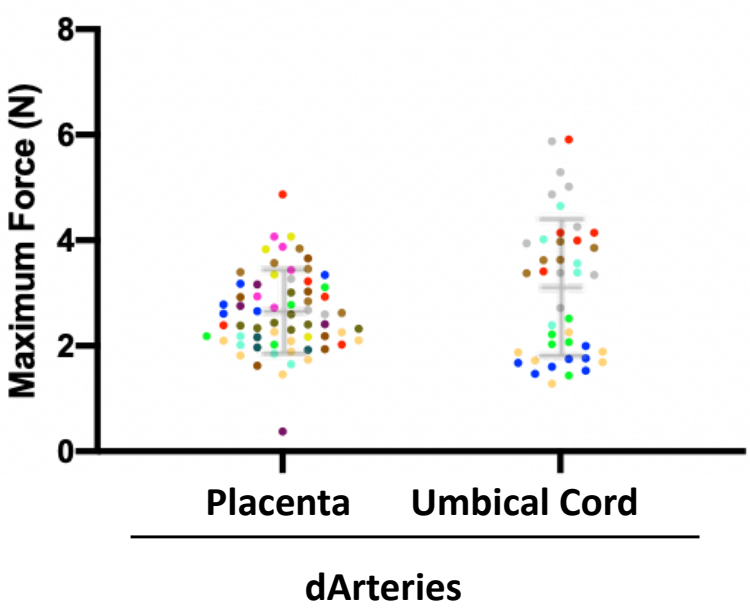

Figure S.2 - Force Max dispersion of decellularized placenta chorion and umbilical cord artery (each color represents a different decellularized artery).

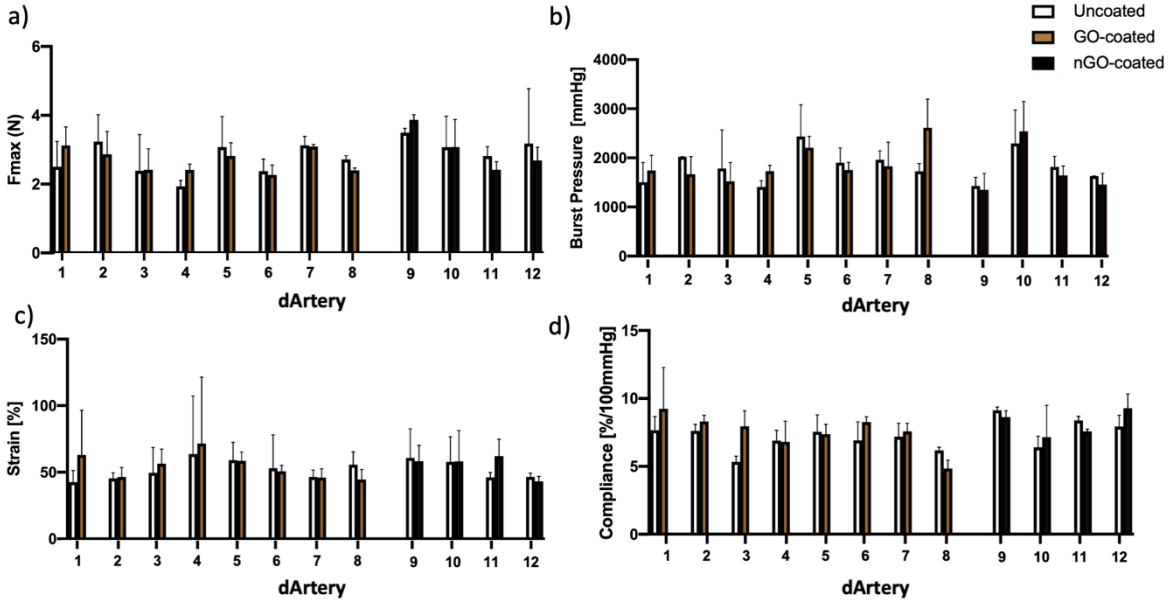

Figure S.3 – Fmax a), burst pressure b), maximum strain c) and compliance of uncoated (white), GO- (Brown) and nGO (Black) -coated decellularized placenta chorion arteries.

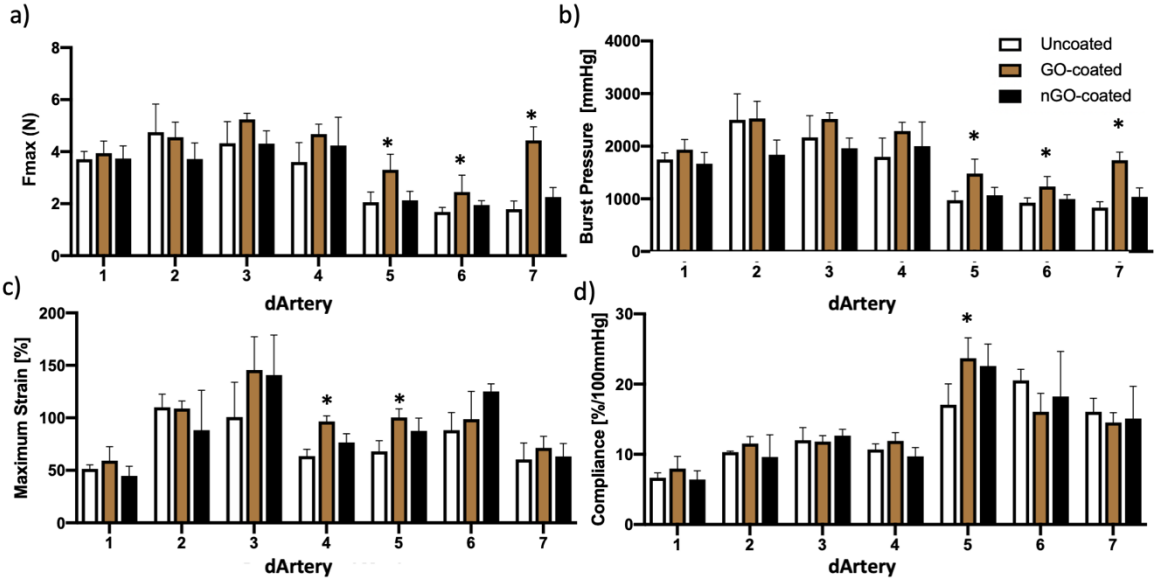

Figure S.4 – Fmax a), burst pressure b), maximum strain c) and compliance of uncoated (white), GO- (Brown) and nGO (Black) -coated decellularized umbilical cord arteries. * ($p < 0.05$ – Two Way ANOVA).

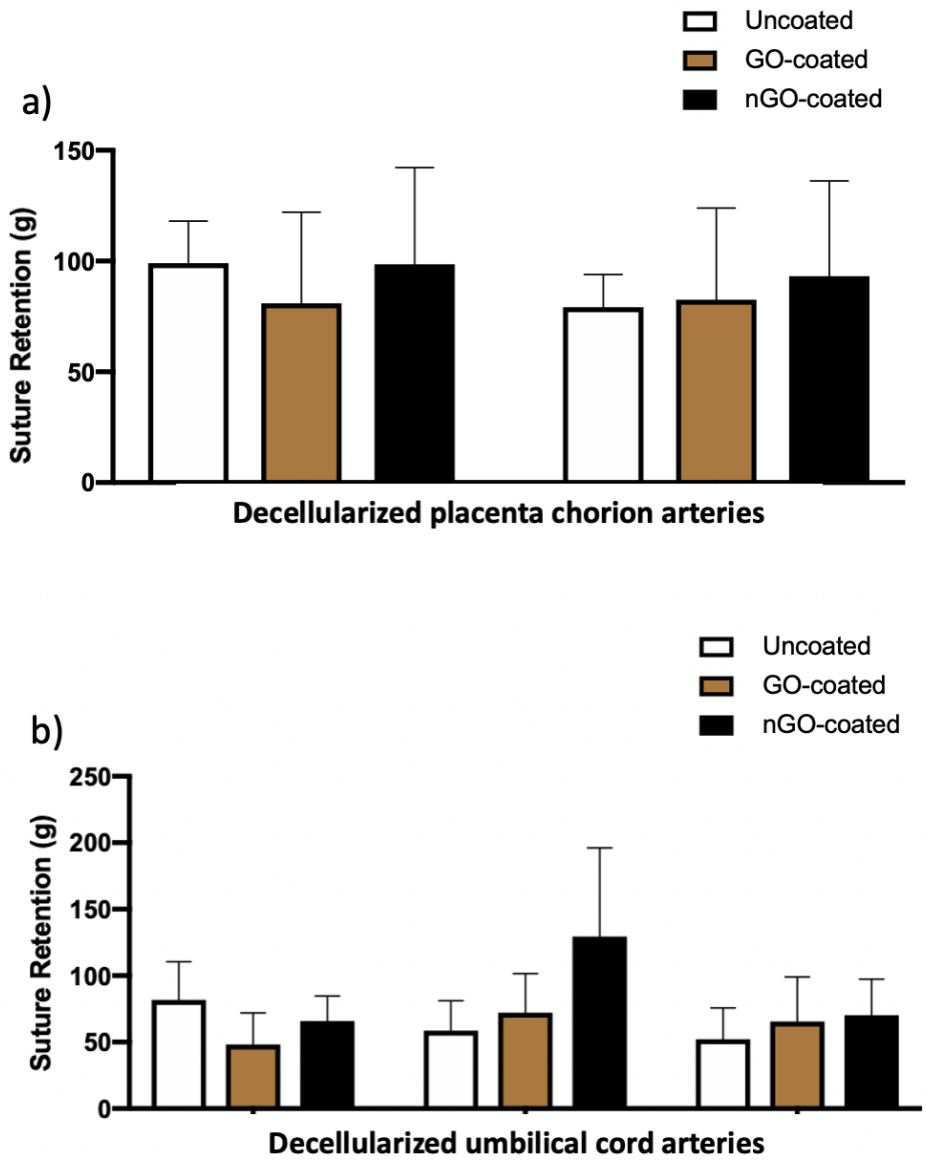

Figure S.5 – Suture retention uncoated (white), GO- (Brown) and nGO (Black)-coated a) decellularized placenta chorion and b) umbilical cord arteries.

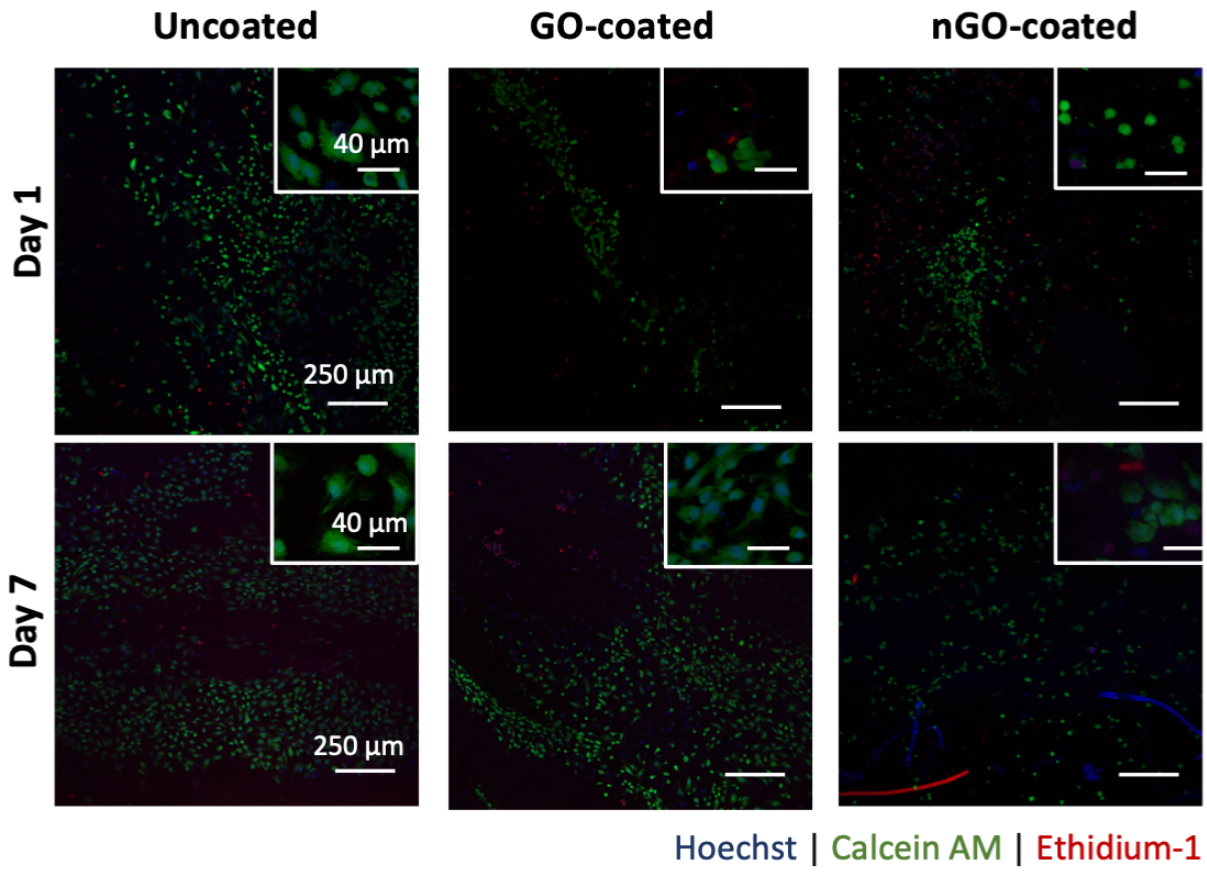

Figure S.6 – Immunofluorescence images of HUVECs adherent to uncoated, GO- and nGO-coated decellularized placenta chorion artery surface after 1 and 7 days of incubation. Cells stained with Hoechst (DNA) in blue, calcein-AM (live cells) in green and Propidium Iodide (dead cells) in red.

Chapter 6

General Discussion, Conclusions and Future Perspectives

In this chapter, the principal results and achievements will be discussed regarding the central problem approached in this study, the design of blood-contacting devices. The main conclusions of the last 3 years' work will be sum up and several cues for way forward on this subject will be provided namely regarding the future usage of graphene-based materials in the design of blood-contacting devices.

6.1 General discussion

The evident lack of hemocompatible materials for the development of blood contact devices (BCDs) awake a clear need for the design of new biomaterials, which were the main focus of this work. Using two different approaches, a set of novel biomaterials with the potential to be applied in the design of BCDs were generated, being their cytocompatibility demonstrated *in vitro* and hemocompatibility *in vitro* and *in vivo* (acute study).

pHEMA, a non-fouling material, which exhibits low adhesion of blood components, bacteria and cells (passive approach), was modified using different graphene-based materials (GBMs) as filler to improve the mechanical properties, aspiring its application as BCDs. In this study, the polymerization of pHEMA was observed in the presence of all GBMs. A relation between filler concentration and the reached pHEMA mechanical features was established, showing, for the highest tested concentration (5% (w/v)), an impressive increase in stiffness (8.3x) and tensile resistance (7.4x) reaching values of 6.5 MPa and 1.14 MPa, respectively. These order of improvements in stiffness and tensile resistance have only been surpassed when GO is incorporated in polyacrylic acid, as very recently reported by Wang *et al*. [1] Besides the concentration effect, the features of the used GBMs also play a critical role in the mechanical properties of pHEMA, being an improvement achieved only when oxidized GBMs are included. The developed composites maintain the cytocompatibility and hemocompatibility of pHEMA, even *in vivo* for pHEMA/GO 1% (acute study).

Beyond pHEMA/oxidized-GBMs application as BCDs, other applications could be envisaged. Their swelling, hydrophilic surface, cytocompatibility and YM similar to polydimethylsiloxane (PDMS) [2], cartilage [2], intervertebral disc [3] or arteries walls [2] and UTS similar to polyurethane rigid foams [4], could be an asset in the development of soft robots', packaging, sealing, cartilage, intervertebral disc and hernia repair devices. Specifically, in food packaging, the swelling capacity and non-fouling properties of pHEMA/oxidized-GBMs may provide an efficient water-removal system and prevent the adhesion of bacteria to surface, preventing food contamination. A further step in pHEMA/oxidized-GBMs hydrogels formulation could be needed, since in the last decade there has been a constant search for biodegradable materials for packaging [5]. Based on the promising results obtained in this work, a further step in pHEMA/oxidized-GBMs hydrogels formulation to make it biodegradable is currently being attempted in our group, in order to widen even more the range of applications of these new composite materials. The biomaterials used nowadays in the design of hernia repair meshes can also be either non-biodegradable, such as polypropylene, polyester, and expanded polytetrafluoroethylene, or biodegradable, such as decellularized matrices [6]. They exhibit poor outcomes, being associated with several problems such as infection, peritoneal adhesions, hernia relapse, obstruction, mesh migration

and mesh shrinkage (contraction) [6]. pHEMA/oxidized-GBMs non-fouling properties could be an asset in the development of hernia meshes, at least preventing infection-related problems. Taking into account the values of abdominal pressure achieved during coughing and jumping (14-33 kPa), pHEMA/oxidized-GBMs composites exhibit the required mechanical properties, but the available meshes are more elastic (150-340% strain) [6, 7], which would require further optimization. Moreover, these devices are attached to the peritoneum by gluing or stapling. However, as non-fouling material that has anti-adhesive properties, gluing pHEMA/oxidized-GBMs to peritoneum would be difficult, and stapling could be restrictive due to the reduced suture retention capacity of pHEMA/oxidized-GBMs.

Regarding the application of pHEMA/oxidized-GBMs in the design of BCDs, they could be potentially used without further modification for storage bags, tubing for blood accessing (catheters), and components of hemodialysis machines. When compared with commercially available materials, such as ePTFE, PU or silicone, pHEMA/oxidized-GBMs could provide better performance for these applications, since they exhibit a low platelet adhesion and infection potential. Heparinization of these commercially available biomaterials is the main strategy currently applied in the clinics to reach improved outcomes. Still under research are several strategies to modify the surface of materials, namely using non-fouling polymers or bioactive molecules [8-11]. The lack of stability, as well as the long protocols associated to these approaches are the main concerns reflecting poor performance, but the high production costs are also a critical factor in the design of BCDs [12]. Since the herein developed pHEMA/oxidized-GBMs composites exhibit inadequate suture retention capacity, applications as vascular grafts and heart valves, that require this step, are most likely unfeasible. This suture retention capacity would need to be improved, possibly by optimizing the 3D conduits production technique, since in this study the composites were produced, as proof of concept, by molding to create either 2D films or 3D tubular structures. Moreover, depending on BCDs, different strategies could also be envisaged. In particular for the design of small-diameter vascular grafts (<5 mm), a bioactive strategy could be pursued, aiming to support adhesion of blood-derived endothelial cells, progenitor cells, and stem cells [13-17]. For this, besides the improvement of suture retention, pHEMA/oxidized-GBMs would need to be capable of supporting endothelial cells adhesion, growth and proliferation, without compromising their non-fouling properties for blood components and bacteria. Finally, for pHEMA/GO to be used in the design of small-diameter vascular grafts, degradability and elasticity should also be improved.

This bioactive strategy was also explored in this study, namely through the use of decellularized arteries for the development of small diameter vascular grafts (<5 mm). Human placenta chorion and umbilical cord decellularized arteries, which exhibit the natural architecture and biological cues to promote cell adhesion and proliferation, were coated

through automatic reperfusion of GO solutions to improve their mechanical properties and decrease collagen exposure, which are associated with high thrombogenic and infection potential [18]. An increase of 29% for maximum force and 27% for burst pressure was observed for decellularized umbilical cord arteries reaching values of mechanical properties similar to the saphenous vein, which is the gold standard for vascular replacement. This increase in the mechanical properties is higher than the reported in the literature for GO adsorption to an acellular dermal matrix, where an increase of 10% in tensile resistance was reported [19]. Better resistance platelet adhesion was reached without affecting the adhesion of endothelial cells. *In vivo* acute hemocompatibility studies revealed that GO-coated decellularized umbilical cord arteries do not clot upon a further step of heparin functionalization, unraveling the possibility to implant it *in vivo* for further studies. Vascular grafts based in decellularized matrices are already available in the market, namely Artegraft® (Bovine carotid artery), Solcograft (Bovine carotid artery), ProCol® (Bovine mesenteric vein), and SynerGraft® (Bovine ureter) being used for vascular access during hemodialysis or peripheral arterial bypass [13, 20]. However, even when systemic or local anticoagulation is performed, clinical outcomes are not satisfactory due to graft-related thrombosis, infection, and aneurysm, which are associated with a poor endothelialization upon implantation [13]. These poor outcomes, in combination with their high production costs (comparing to available synthetic materials), prevent their extensive use in clinics [20]. Recent studies show good support of endothelial cells, depending on source and decellularization protocol [18, 21-25]. Functionalization of decellularized matrices with bioactive molecules (VEGF and heparin) were also proposed, despite none has reached the market yet [13]. GO coating of decellularized umbilical cord arteries emerges as an alternative approach to achieve better performance. Further mechanical and biological improvements of decellularized matrices could be idealized, namely promoting higher tensile resistance, blood compatibility, and a faster reendothelization.

Comparing passive vs bioactive strategies, it is possible to point out advantages and disadvantages to each. Approaches that promote surface endothelialization exhibit more effective outcomes regarding hemocompatibility than non-fouling materials [9] because the establishment of a physiologically functional endothelial layer leads to the constant release of anticoagulant stimulus *in situ*, therefore preventing thrombus formation at the surface. However, the achievement of physiological fully functional endothelium after implantation of BDCs in a suitable time frame is still the main challenge of this strategy. This happens, because, besides the difficulty of achieving a functional endothelial layer**,** bioactive strategies are susceptible to *in vivo* degradation, which requires a good orchestration between vessel remodeling and scaffold degradation. For decellularized arteries, some studies point out a successful reendothelialization before their degradation [18, 23, 26]. As such, the passive strategy seems to be preferable for short term applications, such as blood bags, catheters,

and tubing systems, although the bioactive strategy exhibit better hemocompatibility outcomes in the long-term, which is a requirement for example in the design of small-diameter vascular grafts. In this thesis, GO exhibits a multitasking role, starting with the improvement of the mechanical properties of two biomaterials with different features, pHEMA and decellularized umbilical cord arteries, using two different incorporation techniques (entrapment in the polymeric network and surface coating) and in the case of decellularized arteries, a decreased platelets adhesion was also achieved. GBMs incorporation did not induce cytotoxicity comparing to neat materials in any of the strategies. However, envisioning a future application of these materials in clinics, it is important to discuss some aspects regarding GBMs safety. Despite GBMs showing potential to be biodegraded *in vivo* [27], the used of any nanomaterial in clinical approaches is stills an under-debate issue. In the passive strategy, GBMs are integrated into the pHEMA matrix, a non-degradable polymer, and therefore GBMs will not be in direct contact with biological systems, which could be an advantage for a quicker transition from bed to bench side. In the bioactive strategy, however, GO is used as a coating of decellularized arteries and therefore is exposed to blood and surrounding tissues, which could compromise their application in clinics.

Intravenous administration of GO dispersion has shown their potential to be accumulated in different organs, particularly liver, spleen and lungs, as shown for intravenous administration of GO solutions. However, herein developed GO-coated grafts contain low amount of GO (maximum 4 μg/mL or 282 μg/kg considering a complete adhesion of all GO incubated with decellularized artery and normalizing with the total volume of blood in the human body (~5L) or to 70.8 kg, average weight of european population), which has been described as a safe concentration in several *in vitro (10* μg/mL for HUVECs cells) and *in vivo* studies (1 mg/kg).

6.2 Conclusions

Graphene based materials (GBMs) exhibit capacity to tune the mechanical properties of two different biomaterials described in literature as having good hemocompibility and/or biocompatibility, namely a non-fouling hydrogel and decellularized arteries.

In the case of pHEMA reinforced with GBMs, the oxidation degree and thickness showed to be important features to improve its mechanical properties being GO the most efficient filler. Incorporation of 5% GO leads to impressive increase in stiffness (730%) and tensile resistance (640%), reaching values of 6.5 MPa and 1.14 MPa, respectively, which pave the way for potential application of pHEMA in several fields which were not possible until now. For the development of BCDs, 1% GO seems to be the optimal concentration. The pHEMA/GO composites keep the non-fouling properties of pHEMA, which could be an asset for the BCDs,

preventing endothelial cells, bacteria and human platelets adhesion and resisting clot formation under blood flow in a pig AV-shunt.

In the case of decellularized arteries, GO coatings of the inner lumen were effective to improve the maximum force and burst pressure in 29% and 27% of umbilical cord arteries, respectively, reaching values similar to the saphenous vein, the gold standard for vascular replacement. Moreover, GO/nGO exhibit a protective effect against bacteria and platelet adhesion. These new features of decellularized matrices achieved by GO coatings are a steppingstone on the development of vascular grafts.

As such, the biomaterials developed in this study, pHEMA/oxidized-GBMs and GO-coated decellularized umbilical cord arteries, reveal high potential to be applied in the development of BCDs.

6.3 Future perspectives

Within the development of this work, several questions were proposed, which unveiled a need for further studies regarding this research topic. The effect of GBMs incorporation in mechanical reinforcement of other hemocompatible materials should be addressed to verify the possible universal role of these materials. Due to reduced suture retention capacity, which impairs pHEMA/GO applications in some BCDs, a new 3D production technique or different formulation should be performed. Since the 3D production technique should have a lower impact on biological outcomes than a different formulation, this should be the first approach to improve pHEMA/GO suture retention capacity. Production of pHEMA/GO fibers by electrospinning or 3D printing could help in inhibiting the rupture propagation upon suturing. Regarding the pHEMA/GO formulation, it could be possible to graft HEMA monomers in GO to promote an even better interaction between pHEMA and GO or conjugate pHEMA/GO composites with other polymers to promote an improved reinforcement, such as the development of interpenetrated networks. For a possible application in the design of small-diameter vascular graft, a further optimization step of pHEMA/GO should be performed to induce its endothelialization and biodegradability upon implantation. Some peptides sequence, such as REDV, show potential to induce endothelial cells adhesion without promoting platelet activation. Changing of pHEMA crosslinking agent (TEGDMA) to a biodegradable one, such as N,O-dimethacryloyl hydroxylamine (DMHA) [28], could be an strategy to became pHEMA biodegradable. Depending on BCDs applications, such in the case of implantable BCDs, vascular grafts and heart valves, long-term *in vivo* study with implanted pHEMA/GO should be performed.

Under the scope of GO-coated decellularized umbilical cord arteries, the next step is to evaluate the effect of heparin crosslinking in the mechanical properties of GO-coated

decellularized umbilical cord arteries. Moreover, the long-term implantation of these grafts in rabbit infrarenal aorta, an *in vivo* model for small diameter vascular grafts (i.d. 1-4 mm) should be addressed [13]. This will allow to understand the effect of GO effect in artery remodeling and inflammatory response, and to address GO distribution and its toxicity to other organs. Given the promising antibacterial results obtained *in vitro*, grafts could be tested in challenging *in vivo* conditions, such as the vascular graft infection model [29]. Further mechanical improvements on GO and decellularized arteries could be envisaged using smaller GBMs, which could penetrate between collagen fibers, or promoting a covalent interaction between GO and matrix. Modifications of GO with bioactive molecules might also be performed, such as REDV peptide, VEGF to promote faster remodeling, antimicrobial peptide, antibiotics to improve antimicrobial properties and/or, PEG, PAM, and pHEMA to modulate the inflammatory response.

This work opened a new research area in our team, namely in the reinforcement of different hydrogels such as alginate with GBMs as well as in pHEMA/GO modifications for the design of small-diameter vascular grafts.

6.4 References

[1] Y. Wang, Q. Chang, R. Zhan, K. Xu, Y. Wang, X. Zhang, B. Li, G. Luo, M. Xing, W. Zhong, Tough but self-healing and 3D printable hydrogels for E-skin, E-noses and laser controlled actuators, J of Mater ChemA 7(43) (2019) 24814-24829.

[2] A.J.T. Teo, A. Mishra, I. Park, Y.-J. Kim, W.-T. Park, Y.-J. Yoon, Polymeric Biomaterials for Medical Implants and Devices, ACS Biomater-Sci Eng 2(4) (2016) 454-472.

[3] R.G. Long, O.M. Torre, W.W. Hom, D.J. Assael, J.C. Iatridis, Design Requirements for Annulus Fibrosus Repair: Review of Forces, Displacements, and Material Properties of the Intervertebral Disk and a Summary of Candidate Hydrogels for Repair, J Biomech Eng 138(2) (2016) 021007.

[4] M. Ridha, V.P.W. Shim, Microstructure and Tensile Mechanical Properties of Anisotropic Rigid Polyurethane Foam, Exp Mech 48(6) (2008) 763-776.

[5] R.A. Batista, P.J.P. Espitia, J.S.S. Quintans, M.M. Freitas, M.A. Cerqueira, J.A. Teixeira, J.C. Cardoso, Hydrogel as an alternative structure for food packaging systems, Carbohyd Polym 205 (2019) 106-116.

[6] S. Elango, S. Perumalsamy, K. Ramachandran, K. Vadodaria, Mesh materials and hernia repair, Biomedicine (Taipei) 7(3) (2017) 16.

[7] P.P. Pott, M.L. Schwarz, R. Gundling, K. Nowak, P. Hohenberger, E.D. Roessner, Mechanical properties of mesh materials used for hernia repair and soft tissue augmentation, PLoS One 7(10) (2012) e46978.
[8] B.D. Ratner, Biomaterials: Been There, Done That, and Evolving into the Future, Annu Rev Biomed Eng 21 (2019) 171-191.
[9] M.F. Maitz, M.C.L. Martins, N. Grabow, C. Matschegewski, N. Huang, E.L. Chaikof, M.A. Barbosa, C. Werner, C. Sperling, The blood compatibility challenge. Part 4: Surface modification for hemocompatible materials: Passive and active approaches to guide blood-material interactions, Acta Biomater 94 (2019) 33-43.
[10] R. Gbyli, A. Mercaldi, H. Sundaram, K.A. Amoako, Achieving Totally Local Anticoagulation on Blood Contacting Devices, Adv Mater Interfaces 5(4) (2018).
[11] K.S. Lavery, C. Rhodes, A. McGraw, M.J. Eppihimer, Anti-thrombotic technologies for medical devices, Adv Drug Deliv Rev 112 (2017) 2-11.
[12] I. Sotiri, M. Robichaud, D. Lee, S. Braune, M. Gorbet, B.D. Ratner, J.L. Brash, R.A. Latour, I. Reviakine, BloodSurf 2017: News from the blood-biomaterial frontier, Acta Biomater 87 (2019) 55-60.
[13] C.H. Lin, K. Hsia, H. Ma, H. Lee, J.H. Lu, In Vivo Performance of Decellularized Vascular Grafts: A Review Article, Int J Mol Scie 19(7) (2018).
[14] M.A. Hiob, S. She, L.D. Muiznieks, A.S. Weiss, Biomaterials and Modifications in the Development of Small-Diameter Vascular Grafts, ACS Biomater-Sci Eng 3(5) (2016) 712-723.
[15] D.F. Williams, Challenges With the Development of Biomaterials for Sustainable Tissue Engineering, Front Bioeng Biotechnol 7 (2019) 127.
[16] K.A. Rocco, M.W. Maxfield, C.A. Best, E.W. Dean, C.K. Breuer, In vivo applications of electrospun tissue-engineered vascular grafts: a review, Tissue Eng Part B Rev20(6) (2014) 628-40.
[17] S. Xu, F. Lu, L. Cheng, C. Li, X. Zhou, Y. Wu, H. Chen, K. Zhang, L. Wang, J. Xia, G. Yan, Z. Qi, Preparation and characterization of small-diameter decellularized scaffolds for vascular tissue engineering in an animal model, Biomed Eng Online 16(1) (2017) 55.
[18] K. Schneider, M. Enayati, C. Grasl, I. Walter, L. Budinsky, G. Zebic, C. Kaun, A. Wagner, K. Kratochwill, H. Redl, A. Teuschl, B. K. Podesser, H. Bergmeister, Acellular vascular matrix grafts from human placenta chorion: Impact of ECM preservation on graft characteristics, protein composition and in vivo performance, Biomaterials, 2018.
[19] J. Fu, Y. Zhang, J. Chu, X. Wang, W. Yan, Q. Zhang, H. Liu, Reduced Graphene Oxide Incorporated Acellular Dermal Composite Scaffold Enables Efficient Local Delivery of Mesenchymal Stem Cells for Accelerating Diabetic Wound Healing, ACS Biomater-Sci Eng (8) (2019) 4054-4066.

[20] S. Pashneh-Tala, S. MacNeil, F. Claeyssens, The Tissue-Engineered Vascular Graft-Past, Present, and Future, Tissue Eng Part B Rev 22(1) (2016) 68-100.
[21] K.H. Schneider, P. Aigner, W. Holnthoner, X. Monforte, S. Nurnberger, D. Runzler, H. Redl, A.H. Teuschl, Decellularized human placenta chorion matrix as a favorable source of small-diameter vascular grafts, Acta Biomater 29 (2016) 125-134.
[22] C.H. Lin, K. Hsia, C.H. Tsai, H. Ma, J.H. Lu, R.Y. Tsay, Decellularized porcine coronary artery with adipose stem cells for vascular tissue engineering, Biomed Mater 14(4) (2019) 045014.
[23] A.M. Kajbafzadeh, R. Khorramirouz, S.M. Kameli, K. Fendereski, S.S. Daryabari, S.M. Tavangar, B. Azizi Garajegayeh, Three-year efficacy and patency follow-up of decellularized human internal mammary artery as a novel vascular graft in animal models, J Thorac Cardiovasc Surg 157(4) (2019) 1494-1502.
[24] J. Cheng, C. Wang, Y. Gu, Combination of freeze-thaw with detergents: A promising approach to the decellularization of porcine carotid arteries, Biomed Mater Eng 30(2) (2019) 191-205.
[25] H. Bai, A. Dardik, Y. Xing, Decellularized Carotid Artery Functions as an Arteriovenous Graft, J Surg Res 234 (2019) 33-39.
[26] A. Porzionato, E. Stocco, S. Barbon, F. Grandi, V. Macchi, R. De Caro, Tissue-Engineered Grafts from Human Decellularized Extracellular Matrices: A Systematic Review and Future Perspectives, Inter J Mol Scien 19(12) (2018).
[27] C.M. Girish, A. Sasidharan, G.S. Gowd, S. Nair, M. Koyakutty, Confocal Raman imaging study showing macrophage mediated biodegradation of graphene in vivo, Adv Healthc Mater 2(11) (2013) 1489-500.
[28] M.N. Moghadam, D.P. Pioletti, Biodegradable HEMA-based hydrogels with enhanced mechanical properties, J Biomed Mater Res B Appl Biomater 104(6) (2016) 1161-9.
[29] H. Van de Vyver, P.R. Bovenkamp, V. Hoerr, K. Schwegmann, L. Tuchscherr, S. Niemann, L. Kursawe, C. Grosse, A. Moter, U. Hansen, U. Neugebauer, M.T. Kuhlmann, G. Peters, S. Hermann, B. Loffler, A Novel Mouse Model of Staphylococcus aureus Vascular Graft Infection: Noninvasive Imaging of Biofilm Development in Vivo, Am J Pathol 187(2) (2017) 268-279.